NASA Contractor Report 174964

NASA-CR-174964
19860000994

Film Cooling on a Convex Wall: Heat Transfer and Hydrodynamic Measurements for Full and Partial Coverage

K. Furuhama, R.J. Moffat, J.P. Johnston,
and W.M. Kays

Stanford University
Stanford, California

August 1985

Prepared for
Lewis Research Center
Under Contract NAG 3-3

National Aeronautics and
Space Administration

FOREWORD

This research was supported by the National Aeronautics and Space Administration under NASA Grant NAG 3-3. Dr. Raymond E. Gaugler, of the NASA Lewis Research Center, is the current project officer.

Numerous colleagues made significant contributions during the course of the work. Of particular importance was the work of Mr. Paul Youssefmir, who made major contributions to the modification of the test facility and to the hydrodynamic experiments. Professors J. H. Ferziger (Stanford), S. Honami (Visiting), and N. Kasagi (Visiting) offered many useful suggestions concerning the conduct and interpretation of the experiments, as did Drs. T. W. Simon and J. W. Gillis, who had previously studied the convex problem without injection.

The authors acknowledge their indebtedness to Mr. Robin A. Birch, who built and rebuilt the apparatus, and to Ms. Ann Ibaraki and Ms. Ruth Korb, who produced the report.

This Page Intentionally Left Blank

SUMMARY

Turbine-blade cooling is an important issue for high-efficiency turbine engines, and discrete-hole injection is widely used as a cooling method. The effects of injection and curvature are both important in determining the actual turbine-blade heat transfer. In the present study, detailed measurements were made of the heat transfer and hydrodynamics of a film-cooled flow on a convex wall, both for full and partial coverage.

Discrete-hole injection produces a boundary layer with significant spanwise periodic variations. In the present program, the spanwise-averaged heat-transfer coefficients were measured. Discrete-hole injection poses a three-temperature heat-transfer situation (since the injectant temperature need not be the same as wall temperature); thus two pieces of information are needed to solve a given problem. Results of the present research are reported in terms of two basic Stanton number values: St(0) (Stanton number with $T_2 = T_\infty$) and St(1) (Stanton number with $T_2 = T_w$). These two data sets allow prediction of the Stanton number for any value of injection temperature, using superposition.

Two important parameters were altered: the blowing ratio, m, and the number of rows of injection holes. Three values of m were tested: $m = 0.2$, 0.4, and 0.6. In the blown region, $m = 0.4$ results in the lowest Stanton numbers of the three blowing ratios tested ($m = 0.2$, 0.4, and 0.6). This indicates that the value of $m = 0.4$ is near optimum on the convex wall from the point of view of cooling effect by injection. Plotting the St(1) data on $St - Re_{\Delta_2}$ coordinates reveals that the local response of the boundary layer for $m = 0.2$ and 0.4 is still governed by the convex-curvature effect, but that for $m = 0.6$ the large amount of injection alters the local nature of heat transfer. In the recovery region, both St(1) and St(0) gradually approach the no-injection values. Although the heat-transfer behavior during recovery from injection looks relatively complicated, the behavior of St(0) and St(1) can be explained in terms of two mechanisms: recovery from the thermal effect of injection and recovery from the turbulence

augmentation. This interpretation of the data is supported by the hydrodynamic and temperature-profile measurements.

For partial blowing cases, the data for St(1) follow the full-coverage values inside the blown region. In the unblown region, both in the curved and in the flat plate, the effect of the number of blown rows is clearly seen.

Hydrodynamic boundary-layer profiles were measured with the aid of a triple hot-wire probe. Three mean-velocity components and six turbulence quantities were simultaneously measured, and inside the blown region strong three-dimensionality was observed.

It seems appropriate to divide the flow field in two alternate lanes in the spanwise direction--lanes with injection holes and lanes without. The profiles in the lane with holes were strongly affected by the injection, but in the lane without holes only small effects were observed.

The turbulence structure in the blown region can be described by the superposition of two streamwise evolutions: a small-scale evolution (between consecutive holes) and a large-scale evolution. The patterns shown in both evolutions depend upon the blowing ratios.

A prediction program, STAN-FC-CRV, a combination of STANCOOL and STANCURV, was tested for four representative cases. The comparison between the prediction and the experimental data reveals that further modification is necessary for the injection model.

TABLE OF CONTENTS

NOMENCLATURE

D	Diameter of an injection hole
h	Heat transfer coefficient
m	Blowing ratio: $m \equiv \rho_2 U_2 / \rho_\infty U_\infty$
P	Pitch between two consecutive holes
P_d	Dynamic pressure
P_s	Static pressure
$P_{s,w}$	Wall static pressure
Q^2	Turbulence kinetic energy: $Q^2 \equiv \overline{U'^2} + \overline{V'^2} + \overline{W'^2}$
R	Radius of curvature
Re	Reynolds numbner
Re_{Δ_2}	Enthalpy thickness Reynolds number
St	Stanton number
$St(1)$	Stanton number with $T_2 = T_w (\theta = 1.0)$
$St(0)$	Stanton number with $T_2 = T_\infty (\theta = 0.0)$
St_o	Stanton number with no injection
$St_{m=o}$	Stanton number with no injection but with injection holes open
T	Temperature
T_w	Wall temperature
T_2	Injection air temperature
T_∞	Free-stream temperature
U,V,W	Mean velocities
$\overline{U'^2}$, $\overline{V'^2}$, $\overline{W'^2}$	Reynolds (normal) stresses
$\overline{U'V'}$, $\overline{V'W'}$, $\overline{W'U'}$	Reynolds (shear) stresses
U_p	Potential flow velocity
U_{pw}	Wall potential flow velocity

x Streamwise distance: $x = 0$ at the beginning of the curve

y Normal distance: $y = 0$ at the wall

z Spanwise distance: $z = 0$ at the centerline

Greek Letters

θ Non-dimensional injection air temperature:

$$\theta \equiv (T_2 - T_\infty)/(T_w - T_\infty)$$

ρ Density

δ Boundary-layer thickness

η Film-cooling effectiveness:

$$\eta \equiv (St(0) - St(1))/St(0)$$

Δ_2 Enthalpy thickness

Subscripts

∞ Values at free stream

w Values at wall

2 Values of injection air

Chapter 1

INTRODUCTION

1.1 Gas Turbine and Turbine Blade Cooling

Gas turbine engines are widely used for aircraft engines and for stationary power plants and inlet temperature plays a key role in setting their performance. Higher turbine inlet temperatures produce higher engine performance and improved efficiency. For these reasons, the future of gas turbine engines is strongly dependent on the operating temperatures which can be tolerated.

One of the difficulties to be overcome in increasing the turbine inlet temperature is protecting turbine blades from the hot gases. Many ways of cooling turbine blades have been designed and tested. In Fig. 1.1, three typical cooling methods are illustrated: convective cooling, discrete hole injection, and transpiration. The last two methods are called "film cooling" because the coolant is injected through the surface and covers the surface as a film. Discrete hole injection cooling is the most promising and practical method among the three, because it produces greater cooling effects than does convective cooling, and is easier to manufacture, and less harmful to blade strength than is transpiration. At the same time, however, discrete hole injection is the method whose characteristics and behavior are least understood, mainly because of the complex geometry of the system and the large number of parameters that govern its heat transfer and hydrodynamic characteristics. Some of the parameters are injection angle, blowing ratio (ratio of the injected flow to the main flow), number of rows of holes, pitch to diameter ratios, and so forth. The problem is further complicated by the effects of curvature.

1.2 Previous Work

In the present study, discrete hole injection with the effects of streamwise convex curvature is experimentally investigated. Indeed, numerous studies have been undertaken to investigate each of these effects.

1.2.1 Film Cooling with Discrete Hole Injection

Film-cooling research began in the early 60's. The early stage of the work was on greatly simplified geometries such as transpiration, injection through a two-dimensional slot or through a single hole. In the case of transpiration, Kays et al. [1] published a summary of research at Stanford University. Classical studies on slot or hole injection were well summarized by Goldstein [2]. In these early studies, film-cooling effectiveness, defined as $\eta \equiv (T_{aw} - T_\infty)/(T_2 - T_\infty)$, was used as a measure of the performance. The heat transfer coefficient was then defined in terms of T_{aw} as $\dot{q}_o = h^*(T_w - T_{aw})$.

More recently, multiple rows of injection and full-coverage cooling has attracted attention. Jabbari and Goldstein [3] conducted experiments for two rows of injection holes on a flat plate. They found that two staggered rows produced more effective cooling than two in-line rows. Two rows of injection has been extensively studied, as a simple case of multiple rows of injection and because it is widely used for actual turbine blades. Bergeles et al [4] and Afejuku et al. [5] also worked on two rows of injection. Numerical as well as experimental analyses were conducted in Ref. 4. Afejuku et al. [5] changed the flow rates of injection from the two rows independently and made a map showing the optimum combinations for a fixed total injection rate. Full-coverage cooling has been studied by several researchers. Metzger et al. [6] investigated heat transfer behavior of a flat plate with full-coverage film cooling. For full-coverage cooling, strong three-dimensionality is expected because of its geometry, and this three-dimensionality makes experimental work difficult. Two different approaches have been reported. One consists of measuring local values of wall temperature and heat transfer coefficients [7,8,9], whereas the other treats the flow as though it were two-dimensional and measures the spanwise-averaged values [11,12,13]. Sasaki et al. [7] measured wall temperature distributions with a scanning infrared camera, and Kasagi et al. [8] used a thin-film of liquid crystal to visualize the wall temperature. Kumada et al. [9] measured local heat transfer coefficients using the naphthalene sublimation technique.

As an alternative to the use of effectiveness and adiabatic wall temperature, one can use a heat transfer coefficient based on the actual difference between gas and wall temperature. In this method, the value of h is a function of the temperature of the injected fluid as well as the hydrodynamic parameters. The two descriptors are then h and θ, instead of η and T_{aw}, where θ is defined as $\theta = (T_2-T_\infty)/(T_w-T_\infty)$. This approach was first introduced by Metzger et al. [10] and developed by Choe et al. [11]. The Stanford program on film cooling follows the h, θ, approach. Data concerning full-coverage film cooling on flat plates were reported by Choe et al. [11] for normal injection, by Crawford et al. [12] for 30° inclined angle injection, and by Kim et al. [13] for 35 × 45 compound angle injection. The consensus from this series of studies is that Stanton number reaches a minimum at about $m = 0.4$ and increases for higher values of m, where m is the blowing ratio.

For the case of discrete hole injection, many combinations of geometric and hydrodynamic parameters have been investigated. Metzger et al. [14] varied the number of rows from one to four for both staggered and in-line geometries. The effect of hole spacing was tested by Sasaki et al. [7], by Crawford et al. [12] and Metzger et al. [14]. Pitch to diameter ratio (P/D) in the streamwise direction was changed for $P/D = 5$ and 10 with P/D in spanwise direction kept at 3 in Ref. 7. Crawford et al. [12] tested $P/D = 5, 10$ in both directions and Metzger et al. [14] used $P/D = 4$ and 8. Of the many hydrodynamic parameters, the blowing ratio, m, defined as the ratio of injection air mass velocity and main stream mass velocity, seems to be most crucial. The range from $m = 0.1$ to $m = 1.0$ has been most commonly tested. For example, Bergeles et al. [4] tested the range from 0.25 to 1.0, Crawford et al. [12] used $m = 0.2$, 0.4, 0.6 and 0.9 and Metzger et al. [14] tested $m = 0.1$, 0.2, 0.3 and 0.5. The effects of free stream conditions have also been investigated. The effect of free stream turbulence was studied by Kadotani and Goldstein [15], Brown and Saluja [16]. Brown tested turbulence intensities 0.02 and 0.09. Kadotani claims that free stream turbulence of 8.2% significantly affects the mixing process of the jet and the main stream in Ref. 15. Jabbari and Goldstein [17] investigated the effect of free-stream acceleration, obtaining a 15%

decrease of the effectiveness for two rows of injection. Brown [16] tested the case with adverse pressure gradient as well as favorable pressure gradient. Upstream conditions, such as initial boundary layer thickness and initial Reynolds number were tested by Crawford [12] and Kadotani [15], who found that the boundary thickness had a significant influence on the film cooling performance.

Experiments with injection holes on a cylinder were conducted by Taylor and Whitelaw [18] and Luckey et al. [19] to simulate the leading edge of turbine blades and to investigate the heat transfer behavior near the stagnation region. The effect of location with respect to the stagnation line was investigated in both of these studies. The number of rows of injection were varied from one to two to three with injection angle fixed at 30° by Taylor et al. [18]. They found that the effectiveness increases as the blowing ratio and the number of rows increases. Three injection angles, 25°, 35°, and 45° were investigated in the study by Luckey et al. [19]. Experiments using actual turbine blades were carried out by Sakata et al. [20] and Dring et al. [21]. Sakata et al. [20] used two-dimensional vanes with 14 rows of holes. Dring et al. [21] tested a single row geometry for both the suction and pressure surfaces of the rotor blade and compared their results with flat plate results. They found reasonably good agreement betwen flat-plate data and suction-side data, but found only a small cooling effect on the pressure side.

Hydrodynamic measurements of the flow field in the blowing region and its wake have been made in several investigations. Bergeles et al. [22] made measurements of spanwise velocity profiles and static pressure distributions in the region very close to the injection hole. Kadotani and Goldstein [23] measured time-averaged and instantaneous velocities as well as temperature profiles and related their results to the turbulence scale in the mainstream.

Turbulence quantities as well as three components of the mean velocity were measured by Yavuzkurt et al. [24] with a triple hot-wire probe in a full-coverage region as well as in the recovery region. They found that hydrodynamic characteristics of $m = 0.4$ and $m = 0.9$ were significantly different. Colladay and Russell [25] visualized an injected flow at normal, 30° and 30° x 45° compound angle in three rows of

holes and showed detailed streaklines of the turbulent motion of the injection air. Russell [26] conducted smoke visualization of the injection into the cross-flow over cylinder. His results showed a close relation between the flow field and the heat transfer behavior.

1.2.2 Streamwise Curvature Effect - Convex

Investigations prior to 1972 are well summarized by Bradshaw [27]. It is still worthwhile, however, to list some of the classical work which spawned the research interests in this area. Wattendorf [28], in 1938, made measurements of mean velocities and wall static pressures in a fully-developed channel flow, and found significant effects of wall curvature. Eskinazi and Yeh [29] measured some of the turbulence quantities, $\overline{U'^2}$, $\overline{V'^2}$ and $\overline{U'V'}$, of the fully-developed flow. For heat transfer measurements, Schneider and Wade [30] measured wall heat flux along a convex wall and found that the heat transfer coefficients were 50% lower than the flat plate values. In the following section, more recent work will be discussed.

The parameter δ/R (initial hydrodynamic boundary layer thickness over radius of wall curvature) is believed to express the strength of curvature adequately for most purposes. Cases with $\delta/R \sim 0.01$ are considered to be mild curvature. The hydrodynamic effects of mild curvature have been experimentally investigated by Ramaprian and Shivaprasad [31, 32, 33] and Bradshaw and his colleagues [34, 35]. From mean velocity measurements [31], Ramaprian concluded that the effect of curvature was observed in the outer part of boundary layer, while the near-wall region was not affected significantly by curvature. Ramaprian and Shivaprasad also conducted turbulence measurements [32, 33]. They found that convex curvature reduces the length and velocity scales of turbulent motions and shifts the spectral distributions of turbulence kinetic energy and shear stress towards higher wave numbers. Hoffman and Bradshaw [35] tested mild curvature ($\delta/R = 0.01$) and measured velocity fluctuation products up to 4th order. They found that those turbulence quantities were suppressed by convex curvature effect.

Effects of strong curvature were investigated by So and Mellor [36, 37] and by Gillis et al. [38]. So and Mellor [36, 37] used $\delta/R = 0.07$

and made very detailed hydrodynamic measurements. They found that the turbulent shear stress approaches zero in the outer part of the boundary layer. They extended their experimental results to a prediction model [39]. Gillis et al. [38] conducted experiments with $\delta/R = 0.05$ and 0.10 and paid particular attention to isolating the effect of convex curvature from the effect of streamwise pressure gradient at the onset of curvature which usually accomlpanies a curved duct flow. They found that, along a convex surface, the turbulent shear stress was almost zero in the outer part of boundary layer even though the turbulent kinetic energy is not zero. Measurements were also made in the recovery region and it was found that the recovery process from curvature effects takes place very slowly. Efforts were made by Gillis et al. [38], to modify the existing computer program STAN-5 [40] to account for convex curvature effects.

Fewer experiments have been conducted on the heat transfer behavior on a convex surface than on the hydrodynamics. Brinich and Graham [41] measured wall heat transfer rates and temperature profiles in a curved channel. Despite the presence of strong secondary flow, slightly lower heat transfer coefficients were measured on the convex wall. Mayle et al. [42] measured local heat transfer coefficients on convex and concave surfaces with $\delta/R = 0.01$. It was observed by Mayle et al. [42] that the effect of convex curvature reduced heat transfer rates while concave curvature increased them, and that the reduction on a convex surface is about 20%. Simon et al. [43] used the same apparatus as Gillis et al. [38] and made detailed heat transfer measurements including the developing and recovery flat-plate regions. Simon et al. [43] found that Stanton number decreased by 30% at the end of a 90° convex curve and that the heat transfer recovery process took place very slowly, as might be expected from the hydrodynamic recovery observed by Gillis et al., [38]. From their measurements with $\delta/R = 0.10$ and 0.05 , they found that the heat transfer results were not a function of δ/R for large values of δ/R (strong curvature).

1.2.3 Film Cooling with Curvature

Few attempts have been made to study the film cooling on a curved wall. Experiments were conducted with injection holes on a cylinder [18], [19], [26]. The emphasis has been placed on the stagnation region, not on a curved boundary layer surface, for this series of experiments. Studies on two-dimensional injection (slot injection) on a convex wall were carried out by Nicolas and Lemeur [44], Folayan and Whitelaw [45], and Mayle et al. [46]. Nicolas [44] claimed that "Archimedes type force" acted on the injected air and influenced its effectiveness. Their experiments show that on a convex wall the effectiveness is higher than on a constant pressure flat plate. No attempt was made to separate curvature effects and pressure effects. They concluded that the effectiveness on a convex wall was less than on a flat plate for the same pressure gradient. Folayan [46] tested the effect of radius of convex curvature and found that a smaller radius (stronger curvature) increased the effectiveness but tended to separate the flow closer to the slot, which resulted in a rapid decrease of the effectiveness. Mayle et al. [46] also found that film-cooling effectiveness was higher on a convex wall and lower on a concave wall than on a flat plate. Ito et al. [47] extended the force balance analysis and included the effect of injection angle. They claim that if the value $(\rho_2 U_2^2/\rho_\infty U_\infty^2)\cos^2\alpha$, where α is injection angle, is less than unity, the effectiveness on a convex surface is better than on a flat or a concave surface. The experiments were conducted by Ito et al. [47], using an actual turbine cascade with a single row of injection, to test their analyses.

There has been no previous work on film-cooling with multiple rows of injection (2-5 rows) or on full-coverage (more than 5 rows) cooling. Jointly with the present study, Youssefmir and Johnston [48] used the same apparatus and measured mean velocities and flow angles for full-coverage film cooling case with $m = 0.4$, with emphasis placed on the region very close to the injection hole.

1.3 Objective of The Present Study

For turbine blade cooling design, the effects of injection, curvature, rotation, pressure gradient, boundary layer maturity, surface roughness, free-stream turbulence, and so forth, must be taken into account. Studying each effect independently is appropriate, provided that the results of individual studies can be combined in a computer program capable of dealing with the entire problem. This capability has been demonstrated by several programs. One example would be STAN5 [40], a finite difference program which has been adapted to many boundary layer problems, including curvature with injection.

The primary objective of this work is to provide a solid data base for film-cooled flow on a convex wall. The data and discussion presented here should increase understanding of the physics of the flow and form an experimental basis for prediction.

Specifically, the following experiments were planned.

1. Measure spanwise averaged heat transfer coefficients for full-coverage film cooling over a convex surface.

2. Conduct the same heat transfer experiments for partial-coverage film cooling where injection is placed on only part of a convex surface.

3. Measure hydrodynamic boundary layer profiles, both mean and turbulence quantities, for some representative cases studied in the heat transfer experiments.

4. Measure temperature profiles at the same streamwise and spanwise locations as for hydrodynamic measurements.

As a final step of the present study and to prepare for future modeling efforts,

5. Compare the predictions of an existing computer code to the experimental data obtained in the present study and identify areas of the program needing development.

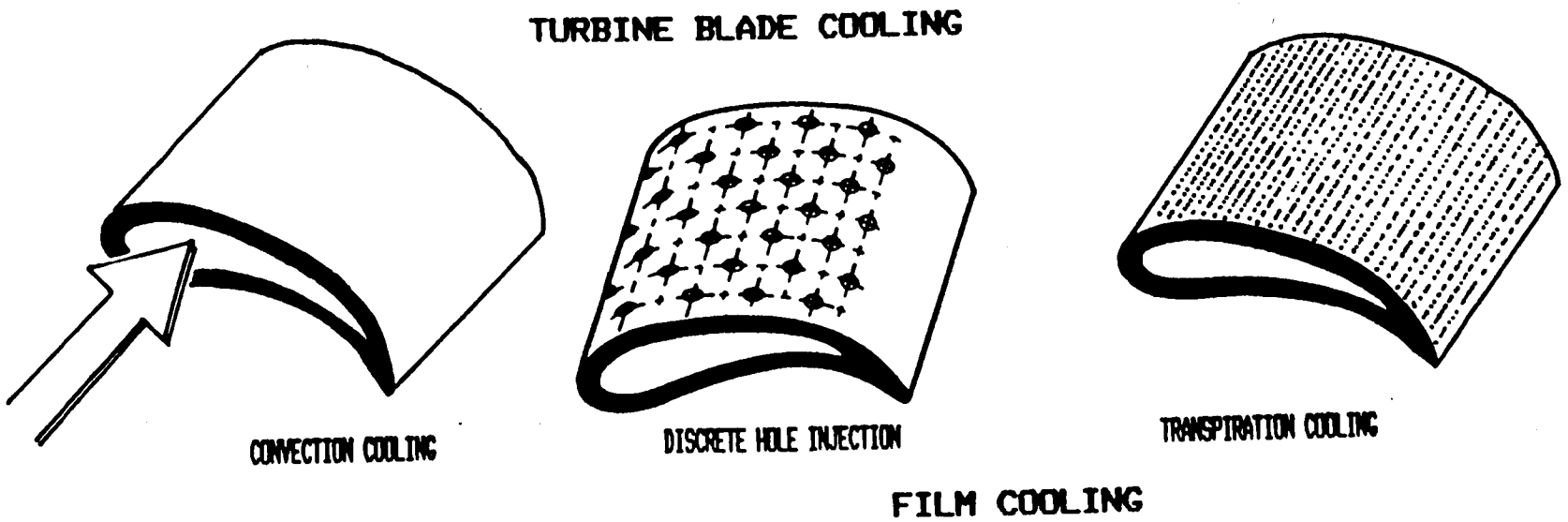

Fig. 1.1. Three typical methods of turbine-blade cooling

Chapter 2

APPARATUS AND INSTRUMENTATION

All experimental appartus and instrumentation used in the present study are described in this chapter. They include a wind tunnel, a triple-hot-wire anemometry, automatic traversing gear, and the data-reduction system. Some of these were built and developed in previous work. A more detailed description can be found in the referenced documents of the previous work.

2.1 Curvature Rig

All experiments were conducted in a closed-loop wind tunnel, shown in Fig. 2.1, originally built by Choe [11] and later modified for the curved-wall experiment by Simon [43]. Detailed descriptions of the tunnel are given in Refs. 11 and 43.

The test section is 3.8 m long and consists of three regions: a developing flat surface, a curved surface with injection holes, and a flat recovery surface. There are two air loops (the main tunnel air flow and the injection air) and two water loops (hot water for heating the plates and cold water for controlling the temperature of the main air flow). Schematics are shown in Fig. 2.2 for these two systems. The free-stream temperature was adjusted by changing the flow rate of make-up water to the recirculating water loop. The experiment was conducted with the free-stream temperature close to ambient to minimize interaction with the room air.

2.1.1 Developing Region

The developing surface is a 1.2 m long flat plate and made of 48 copper strips. The last half of this plate (24 copper strips) can be heated by hot water to a uniform temperature. A thermocouple and a heat flux meter are embedded in each copper strip to measure surface temperature and wall heat flux. Along the surface a turbulent boundary layer is developed which is normal in both hydrodynamic and thermal aspects.

2.1.2 Curved Surface

The curved surface is 0.7 m long with a 90° turn at a radius of curvature of 45 cm. Along the curved surface, there are 14 copper strips. From the second to the last (14th) one, each strip has injection holes. The number of holes in each row is either 8 or 9, starting with 9 holes, and forming a staggered hole pattern. Figure 2.3 is an illustration of the curved surface. The diameter of each hole is 1.03 cm and the spacing between neighboring holes is 5.15 cm in the spanwise directions. Thus, the values of pitch/diameter is 5 in this geometry. The rows are also 5.15 cm apart in the streamwise injected direction. The injected air is at an angle of 30° with respect to the surface tangent. The position and shape of the flexible outer wall of the test section can be adjusted to keep the wall static pressure uniform to within 5% of the dynamic head of the free-stream. By maintaining a constant static pressure, the curvature effect can be isolated from the effect of the streamwise pressure gradient which usually accompanies entry into a curved flow. Three thermocouples are embedded in each copper segment for measuring wall temperature and checking its spanwise uniformity. Each segment is electrically heated, independently, permitting an isothermal wall condition to be achieved.

2.1.3 Recovery Region

The process of recovery from curvature is an important consideration. For the present study, a new, 65 cm long flat plate was inserted in the initial recovery region. This new recovery plate doubled the total length available for heat transfer measurements compared to the study of Simon [43]. In addition, the new plate has the capability of injection, which will be used later for film-cooled flow in the recovery region as well as in the curved region. For the present study, the injection holes were plugged so that the recovery plate was treated as an impermeable wall. This plate is electrically heatable and has four embedded thermocouples in each strip for wall temperature measurement. Since the energy balance method was used for evaluating the wall heat flux in the curved plate and the first recovery plate, the support structure of both plates was heated to a temperature close to the wall temperature for minimizing heat loss. A second recovery plate follows

the initial section. This plate is 1.2 m long, and its first half can be heated by hot water. The structure of this plate is almost idential to that of the developing plate.

2.1.4 Injection Air Loop

The injection air loop has its own blower, heat exchanger, and heater for control of the injection air temperature. The air is divided into 13 paths to feed air separately to each row of injection holes. The flow-rate to each row is measured by hot-wire type flow meter and is adjusted by a gate valve.

The structure and the calibration procedure of the flow meters are described in Ref. [48]. Spanwise uniformity of the injected flow was achieved by small trimming valves, one in each delivery tube. A thermocouple was installed 30 cm upstream of the exit of each delivery tube to measure the injection air temperature. The exit temperature (i.e., T_2) was calculated using a calibrated equation developed by special tests on the injection delivery system. The whole injection air loop is surrounded by an insulation box to minimize heat loss and to establish a uniform temperature for all injection air.

2.2 Flow Measurement Apparatus

2.2.1 Triple Hot-Wire

The triple-hot-wire probe is made of three orthogonal hot wires that allow measurement of the three components of velocity simultaneously. Figure 2.4 shows the structure of the probe. This probe is a standard DISA triple wire probe. the signals are processed by a high speed analog system developed by Yavuzkurt [24] useful in fully three-dimensional flows and further developed by Frota et al. [49] who analyzed the uncertainty of the system and developed the temperature-compensation technique.

The three hot-wire signals are decomposed to calculate instantaneous velocity components, U_i in lab coordinates. High-speed analog processing enables real-time values of U_i to be sensed, and through analog multipliers, six turbulence quantities $\overline{U_i'U_j'}$ as well as three

mean velocity components $\overline{U_i}$ can be calculated. The uncertainty analysis showed that dU/U is 2.1%, dV/U is 1.9% and dw/U is 3.9% for zero pitch angle [49]. The closest point to the wall is at 0.3 cm in the curved region and at 0.4 cm in the recovery region, because of the size of the probe. For the present measurements, a Digital Equipment Corporation MINC-11 laboratory computer was used to acquire the three analog signals sequentially, digitized the signals via a 12-bit successive approximation type A/D converter, and store the data. Details explaining the principles and use of the triple-wire are in Ref. 49.

2.2.2 Automatic Traversing Mechanism

For the boundary layer measurements, the probe was traversed with the automatic traversing device. The traversing mechanism has two axes, y (normal direction) and z (spanwise direction). In both directions, either manual control or computer-aided control is possible. The device was designed by Youssefmir [48], and details of its design and construction are given in that report. Figure 2.5 illustrates the data-acquisition system for hydrodynamic measurements, including the automatic traversing mechanism and the mini-computer.

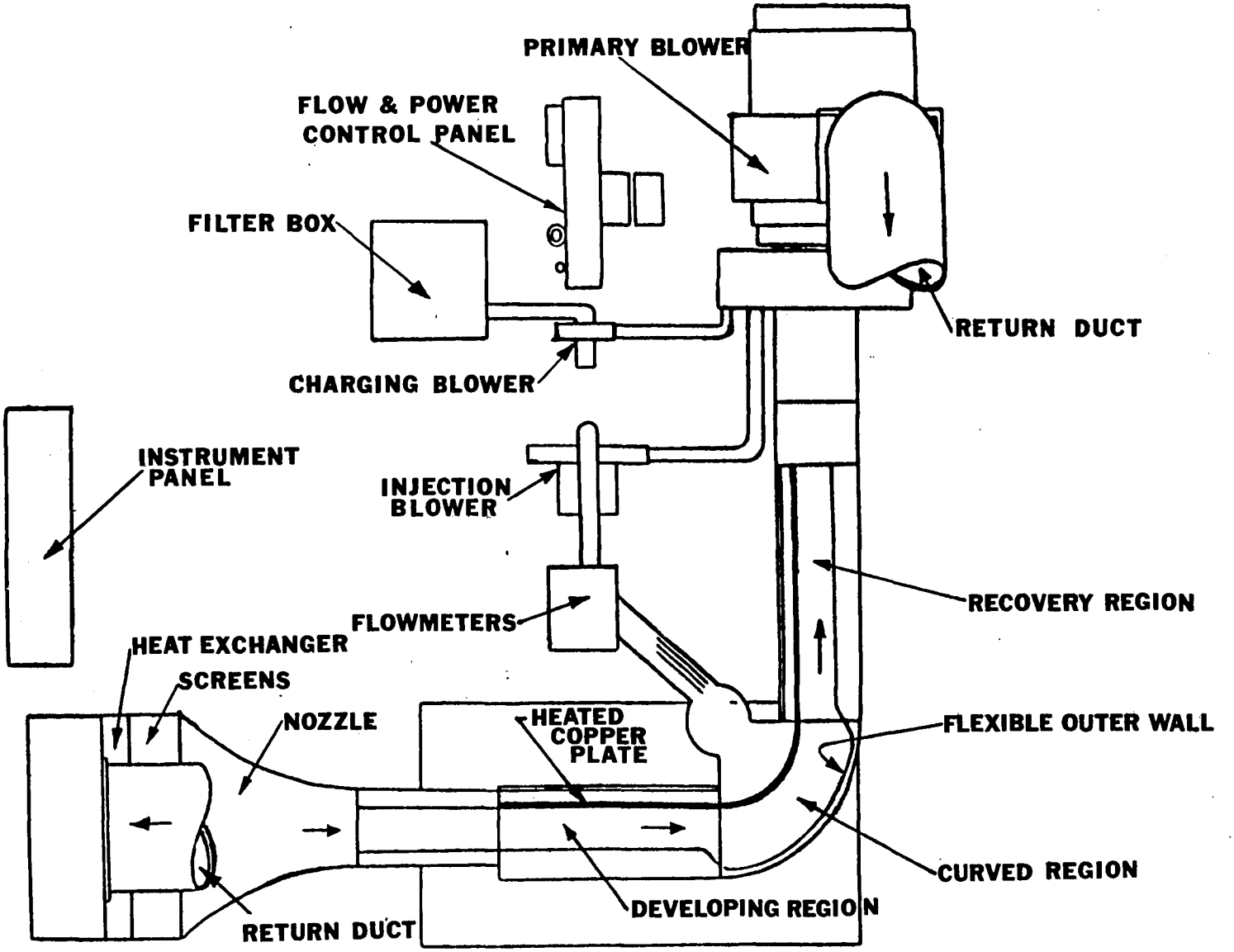

Fig. 2.1. Plan view of curvature rig

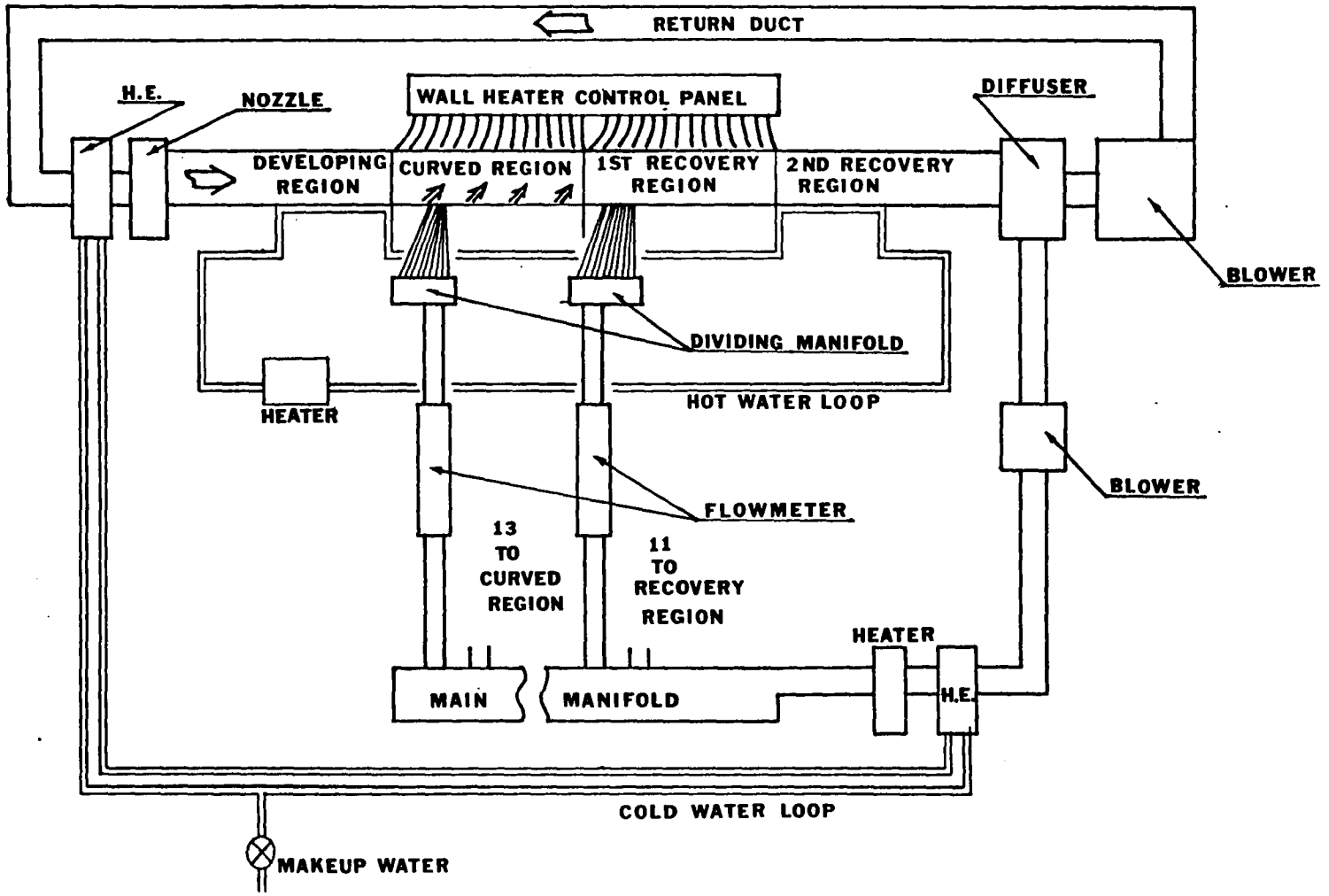

Fig. 2.2. Curvature rig: air loops and water loops

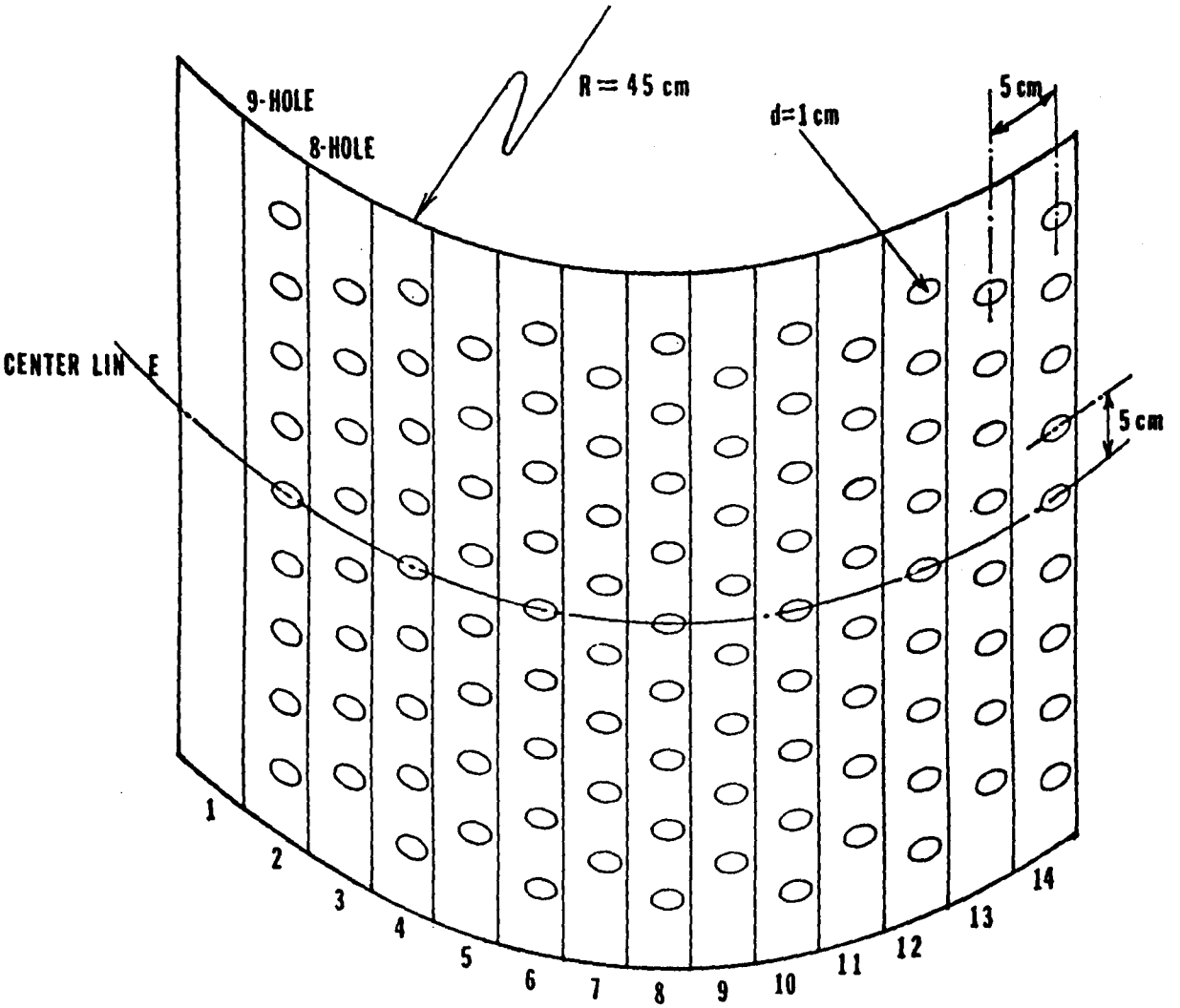

Fig. 2.3. Illustration of curved surface

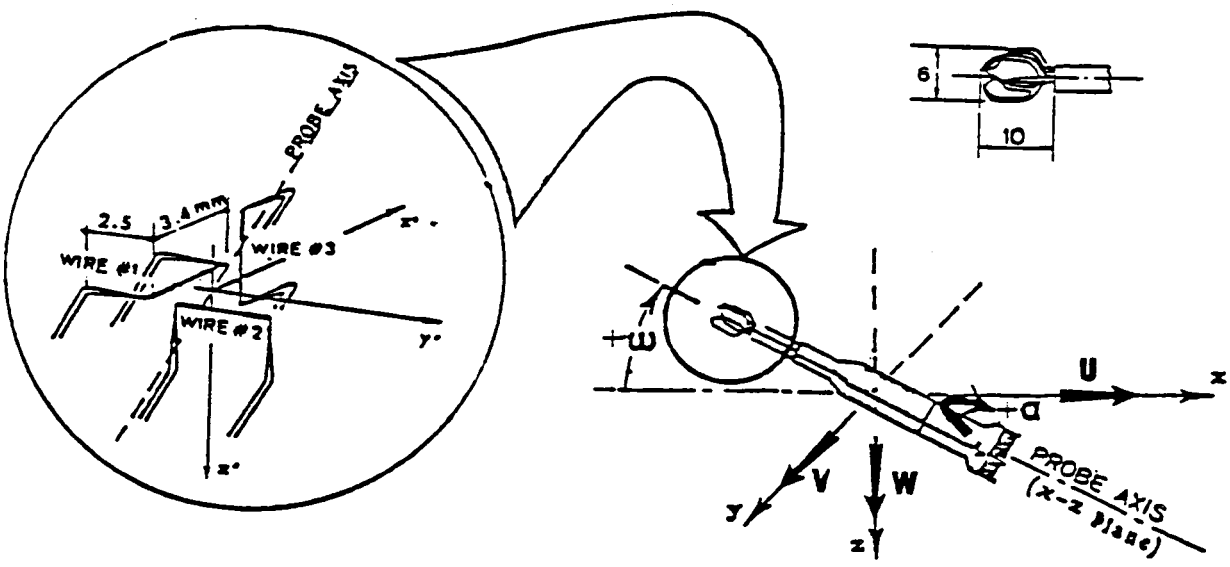

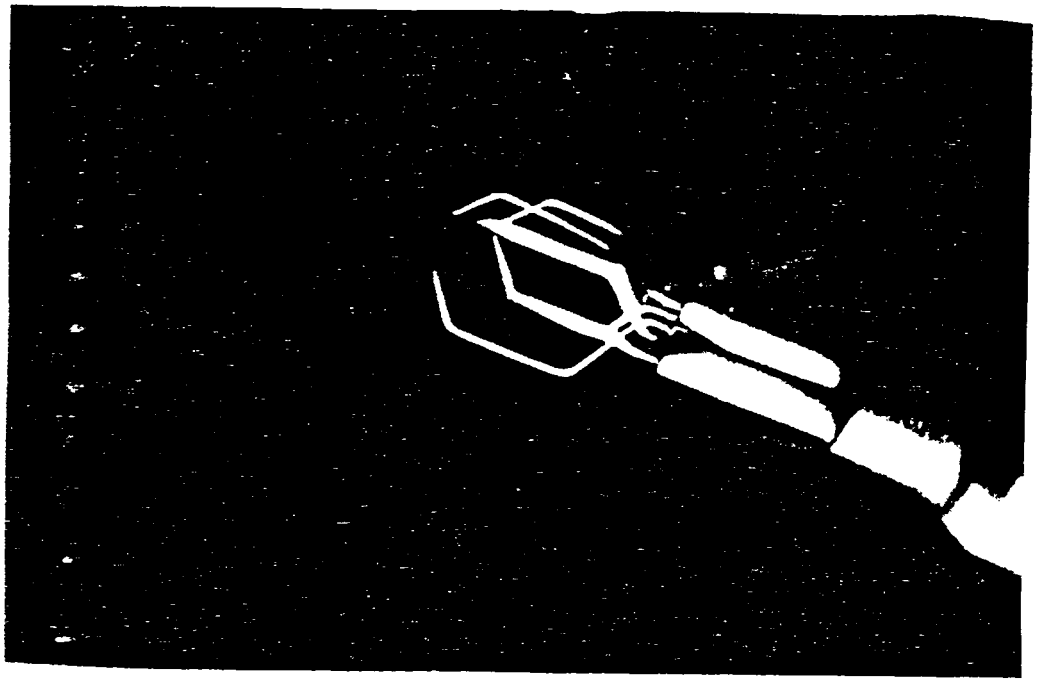

Fig. 2.4. Triple hot-wire probe

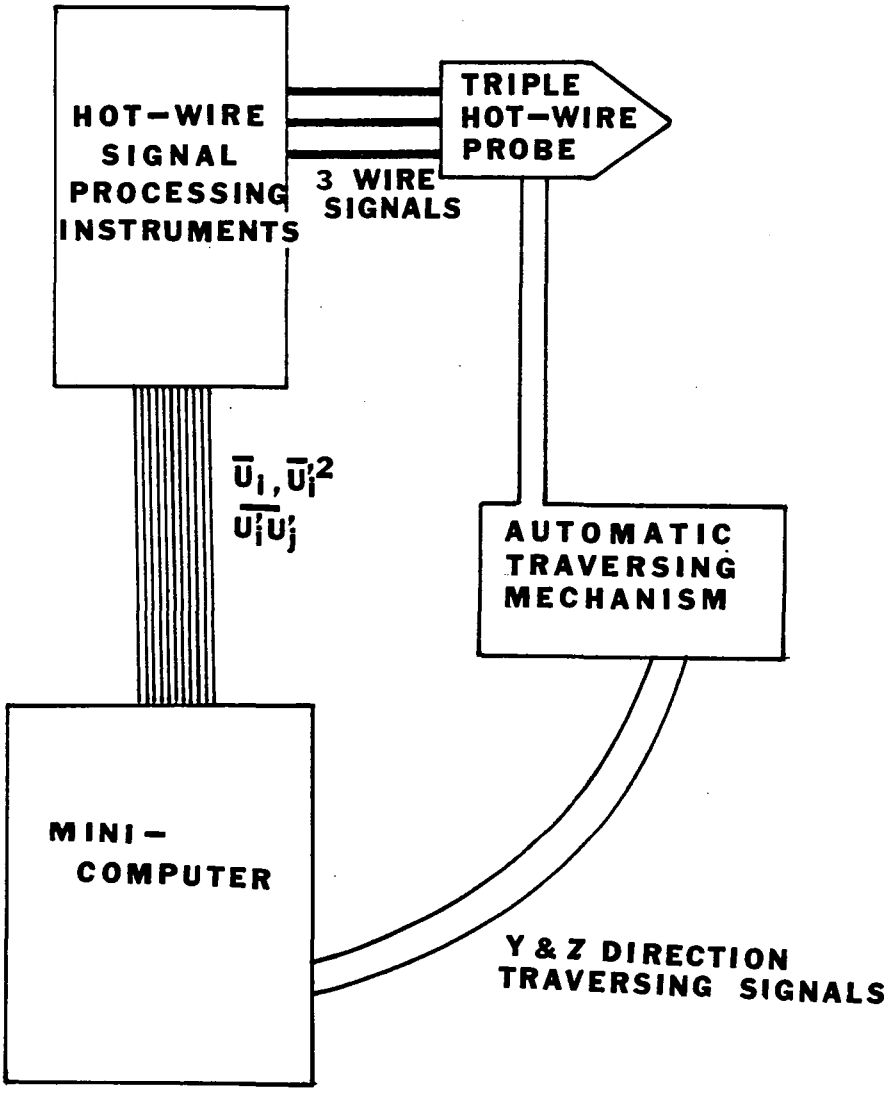

Fig. 2.5. Data-acquisition system for hydrodynamic measurements

Chapter 3

EXPERIMENTAL PROCEDURE

The procedure of the main experiments, both heat transfer and hydrodynamic measurements, is described in the following sections. For heat transfer experiments, two different methods were used for evaluating wall heat flux. The heat transfer data are presented here in terms of h and θ, rather than T_{aw} and η. For boundary layer profile measurements, the relative location of measurements with respect to the injection holes must be precisely pointed out, as well as the streamwise location on the whole test plate. This information is found in this chapter.

3.1 Experimental Conditions

Many parameters can be altered for film-cooling on a convex wall. In the present study, the more important of these parameters were altered and others were held fixed. The blowing ratio, m, defined as the ratio of injection air mass velocity and free steam mass velocity, $\rho_2 U_2/\rho_\infty U_\infty$, is of great importance in discussing film cooling characteristics. Experiments were conducted for three different values of m: $m = 0.2$, 0.4 and 0.6. The value of $m = 0.4$ was found near optimum from the results of earlier flat-plate experiments [11,12,13] and a considerable amount of data exists for $m = 0.4$. For the reasons above, $m = 0.4$ was chosen as the baseline condition for the convex wall study. Injection with $m = 0.2$ and 0.6 were chosen as representative cases for lower and higher blowing.

The number of rows of injection is another parameter which the designer must fix. More rows of injection are expected to give more protection to the surface, but also require more injection air and more manufacturing effort, and weaken the blade. The heat transfer behavior with different numbers of rows was measured to give an idea of how many rows might be sufficient for a particular engine design. For heat transfer (Stanton Number) measurements of the present study, four different cases were examined; full-coverage blowing (13 rows of injection) and partial-coverage with 6,4, and 2 rows. Boundary layer

measurements, i.e., velocity, turbulence and temperature, were also made for the full-coverage case and for two rows of injection as representative of partial-coverage cases.

The following are the fixed conditions: The free-stream velocity is 14 m/s. The ratio of hydrodynamic boundary layer thickness (δ_{99}) and radius of curvature (R) was held at 0.10 at the beginning of the curved surface, which represents strong curvature. The wall temperature was uniform in the streamwise direction, approximately 15°C higher than free stream temperature. The injection angle at the surface was 30° and the ratio of pitch over diameter, P/D , is 5.

3.2 Stanton Number Measurements

3.2.1 Wall Heat Flux

Two different ways of measuring heat flux were used. In the developing plate and the secondary recovery plate, the heat flux from each copper strip was directly measured by an embedded heat flux meter, taking account of radiation loss and the conduction loss to the neighboring strips. The radiation loss was only a small amount, and the conduction loss was minimized by the isothermal wall condition.

In the curved plate and the first recovery plate, an energy balance was executed on each strip, accounting for the radiation loss, the lateral and axial conduction loss, the loss to the support structure and for heat exchange between the wall and the injection air. To minimize the loss to the support structure, the structure was independently heated to approximately the same temperature as the wall. The heat loss to the injection air was calculated using an experimentally determined calibration constant. (See Refs. 11 and 12 for details.) In the case where the injection air temperature was largely different from the free stream, the amount of heat loss was relatively high and the evaluated heat flux had a large uncertainty (+ 8.1%).

3.2.2 Injection Air

For the injected flow, the flow rate and temperature are most critical. The hot-wire type flow meter can measure the flow rate of each row of injection holes within 5%. This value was estimated by uncertainty analysis of the measurement system and was confirmed through the calibration process. The flow rate of the injection air is expressed in terms of the blowing ratio, m, defined earlier.

The temperature of the injected air was measured by embedded thermocouples installed 30 cm upstream of the exit of the injection tube. The exit temperature was calculated by a calibration equation based on heat exchanger theory, and the accuracy is $\pm 0.2°$. References 11 and 12 describe the details. The same idea is applied to calculate the heat flow between the injection air and the surface. Details are also in Ref. 11. The uncertainty of the calibration constant is high, 20%, but the contribution to the total uncertainty (uncertainty of St) is 2.5% for hot run and 5% for cold run.

For discrete hole injection, the injection air temperature is an independent variable which affects the value of the heat transfer coefficient significantly. In order to express the heat transfer coefficient as a function of the injection temperature, heat transfer measurements with two different injection temperatures were made for each set-up. In one case, the injection air was heated so that its temperature became almost equal to the wall temperature (Hot Run) and in the other case, the injection air temperature was approximately equal to the free-stream temperature with the heater off (Cold Run). The difference was seldom more than 3°C.

3.2.3 Superposition Approach

The heat transfer coefficients can be calculated as a function of the injection air temperature, using the linearity of the energy equation for low-speed, constant-property flow. The non-dimensional heat transfer coefficient, St , can be expressed as a linear function of the non-dimensional injection air temperature, θ, as

$$St(\theta) = St(0) - \theta\, St(0) - St(1) \qquad (3\text{-}1)$$

where θ is defined as $\theta \equiv (T_2 - T_\infty)/(T_w - T_\infty)$

$St(0)$ is St with $T_2 = T_\infty$ $(\theta = 0)$

$St(1)$ is St with $T_2 = T_w$ $(\theta = 1)$

A detailed discussion of the superposition approach is given in Ref. 11. From the measured values of St for the hot run (θ_H) and the cold run (θ_c), St(0) and St(1) can be calculated by following equations.

$$St(0) = \frac{(\theta_H)\, St(\theta_c) - (\theta_c)\, St(\theta_H)}{\theta_H - \theta_c} \qquad (3\text{-}2)$$

$$St(1) = \frac{(1-\theta_c)\, St(\theta_H) - (1-\theta_H)\, St(\theta_c)}{\theta_H - \theta_c} \qquad (3\text{-}3)$$

If the values of St(1) and St(0) are given, the Stanton Number values at any θ (any injection air temperature) can be calculated by Equation (3-1). The validity of this superposition approach was experimentally demonstrated. The result is shown in Fig. 3.1. Two sets of St(0.7), one with an experiment and the other with superposition calculation, are compared in the figure. The agreement of the two are excellent in the entire region including the recovery region.

3.3 Boundary Layer Measurements

Boundary layer measurements were carried out for hydrodynamics and temperature. Hydrodynamic measurements were made with a triple hot-wire and included both the mean velocity components and the turbulence quantities. The measurements were conducted at six streamwise stations. The first two stations were inside the curved region and other four stations were in the recovery region. Station 1 was at the third blown row (s = 17.6 cm) and Station 2 was at the eighth blown (s = 42.7 cm). Station 3 was at the very beginning of the recovery plate (s = 73.2 cm). Station 4, 5, and 6 were at s = 103.7 cm, 141.8 cm, and 220.4 cm, respectively. Since the flow field with injection air was expected to be three-dimensional inside the blown region and in the first part of the recovery region, multiple measurements were made in the spanwise

direction. Principally, five spanwise locations were used at Station 1, 2, and 3; $z = 0$ (centerline), $z = \pm 2.54$ cm and $z = \pm 1.27$ cm. The locations $z = 0$ and $z = \pm 2.54$ cm were in line with injection holes and those of $z = \pm 1.27$ cm were in lanes between the holes. At Station 4, three spanwise locations were used; $z = 0$ and $z = \pm 2.54$ cm, to see how the three-dimensionality created by injection decayed in the recovery region. At Station 5 and 6, only the center line location ($z = 0.0$) was used; presuming the flow was two-dimensional. The streamwise and spanwise locations of triple-wire measurements are illustrated in Fig. 3.2, which also shows the relation between the measurement location and the injection holes.

The hydrodynamic measurements were conducted under isothermal conditions. The wall heater was off and the injection air temperature was controlled to be the same as the free stream temperature ($\theta = 0.0$) within 0.3°C. For full-coverage blowing, all three blowing ratios, $m = 0.2$, 0.4, and 0.6 were examined. For partial blowing, the case of two rows of blowing was tested for both $m = 0.4$ and 0.6. Two rows of blowing were the smallest number of rows used in the present series of experiments, and seems to show the characteristics of partial blowing cases very clearly. Also, two rows of blowing are frequently used in actual engine designs.

Temperature profiles were taken with a thermocouple probe (Chromel-Constantan). The probe was driven by an automatic traverse and the data was digitally stored in a mini-computer, as for the triple-wire case. The streamwise and spanwise locations for temperature measurements were identical to those for hydrodynamic measurements except the last location (Station 6). Station 6 is at $s = 163.4$ cm for the temperature profiles because, in the location $s = 220.4$ cm (Station 6 for hydrodynamic profiles), the plate is not heated. Temperature measurements were made for two full-coverage cases ($m = 0.4$ and $m = 0.6$). For $m = 0.4$, both a hot run ($\theta \sim 1.0$) and a cold run ($\theta \sim 0.2$) were examined. For $m = 0.6$, only a hot run was tested. The hot run was felt to be more important from the application point of view and because heat transfer experiments indicated that St(1) showed distinctive differences between $m = 0.4$ and $m = 0.6$. As a practical blowing case, two rows of blowing with $m = 0.4$ (hot run) was tested, which was the most representative case.

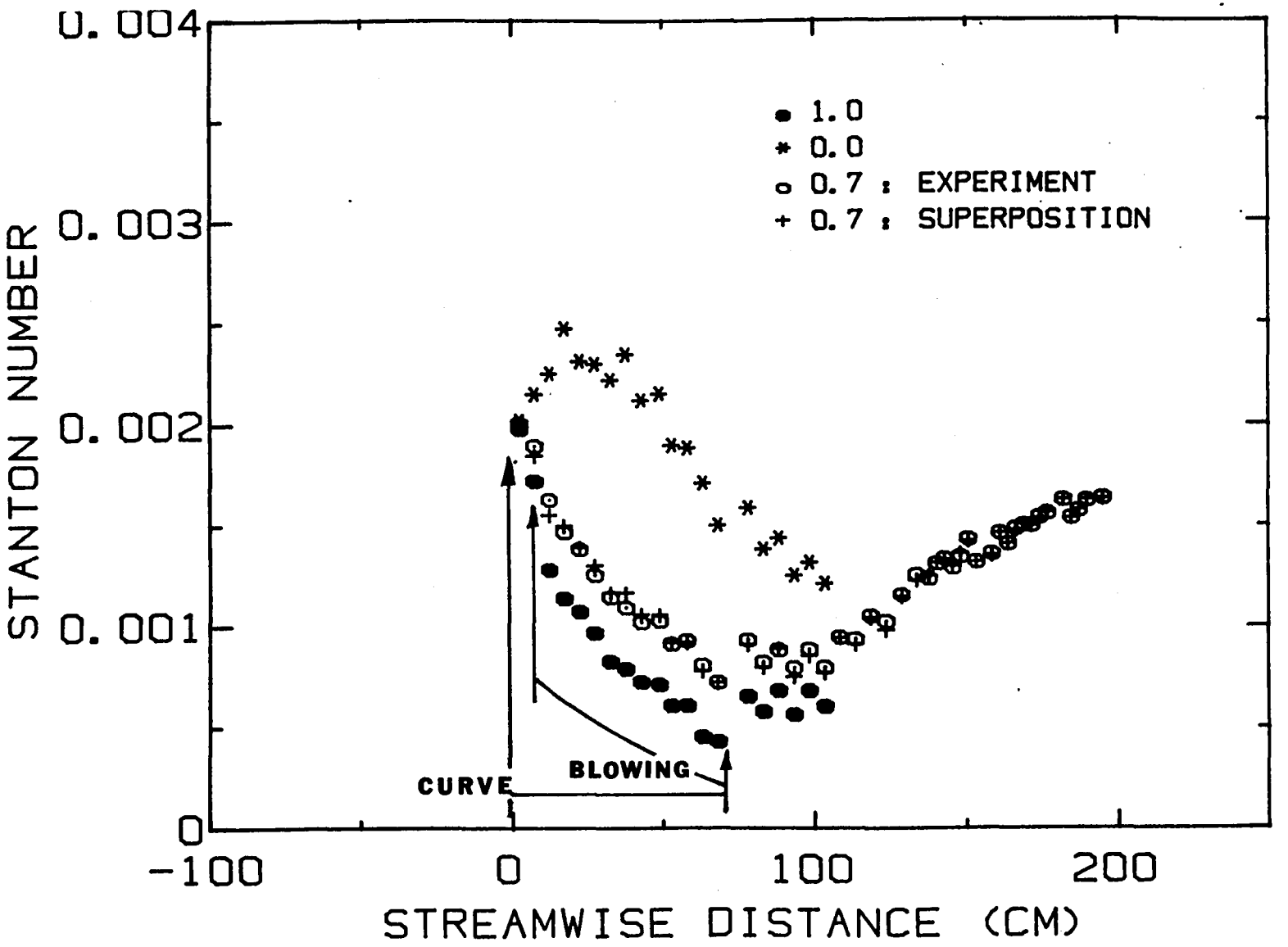

Fig. 3.1. Comparison of St(0.7) data: experiment and superposition calculation

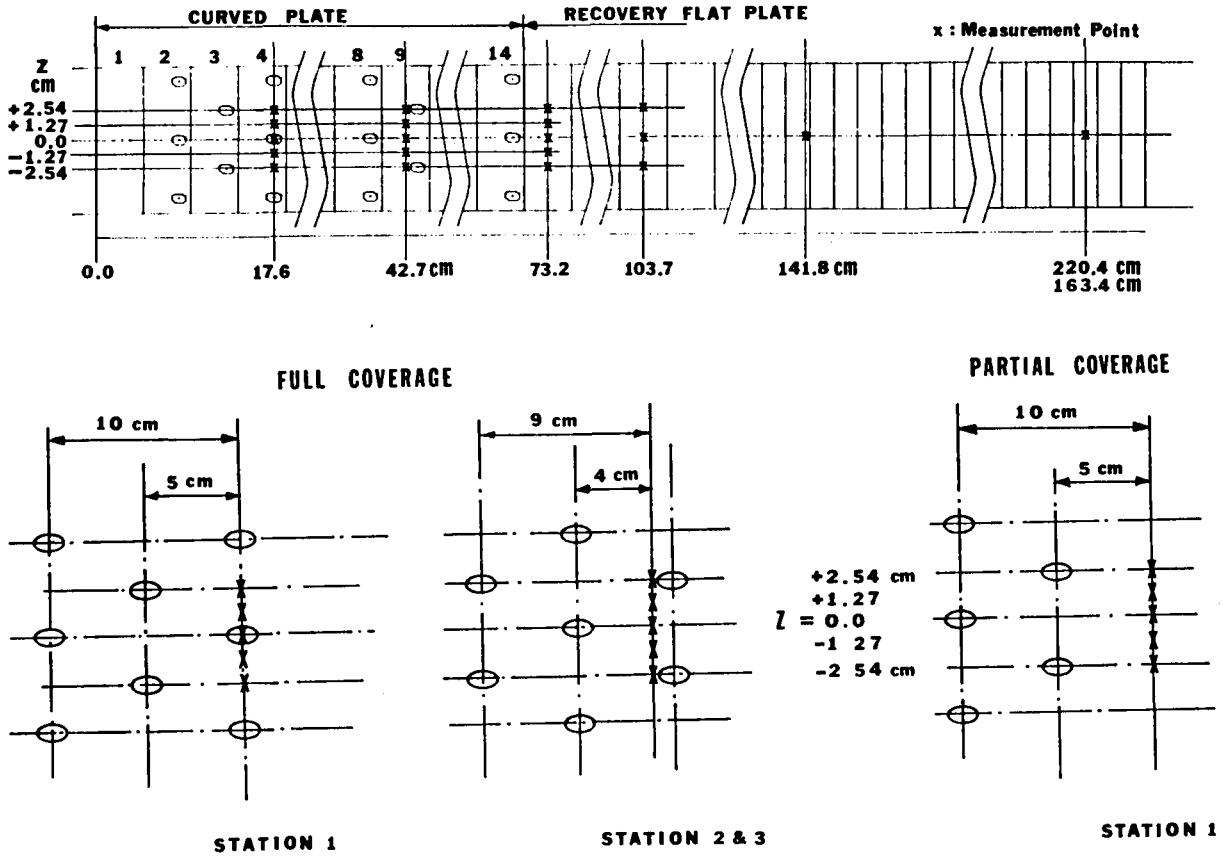

Fig. 3.2. Measurement locations of boundary-layer profiles

Chapter 4

QUALIFICATION TEST

Prior to the main experiments, extensive tests were conducted in order to qualify the experimental apparatus and instrumentation and to verify the experimental procedure. The qualification tests were carried out on both heat transfer and hydrodynamic aspects. The results of these tests are shown in the following section and provide the proof of the validity of the data of the main experiments. An uncertainty analysis is presented which allows an estimate of the accuracy of the data.

4.1 Main Stream Condition

Approaching the curve, the boundary layer was uniform within $\pm 5\%$ of momentum thickness in the spanwise direction. The free stream was uniform within 0.05°C, constant with time, and had a turbulence intensity of less than 0.5%. Within the curved region, secondary flow caused less than 2° convergence of the streamlines within the center 13 cm span of the boundary layer. This low value was achieved using side-wall fences and boundary layer bleed on the side.

4.2 Energy Balances

4.2.1 Run with No Heat Flux

As described in the previous chapter, the energy balance method was used at each copper strip to calculate wall heat flux. Heat losses considered to be significant compared to the wall heat flux were calculated by using calibration constants obtained through independent experiments. Special test conditions were set up, with large temperature differences intentionally exaggerating the losses, to get more accurate values of the constants. The constant describing heat loss to the support structure was measured with the wall heated and the structure cooled. The constant for heat exchange between the tube wall and the injected flow was evaluated with the wall hot but the injected air cold. In actual running, the structure was heated nearly to wall temperature and the delivery tube was insulated to minimize losses.

The accuracy of the measured heat transfer coefficient is largely dependent on the accuracy of these constants. As a final check, energy balance tests were performed as follows. The wall was insulated in the same way as for the calibration experiments. The wall, injection air and support structure were all heated. The heat flow from one copper strip is to the injection air, the support structure and the neighboring strips caused by the small temperature difference. The amount of this heat loss is supposed to be calculated by the calibration constants. The comparison is made between the calculated and the measured heat loss and the significance of the difference was tested in terms of the ratio of the difference over the wall heat flux in the main experiment. The result is surprisingly good with the maximum value 4.5%, which is less than the uncertainty of the measured Stanton number shown in the following section.

4.2.2 Enthalpy Thickness

Enthalpy thickness can be calculated by two independent methods; one by integrating the Stanton number and injection air in streamwise direction and the other by integrating the velocity and temperature profiles in the normal direction. It is good practice to compare the values of enthalpy thickness calculated by these two different methods to check the energy balance closure of the experimenal apparatus. In the present study, this energy balance test was conducted for the base-line case of $m = 0.4$. The comparison was made at two stations; one inside the curved blown region (9th plate in the curved plate) and the other in the flat recovery region (6th plate in the first recovery region). It is worth noting that the definition of the enthalpy thickness is slightly different from the conventional flat plate definition, as Honami [50] suggested. From the energy balance,

$$\int_0^{\Delta_2} U_p (T_w - T_\infty)\, dy = \int_0^{\infty} U(T-T_\infty)\, dy$$

Using the relation $U_p = \dfrac{U_{pw}}{1 + (1/R)y}$, where R is a wall radius,

$$\Delta_2 = R \exp\left[\frac{1}{R}\int_0^{\infty} \frac{U}{U_{pw}} \frac{T-T_\infty}{T_w-T_\infty}\, dy\right] - 1$$

It is also important to notice that in the curved region, the velocity and temperature profiles show strong three-dimensionality because of injection (see Chapter 5) and that a proper way of averaging is required. From the conserved property of energy, the value of $U(T-T_\infty)$ was averaged in spanwise direction then the averaged value was substituted into the enthalpy thickness equation shown above.

The result is shown in the following table and shows good energy closure of the system. The larger difference observed in the curved region is an expected result because the enthalpy flux calculated from velocity and temperature has a higher uncertainty in the region of fully three-dimensional flow.

Table 4.1

Enthalpy Thickness

Hot Run ($\theta \sim 1.0$) : Full-Coverage : m = 0.4

Station	Δ_2 by Streamwise Integration	Δ_2 by Normal Integration	Difference
2	0.717 cm	0.764 cm	6.2%
4	1.069 cm	1.118 cm	4.4%

4.3 Uncertainty Analysis of Stanton Number Measurements

For Stanton Number measurements, the measured values (temperature, heat flux meter reading and watt meter reading) were used in a data-reduction computer program with all corrections. Each measured value and calibration constant for corrections has its own uncertainty. The uncertainty of Stanton number, δSt_i, caused by each variable, x_i, can be calculated as $\delta St_i = \delta x_i(\partial St/\partial x_i)$. The total uncertainty of Stanton Number is then evaluated by collecting all individual uncertainties as $\delta St = \sqrt{\Sigma(\delta St_i)^2}$. In Table 4.2, the estimated uncertainty of each value is listed. The total uncertainty of Stanton Number in each region is tabulated in Table 4.3. As expected, the uncertainty is highest in the curved region for cold run, 8.1%. This is mainly because of uncertainty in the correction for the heat transfer between the test wall and the injected air. The constants used in calculating the heat flow from the wall to the injection air contributed significantly to the high uncertainty in St (see Appendix for a full presentation of the analysis).

Table 4.2

Variables	Uncertainties	Regions
T. C. Calibration Constant	50%	1,3.4
Ambient Temperature	1°F	All
Ambient Pressure	0.05 in Hg	All
Free Stream Temperature	0.005 MV	All
Dynamic Pressure Difference	0.002 In H_2O	All
Gauge Static Pressure	0.002 In H_2O	All
Wall Temperature	0.003 MV	All
Heat Flux Meter Reading	0.6%	1,4
Pressure Coefficient	0.001	All
Axial Heat Loss Constant	20%	All
Heat Flux Meter Constant	3%	1,4
Shape Factor	10%	All
Emissivity	10%	All
Watt Meter Reading	0.1 Watt	2,3
Constant for Heat Loss to Support Structure	20%	2,3
Support Temperature	0.5°F	2,3
Measured Injection Air Temperature	0.010 MV	2
Injection Air Flow Rate	4%	2
Constant for Calculating Heat Flow between Wall and Injection Air	20%	2
Constant (Power) for Heat Flow between Wall and Injection Air	10%	2
Constant for Calculating Injection Air Exit Temperature	10%	2
Resistance etc. of Power Line	5%	2,3

Table 4.3

Total Uncertainty of St

Region and Case	δSt/St
Developing Region	3.4%
Curved Region (Hot Run)	5.7%
Curved Region (Cold Run)	8.1%
1st Recovery Region	3.9%
2nd Recovery Region	3.7%

4.4 Qualification of Boundary-Layer Measurements

4.4.1 Triple-Wire Anemometry

The accuracy of triple-wire measurements of turbulence quantities was reported by Frota et al. [49]. Results of his uncertainty analysis are shown in Fig. 4.1, in which values of dU/U, dV/U, and dW/U are plotted as a function of pitch angle, ω (see Ref. 49 for definition of ω). For zero pitch angle, dU/U is 2.1%, dV/U is 1.9%, and dW/U is 4.0%. In the blowing region, near the injection hole, the velocity vector is considerably off the probe axis when the probe axis is tangent to the surface. The maximum deviation angle could be 30°, the injection angle at the exit of the hole. The uncertainty in measured V, dV/U becomes higher as the pitch angle increases, and for $\omega = 30°$, is about 7%.

Mean velocity and turbulence measurements in a two-dimensional channel flow and in a boundary layer are made with a triple-hot-wire probe fabricated by Frota et al. [49]. Figures 4.2 and 4.3 show the results. Figure 4.2 shows the three mean-velocity components in a flat-plate boundary layer, while Fig. 4.3 shows the shear-stress profile and turbulence-kinetic-energy profile in a fully developed two-dimensional channel flow. In both cases, the results agree with data obtained by other methods. These results verify the accuracy of the triple-wire probe.

Youssefmir et al. [48] used a "four-hole probe" and measured mean-velocity distributions for the full-coverage cooling case with $m = 0.4$.

Data from the triple-wire probe and the "four-hole probe" (at Station 1) are compared in Fig. 4.4. The "four-hole probe" can make measurements closer to the wall than the triple-wire can. The agreement of the two sets of data, one with the "four-hole probe" and the other with the triple wire, is very good in this quantity. In Fig. 4.5, the values of V/U (degree) were compared. The agreement is not very good near the wall (until $y = 1$ cm), where noticeable differences are observed. It is not certain whether this difference is attributable to uncertainty in the measurement systems or to the other causes.

Mean velocity data measured by Youssefmir and Johnston [48] showed the following hydrodynamic behavior. The profile in the near-wall region was distorted by the injected jet as far as 5 cm downstream of the hole ($y \leq 0.4$ cm). The profiles at $z = 0.0$ and $z = 2.54$ cm show this effect clearly, while the profile at $z = 1.27$ cm, which is in the lane with no holes, shows hardly any effect of the jet. The u-component of the jet velocity is uniform in the y direction, out to about $7 = 0.3$ cm, with $U = 7$ m/s right at the hole. As far as 5 cm downstream of the hole ($z = 2.54$ cm profile), the boundary-layer profile still shows a uniform velocity in the inner region, but at 5 m/s, not 7 m/s.

4.2.2 Data-Acquisition System

As described in Chapter II, the data for boundar-layer profiles, hydrodynamics, and temperature were read by a mini-computer and stored on discs. Sample number and frequency are important for obtaining reliable averages, and were conducted to determine the combinations which would be used. For hydrodynamic measurements, three samples were taken at a sampling rate of 100 Hz for each of ten components ($\overline{U}_i$, $\overline{U'_i U'_j}$, and Q^2). The scanning was repeated 100 times and then averaged. Triple-wire outputs were filtered through a low-pass filter before they were read by the computer; this procedure helped to stabilize the output signal.

For temperature measurements, a thermocouple signal was sent to a computer. Since the signal was very low, on the order of 1 mV, the signal was amplified by a factor of 1000, which eliminates the noise

from the output signal. For averaging the temperature signal, 100 samples were taken at 20 Hz.

4.3 No-Injection Run

As part of the qualification tests, a heat transfer experiment was run with a smooth wall (all injection holes closed) to compare with Simon's data [43]. Since the new recovery plate was inserted for the present study, this run was to make sure that the modification of the tunnel did not change the experimental conditions. The result of the comparison is shown in Fig. 4.6. The agreement is excellent in the developing region and in the curved region. In the recovery region, the last two points of Simon's data are low compared to the present data. The difference for these two data points is approximately equal to the maximum expected difference, due solely to random uncertainty (7% at 20:1) and may or may not be significant.

There is one thing worth noting. In the case of the smooth wall run in the present study, a sharp increase of Stanton number was observed between the curved and the recovery region as seen in Simon's case [43]. The first recovery plate for the present study was newly inserted after Simon's experiment, and the method of acquiring wall heat flux was different in each case. This fact indicates that this rapid increase is a real phenomenon.

The next test was carried out with all injection holes open but with no injection flow. The results are also shown in Fig. 4.6. The difference is most noticeable in the first part of the curved region. Values of Stanton number with open holes lie about 7% above those of the smooth wall. This high values of Stanton Number seem to be caused by the roughness effect of the open injection holes, which increase the turbulence mixing and heat transfer. Farther downstream, as the boundary layer thickens, the effect of the open holes decreases. Finally, in the last part of the curved region and in the recovery region, there is essentially no difference.

For the partial blowing cases discussed later, other rows of injection holes were left open; therefore the effect of open holes was present in the curved unblown region. However, the effect was minor compared with the effect of injection air.

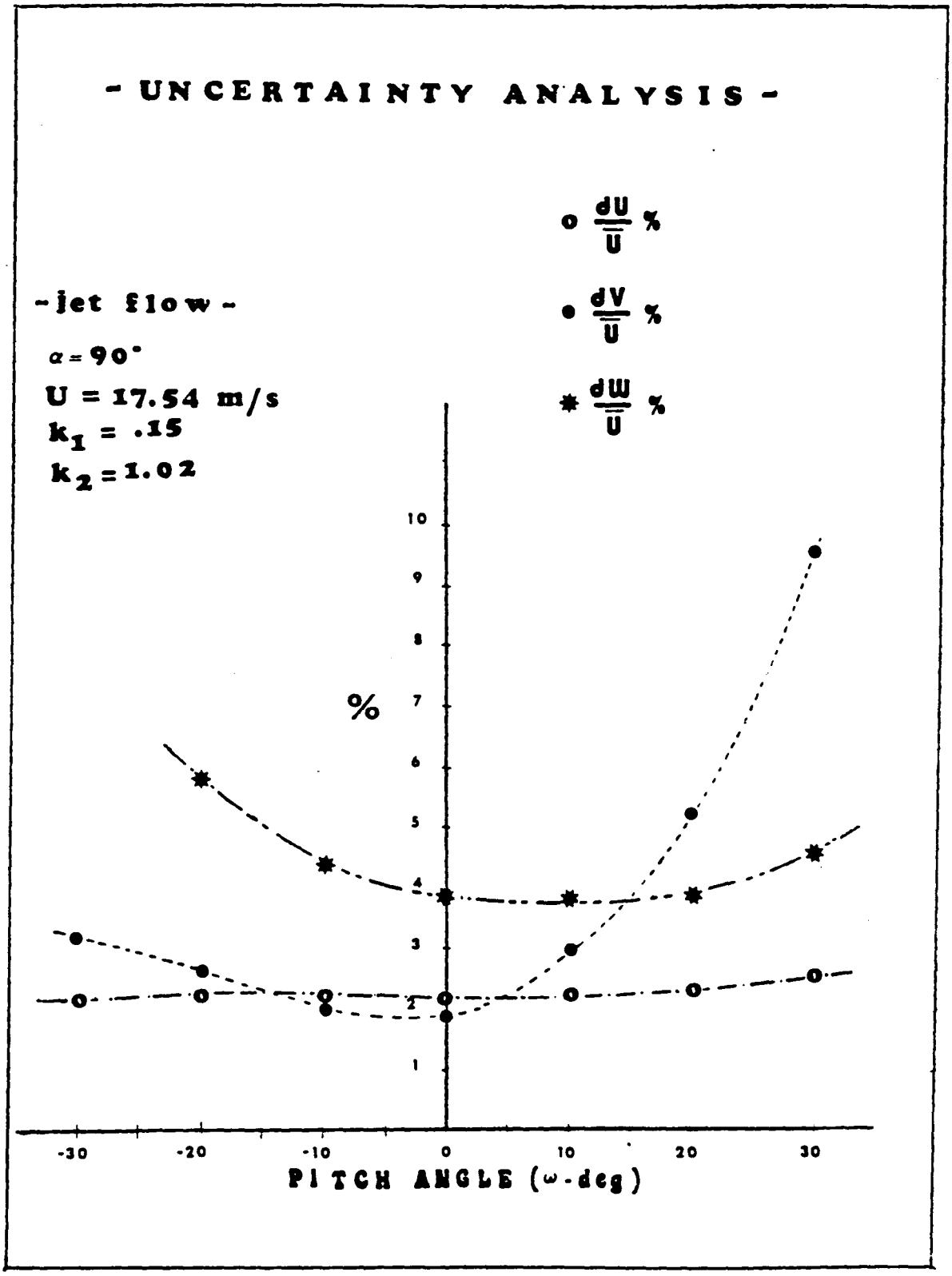

Fig. 4.1. Uncertainty of triple hot-wire signals [49]

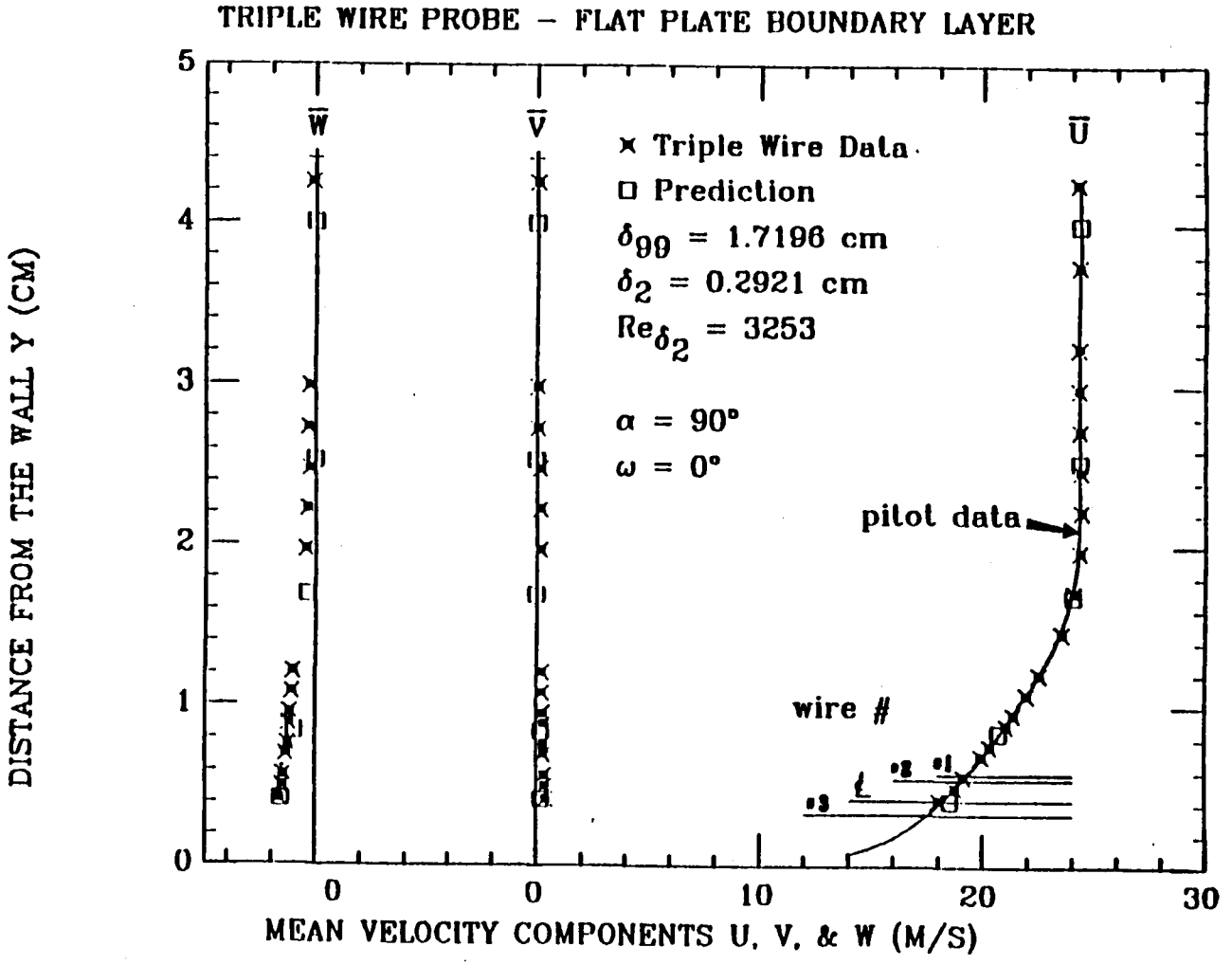

Fig. 4.2. Mean-velocity profiles of flat-plate boundary layer measured with a triple hot-wire probe [49]

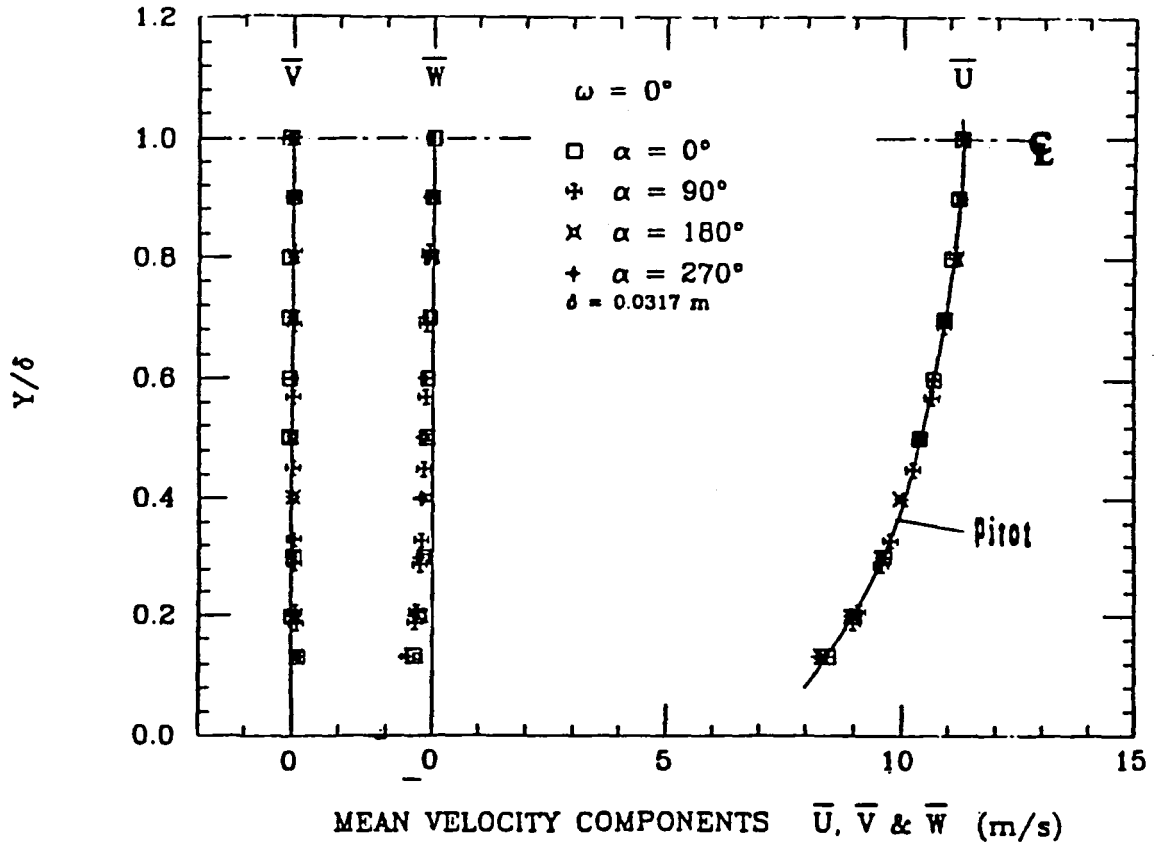

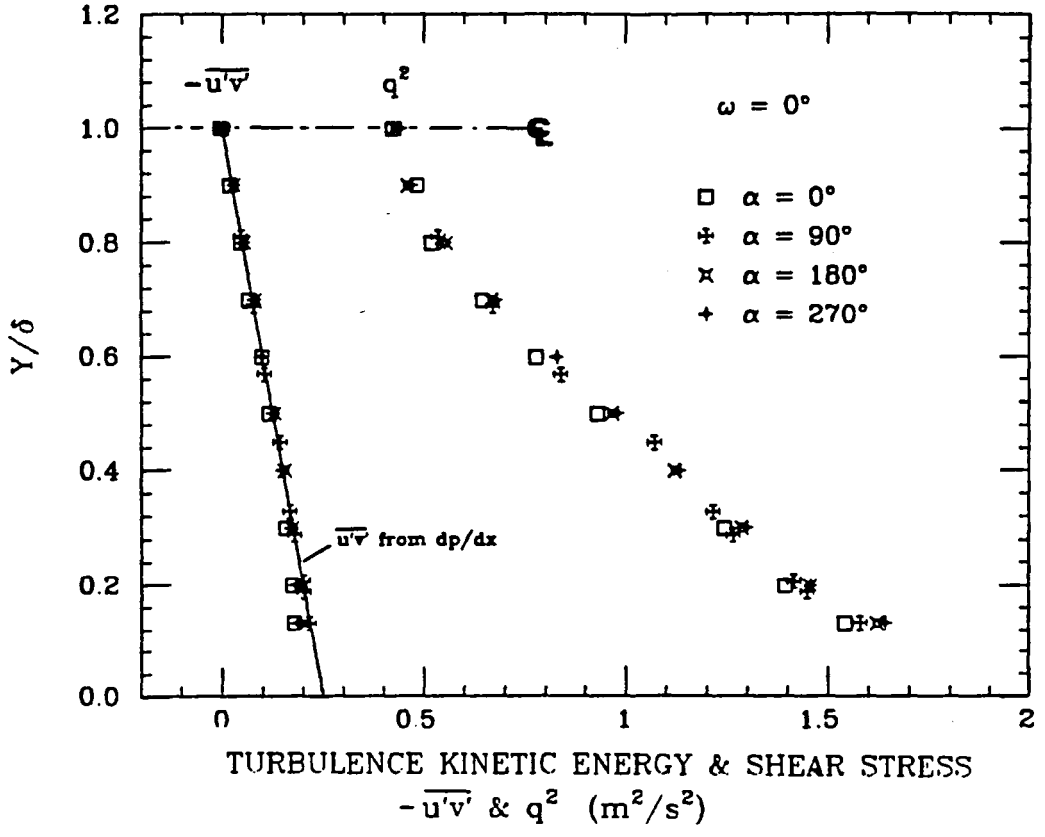

Fig. 4.3. Mean velocity, turbulence kinetic energy, and shear stress profiles of 2-D channel flow measured with a triple hot-wire probe

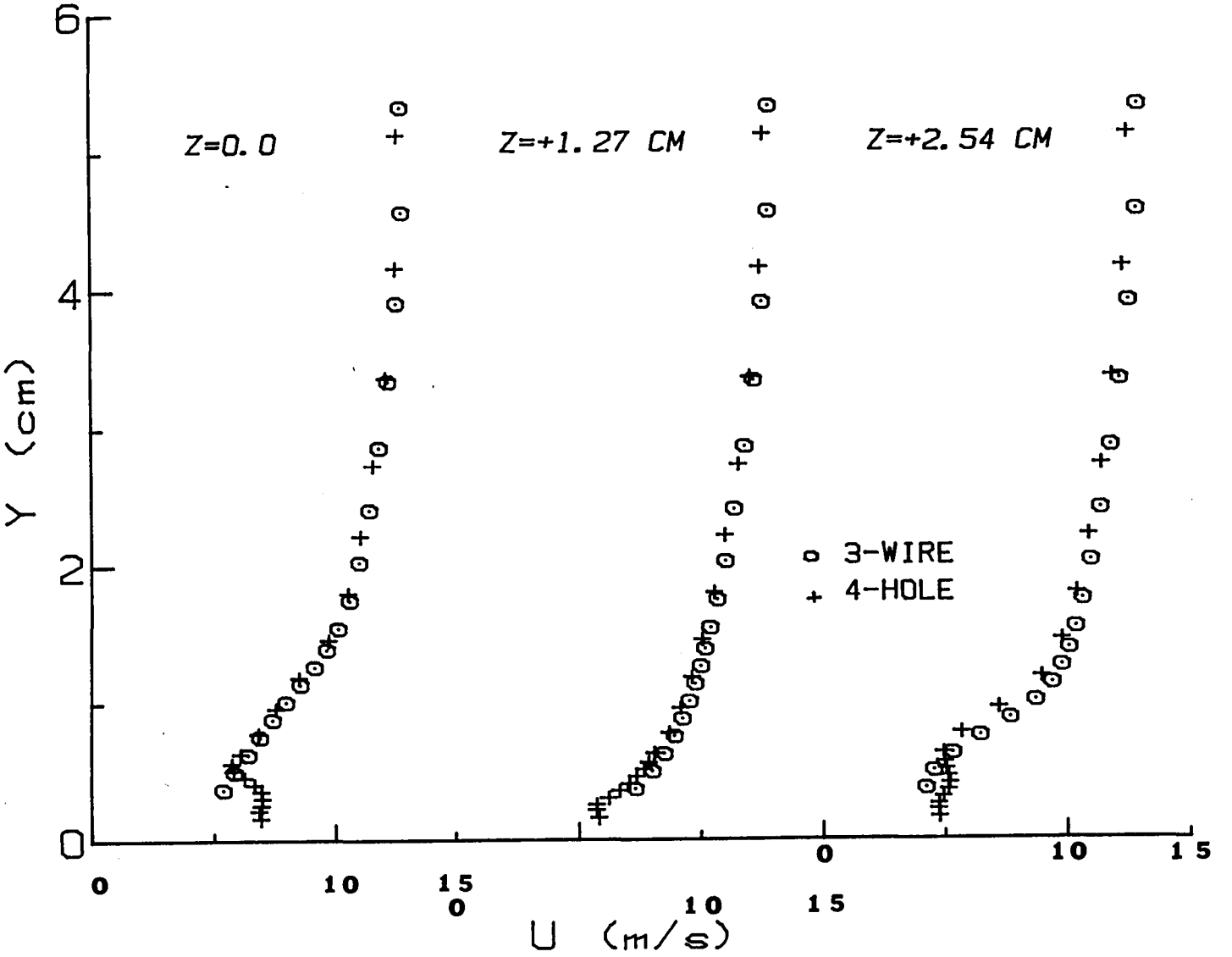

Fig. 4.4. Mean velocity (U) profiles in the curved blown region with m = 0.4: comparison of two data sets with a triple hot-wire probe and a "four-hole" probe [48]

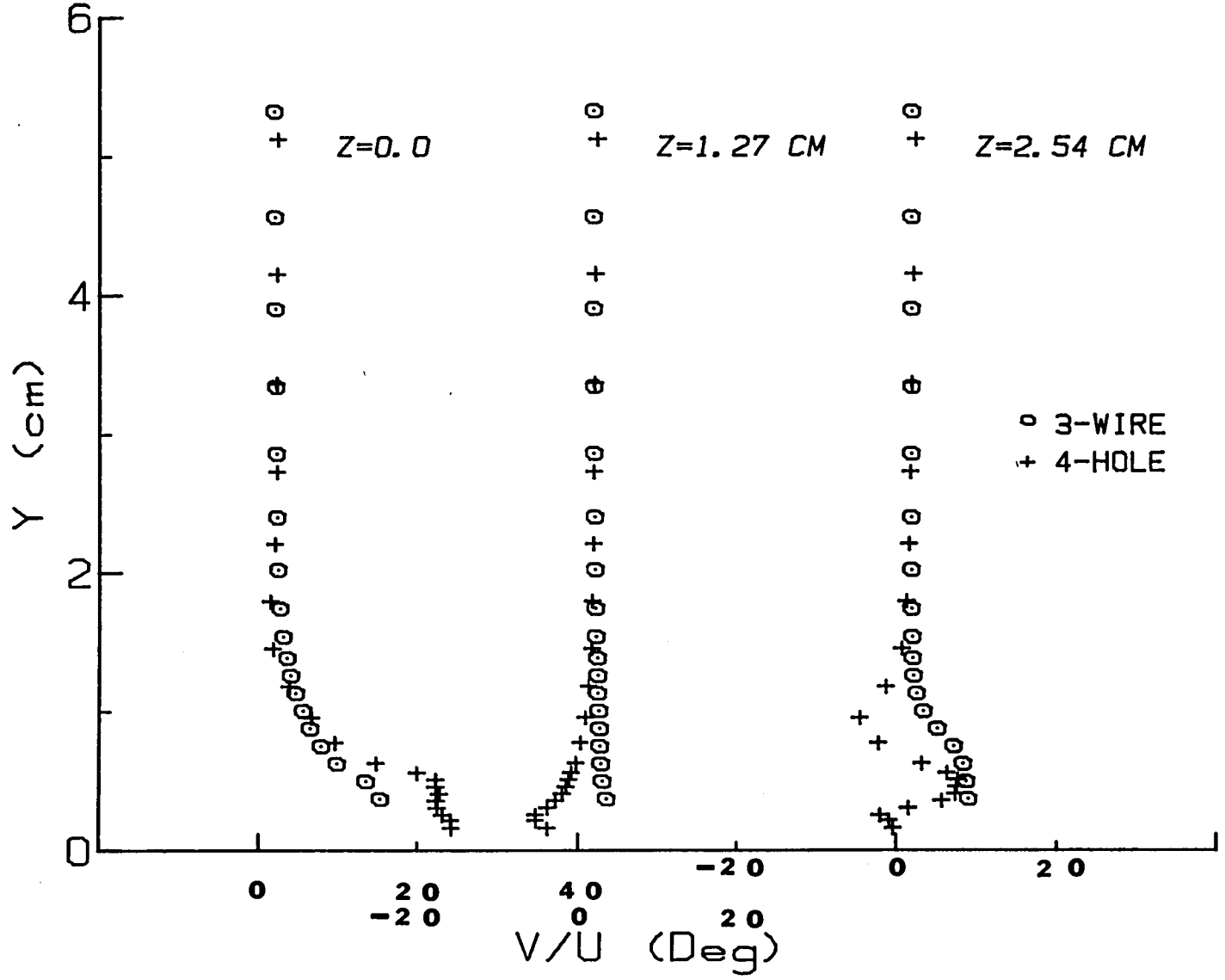

Fig. 4.5. Flow angle (V/U) profiles in the curved blown region with m = 0.4: comparison of two data sets with a triple hot-wire probe and a "four-hole" probe [48]

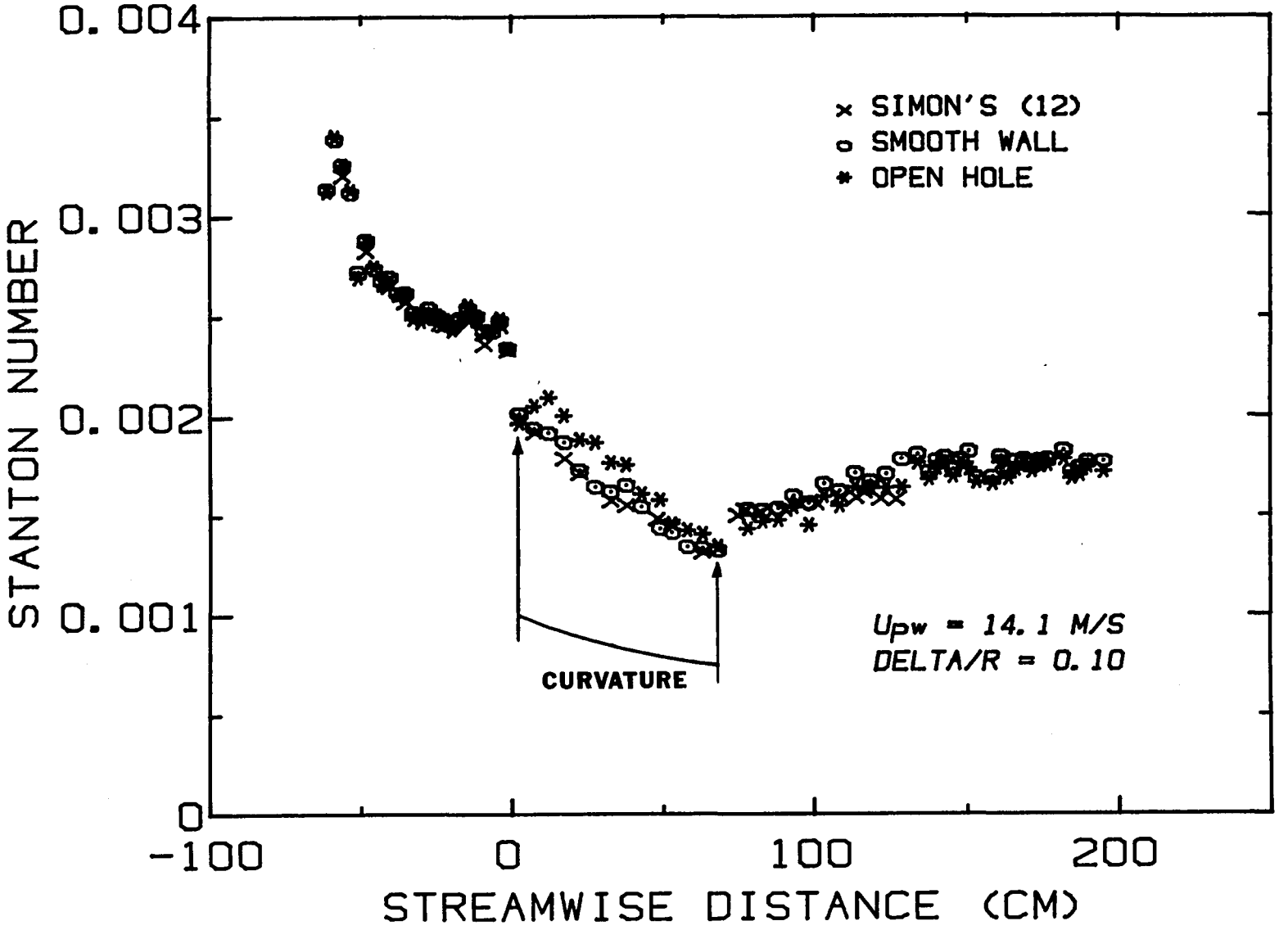

Fig. 4.6. Stanton numbr with no injection: smooth-wall data (St_o) and open-hole data ($St_{m=o}$)

Chapter 5

EXPERIMENTAL RESULTS AND DISCUSSION

Three major experiments were conducted in the present study: heat transfer coefficient measurements, hydrodynamic profile measurements and temperature profile measurements. For heat transfer coefficient measurements, results are presented and discussed in terms of two basic Stanton Number values, St(0) and St(1) (see Section 3.2.3 for the definition of St(0) and St(1)). For hydrodynamic profile measurements, both mean and turbulence quantities are presented. Hydrodynamic and temperature profiles were taken for some, but not all, of representative cases of the heat transfer experiments.

5.1 Stanton Number Data

The first series of the experiments in the present study measured the spanwise averaged heat transfer coefficient (Stanton Number) along the plate. The baseline case was injection of air with full-coverage blowing (13 rows of blowing) and a blowing ratio, m, of 0.4. For this case, a larger amount of data was taken than for any other case. This set of data was intended to give a very detailed description of the film-cooled flow and to provide the basis for computer modeling of the heat trnasfer and hydrodynamics. The value, $m = 0.4$, was chosen because it is close to the optimum value, based on the results of flat plate experiments [12].

Four smaller scale experiments were then conducted, each changing one of the parameters. Using the data of full-coverage with $m = 0.4$ as a baseline case, comparison was made with other cases to determine the effects of these parameters. In the first of the four experiments, the number of rows of blowing was reduced: two, four, and six rows were studied. The effect of blowing ratio, m, was tested in the second and third experiments: $m = 0.2$ and $m = 0.6$. The blowing rate experiments were conducted both for full-coverage and partial coverage cases. The fourth experiment tested the cases with rows of blowing starting at different locations of the curved plate.

The results of each test will be discussed from two different aspects: presentation of the data and interpretation of the data. In the section presenting the data, the trends of the data are described. In the section on interpreting the data, the reasons and the mechanisms of the phenomena (why and how it occurs) are discussed.

5.1.1 Full-Coverage Film Cooling

5.1.1.1 Data for m = 0.4

The results of the baseline case (full-coverage with $m = 0.4$) are shown in Fig. 5.1. Values of Stanton Number with $\theta = 0.0$, (i.e., St(0)) and with $\theta = 1.0$ (i.e., St(1)) are shown together with St_o, the no-injection values taken on a smooth wall. In the developing region and for the first data point in the curved region, where there are no injection holes, the data for St(0), St(1), and St_o collapse onto one another, showing that there is no effect of injection upstream of the blown region.

Data for $\theta = 1.0$

For $\theta = 1.0$, Stanton Number falls rapidly immediately after the blowing begins and the values of St(1) in the blown region are much lower than the St_o values. At the end of curved region, the value of St(1) is less than half of the no-injection value. This reduction clearly demonstrates the cooling effect of the injection. After the blown region, values of St(1) show an rapid increase similar to that seen with curvature but no injection. In the recovery region, St(1) values gradually approach the no-injection values. However, even at the end of the recovery plate, 1.2 m downstream of the end of the blown region, the value of St(1) is still 20% lower than that of St_o.

Data for $\theta = 0.0$

On the other hand, for $\theta = 0.0$, Stanton Number increases when blowing starts, has its maximum value somewhere between the third and fifth rows of holes, and then begins to decrease. Inside the blown region, the value of St(0) is always higher than St_o. The same phenomenon was seen in the flat plate blowing case [12].

It is worth noting that St(0) continues to decrease into the first part of the recovery region: there is no rapid increase at the end of curvature as was noted for St(1) and St_o. The minimum in St(0) occurs about 20 cm downstream in the recovery region. Injection of fluid at the same temperature as the free stream temperature clearly alters the response of the boundary layer to the release of wall curvature. Values of St(0) return toward St_o values after the minimum value and the recovery looks quicker than that of St(1). In the last part of the recovery region, the last 40 cm of the 1.2 m recovery region, the St(0) data lie above St_o. This is believed to be a real occurrence, not just uncertainty in the data.

5.1.1.2 Data for m = 0.2 and 0.6

Two additional full-coverage blowing cases were tested: m = 0.2 and m = 0.6. Those two values are considered to be significant and representative cases of higher and lower blowing than the baseline case of m = 0.4. Figure 5.2 and 5.3 show the full-coverage data for m = 0.2 and 0.6, respectively. The general trends of the data for both St(1) and St(0) are similar to that seen in the case of m = 0.4, but the boundary layer structure changes significantly for m = 0.6.

The data for St(0) rise downstream of the first row of holes, reaching a maximum between the 5th and 7th row. Beyond the 7th row, St(0) decreases, and continues to decrease well into the recovery region. As was seen in the case of m = 0.4, the St(0) data for both m = 0.2 and 0.6 continue to decrease after the end of the curved region, reaching a minimum within the recovery region. The response of the boundary layer to the release of curvature, reflected by this behavior of the St(0) data, seems to be characteristic of full-coverage cooling on a convex wall. The St(0) values in the recovery region merge to the no-injection values in a shorter distance for m = 0.2 than for m = 0.4. The St(0) data appear to rise above the no-injection values in the last part of the recovery region. This is believed to be real, not an artifact or scatter. This phenomenon was also seen for the case of m = 0.4. It will be discussed in detail in the following sections.

The data for St(1) lie far below the no injection data, due to the cooling effect of the injection air. The St(1) data with m = 0.6 recovers only slowly and does not reach the no-injection data within the recovery region, but the St(1) data with m = 0.2 appears to complete the recovery approximately at 1.0 m downstream of the end of the blown region. The St(1) data for the three blowing ratios will be compared in detail in a later section.

5.1.1.3 Interpretation of the Data

Effect of m

It is important to have accurate knowledge of the effect of the injection parameter, m , in order to identify the optimum value for a given cooling application. Three full-coverage cases with different blowing ratios, m = 0.2, 0.4, and 0.6 were studied in this program. Here, the results are compared from the point of view of the cooling effect.

Under isothermal wall conditions, the heat load on the wall is proportional to the area under the St vs. X-curve. The relationship between current engine design practice leads to the cooling air being nearly at wall temperature when injected, thus examining only the values of St(1), will show at least the main trends of the cooling effect of discrete hole injection under engine conditions.

Figure 5.4 shows St(1) data for the three values of m, each with 13 rows of blowing (full-coverage). The data for m = 0.4 show lower St(1) values, i.e., higher cooling effect than the data for m = 0.2 both in the curved blown region and in the recovery region.

Below m = 0.4, increasing the amount of injected flow provides more protection at the wall. However, comparison of the data for m = 0.4 and m = 0.6 gives different results. In the blown region, the St(1) values for m = 0.6 are higher than those for m = 0.4 despite the additional air injected.

In the recovery region, the St(1) data for m = 0.6 recover very slowly toward the no-injection values. As shown in Fig. 5.4, the St(1) data for m = 0.6 are above the data for m = 0.4 within the curved

region, but meet the $m = 0.4$ data about one-third of the way down the recovery region. Through the rest of the recovery region, the data for $m = 0.6$ are lower than for $m = 0.4$.

Effect of Curvature and Injection on Heat Transfer

Heat transfer on a convex wall with discrete hole injection at $\theta = 1$ is affected by three mechanisms: (1) the convex curvature effect, which decreases the heat transfer coefficient, (2) injected air at the same temperature as the wall temperature, which reduces the heat exchange between the wall and free stream, and (3) the hydrodynamic disturbance caused by injecting the air into the boundary layer which causes higher turbulence mixing and tends to raise the heat transfer rate. The recovery region is a flat plate with no injection in which the boundary layer recovers towards a normal flat plate condition. The effects of the curved, blown region are still important in setting the heat transfer behavior for some distance downstream, but do so only through their effect on the condition of the boundary layer at the beginning of the recovery region. The boundary layer thickness and the distributions of velocity, temperature and turbulence kinetic energy at the beginning of the recovery region are all strongly dependent on the curvature and the blowing condition upstream. These determine the behavior in the recovery region, and the heat transfer results shown in Fig. 5.1, 5.2, 5.3 and 5.4, can be explained in those terms.

Curved, Blown Region

Stanton number with injection at $\theta = 1.0$ in the curved region is lower than that on a convex wall with no injection, for all values of m studied in this work. This indicates that the protective effect of the injection gas overcomes the effect of increased turbulence mixing over the entire range. The values of $St(1)$ for $m = 0.6$ are higher than for $m = 0.4$, however, which shows that the turbulence mixing caused by injection at $m = 0.6$ was more important than the additional cooling, resulting in an enhanced heat transfer. This view is supported by a comparison of the turbulence data, presented later, in Section 5.3.1, which shows higher q^2 values for 0.6 than 0.4.

At the end of the curved, blown region, a rapid increase of St(1) is seen because two effects tending to reduce the heat transfer rate, injection at wall temperature and convex curvature, are simultaneously stopped. A similar rapid increase was seen when injection at $\theta = 1$ was terminated on a flat plate [12]. A similar rapid increase in St_o has been seen at the end of a curved surface, with no injection, by Simon [43]. Thus, when both curvature and injection simultaneously end, a pronounced rise should be expected.

The situation is different when blowing is terminated inside the curved wall. No rise is seen. This will be discussed later, in Section 5.1.2.

For injection with $\theta = 0.0$, there is no protecting effect of the injection air because the injected air is at free stream temperature. Both the augmented turbulence and the altered mean temperature tend to increase Stanton number. The higher value of Stanton number seen in the first part of blown region is caused by a higher turbulence mixing. The reduction of Stanton number after that region is probably because of convex curvature effects but the increased turbulence mixing always keeps St(0) higher than St_o, the no-injection value on a convex wall. Convex curvature changes the turbulence structure, reducing the thickness of the active shear layer and the scale of turbulence mixing. This was experimentally found by Gillis et al. [38] and contributes to the lower Stanton number along a convex surface, as found by Simon et al. [43].

Recovery Region

The recovery plate is a flat wall with no injection. Thus, the recovery process is a twofold one: from both the curvature effect and the effect of injection, at the same time. The boundary layer in the recovery region can be viewed as divided into two layers: an inner layer which is developed on the recovery plate, and an outer part which reflects the nature of the upstream curved, blown region.

A special test was conducted to investigate the inner region behavior in the recovery region for the case of recovery after a curved flow with no injection. Heating was started just at the beginning of the

recovery region. The momentum thickness was measured, to provide an initial condition of the hydrodynamic boundary layer in the recovery region and a virtual origin calculated from the momentum thickness, assuming that the upstream plate had been flat. The distribution of Stanton number in the recovery region was then calculated using the flat plate, unheated starting length equation and compared with the experimental data [43]. Good agreement was obtained. This result indicates that the inner part of the boundary in the recovery region following convex curvature behaves as though it were a normal flat plate boundary layer.

The present study combines curvature and injection, and even here it seems that the inner part of the boundary layer, in the recovery region, behaves like a normal flat plate boundary layer and that the only outer part contains the upstream effect (curvature and injection). As seen in the data, the heat transfer characteristic in the recovery flat plate differs significantly from that of a normal flat plate boundary layer, but this difference is attributed mainly to the initial conditions.

All three full-coverage cases $m = 0.2$, 0.4, and 0.6 show qualitatively the same behavior in the recovery region. Fig. 5.5 schematically illustrates the behavior of $St(1)$ and $St(0)$ in the recovery region. Three regions of behavior are shown. The behavior of Stanton number in each region can be explained by reference to the temperature profiles and the turbulence kinetic energy distributions in the boundary layer in these different regions.

Recovery for $\theta = 1.0$

Stanton number with $\theta = 1.0$ demonstrates a monotonic recovery towards St_o, the no-injection values. For $St(1)$, the secondary air is injected at the wall temperature, which keeps the boundary layer fluid temperature near wall temperature, even far from the wall as shown in the temperature profile at Stations 3 and 4 (see Fig. 5.54). This effect is significant throughout the boundary layer, extending even to the outer part $(y/\delta \sim 0.8)$. The temperature profile must approach the no-injection profile far downstream in the recovery region but the recovery is very slow for two reasons: (1) the whole boundary layer is

involved, and (2) the recovery process must begin at the outer edge of the layer, and must penetrate all the way to the wall by turbulent diffusion. The St(1) data for all three blowing ratios clearly show that the larger the blowing ratio, the slower the recovery. The larger amounts of injection air cause the temperature profile in the first part of recovery region to differ more significantly and the boundary layer to be thicker. Together, these result in the slower recovery.

Recovery for $\theta = 0.0$

The recovery process of St(0) is not as simple as of St(1). The curve of St(0), starts with a decrease and has both a minimum and a maximum within the recovery region. Three regions can be identified, in each of which a different effect governs the heat transfer behavior. The first region is from the beginning of recovery to the location of the minimum value. The second region extends to the location of the maximum value. The third region extends till final recovery to St_o.

First of all, it is worth noting that the value of St(0) shows a smooth transition from the curved blown plate to the recovery plate: there is no rapid rise as was seen for $\theta = 1$. This appears understandable. A sharp increase in St_o was observed at the end of convex curvature by Simon [43], and a steep decrease in St was reported at the end of blowing with $\theta = 0.0$ on a flat plate [12]. Thus convex curvature and discrete hole injection have opposite effects on the turbulence. When both effects are applied at the same location, they appear to cancel one another.

Moving now into the first portion of the recovery region: in Region I St(0) decreases. This trend can be explained in terms of the temperature profiles and the turbulence kinetic energy levels, since both are changing in such a way as to reduce the Stanton number.

The temperature profile entering the recovery region is significantly distorted for $\theta = 0.0$ and has a sharp gradient at the wall as shown in Fig. 5.52, Section 5.4.1. This distortion will be reformed in a relatively short distance and as the profile approaches a normal (monotonic) shape, the gradient at the wall becomes less sharp and the heat transfer rate is reduced. Larger distortion of the temperature profile

is seen for higher blowing ratio. This indicates that a longer distance will be necessary for the profile to come back to a normal shape, which is consistent with the results that St(0) for $m = 0.6$ has the longest distance of the Region I.

The difference between the temperature profiles for St(1) and St(0) in the blown region must be mentioned here. Both profiles are affected by injection, but in one case ($\theta = 1.0$) the air is injected at wall temperature, and in the other ($\theta = 0.0$), it is injected at free stream temperature. Injection at wall temperature results in a large region of fluid near the wall nearly at wall temperature. Thus, for $\theta = 1.0$, as the profile relaxes towards the no-injection profile the slope at the wall becomes steeper, and this increases the heat transfer rate. This is an opposite result to the cold run case ($\theta \sim 0.0$). A sketch of these profiles for both cold and hot runs are shown in Fig. 5.6.

The second mechanism is related to the turbulence kinetic energy, TKE, under the assumption that turbulent transport is related to TKE . The level of TKE decreases after termination of injection as shown in the experimental data of Fig. 5.28, 5.29, and 5.30. These show noticeable reduction of Q^2 between Station 3 and 4 for $m = 0.6$ but does not show a significant change for $m = 0.4$ and 0.2, probably because of the trade-off with the increase caused by the release of curvature. This result also agrees with the fact that the minimum value of Stanton number occurs further downstream for $m = 0.6$ (i.e., Region I is large).

In Region II, once the normal (monotonic) profile is established, the recovery for St(0) is similar to the case of St(1) with one significant difference. St(0) is recovering faster than St(1) (since the inner region defect is less). As a consequence, the local TKE where St(0) is nearly recovered, is high, and the St(0) shows a higher level of Stanton number than would St_o. This behavior is illustrated by the maximum value between Regions II and III and can be explained by the fact that the turbulence kinetic energy in this location is still higher than for no-injection case. Region III is characterized by the recovery from the higher level of TKE to the normal no-injection level.

The over-shoot discussed above does not happen for St(1) because the recovery of the temperature profile in the case of $\theta = 1.0$ takes so long that the level of TKE has come back to the level of no-injection case by the location where the recovery of temperature profile is completed.

Local Responses

It is common to plot heat transfer data on St-x coordinates, but such a treatment is ambiguous when the boundary conditions change in the x-direction. For example, it is well known that thick boundary layers result in low heat transfer coefficients: as a normal turbulent boundary layer develops downstream, "h" gets steadily lower. Thus, evidence of low "h" is not sufficient to demonstrate any "unusual behavior". What must be shown is low "h", considering the local state of the boundary layer. For this reason, it is frequently desirable to plot Stanton number against the enthalpy thickness Reynolds number--a measure of the thermal boundary layer thickness. This incorporates the history effect into the enthalpy thickness Reynolds number and reveals the local response of the boundary layer to its present condition. In Fig. 5.7, values of St(1) for $m = 0.2$, 0.4 and 0.6 , are replotted on St-Re_{Δ_2} coordinates. For both $m = 0.2$ and $m = 0.4$, in the curved region, the St(1) data lie on the same line as for no-injection, a line of (-1) slope. The appearance of the (-1) slope in St-Re_{Δ_2} coordinates is one of the most noticeable characteristics of the convexly curved boundary layer heat transfer [43]. From fact that both $m = 0.2$ and $m = 0.4$ show the same slope (-1), it can be concluded that the local response of the boundary layer is same as in the case of convexly curved boundary layer and is still dominated by curvature effect. The stabilizing effect of convex curvature seems to enhance the cooling effect and as long as the local response is controlled by the curvature effect, the cooling capability depends directly on the amount of injected air.

For $m = 0.6$, however, the St(1) data behave differently. Throughout the curved region, the data for $m = 0.6$ lie above the line of (-1) slope. Near the downstream end, the data appear to be falling rapidly toward the -1 slope, but the present data are not sufficient to establish that this is significant. This behavior indicates, however,

that the local response of the boundary layer alters, at some critical "m" value between $m = 0.4$ and $m = 0.6$, and that above that value of m, the cooling effect decreases even if the blowing ratio increases. Similar behavior was seen in earlier studies of flat plate heat transfer.

In the recovery region, all values of blowing ratios ($m = 0.2$, 0.4 and 0.6) show similar responses on $St\text{-}Re_{\Delta_2}$ coordinates. They lie on parallel lines with the same slope. This suggests that there is no large differences in the local response of the boundary layer among three blowing ratios, and that the main differences are due to the different initial conditions. This result confirms that heat transfer in the recovery region is mainly affected by its upstream history, principally the amount of injected air.

5.1.2 Partial-Coverage Film Cooling: 2, 4 and 6 Rows

5.1.2.1 Data for $m = 0.4$

Partial-coverage blowing was tested, using the first two, four, and six rows of injection holes. Figsures 5.8, 5.9, and 5.10 show three partial blowing cases (two, four, and six rows) with $m = 0.4$.

Data for $\theta = 0.0$

Within the blown region, the St(0) data for six rows of blowing follow the full-coverage data very closely, reaching a sharp peak at the third row of holes. The St(0) data for four rows follow the full-coverage data for the first two rows, but the third data point is not as high, being no higher than the second. The St(0) data for two rows do not rise as rapidly, and show the maximum Stanton number at the third, not the second, row. The fact that the behavior in the first few blown rows depends on how many more rows downstream are blown suggests that the problem is not entirely parabolic. The downstream condition, how many rows of injection holes downstream, is affecting the upstream behavior. The most likely cause of this phenomenon is the pressure field established by the interaction of the injection jets with the boundary layer. If there were no pressure effects, the boundary layer behavior would be purely parabolic, hence there could be no upstream propagation of downstream events. The wall static pressure was measured

and found to show an "island" of higher static pressure within the jet field. These data are discussed in a later portion of this chapter.

For two rows of blowing, St(0) returns to the no-injection data by 15 cm downstream of the end of injection. For four rows, recovery takes about 20 cm and for six rows about 30-35 cm.

Data for $\theta = 1.0$

Values of St(1) for partial blowing follow the line of full-coverage St(1) until the end of blown region. When blowing terminates, St(1) does not return immediately to the unblown line, however, as might be expected. After the blowing terminates, St(1) values depart from the full-coverage line, but they continue to decrease only slowly. The slope of this gentle decrease is approximately the same in every partial blowing case.

For two rows of blowing, the transition from the blown region to unblown curved region is somewhat different from other cases (four and six rows). The first measuring point downstream of the blown region is still on the line of the full-coverage case ($m = 0.4$). One point to keep in mind in examining these data is that the injection holes are near the downstream edge of each copper strip yet have a strong effect on the average heat transfer to that strip. For the next two measuring points, an increase of Stanton number is observed, which is believed to be a real phenomenon, rather than experimental uncertainty. This behavior is not found for either four rows or six rows of blowing at $m = 0.4$. After the re-rise, the data for two rows of blowing gradually decrease, as do those for four and six rows. At $m = 0.4$, this "re-rise" is only seen for two rows of injection, but for other injection rates a "re-rise" is seen for some conditions. It seems that the convex curvature effect prevents the heat transfer coefficient from starting to increase after the end of blowing. St(1), unlike St(0), does not recover to the no-injection values inside the curved region. From the behavior of St(1), it is clear that more rows of injection gives lower values of St(1) (i.e., higher cooling effect) both in the curved and the recovery region. However, the "best" number of rows for a given engine will depend on the engine design because more rows of blowing

requires more injection air and more manufacturing work, and does not necessarily provide an over-all increase in performance.

5.1.2.2 Data for $m = 0.2$ and 0.6

Partial coverage tests were also conducted for two other blowing ratios, $m = 0.2$ and 0.6. Figures 5.11 through 5.15 shows the data of these conditions: for $m = 0.2$, both two and six rows of blowing were tested (Figs. 5.11 and 5.12) and for $m = 0.6$, two, four, and six rows of blowing were tested (Fig. 5.13, 5.14, and 5.15). In this section, the behavior of St(0) and St(1) for each blowing ratio is described, pointing out the characteristics of the data which are believed to be important for checking prediction models. Comparison will also be made among the runs with different number of rows with m fixed and among three blowing ratios with the same number of rows.

Curved Region for $m = 0.2$

For $m = 0.2$, the St(0) data for six rows of blowing follows the full-coverage line until fourth blown row but the last two data points (5th and 6th) are lower. For two rows of blowing, the rise of St(0) is not as high as was seen for the full-coverage cases. These seem to be caused by the effect of a pressure "island" associated with the injected jets. The St(0) data, as expected, recovers to the $St_{m=0}$ data (Stanton Number with no-injection (but with the injection holes open) inside the curved region. The St(0) data in the curved region for two rows of blowing is exactly the same as for two rows of blowing with $m = 0.4$. For six rows of blowing, the sets of St(0) data with $m = 0.2$ and with $m = 0.4$ are still very close.

The behavior of St(1) is more interesting. The data for two rows of blowing with $m = 0.2$ show an increase of St(1) after the end of injection. This rise begins right after the end of injection; i.e., there are no data points which remain on the full-coverage line after the blown region. The re-rise after the end of injection is more noticeable than that seen for $m = 0.4$. The St(1) data recover to the $St_{m=0}$ values after this rise and follow the line of $St_{m=0}$ thereafter. For six rows of blowing with $m = 0.2$, a similar rise is observed right after the blown region. However, the rise is not as

significant as for two rows, and the St(1) data do not reach the $St_{m=0}$ line.

Recovery Region for m = 0.2

In the recovery region (m = 0.2), the St(0) data do not differ from $St_{m=0}$, either for two rows or six rows of blowing. Neither shows an over-shoot between Regions I and III near the end of the recovery region. This means that the effect of injection has been wiped out for St(0) in the curved region, both as to the thermal effect of injecting at free stream temperature and the augmentation of turbulence. The only effect left to recover from, in the recovery flat plate, is the curvature effect. Thus, the recovery region data look very much like the unblown data.

In the case of $\theta = 1.0$, the story is different. For two rows of blowing, there is no visible effect of injection visible; i.e., St(1) = St(0). For six rows of blowing, however, in the first half of the recovery plate, the St(1) data are lower than the St(0) data, showing the thermal effect of injection. The hydrodynamics should be the same for both $\theta = 0.0$ and $\theta = 1.0$, but the thermal effect of injection at wall temperature remains for a longer distance than that of injection at free stream temperature.

Curved Region for m = 0.6

For the blowing ratio of m = 0.6, three partial-coverage tests were conducted: two, four, and six rows of blowing. St(0) data for six rows of blowing (Fig. 5.15) follows the full-coverage line until the last blown row (6th blown row) and then falls toward the no-injection but open-hole data, $St_{m=0}$ with a steeper slope than for the full-coverage. The St(0) data for 6 rows appears to reach the $St_{m=0}$ value at the very end of curved region (about 40 cm downstream of the last blown row). For four rows of blowing, the St(0) data follow the full-coverage data for three blown rows, but the value at the 4th row is lower than the full-coverage point. The data finally recover to the $St_{m=0}$ values, about 30-35 cm downstream of the end of blowing. For two rows of blowing, the values of St(0) in the blown region are lower than those for the full-coverage. This behavior was seen both for m = 0.2 and m = 0.4, for the case of two rows of blowing. Recovery to

the $St_{m=0}$ values is completed about 20 cm downstream of the end of injection.

The data of St(1) with $m = 0.6$ in the curved region shows very interesting behavior. For $m = 0.6$, and 6 rows of injection, the St(1) values downstream of the injection region, but still inside the curved region, are identical to the full-coverage values. For four rows of blowing, there are small differences, but even for two rows of blowing, the differences are not large--certainly much smaller than was seen for two rows of blowing with $m = 0.4$ and $m = 0.2$.

Comparison of the data for $m = 0.4$ and $m = 0.6$ in that region (curved, unblown) reveals that the St(1) data for $m = 0.6$ are higher at the beginning but merge with data of $m = 0.4$ in the last part. The two sets of data, one for $m = 0.4$ and the other for $m = 0.6$, coalesce in a shorter distance for fewer rows of blowing. For two rows of blowing, the data are together in the entire region, except for the first point downstream of the blown region.

Recovery Region for $m = 0.6$

The St(0) data with $m = 0.6$ in first part of the recovery flat plate are lower than $St_{m=0}$ data, as seen in the full-coverage case. The difference of two values, St(0) and $St_{m=0}$, and the distance through which this difference is observed are small, and are proportional to the amount of injected air; i.e., the number of rows of injection. For the partial-coverage cases, the St(0) data recovers to the $St_{m=0}$ data by the middle of the recovery region and no overshoot is observed. The recovery of St(1) is slower than that of St(0) as has been seen before, indicating that the thermal effect for $\theta = 1.0$ remains effective over a longer distance than for $\theta = 0.0$. This was also observed for $m = 0.2$ and 0.4. The more air that has been injected in the curved region, the lower is the Stanton number in the recovery region. A larger cooling effect is obtained in the recovery region for $m = 0.6$ than for $m = 0.2$ or $m = 0.4$ with the same number of rows of blowing. This is consistent with the results for full-coverage.

5.1.2.3 Interpretation of the Data

In this section, the behavior of St(0) and St(1) is discussed in terms of various effects of the curved, film-cooled flow discussed for the full-coverage cases: curvature effect, thermal protecting effect of injection and turbulence augmentation by the injected jets. The data discussed here is for $m = 0.4$, which is a representative case for partial blowing, unless otherwise mentioned. However, the general ideas can be applied to the other two cases.

Curved Region for $\theta = 0.0$

As briefly discussed in the previous section, the St(0) data in the blown region for partial coverage do not exactly follow the full-coverage data. The St(0) data for 6 rows of blowing do follow the full-coverage data throughout the blown region, but for 4 rows of blowing, the St(0) data follow the full-coverage ones only until the second blown row. For 2 rows of blowing, the rise of St(0) data at the first blown row is less steeper than for other cases. This trend of the St(0) data suggests the existence of the effects of slight differences of wall static pressure distributions. If there were no pressure effects, the data for partial injection should lie directly on the corresponding data for full-coverage.

The wall static pressure distributions were measured and found to be small, averaging about 3% of the velocity head of the main stream. For partial injection, the pressure "island" occupied the blown rows, rising on the first blown plate and dropping after the last. The extent of the pressure island corresponded to the number of blown plates.

In Fig. 5.16, the distributions of the wall static pressure, $P_{s,w}$, are shown, along with schematics which highlight the features the data reveal. In Fig. 5.16a, measured values for full- and partial-coverage cases (two, four, and six rows) are plotted, while in Fig. 5.16b, the schematic illustrations of the wall static pressure distributions are shown. For the full-coverage case, the wall static pressure, $P_{s,w}$, increases abruptly at the beginning of the blown region. This rise is believed to be due to the deflection of the mainstream by the injection. The $P_{s,w}$ wall static values stay high for several rows of injection

holes and then gradually decrease. For the partial blowing cases, the same rapid increase is observed in the beginning of the blown region as for the full coverage. However, for partial blowing, right after the end of the blown region, the values of $P_{s,w}$ drop very sharply. High $P_{s,w}$ values are seen only in the injection region and form a "pressure island" there.

The turbulence data show no significant differences in this region between the full-coverage and the partial coverage. The mechanism by which this pressure island interacts with the flow to affect Stanton number is not known.

In the curved region downstream of the blown region, for all three cases (two, four, and six rows), the data of St(0) approach and reach the no-injection Stanton Number. Two mechanisms contribute to the high values of St(0) in the blown region: (1) the increased turbulence caused by injected air, and (2) the thermal effect of injection at free stream temperature. Recovery from injection takes place inside the curved region, and the effect of the convex wall suppresses the turbulence activity. This allows the recovery to the no-injection value to occur in a shorter distance than for the full-coverage cases, where recovery occurs in the flat-plate wall region.

Curved Region for $\theta = 1.0$

The partial coverage St(1) data in the blown region follow the full-coverage values. This is an expected result from the parabolic nature of the boundary layer heat transfer situation. The effect of the pressure gradient observed for the St(0) data is not seen here. The heat transfer behavior in the blown region is dominated by the thermal protection effect of the injection air at wall temperature and the pressure effect seems to be small enough to be hidden by this strong thermal effect.

The rapid increase of the St(1) data right after the blowing region, which was seen for both the flat plate injection case and the full-coverage case in the present study, is not visible for the partial blowing cases. The sharp increase is caused by the sudden cessation of injection and the resultant abrupt decrease of the thermal protection

effect. The turbulence level, however, remains high. Convex curvature has a stabilizing effect and softens the abrupt transition by suppressing the turbulence. This prevents the end of the thermal protection zone from being visualized as a rapid increase in Stanton number.

The unblown region downstream of the blown region is still on a convex curve. The St(1) data in this region continues to decrease, even though the slope is less steep than in the blown region. This seems to be because the convex curvature, again, plays a role. The turbulent mixing is suppressed, which is the original effect of convex curvature on heat transfer reported by Simon [43] and Gillis [38]. The recovery process from the thermal effect of injection takes place in the same way as for the full coverage cases, but the convex curvature effect on heat transfer prevents the St(1) data from increasing inside the curved region.

Recovery Region

In the following paragraphs, the behavior of St(0) and St(1) in the recovery region will be discussed. For $\theta = 0.0$, even for six rows of injection, the Stanton number has recovered to the no-injection values inside the curved region. The behavior of St(0) in the recovery flat plate is also similar to the no-injection case. The recovery region effects seen in the full-coverage cases are not visible for partial coverage.

A rapid increase is observed for St(1) between the curved and the flat plates. The step is about the same size for full and partial coverage and is caused by the release of curvature, as was seen for the no-injection curved flow. The St(1) data are low at the beginning of the recovery region and gradually increase. This represents the relaxation of the temperature profile. This behavior can be contrasted with the recovery on the curved region where curvature suppressed the turbulence and Stanton number continued to decrease after the end of injection. The recovery to the no-injection values is quicker for partial blowing than for full-coverage. The distance necessary for recovery is more or less proportional to the amount of injected air, i.e., the recovery after six rows needs the longest distance and that for two rows needs the shortest distance. There is no over-shoot in the recovery region,

even though the recovery takes place in a shorter distance than for full-coverage case. The level of turbulence at the beginning of the recovery region is not as high as for the full-coverage because of fewer rows of injection, hence there is little or no tendency for the Stanton number to overshoot.

Partial Blowing on $St\text{-}Re_{\Delta_2}$ Coordinates

In Fig. 5.17, the St(1) data for all cases with $m = 0.4$, both full and partial coverage, are plotted on $St\text{-}Re_{\Delta_2}$ coordinates. All partial blowing cases with $m = 0.4$ stay on the same line as the full-coverage blowing, a line of (-1) slope. This result shows the well ordered nature of this situation, because the partial blowing cases are bounded by the full-coverage case and the no-injection case, and all three cases are now seen to lie on the same line.

It is interesting to see how partial blowing with $m = 0.6$ behaves in $St\text{-}Re_{\Delta_2}$ coordinates. As shown in the previous section, values of St(1) for full-coverage with $m = 0.6$ lie above the (-1) slope line. Figure 5.17 shows the St(1) data of $m = 0.6$ for both partial- and full-coverage. Recall that for partial coverage at $m = 0.4$ the St(1) data remained on the full-coverage line throughout the curved region. For $m = 0.6$, however, the local response of the boundary layer to partial blowing is different. For the partial blowing cases, St(1) for $m = 0.6$ follows the line of the full-coverage values for $m = 0.6$ only until the last blown row. From then on, the St(1) data come down rapidly, approaching the extension of the line of no injection (-1 slope). Since the recovery from blowing proceeds inside the curved region, the recovery process is different from that following full-coverage, where the recovery took place on a flat surface. The value of St(1) for partial injection continues to decrease after the cessation of blowing, because of the effect of convex curvature in suppressing turbulence. The local response of the boundary layer shown in $St\text{-}Re_{\Delta_2}$ coordinates recovers to the line characterized by curvature.

A blowing ratio of $m = 0.2$ shows the same results for partial blowing as $m = 0.4$, staying on the line of -1 slope throughout the curved region. This result confirms the well-ordered nature of the situation, because both full and partial coverage St(1) data for $m = 0.4$,

and St with no injection, lie on the same line. Figure 5.19 shows the data for St(1) with m = 0.2 for two, six, and thirteen rows of blowing. The St(1) data for the partial blowing cases increase slightly just downstream of the blown region and thereafter stay on a line of (-1) slope, but slightly above the line describing the full-coverage case. This shift is attributed to the effect of open holes with no flow. As mentioned before, for the partial blowing cases, the unblown injection holes were left open but with no flow. These open holes increased the heat transfer rate, as a roughness effect. The small amount of injection air and the thin boundary layer associated with partial injection at m = 0.2 do not thicken the boundary layer enough to wipe out the effect of the open holes. A similar shift was observed for the case of no blowing with open holes.

5.1.3 Partial Blowing: Injection at Different Locations

5.1.3.1 Experimental Data

In Fig. 5.20 and Fig. 5.21, additional data are shown for two rows of blowing at m = 0.4 , but for different locations in the curved region. For the data in Fig. 5.20, injection was located in the middle of curved region (7th and 8th copper strips, starting at 41.5°) and for the data in Fig. 5.21. at the end of curved region (13th and 14th copper strips, starting at 80.3°). In the region ahead of injection, the data for both cases follow those with open holes with no flow. Once the blowing starts, they behave in the same general manner as the foregoing cases with blowing, i.e., St(0) first increases then starts decreasing and St(1) becomes lower than the non-injection value. Comparing the three cases having two rows of injection, Fig. 5.8, Fig. 5.20 and Fig. 5.21, the effect of injection persists for about the same distance, 60 cm downstream of the last injection row, regardless of where the injection begins. The data of St(0) in Fig. 5.21 (injection at the end of curved plate) show a smooth transition from the curved region to the recovery region, as was seen in the full-coverage blowing cases.

5.1.3.2 Interpretation of the Data

The hydrodynamic and thermal structure of the boundary layer differs at different locations of the curved plate, for the curved flow with no injection. However, the response to injection appears to be the same for the three different locations inside the curve. The injection alters the boundary layer structure so drastically that the difference observed for the no-injection flow becomes minor in the blown region.

The transition from the curved plate to the flat plate, for the case where two rows are at the end of the curved plate, is smooth as it was for the full-coverage case. The response to the release of the curvature for St(0) data is more dependent on the location of the last blowing row than on the amount of injected air or on the thickness of the boundary layer. The data of St(1), however, always show a rapid rise between the curved and the recovery region. On the St-Re_{Δ_2} coordinate, all three cases discussed here show the same behavior. Inside the curved region, either in the blown or in the unblown region, the St(1) data lie on the same line of (-1) slope. By the end of the curved region, the total energy input by injection is the same for all three cases, regardless of where the injection begins, hence the line of -1 slope ends at the same location. The behavior in the recovery region is slightly affected by the location of injection, but the difference is small. The St(1) data at the beginning of the recovery plate are slightly lower for the case of injection just before the recovery region.

5.2 Effectiveness Calculation

5.2.1 Full-Coverage

The film-cooling effectiveness, η, is frequently used in discussing the cooling effect of discrete hole injection. As mentioned earlier, the film-cooling effectiveness can be calculated from the two basic values of Stanton Number, St(0) and St(1). Figure 5.22 shows values of η for three cases: $m = 0.2$, 0.4, and 0.6. For all cases, effectiveness rises rapidly downstream of the first row of holes and, once again, $m = 0.4$ appears to be near an optimum value.

In the blown region, the effectiveness for $m = 0.4$ shows the highest value among the three. In the recovery region, on the other hand, the effectivenss for $m = 0.6$ becomes highest.

Figure 5.22 also shows (dashed times) the effectiveness calculated from the flat plate data with $m = 0.4$ [12]. The effectiveness on a convex wall (present study) shows a higher value than that on a flat plate. This result agrees with the conclusion by Ito et al. [47], who claims that the effectiveness on a convex wall is higher than that on a flat plate if $m < 1.15$, $\rho_2 = \rho_\infty$ and $\alpha = 30°$.

From the results above, two conclusions can be drawn. First, in the blown region, $m = 0.4$ is the optimum blowing ratio. Second, in the recovery region downstream of the blown region, the injection with $m = 0.6$ can keep the cooling effect for the longest distance.

5.2.2 Partial-Coverage: 2, 4 and 6 Rows with $m = 0.4$

In Fig. 5.23, the effectiveness calculated by using the St(0) and St(1) is plotted for $m = 0.4$ with two, four, and six rows of injection. Within the blowing region, the effectiveness followed the same line for both full- and partial coverage. Immediately after the last blown row, the partial coverage data depart from the full-coverage data and start decreasing. The number of rows of injection in the curved region clearly affects the effectiveness in the recovery region. For two rows of blowing, there is very little effect of cooling (i.e., the effectiveness is near zero) in the recovery region.

5.2.3 2 Rows of Injection at Different Locations

Figure 5.24 shows the calculated values of effectiveness for three cases of two rows of blowing ($m = 0.4$) at different locations inside the curved plate. In the blown region, high values of film-cooling effectiveness are obtained, showing the cooling effect of the injected air. In the region downstream of injection, the effectiveness gradually decreases and asymptotically approaches zero.

The effectiveness curves for injection at the beginning of the curve and for injection at the middle show a very similar shape: a

linear translation in x-direction would collapse the two curves. The curve for injection at the end of curvature appears somewhat different from the other two but this is not real. The apparent peak value in this case is about 20% lower and is located at the second row of injection, but the rig structure is such that one data point is missing: that which would have been the highest had the profiles been similar. For the other two cases, the maximum value is obtained at the third data point, one strip downstream of the last (2nd) injection row. At present, it seems safe to say that all three curves are nearly the same.

5.3 Hydrodynamic Measurements

As mentioned in the earlier chapter, by means of a triple-hot-wire probe, three mean velocity components, U_i, and six turbulence quantities, $\overline{U'_i U'_j}$ were simultaneously measured. Among the ten quantities (nine described above plus $Q^2 = U'^2 + V'^2 + W'^2$), the U component of the mean velocities, the Turbulence Kinetic Energy, Q^2, and the two dimensional shear stress, $\overline{U'V'}$, will be primarily discussed. These three are considered to be most important in describing the flow characteristics. They are also crucial for modeling efforts. Emphasis is placed on the streamwise evolution of the flow--both small scale and large scale. The small scale evolution denotes the streamwise evolution from one hole to the next hole at the same z-location (i.e., between rows) while large scale refers to the streamwise changes in profiles at the same relative location to the injection hole but in the different positions inside the array.

The quantities, V, W, $\overline{U^2}$, $\overline{V'^2}$, $\overline{W'^2}$, $\overline{V'W'}$, $\overline{W'U'}$, are presented, but are discussed in less details.

5.3.1 Full-Coverage Film Cooling

5.3.1.1 Mean Velocity: $\bar{U}$

Hydrodynamic measurements were made for three cases of full-coverage blowing, m = 0.2, 0.4, and 0.6. Figures 5.25, 5.26, and 5.27 show the streamwise evolution of the mean velocity profiles for m = 0.2, 0.4, and 0.6, respectively. Profiles at the three stations within the blowing region show pronounced three-dimensionality (i.e., spanwise non-

uniformity) in the inner region of the boundary layer for all values of blowing. The three-dimensional effects extended out from the wall to $y/\delta \sim 0.35$, a distance which appears to be almost constant in the streamwise direction. This spanwise variation is a result of the injected flow and shows a regular periodic pattern. Profiles at the same spanwise location relative to the injection holes show good agreement (see, for example, the pair of profiles at $z = +2.54$ cm and at $z = -2.54$ cm, and the pair at $z = +1.27$ cm and at $z = -1.27$ cm). For each measuring station, the profiles from the outer part of the boundary layer in different spanwise locations collapse to one, indicating two-dimensional flow in the outer region. A momentum defect is observed, however, relative to the no-blowing curved boundary layer profiles reported by Gillis [38]. The defect is not proportional to the blowing rate, but seems independent of it, in the coordinates of U/UP vs. y/δ. The defect is observed to become larger farther downstream. At Station-1, there is almost no defect, but at Station-2, the defect is clearly shown in the outer part of the profiles. Qualitatively, these same phenomena, in both inner and outer regions of the boundary layer, were observed by Yavuzkurt [24] in the studies of the hydrodynamics of discrete-hole injection on a flat plate.

The profiles of $z = 0.0$ at Station-1 were measured at the center of the injection hole (3rd row of holes) 4 mm above the wall. The effect of the jet from the injection hole at the probe location can be seen for $m = 0.6$, where the profile shows a negative velocity gradient for the first three points. However, that same profile, outboard of the first three points, is affected also by the jets ejected from the holes upstream (in this case, the first row of holes). For $m = 0.4$ and 0.2, the effect of the jet at the third row at this measuring station is hardly seen in the profile, but it would probably have been seen if data could have been taken in the region very close to the wall. The size of the probe prevents measurements closer than 3.8 mm to the wall. For $m = 0.4$, Youssefmir and Johnston [48] measured the mean velocity profiles very close to the hole and found a very strong effect of injected jet in that region (see Fig. 4).

At Stations -2 and -3, measurements were made in the same locations relative to the injection holes: 4 cm downstream of the nearest injection hole for the station at $z = 0.0$, 9 cm downstream at $z = \pm 2.54$ cm and on a line between holes at $z = \pm 1.27$ cm. For $m = 0.6$, the profile at $z = 0.0$ is significantly distorted, showing a sharp break at $y/\delta \sim 0.15$, while the profiles at $z = 2.54$ cm are flattened. This difference indicates that, for $m = 0.6$, the mixing between the jet and the mainstream has not progressed far by 4 cm downstream but is relatively complete by 9 cm downstream. For $m = 0.4$, the center line profiles at Station 2 and 3 (4 cm downstream of a hole) also show breaks, but they are much less noticeable than those seen for $m = 0.6$. The very inner-region profile ($y < 0.3$ cm) taken by Youssefmir and Johnston [22], however, show the effect of jets. The mixing process between the jet and the mainstream for $m = 0.4$ seems to be in largely completed by 4 cm downstream. The profiles at $z = \pm 2.54$ cm are different from those at $z = 0.0$ only in the first three points. This behavior also indicates that the interaction between the jet and the mainstream is not very active between 4 cm and 9 cm downstream of the jet. The interaction is nearly complete by 4 cm downstream, as described above, for $m = 0.4$. For $m = 0.2$, even the center profiles are smooth with no break. However, the difference between the profiles at $z = 0.0$ (4 cm downstream) and those at $z = \pm 2.54$ cm (9 cm downstream) shows the same behavior as for $m = 0.4$: only the first three points are changed, at both Stations 2 and 3. The mixing process for $m = 0.2$ seems essentially the same as for $m = 0.4$. The profiles at $z = \pm 1.27$ cm (a lane between holes) show momentum defects compared to the no-blowing profiles of Gillis [38] for all blowing ratios. The defects become larger farther downstream (i.e., larger at Station 2 than at Station 1), especially in the region from $y/\delta \sim 0.2$ to $y/\delta \sim 0.4$. (The defect probably becomes still larger at Station 3, but there are no no-injection profiles available at Station 3). The defect is approximately the same for all three values of m.

In the recovery region, for all blowing ratios, the three spanwise profiles ($z = 0.0$ and ± 2.54 cm) collapse on one another at the first recovery station (30 cm downstream of the end of curved region). The momentum defect is clearly seen in the profiles at Station 4 and 5,

although it becomes smaller farther downstream. At Station 6, profiles for all blowing ratios are identical.

5.3.1.2 Turbulence Kinetic Energy: Q^2

Figures 5.28, 5.29, and 5.30 show distributions of turbulence kinetic energy, Q^2 for full-coverage cooling cases with $m = 0.2$, 0.4 and 0.6, respectively. Three-dimensional effects are confined to the region near the wall in the blown curved plate. In the unblown recovery region and outboard of $y/\delta = 0.4$ in the blown region, the distributions are spanwise uniform within the uncertainty of measurement.

Measuring Station 1 is on the fourth plate, but there are only two rows of holes upstream. The center profile ($z = 0.0$) at Station 1 was measured directly over the center of the injection hole. For $m = 0.6$, the first three points show the effect of the jet ejected through that hole; a high peak value at the second point and an abrupt decrease at the third point. Above those points, the profile shows the effect of the jet upstream. For $m = 0.4$, only the first point shows any trace of a negative slope, while for $m = 0.2$, the effect of the 3rd row jet is not visible in the profile. Again, probing the region closer to the wall would probably make that effect more clearly seen.

The profiles of $z = \pm 2.54$ cm at Station-1 are 5 cm downstream of the nearest injection holes and are noticeably different from the center profiles. The side profiles (± 2.54 cm) will also be seen to be similar to the center profiles at Station 2 and 3, which are also about 4 cm downstream of the nearest hole. Profiles taken 4 or 5 cm downstream of the nearest hole and in line with the hole can be described as a three zone system: an inner zone in which Q^2 is substantially uniform in the y-direction, an outer, two dimensional flow zone; and an intermediate, 3-D mixing zone. The innermost zone is strongly three dimensional in the spanwise sense, due to the influence of the jet. The level of Q^2 in that zone is the highest seen anywhere in the profiles at the same station. The "streamwise evolution" of the profiles will be discussed in the next section.

In the recovery region at Station 4, three profiles ($z = 0.0$ and $z = \pm 2.54$ cm) collapse on one another. This is the same result as was

found in the mean velocity measurements. Values of Q^2 at Station 4 are highest for $m = 0.2$ and those for $m = 0.4$ are second highest. At Station 5, profiles for $m = 0.2$ and 0.4 are identical and show higher values than that for $m = 0.6$ does. At Station 6, profiles for all blowing ratios become identical. These results in the recovery region are not inconsistent with the heat transfer results in that region, i.e., $m = 0.6$ shows the lowest values of St(1) and $m = 0.2$ shows the highest values. However, even in the region where the profiles for $m = 0.2$ and 0.4 become identical, the heat transfer coefficients are different. The difference of measured heat transfer coefficients is largely due to the differences in the boundary layers, which reflect their upstream history. The same phenomena would be observed at Station 6 if the heat transfer measurement were made.

5.3.1.3 Shear Stress: $\overline{U'V'}$

In Fig. 5.31, 5.32 and 5.33, the profiles of $-\overline{U'V'}$ are shown for full-coverage cases with $m = 0.2$, 0.4 and 0.6. The center profiles ($z = 0.0$) at Station 2 and 3, for $m = 0.4$ and $m = 0.6$, show similar shapes, starting with very low values of $-U'V'$ close to the wall, increasing and showing a high peak at $y/\delta \sim 0.15$, and then decreasing until the low peak at $y/\delta \sim 0.2$, increasing again and showing the second high peak at $y/\delta \sim 0.25$, then gradually decreasing and approaching the zero value. Comparing profiles of $m = 0.4$ and $m = 0.6$, however, shows that the magnitude of these peaks is much larger for $m = 0.6$. Especially for $m = 0.6$, large negative values of shear stress were found in the near-wall region, in which a negative mean velocity gradient was also found. For $m = 0.4$, such negative values were not seen. For $m = 0.2$, the center profile at the same stations (2 and 3) starts with a low value of $-\overline{U'V'}$ and show a high peak at $y/\delta \sim 0.15$, but, unlike $m = 0.4$ and 0.6, there is neither a low peak nor the second high peak. The side profiles ($z = \pm 2.54$ cm) for $m = 0.2$ are very similar to the center profiles, indicating how the small scale evolution of shear stress has proceeded between 4 cm and 9 cm downstream of the hole. The side profiles for $m = 0.4$ resemble those for $m = 0.2$, while those for $m = 0.6$ are different, showing very high values in the closest region to the wall. For shear stress, it seems that the

small-scale evolution has substantially been completed by 4 cm downstream of the hole for $m = 0.2$, between 4 cm and 9 cm for $m = 0.4$, and is still proceeding at 9 cm downstream for $m = 0.6$. The profiles at $z = \pm 1.27$ cm (the lane without holes) for all blowing ratios show lower shear stress than the profiles in the lanes with holes at all stations in the blown region.

In the outer part of the boundary layer in the blown, curved region (about $y/\delta \sim 0.5$), the shear stress becomes zero and even shows a small negative value. This is one of the characteristics of the convexly curved boundary layer observed by Gillis et al. [38]. The current results clearly indicate that the outer half of the boundary layer is not much affected by injection.

In the recovery region at Station 4, three measured profiles show no difference, as seen in the mean velocity and Q^2 profiles. All profiles in the recovery region, for all blowing ratios show a high peak at $y/\delta \sim 0.4$ and the values of shear stress near that peak are much higher than that with no-injection [38]. At Station 4, $m = 0.2$ shows the highest values, with $m = 0.4$ the second, and $m = 0.6$ the lowest. At Station 5, profiles for $m = 0.2$ and for $m = 0.4$ are identical, and that for $m = 0.6$ is lower. At Station 6, far downstream, all three blowing ratios show the same profile. This result is the same as for mean velocity and turbulence kinetic energy. From those results, it can be concluded that the hydrodynamics of $m = 0.2$ and $m = 0.6$ become identical by 70 cm downstream of the end of the blown region, and the hydrodynamics of $m = 0.6$ becomes identical to that of the other two blowing ratios by 150 cm.

5.3.1.4 Flow Angle: V and W

One advantage of using a triple hot wire is the capability of measuring the three mean velocity components $\overline{U}$, $\overline{V}$, and $\overline{W}$ at the same time. In the present study, the injection air is ejected at 30°, thus the components $\overline{V}$ and $\overline{W}$ are not small in the blowing region. From Figs. 5.34 to 5.37, values of flow angle, $\overline{V}/\overline{U}$ and $\overline{W}/\overline{U}$, are shown for $m = 0.4$ and 0.6. All data were taken at Station 2, in the middle of blown region. For the $\overline{V}$ component, the shapes of the profiles are

alike for $m = 0.4$ and $m = 0.6$. In the lane with holes ($z = 0.0$ and $z = 2.54$ cm), the highest value appears at the closest point to the wall. The magnitude of that value is larger for $m = 0.6$: 18° at $z = 0.0$, and 7° at $z = 2.54$ cm for $m = 0.6$ and 12° at $z = 0.0$ and 6° at $z = 2.54$ cm for $m = 0.4$. In the lane without holes ($z = 1.27$ cm), $\overline{V}/\overline{U}$ is near zero, indicating that the injection has very little effect on the lane without holes. In the part near the wall, $\overline{V}$ for $m = 0.6$ shows negative values, while $\overline{V}$ for $m = 0.4$ does not. This indicates that the entrainment characteristic for $m = 0.6$ is more visible than for $m = 0.4$, which probably contributes to the high heat transfer coefficients for $m = 0.6$.

For the $\overline{W}$ component, similar shapes of the profiles are seen for $m = 0.4$ and $m = 0.6$. The only visible difference is that $\overline{W}/\overline{U}$ at $z = 0.0$ shows a higher value on the positive side for $m = 0.6$ than for $m = 0.4$. Note that in the negative side, both $m = 0.4$ and $m = 0.6$ show about the same magnitude.

5.3.1.5 Reynolds Stresses

With a triple-wire probe, all six Reynolds stress components can be measured. Examples of these data are shown in Fig. 5.38 to 5.41. Figures 5.38 and 5.39 show normal stresses and Figs. 5.40 and 5.41 show shear stresses. Both data were taken at $z = 0.0$ (4 cm downstream of the hole) at Station 2. Other data are listed in Appendix. In each figure, the data for $m = 0.4$ and $m = 0.6$ are shown side by side. For the normal stresses, high values are seen in the near region and the level of $\overline{U'^2}$ is approximately half as high as the other two, which show about the same level. The shape of the normal stress distributions for the two blowing ratios is very similar and for $m = 0.6$, the magnitude is about twice as for $m = 0.4$. For the shear stresses, $-\overline{U'V'}$ and $-\overline{U'W'}$ show about the same shape and level. Values of $-\overline{V'W'}$ in the near wall region are negative and the magnitude is considerably higher for $m = 0.6$ than for $m = 0.4$.

5.3.1.6 Hydrodynamic Measurements: Streamwise Evolution of the Q^2 Profile

The boundary layer hydrodynamic measurements indicate that the flow field in the blown region appears to be divided into two lanes: one which contains holes and one which does not. The distribution of Q^2 along a lane between columns of holes ($z = \pm 1.27$ cm) shows lower values of Q^2 than in the lanes with holes and is closer to the Q^2 distribution of the no-injection flow on a convex wall [38]. Along a lane containing holes, there appear to be both "large scale" and "small scale" patterns of evolution.

For discrete hole injection, the streamwise evolution from one hole to its next downstream hole is of interest; i.e., how the jet from the hole merges into the boundary layer. This evolution between two holes will be called "small scale" evolution.

It was not possible to make several profile measurements at different streamwise locations between any two consecutive hole, because of the structure of the facility. Instead, at any one station in the blowing region, profiles at $z = 0$ and at $z = \pm .54$ cm were compared, to represent the "small scale" evolution. To illustrate, at Station 2, the center profile ($z = 0.0$) is 4 cm downstream of the hole in the seventh row while the side profile ($z = \pm 2.54$ cm) is 9 cm downstream of the hole in the sixth row. Comparison of these two profiles gives a reasonable picture of the "small scale" evolution.

The term "large-scale" refers to the gradual changes in the small scale pattern between the upstream and downstream portions of the test surface. This type of evolution is particularly important for full-coverage cooling where multiple rows of injection will be used. The "large scale" evolution can be examined, at least to some extent, examined by comparing profiles at different stations but at the same location relative to the injection hole.

As to "small scale evolution", the following features were found from the experimental data, considering the Q^2 behavior in a lane with holes. The center profiles ($z = 0.0$) at Stations 2 and 3 were measured 4 cm downstream of the holes. They show very high values of Q^2

in the inner region of the boundary layer for all values of m. For m = 0.2 and m = 0.4, by 9 cm downstrean of the hole (see the profiles at z = 2.54 cm), these high values have decreased and the profiles are very similar to the profiles in the lanes without holes (z = ±1.27 cm). However, for m = 0.6, even by 9 cm downstream of injection (z = 2.54 at Station 2 or 3) the values of Q^2 in the inner region remain above the value in the lanes without holes. The location 9 cm downstream of the injection holes is right in front of the next injection hole. From these observations, one can propose the following description. For m = 0.2 and 0.4, the Q^2 levels in the inner region returns to the lowest possible value (the value in the lanes without holes) before the next row is encountered. For m = 0.6, the level of Q^2 does not return to that value, but remains high in the inner region when the next row is encountered. The Q^2 values in the lanes without holes change monotonically: there is no "small scale" evolution in these lanes.

The profiles measured 5 cm downstream of a hole show a high level of Q^2 in the near wall region. For m = 0.4, this high level remains about the same in the stations downstream (see the center profiles at Stations 2 and 3). For m = 0.6, however, the peak value of Q^2 becomes higher, farther downstream; i.e., the center profile at Station 2 shows higher level than at Station 1 (z = ±2.54 cm) and at Station 3, becomes still higher. On the other hand, for m = 0.2, the value of the highest Q^2 becomes smaller and at Station 3, the center profile is so smooth that the near wall region and the intermediate region are hardly different at all.

For m = 0.6, there appears to be less interaction between the lanes with holes and the lanes without than was found for lower m. The value of Q^2, at the same station, is smaller for m = 0.6 than for m = 0.4 or m = 0.2, and the difference becomes larger farther downstream.

There is an abrupt increase in Q^2 at each row of injection holes, and Q^2 is highest in the near wall region. For m = 0.2 and m = 0.4, the "small scale" evolution indicates that along the streamwise line passing through a hole, the level of Q^2 in the inner region decreased almost to the no-injection level before the flow reached the

next hole. At each successive hole, an increase in Q^2 occurs for $m = 0.4$. The level of Q^2 measured 4 cm downstream of a hole remains constant: there is no "large scale" evolution. For $m = 0.2$, however, the maximum value of Q^2 in the inner region decreases in the streamwise direction; i.e., the values at Station 3 are lower than at Station 1 or 2. This indicates that for $m = 0.2$, evolution shows a decrease in Q^2 with distance. This may either be because the increase of Q^2 at each injection location is less in the downstream region than the early region, or that the dissipation of Q^2 or the transfer of Q^2 to the lanes between holes takes place more quickly farther downstream. Either or both of these mechanisms would account for the lower values of Q^2 measured 4 cm downstream of the injection hole at Station 2 and the still-further reduced values at Station 3. The decrease of Q^2 for $m = 0.2$ might be due to the curvature effect, since convex curvature is known to suppress turbulence [38]. The injection rate is low for $m = 0.2$; hence there is little or no augmentation of turbulence by the injection. Under these conditions, it may be that the effect of convex curvature is dominance.

For $m = 0.6$, the values of Q^2 in the inner region of the center profile become larger at each successive station downstream. This result is explained by the "small scale" evolution. The increase in Q^2 produced by the jets is not offset by the decrease in the lane without holes before the next injection hole. Thus, at the next hole, the level of Q^2 is the sum of that left over from the hole upstream and the new addition at the hole just encountered.

Figure 5.42 schematically shows the streamwise evolution of Q^2, both "small scale" and "large scale". The figure illustrates the three consecutive injection rows and provides the sketch of how these two "evolutions" link with each other.

Measurements at many locations between two consecutive holes would reveal the behavior of the decay of Q^2 in the inner region. This experiment is strongly recommended for future work.

5.3.1.7 Detailed Spanwise Measurements

In the last section, it was pointed out that the flow field in the blown region can be divided into two types of lanes. The lanes located at $z = 0.0$ and $z = \pm 2.54$ cm contain injection holes, while the lanes located at $z = \pm 1.27$ cm have none. Measurements were made for $m = 0.4$ in the region between $z = +1.27$ cm and $z = -1.27$ cm at Station 2. The data were taken 0.43 cm upstream of the leading edge of the eighth row of injection holes. The objectives of these measurements are first to detect the sensitivity to the misalignment of the probe in the spanwise direction and second to make a detailed measurement across one representative span covering both types of lanes. The results are shown in Figs. 5.43 and 5.44. Figure 5.43 shows the mean velocity profiles, and Fig. 5.44 shows the turbulence kinetic energy profiles. The data of both $\bar{U}$ and Q^2 demonstrate that the centerline of the jet lies between $z = 0.0$ and $z = +0.25$ cm. The jet is indicated to be tilted about 1° upward. For the mean velocity profiles, two profiles at the center ($z = 0.0$, $z = +0.25$ cm) show the relatively strong effect of the injected jet with the peak at $y/\delta = 0.15$. The profiles next to these also show the peak, which, however, is much less noticeable. For Q^2 profiles, four profiles at the center ($z = -0.25$, 0.0, +0.25, and +0.51 cm) show the characteristics of the lane with holes and all four profiles are alike. From these results, it can be said that the width of the lane with holes is approximately 1 cm and that the border between two lanes for mean quantity show a gradual transition while that for turbulence quantity shows a more abrupt change.

5.3.1.8 Spanwise Average

As has been seen already, the flow field near the wall in the blown region is fully three-dimensional because of the injection. From the point of view of modeling, two-dimensional analyses are easier to make and two-dimensional codes are more compact. Spanwise averages of the hydrodynamic data are important in that sense. A mass-weighted average was used for $\bar{U}$ and Q^2 and an area average for $-\overline{U'V'}$. The span from $z = -2.54$ cm to $+2.54$ cm is considered to be one unit, because this pattern of geometry repeats in the spanwise direction. Averaging was

carried out by using five spanwise measurements: $z = 0.0$, ± 1.27 cm, and ± 2.54 cm. Special care must be taken for dealing with the profiles at $z = \pm 2.54$ cm, because these two locations are at the boundary of the unit width. Half as much weight as for other profiles should be used for each of these two profiles. Results are shown in Figs. 5.45, 5.46, and 5.47: mean velocity in Fig. 5.45, turbulence kinetic energy in Fig. 5.46, and the area-averaged shear stress in Fig. 5.47, with three blowing ratios, 0.2, 0.4, and 0.6. The figures show the results only in the blown region (Stations 1, 2, and 3).

The effect of m on the profile shape becomes more noticeable farther downstream; i.e., the largest effect of m is seen at Station 3 for all three quantities, $\overline{U}$, Q^2, and $\overline{U'V'}$. This may be attributed to the large scale evolution.

For $\overline{U}$ profiles, the two lower blowing ratios ($m = 0.2$ and 0.4) show similar profiles, although the profile for $m = 0.4$ is slightly distorted. For $m = 0.6$, the profile is significantly different from the other profiles, showing a break at about $y/\delta = 0.1$ which lower m does not produce. The $m = 0.6$ data are noticeably different from tha for other blowing ratios throughout the inner part of the boundary layer. At Station 1, the Q^2 profiles for all three blowing ratios are very close to one another. At Station 2, the Q^2 profile for $m = 0.4$ is slightly lower than the other two, but the difference is very small. At Station 3, relations among three profiles are more complicated. In the inner part of the boundary layer ($y/\delta \sim 1.5$), Q^2 for $m = 0.6$ shows the highest value, probably strongly affected by the very high level of Q^2 at $z = 0.0$. Above that region, Q^2 for $m = 0.6$ decreases rather abruptly, while Q^2 for $m = 0.2$ and $m = 0.6$ sustain relatively high values farther out in the boundary layer.

The $\overline{U'V'}$ profiles clearly show the difference among three blowing ratios. The profiles for $m = 0.2$ are smooth and show the highest values of $-\overline{U'V'}$ of all three cases studied. The profiles for both $m = 0.4$ and $m = 0.6$ show breaks at about $y/\delta = 0.1$, and their general shapes and magnitudes are very similar.

5.3.1.9 Stanton Number and The Hydrodynamic Boundary Layer

In the section discussing the Stanton number data, the heat transfer behavior for each blowing ratio was discussed in terms of the hydrodynamic and thermal effects of injection. Hydrodynamic measurements should support these discussions. In this section, the results of hydrodynamic measurements are examined from this point of view.

In the blown region, the values of St(1) for $m = 0.6$ are higher than for $m = 0.4$, despite the higher amount of wall temperature air injected. Higher turbulent mixing caused by injection with $m = 0.6$ was considered to be the reason for this phenomena. Comparison of the turbulence kinetic energy data reveals that the values of Q^2 in the lane with holes ($z = 0.0$ and $z = 2.54$ cm) are significantly higher for $m = 0.6$ than for $m = 0.4$. However, the Q^2 data in the lane without holes are lower for $m = 0.6$. The spanwise-averaged value of Q^2 for $m = 0.6$ is thus only slightly higher than for $m = 0.4$. These results are not fully supportive of the idea that the heat transfer increase was due to the level of turbulence mixing, but do not contradict it. Measurements of local heat transfer coefficients and more detailed (both in spanwise and in streamwise) hydrodynamic measurements would be needed to make a full understanding of the relation between heat transfer and increased turbulence. The local heat transfer behavior may be more-than-linearly influenced by the level of turbulence, which would raise the spanwise averaged heat transfer coefficient more than the average turbulence.

It should be noted that the level of $\overline{V'^2}$ for $m = 0.6$ is more than twice as high as that for $m = 0.4$ near the wall. The level of U'^2 is only 50% higher for $m = 0.6$ (see Figs. 5.38 and 5.39). The turbulent transport of heat is measured by $\overline{v't'}$. Thus the V'^2 value may be more important than U'^2 or Q^2 for explaining the heat-transfer behavior in the turbulent boundary layer. Quite high values of V'^2 for $m = 0.6$ might play a key role in higher heat-transfer coefficients for $m = 0.6$.

Mean velocity measurements support the evidence of higher St(1) for $m = 0.6$: the injected air remains in the shape of a jet for a longer distance. This would mean that, for $m = 0.6$, the jet and the

main flow do not mix well and the area covered by injected jet is small near the injection hole, and the near-jet effect of the thermal protection by injection is decreased compared to $m = 0.4$. On the other hand, the mixing process between the jets and the main flow appears similar for $m = 0.4$ and $m = 0.2$. For these values of m, the effect on Stanton number is somewhat proportional to the amount of injected air.

Flow angle measurements reveal that in the lane without injection holes, for $m = 0.6$, larger values of negative angle of $\overline{V}/\overline{U}$ are measured, suggesting that a large amount of entrainment may be taking place for $m = 0.6$.

In the recovery flat plate, the value of Q^2 for $m = 0.6$ is lowest, while that for $m = 0.2$ is highest. This trend is clearly seen at Station 4 (30 cm downstream of the end of curved blown region). The mechanism responsible for this is not identifiable from the present data, but may be related to the highly localized distribution of Q^2 in the blown region for $m = 0.6$. This seems to be one of the reasons which explain the behavior of $St(0)$ in Region 1 (see Fig. 5.5). In this region, $St(0)$ data decrease. This reduction of $St(0)$ was related to the cessation of turbulence production by injection. The large reduction of $St(0)$ for $m = 0.6$ between the end of injection to the location of Station 4 is believed to be a consequence of the large reduction of Q^2 near the wall for $m = 0.6$.

The behavior of $St(1)$ in this region was mainly explained in terms of the recovery of the temperature distribution. The level of Q^2 appeared to be a secondary effect. The low level of Q^2 for $m = 0.6$ may play a role in the slow recovery of $St(1)$ for $m = 0.6$.

The measurements at Station 5, approximately at the end of Region II, show a higher value of Q^2 than for the no-injection case, for all three blowing ratios. This is clear support for the idea that the higher level of turbulence observed with injection causes higher values of $St(0)$ than those for no-injection.

5.3.2 Partial-Coverage Film Cooling

As partial-coverage cases, the case of two rows (first and second) of blowing was chosen. The most interesting behavior is the recovery from blowing, inside the curved region. Two blowing ratios were used: $m = 0.4$ and 0.6. For the boundary layer measurements, the unblown holes were closed with tape so that the effect of the open holes was eliminated.

In Figs. 5.48 and 5.49, mean velocity profiles are shown for $m = 0.4$ and $m = 0.6$, respectively. At Station 1, 5 cm downstream of the second row of injection holes, profiles for both $m = 0.4$ and $m = 0.6$ are similar to those in the blown region of the full-coverage cases for each blowing ratio. At this station, the profiles were taken 5 cm downstream of the injection hole at $z = \pm 2.54$ cm and 10 cm downstream at $z = 0.0$. Profiles at Station 2, still inside the curved region but 30 cm downstream of the last blown row, show no spanwise variation, demonstrating the quick recovery from the three dimensionality caused by the injection. After Station 2, profiles at each station for both blowing ratios collapse on each other.

Turbulence kinetic energy profiles are shown for $m = 0.4$ and $m = 0.6$ in Figs. 5.50 and 5.51, and shear stress profiles ($-\overline{U'V'}$) in Figs. 5.52 and 5.53. For both Q^2 and $-\overline{U'V'}$ in the blown region (Station 1), the profiles show litte difference in shape and magnitude between two blowing ratios. The heat transfer behavior in that region is considerably different. It is still uncertain whether this set of data is enough to show the hydrodynamic behavior of the flow. More detailed measurements, especially for spanwise evolution, would be necessary before one could fully understand the hydrodynamic behavior and to explain the heat transfer results.

The three-dimensionality of the mean velocity profiles, is wiped out before the end of the curved surface for partial coverage (i.e., by Station 2) and the profiles for both blowing ratios become identical by 30 cm downstream of the last injection row. In the full-coverage cases, spanwise non-uniformity also vanished by 30 cm downstream of the last row of injection but the profiles for different blowing ratios were different. The profiles in the unblown region for partial coverage are

two dimensional (i.e., spanwise uniform) and very similar to those from an unblown layer. For full-coverage, the relaxed 2-D profiles still differ significantly from unblown profiles. This result seems to be because of the small total amount of injection air for partial coverage (two rows) and the stabilizing effect of convex curvature.

5.4 Temperature Profiles

5.4.1 Full-Coverage with $m = 0.4$

Temperature profiles were taken as part of the boundary layer measurements. For this series of experiments, the wall was heated to an isothermal condition as though for Stanton number measurements, with full-coverage blowing at $m = 0.4$ since this is the baseline test case. Temperature profiles were taken for two case values of θ: a hot run ($\theta \sim 1.0$) and a cold run ($\theta \sim 0.2$). Measurements were made at the same streamwise locations used in the hydrodynamic measurements, except at Station 6. Station 6 for temperature profiles is at $x = 163.4$ cm, which is in the very last part of heating region while Station 6 for the hydrodynamic measurements was at 220.4 cm.

Figure 5.54 shows the temperature profiles for the hot run with $m = 0.4$. In the blown region (Stations 1, 2, and 3), the three-dimensionality is clearly seen. The region with significant spanwise non-uniformity extends out to $y/\delta \sim 0.4$, the same as in hydrodynamic profiles. In these figures, the y-coordinate is normalized with hydrodynamic boundary layer (δ_{99}) to make possible a direct comparison.

At Station 1, the profile at $z = 0.0$ was taken directly above the center of the injection hole. The centerline of the temperature probe could get within 0.5 cm of the wall. The profile can be divided into three regions: the inner most part (the first three points out to $y/\delta \cong 0.1$) is directly affected by the jet; the intermediate part (from $y/\delta \sim 0.1$ to 0.4) is affected only by the wake from the inline jet upstream of the probe (i.e., in the first row); and the outer part of the profile is two-dimensional and shows no effect of injection. The side profiles ($z = \pm 2.54$ cm) at Station 1 show the same effects of injection between y/δ of 0.1 and 0.4 , but do not show any direct effect of the jet very near the wall ($y/\delta < 0.1$). The side profiles and the

profiles between holes ($z = \pm 1.27$ cm) at Stations 1 and 2 demonstrate the symmetry of the temperature field, as was seen in hydrodynamics.

At Station 2, the center profile shows negative values of $(T_w-T)/(T_w-T_\infty)$ in the part of $y/\delta \sim 0.1$. This location is only 4 cm downstream of the nearest hole and the injection air temperature at that hole was slightly higher than the wall temperature (i.e., $\theta \simeq 1.03$). By 9 cm downstream of the hole ($z = 2.54$ cm), the temperature field is relatively smoothed out. The measurement location at Station 3 is in the same position, relative to the injection hole, as is the location at Station 2. The center profile looks different from the one at Station 2, but this is simply because the injection air temperature at 13th row is lower ($\theta \sim 0.9$) . For the "hot" case, the profiles in the lane between holes ($z = \pm 1.27$ cm) at three stations (Stations 1, 2 and 3) show that the thermal effect of injection accumulates in the streamwise direction: the average temperature near the wall moves steadily towards the wall temperature. This indicates that the thermal effect spreads in the spanwise direction from the lanes with holes to the lanes between holes: a "large scale" evolution. In the recovery region, spanwise non-uniformity vanishes by 30 cm downstream of the last row of injection as was seen in hydrodynamic study. At Station 4, however, although the profile is spanwise uniform, it is considerably different from the no-injection profile at that same location [38]. The profile with injection changes only slowly in the streamwise direction, shows no signs of a rapid return to the "unblown" profile.

In Fig. 5.55, temperature profiles are shown for the cold run with $m = 0.4$. In the blown region, the effect of injection is much less than for the hot run, except the center profile at Station 1, for which the first three points clearly show the effect of cold air injection ($\theta \sim 0.2$). The injection air temperature is not much different from the temperature in the inner region of the boundary layer.

At Station 4, the first station in the recovery region, the profile shows only small differences from the no-injection profiles, much smaller than for the hot run.

At Station 6, in the recovery region, the profile is considerably different from the hot run profile and appears to be very similar to the no-injection profile.

5.4.2 Full-Coverage with $m = 0.6$

As a full-coverage case, the hot run with $m = 0.6$ was also tested (Fig. 5.56). The discussion made for the hot run with $m = 0.4$ can be qualitatively applied to this case. The three-dimensionality extends somewhat further out, to $y/\delta \sim 0.5$. The effect of the jet below the probe is seen in the center profile at Station 1 and is more noticeable than for $m = 0.4$. A stronger distortion of the profile (an effect of the jet) is seen at 9 cm downstream of the hole ($z = \pm 2.54$ cm at Stations 2 and 3) for $m = 0.6$ than for $m = 0.4$, which is consisent with the hydrodynamic results. In the blowing region, typically at Station 2, the temperature near the wall for $m = 0.6$ is farther from the wall temperature than for $m = 0.4$. This results in sharper temperature gradient at the wall and produces a high heat transfer rate at the wall. In the recovery region, even at Station 6, profiles for $m = 0.4$ and $m = 0.6$ differ from each other.

The profile for $m = 0.4$ at Station 6 is closer to the no-injection temperature profile. This indicates that the recovery of the temperature profile from the effect of injection is more complete than for $m = 0.6$.

5.4.3 Partial-Coverage with $m = 0.4$

As a representative case of partial coverage, two rows of blowing with $m = 0.4$ was tested for $\theta \simeq 1.0$ (Fig. 5.57). At Station 1 (blown region), three-dimensionality was observed in the inner region ($y/\delta \leq 0.4$) as a result of injection. The shape of profiles at this station is qualitatively the same as those in the blown region for full-coverage cases. By Station 2 (30 cm downstream of the blown region but still inside the curved plate), the three dimensionality is gone, as was seen in the hydrodynamic measurements. In the flat plate region, the profile is close to the no-injection profile [38] at Station 4. The profile probably recovers to the no-injection shape by the end of heated flat plate as do the Stanton number data.

5.4.4 Stanton Number and Temperature Distribution

Measurements of temperature profile were made only for $m = 0.4$ and 0.6 . The results were presented in the previous sections. Here, the results will be listed which were important in explaining the behavior of $St(0)$ and $St(1)$.

1) In the blown region (hot run: $\theta \sim 1.0$), the temperature gradient at the wall appears to be steeper for $m = 0.6$ than for $m = 0.4$, which supports the higher value of $St(1)$ for $m = 0.6$ in the blown region.

2) At the end of the blown region (cold run: $\theta \cong 0.2$) the temperature profile was very distorted near the wall. There was a steep gradient at the wall, supported by a region strongly affected by the injected fluid extending out to y/δ of about 0.2. Beyond that height, the profile was nearly normal. The relaxation of the temperature distribution in this inner region is responsible for the rapid drop of $St(0)$ in Region I of the recovery plate.

3) The temperature distribution with injection (both the hot run and the cold run) approaches that for no-injection as the recovery proceeds. There is a large difference between the profiles for the hot run and no injection run. The hot run needs a long distance for the recovery of the temperature distribution: almost the entire length of the recovery plate. This is why $St(1)$ recovers so slowly. On the other hand, by Station 4 the cold run differs only slightly from the no-injection case, and recovers in a shorter distance. Recovery of the temperature distribution for the cold run appears to be complete by the end of Region II of the recovery plate.

4) The profile for the cold run at Station 6 appears to collapse to the no-injection profile, indicating that recovery of the temperature distribution has been completed. On the other hand, for the hot run, the temperature profile has not recovered by Station 6: further evidence of the slow recovery of $St(1)$ toward the no-injection value.

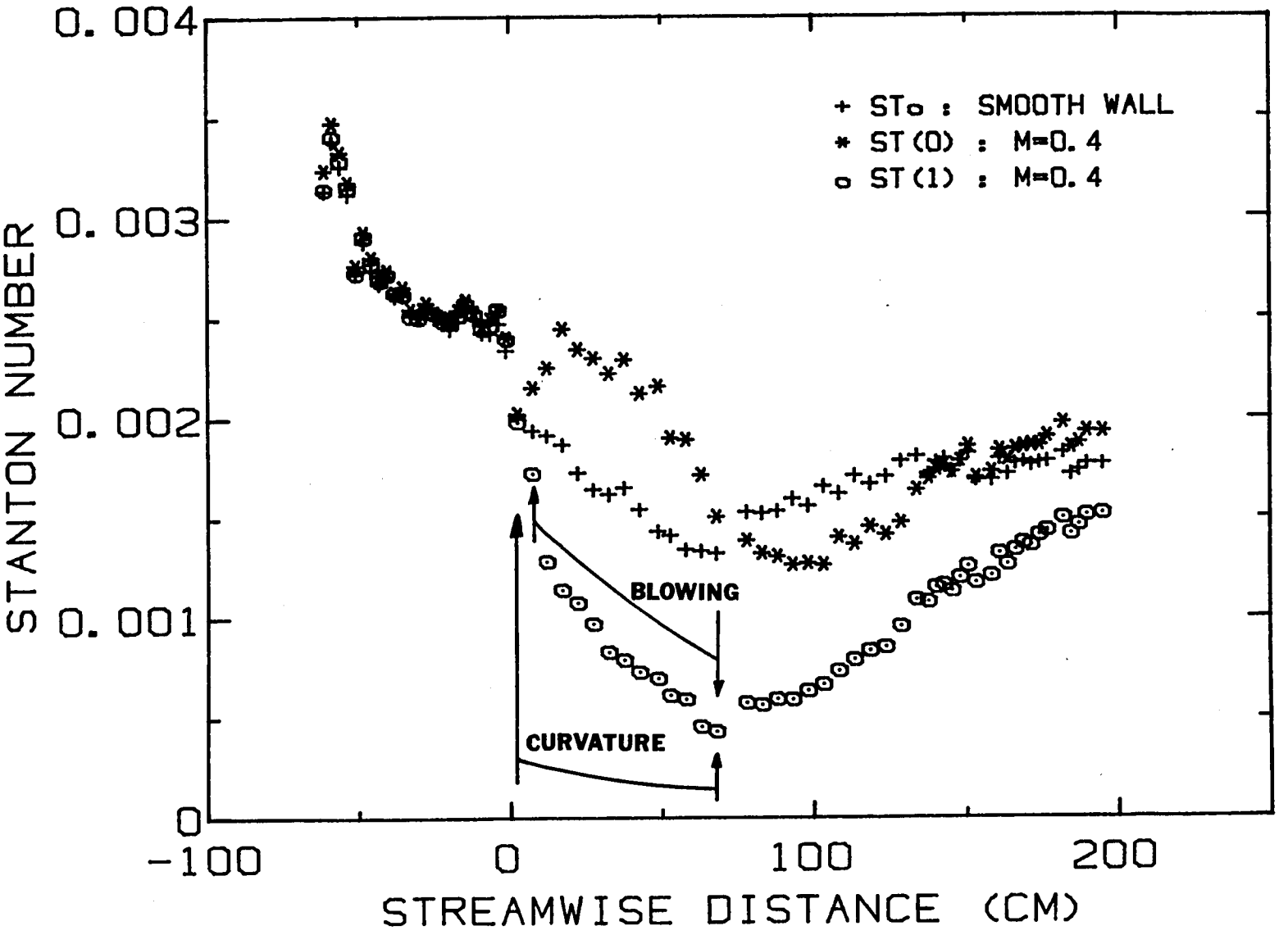

Fig. 5.1. Stanton number for full-coverage cooling with m = 0.4

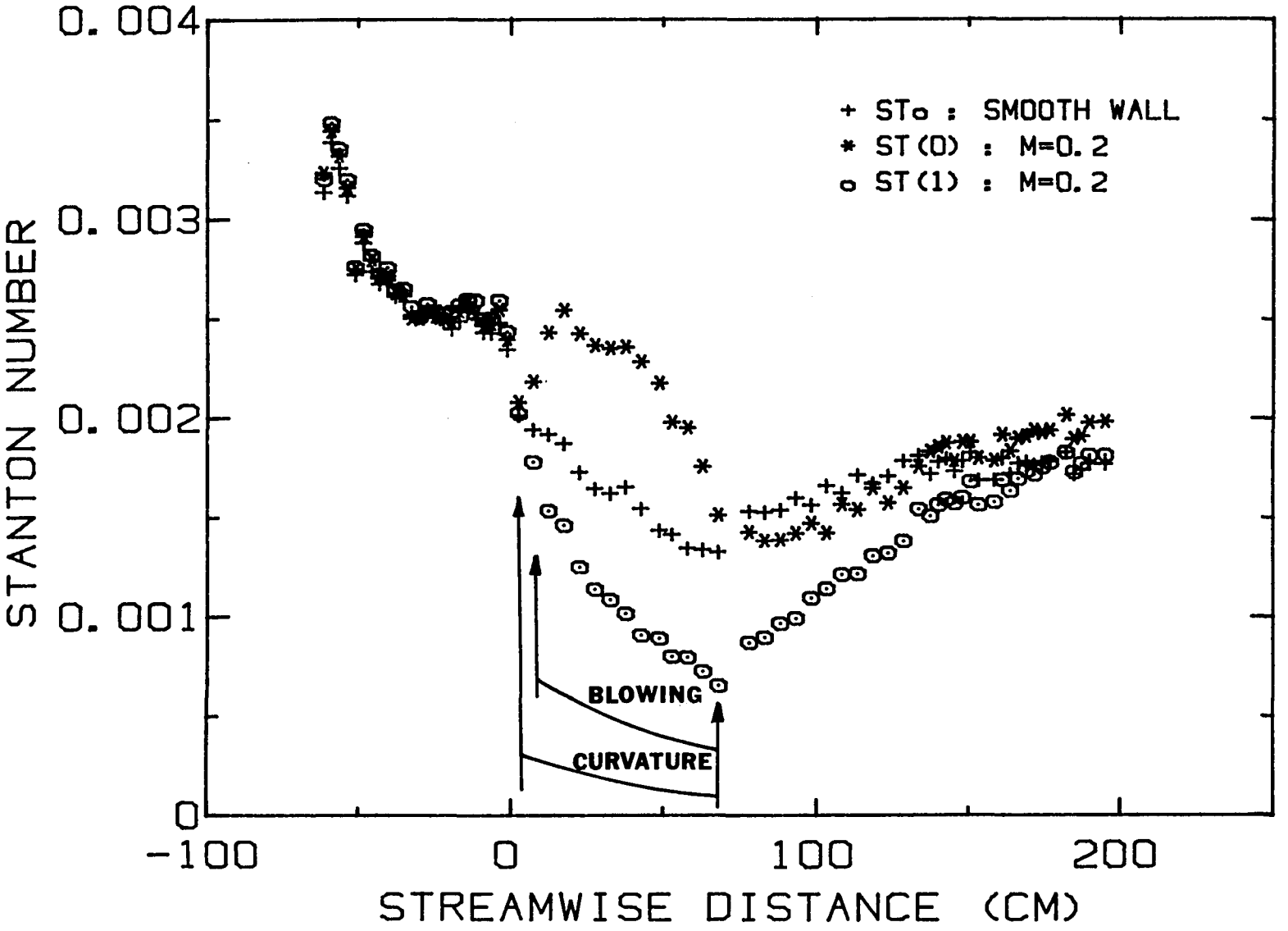

Fig. 5.2. Stanton number for full-coverage cooling with m = 0.2

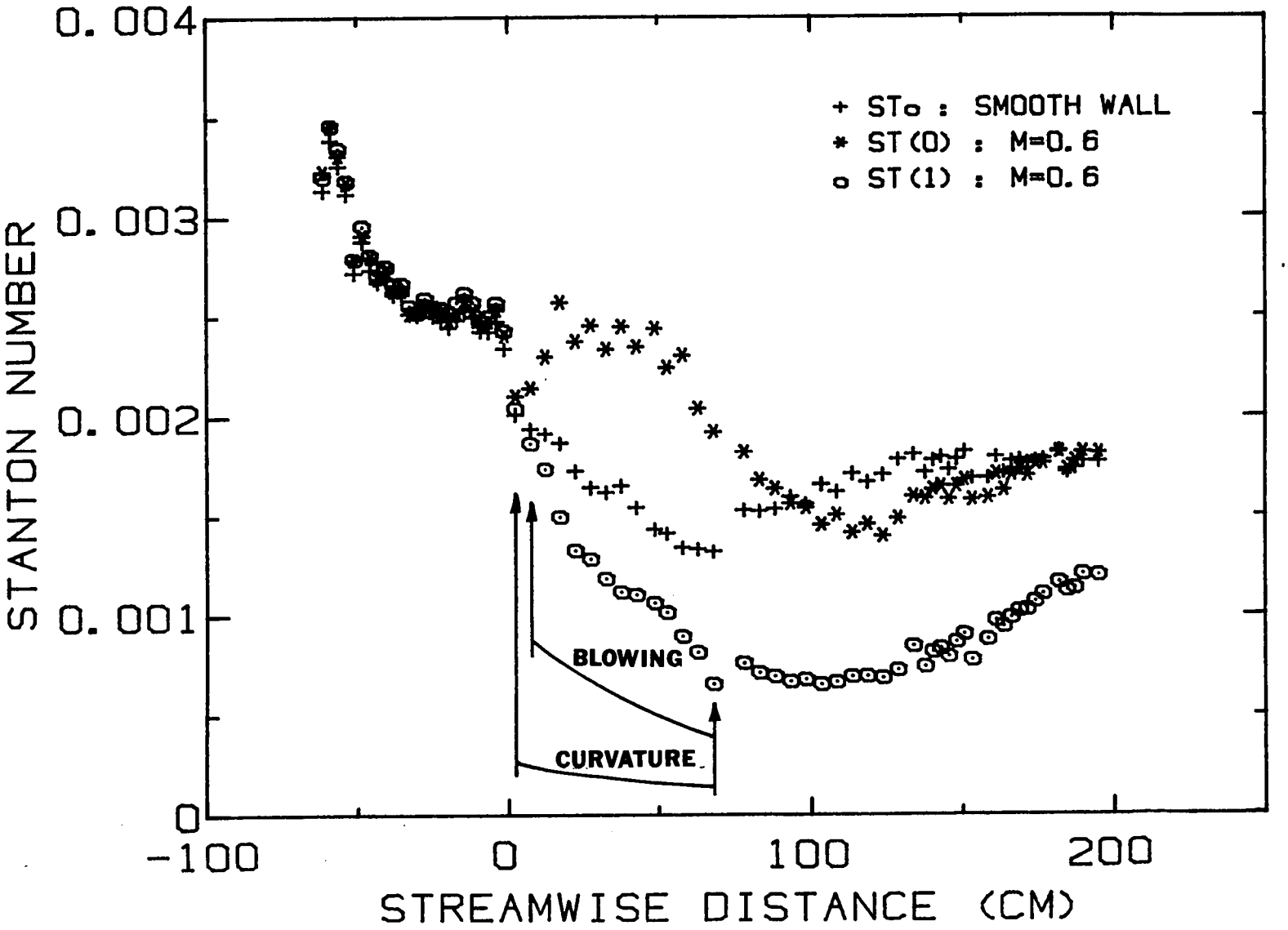

Fig. 5.3. Stanton number for full-coverage cooling with m = 0.6

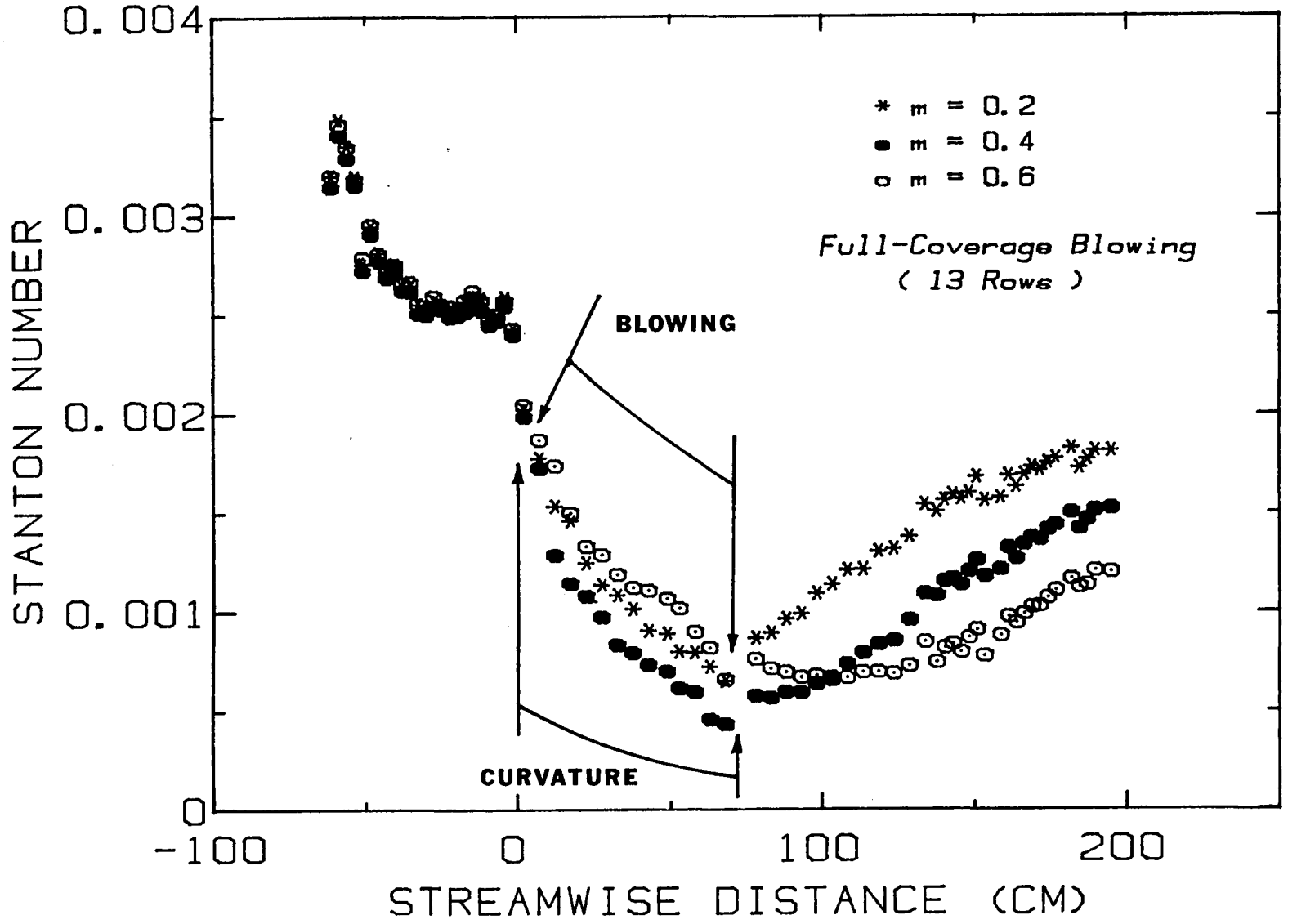

Fig. 5.4. Stanton number with $T_2 = T_2$ ($\theta = 1.0$) for full-coverage cooling: m = 0.2, 0.4, and 0.6

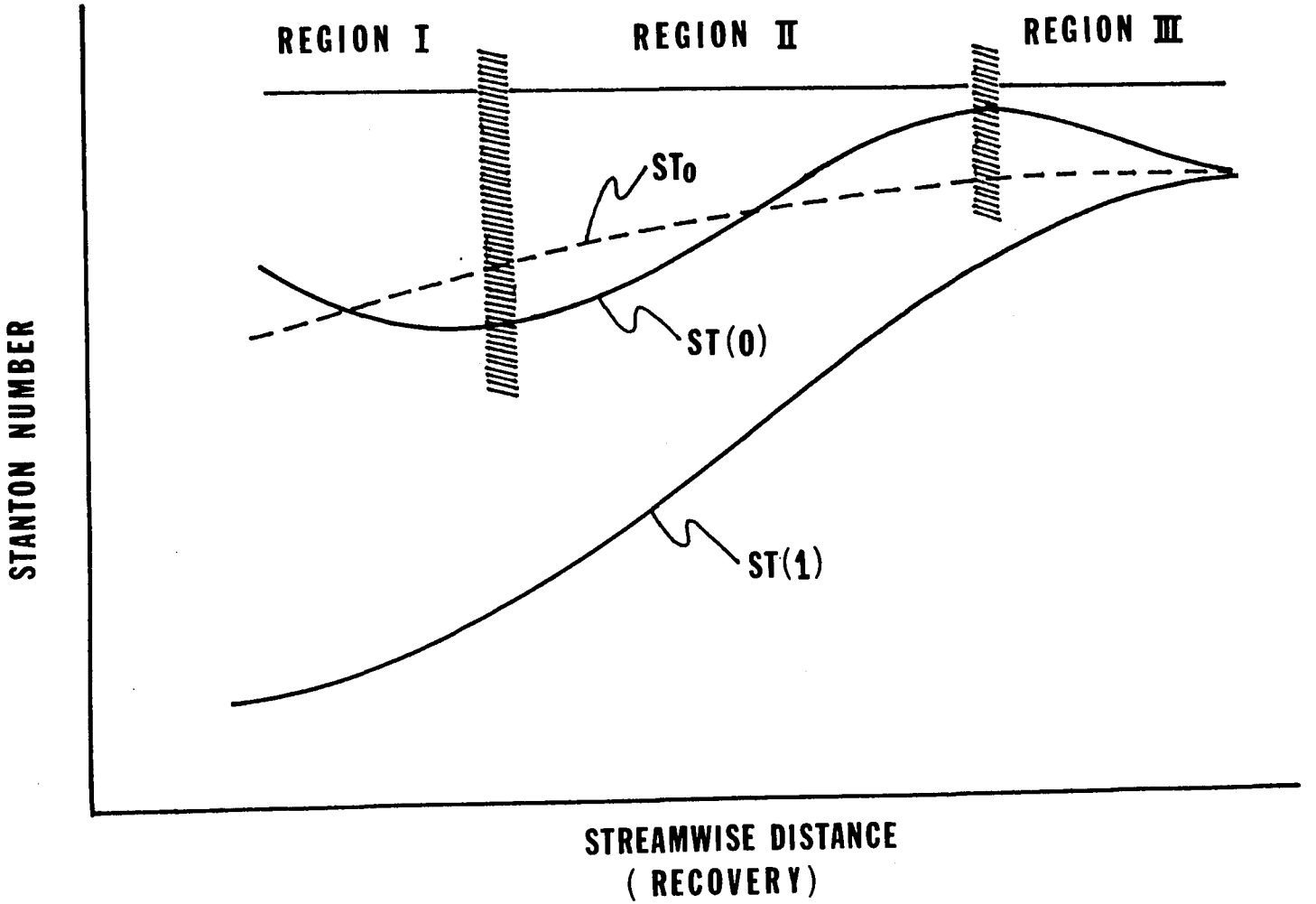

Fig. 5.5. Recovery process of Stanton number on a flat plate after full-coverage cooling on a convex surface

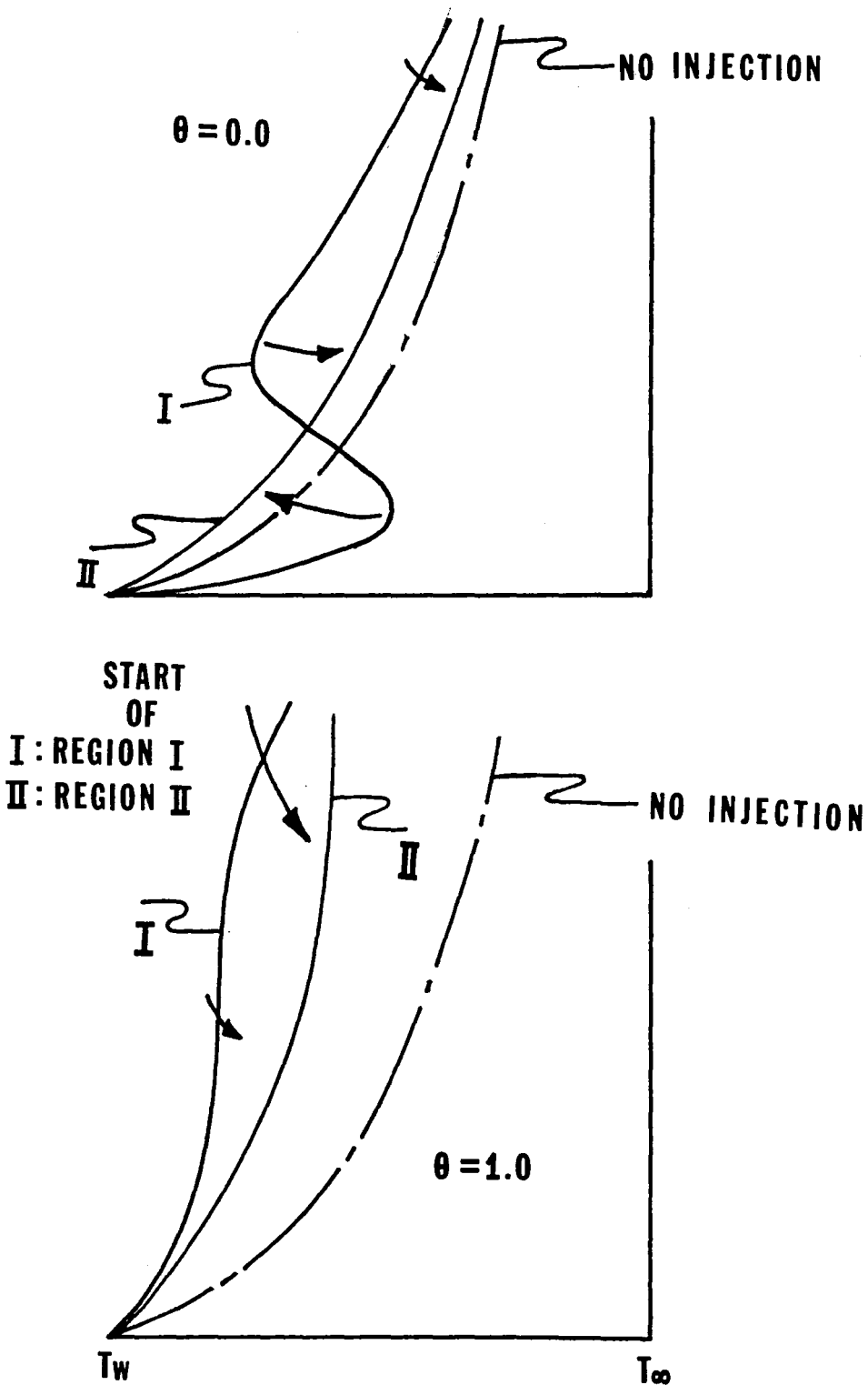

Fig. 5.6. Recovery process of temperature distribution on a flat plate after full-coverage cooling on a convex surface

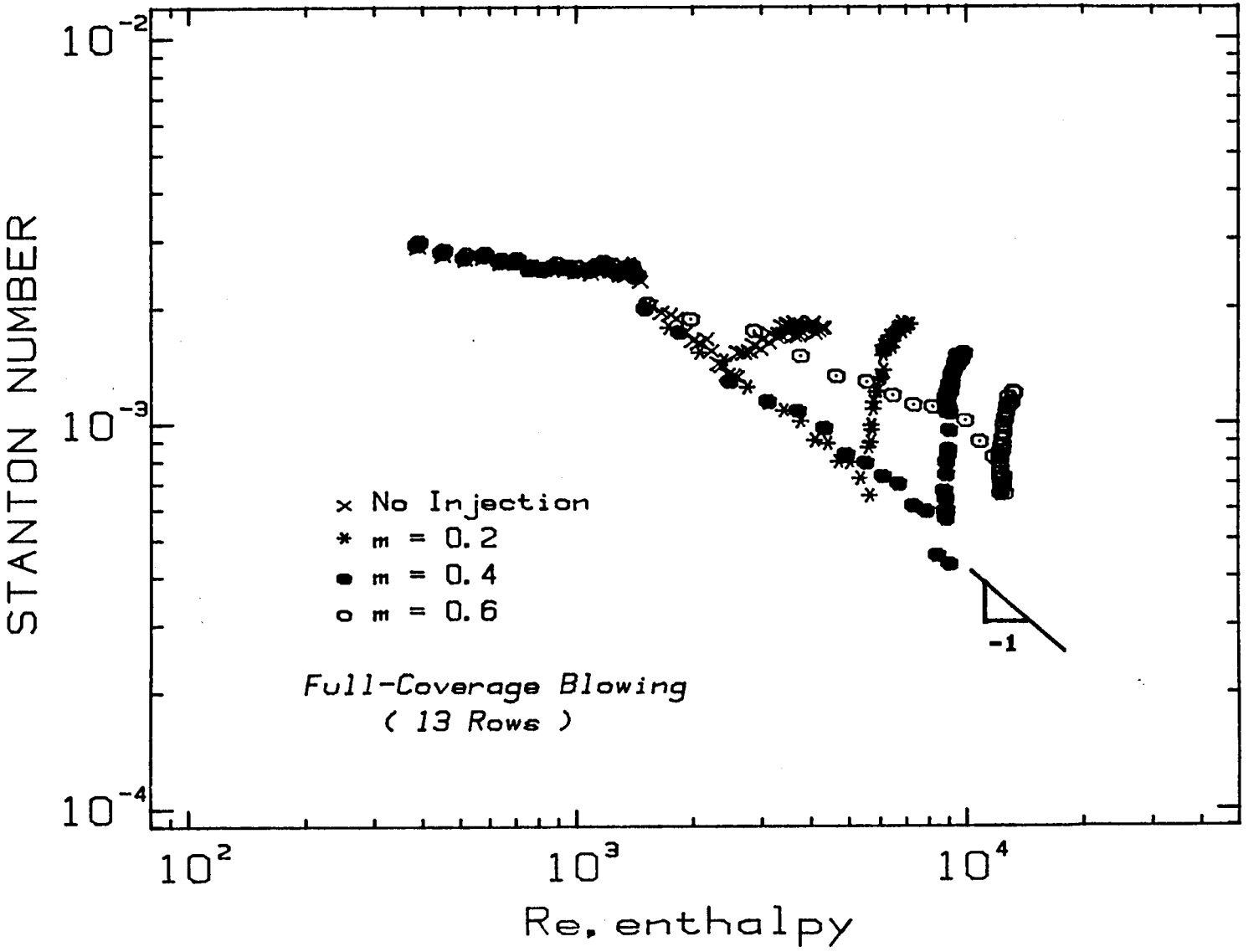

Fig. 5.7. Stanton number with $T_2 = T_w$ ($\theta = 1.0$) for full-coverage cooling: m = 0.2, 0.4, and 0.6, on St - Re coordinates.

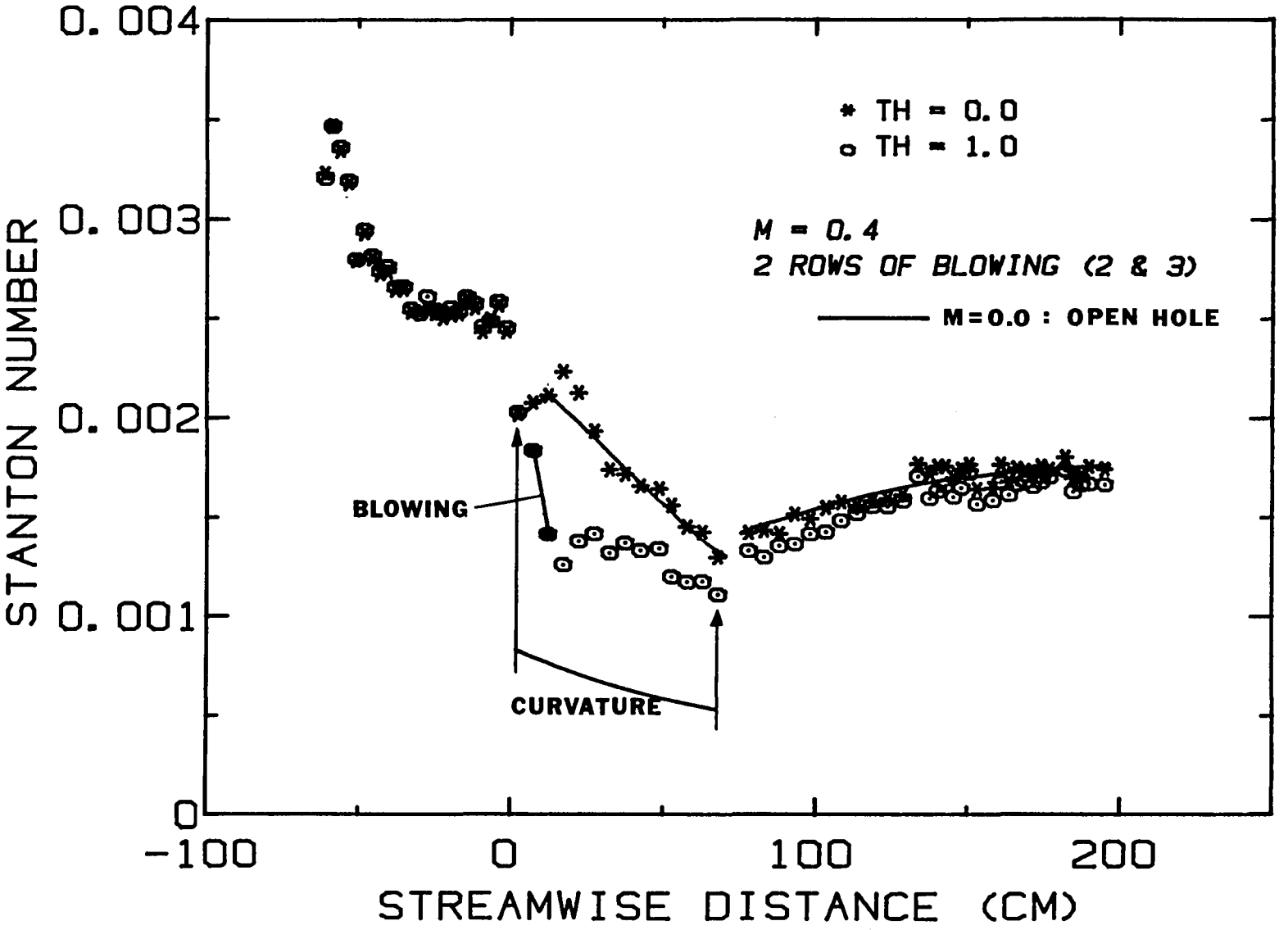

Fig. 5.8. Stanton number for partial-coverage cooling (two rows of injectin) with m = 0.4

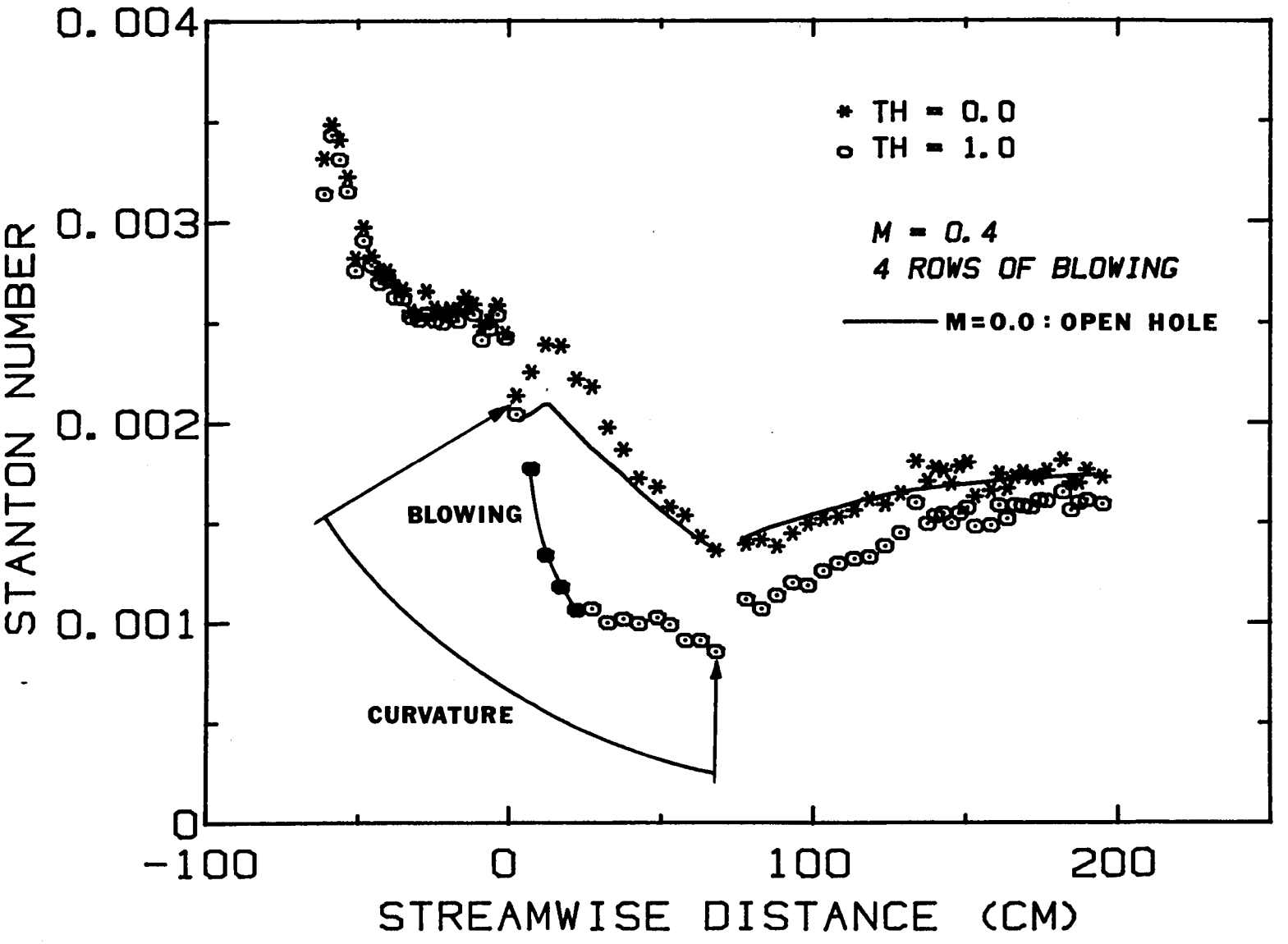

Fig. 5.9. Stanton number for partial-coverage cooling (four rows of injection) with m = 0.4

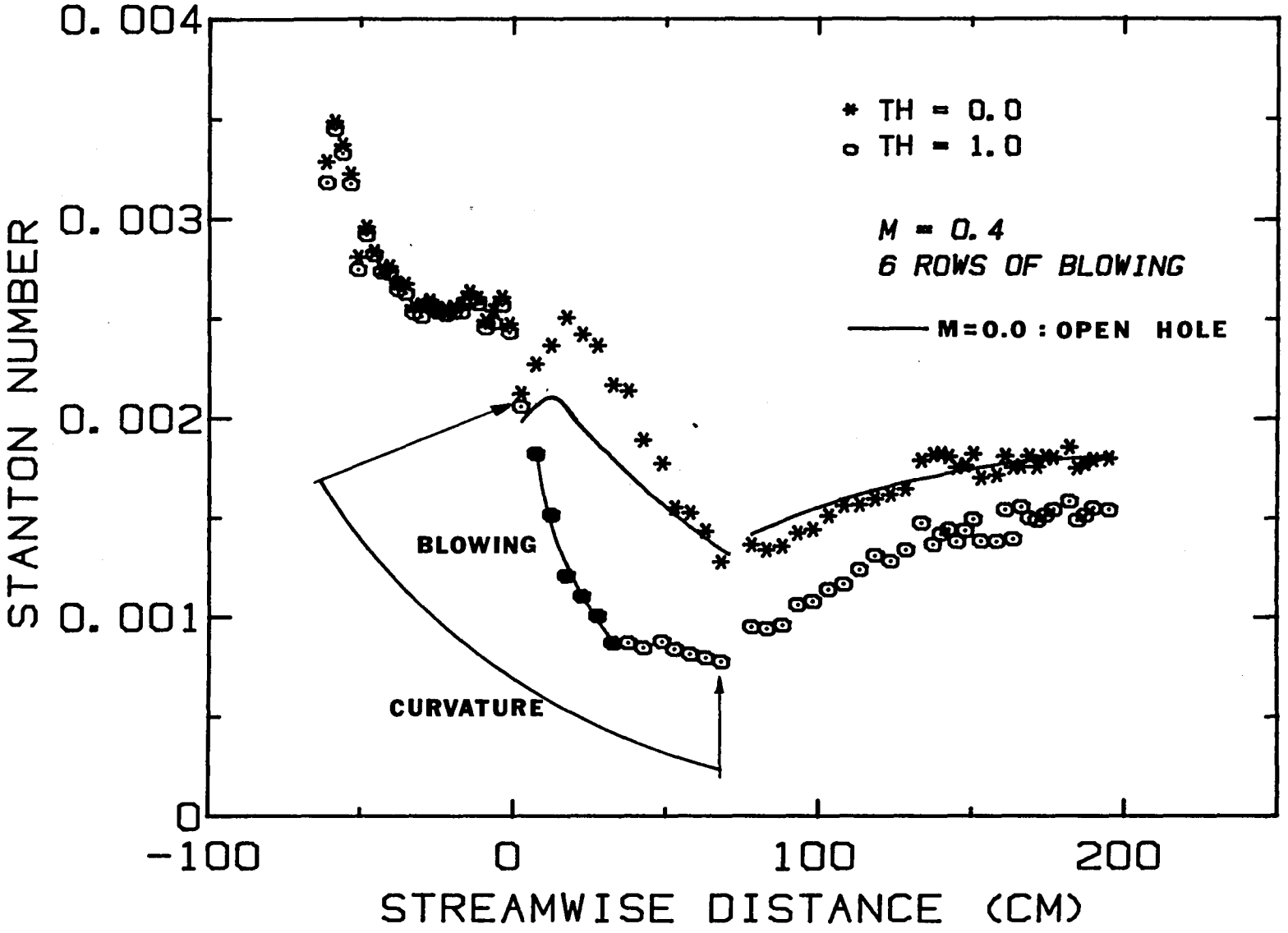

Fig. 5.10. Stanton number for partial-coverage cooling (six rows of injection) with m = 0.4

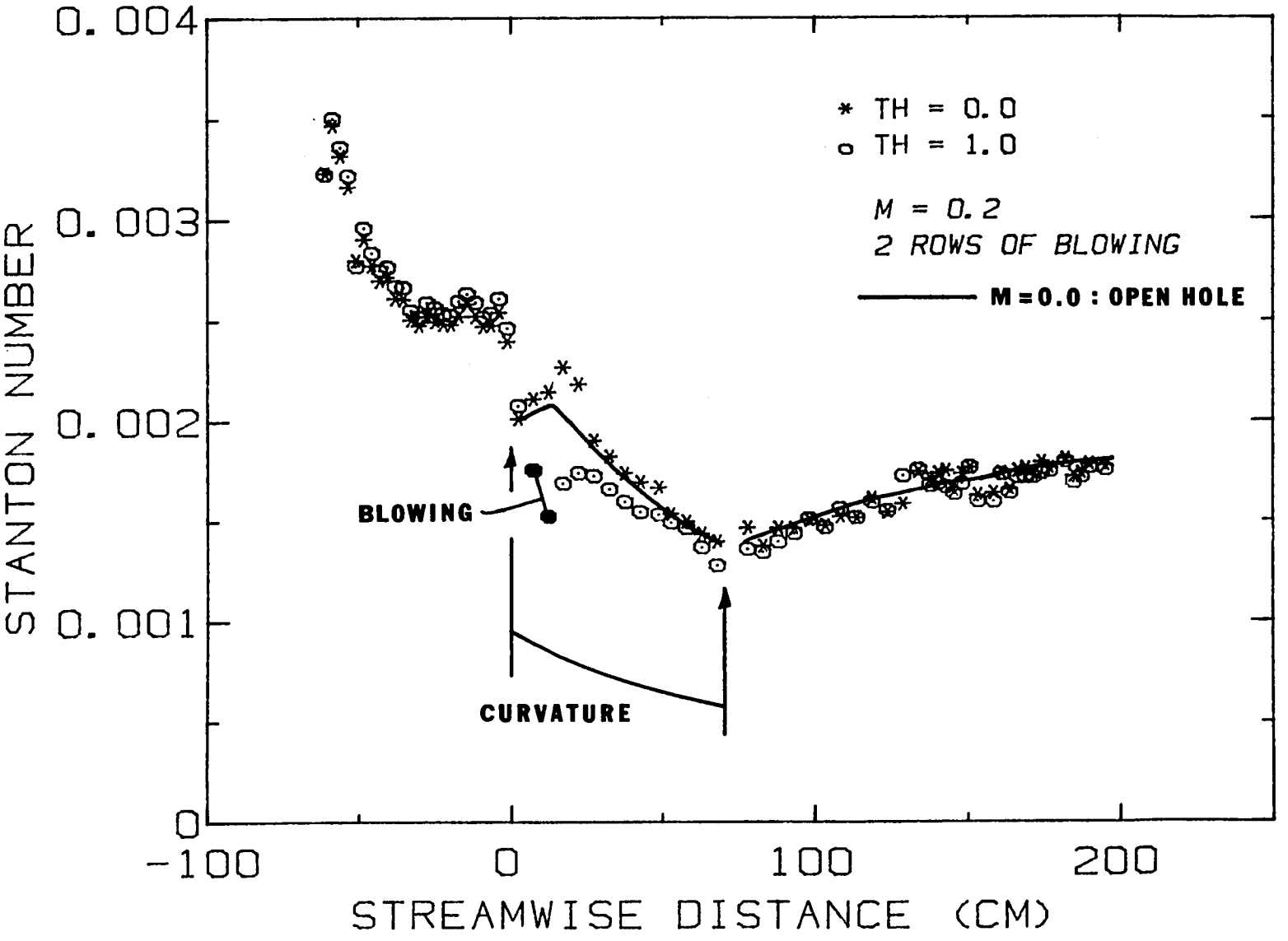

Fig. 5.11. Stanton number for partial-coverage cooling (two rows of injection) with m = 0.2

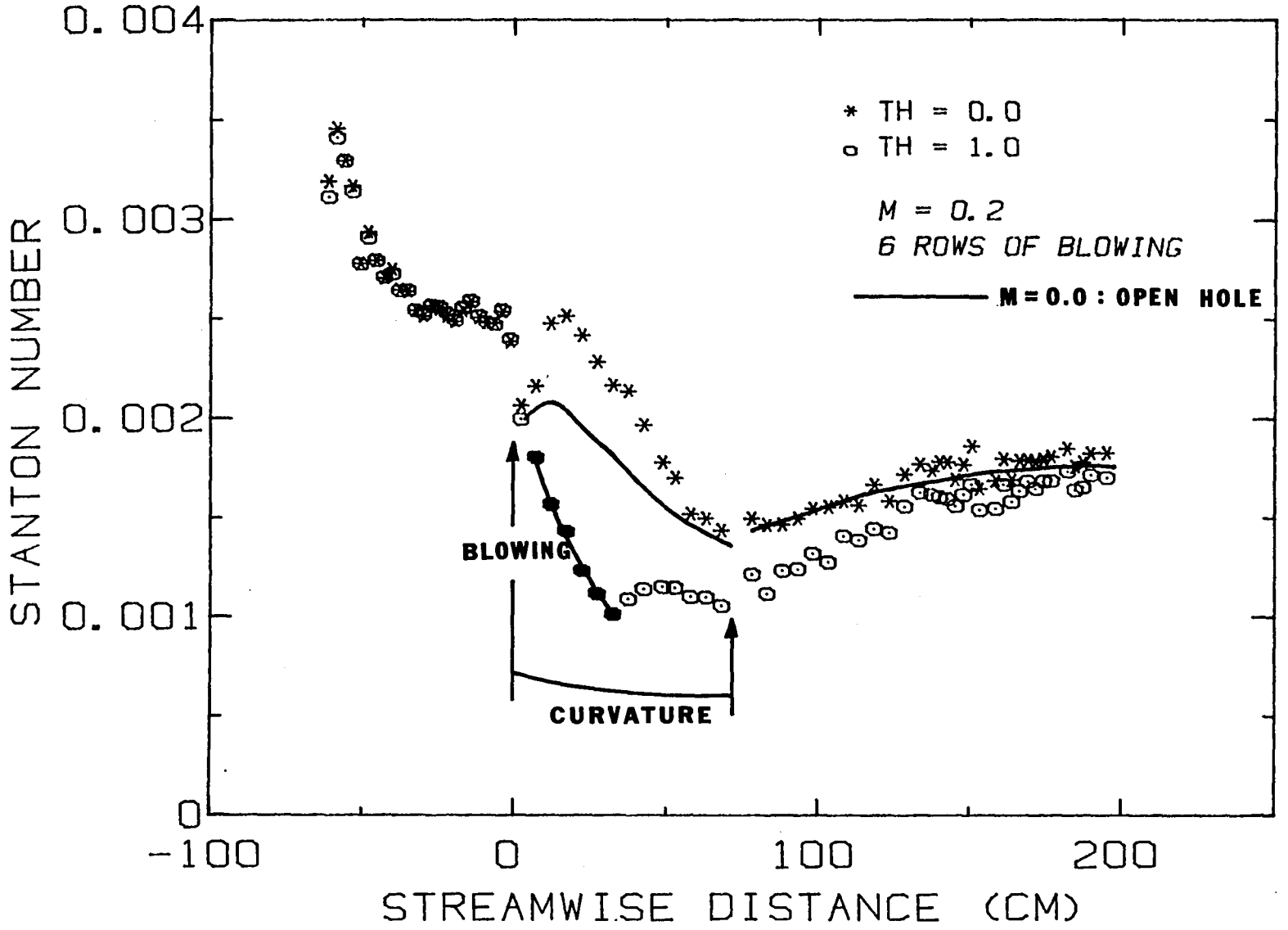

Fig. 5.12. Stanton number for partial-coverage cooling (six rows of injection) with m = 0.2

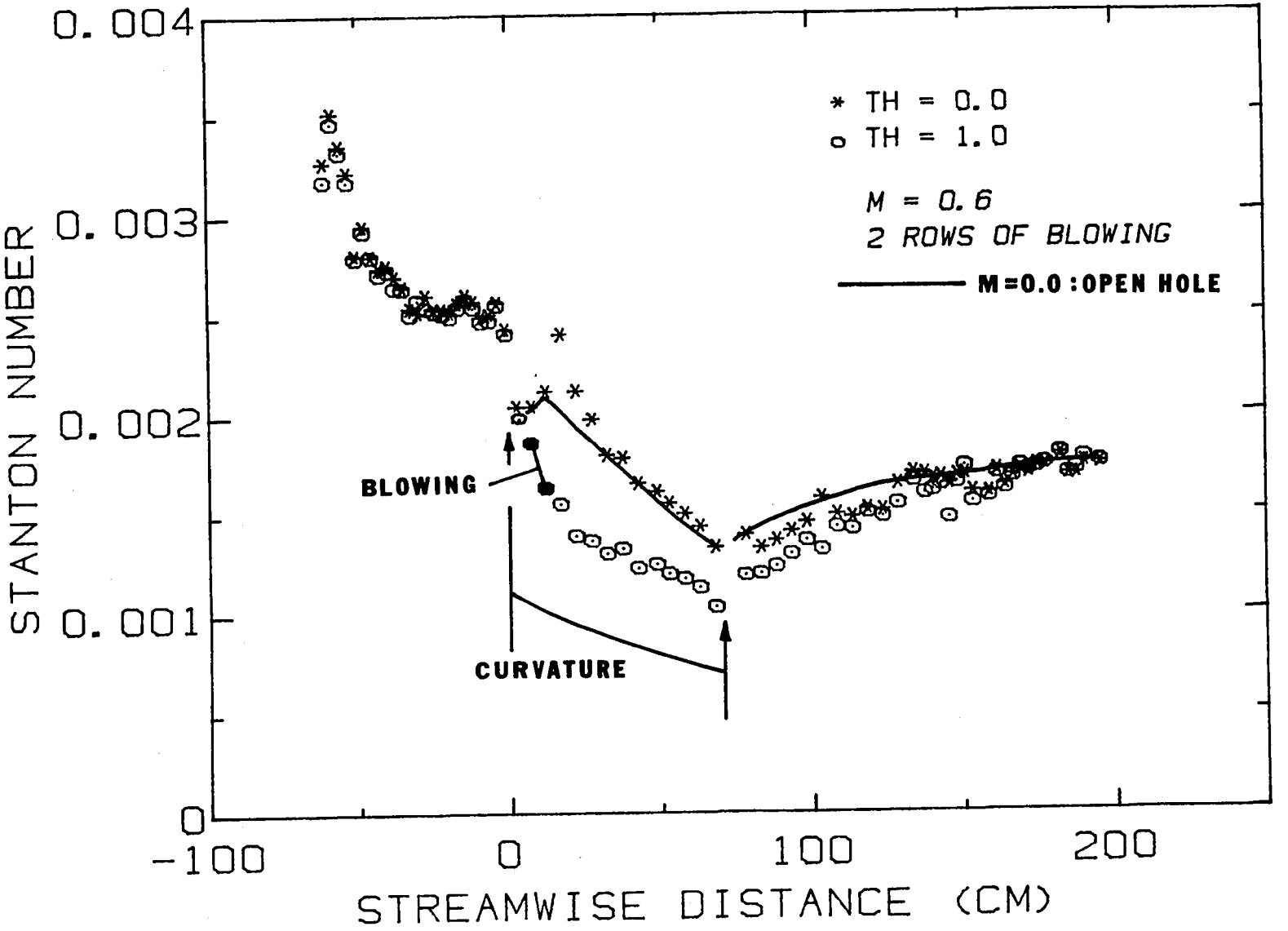

Fig. 5.13. Stanton number for partial-coverage cooling (two rows of injection) with m = 0.6

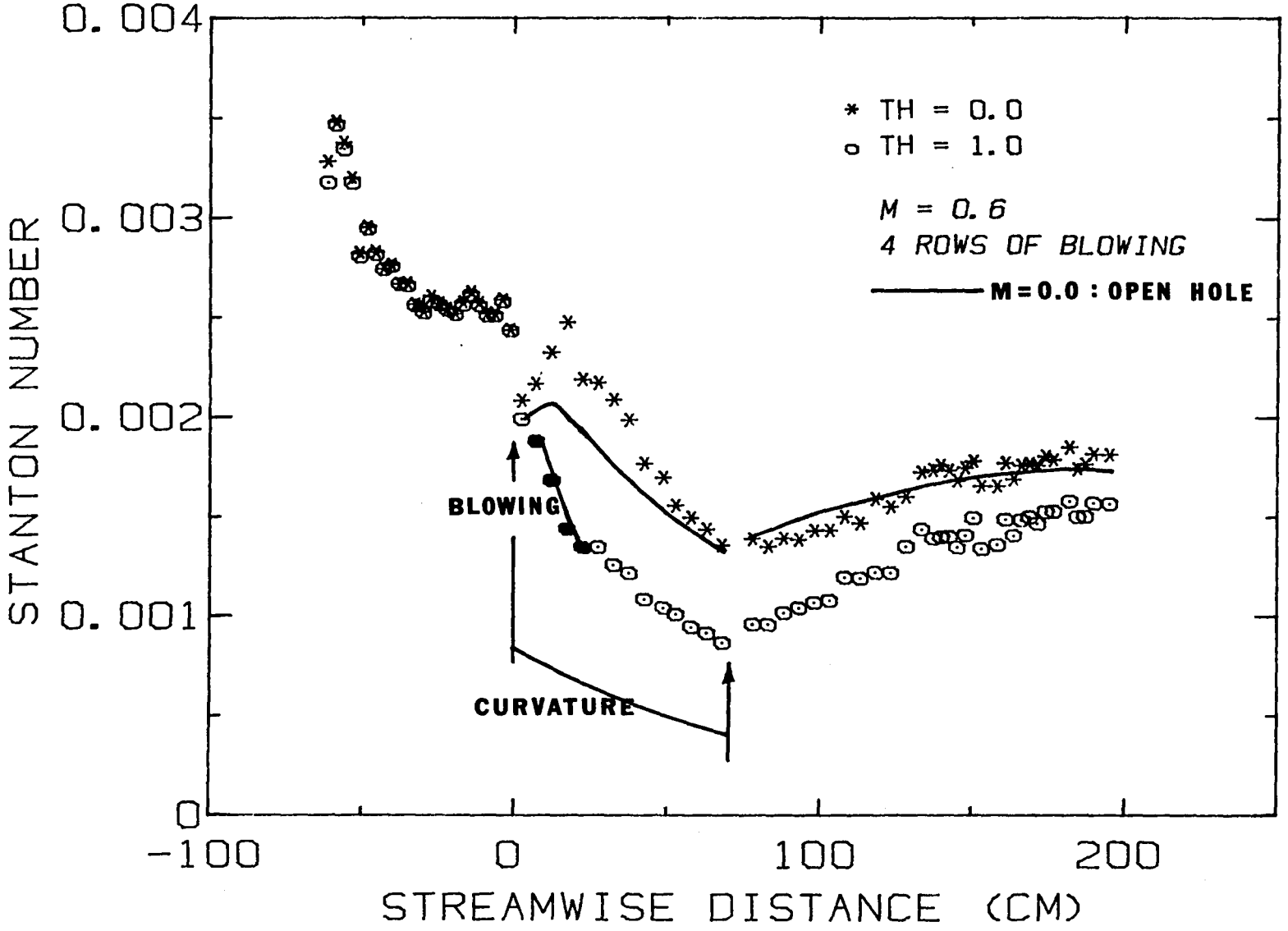

Fig. 5.14. Stanton number for partial-coverage cooling (four rows of injection) with m = 0.6

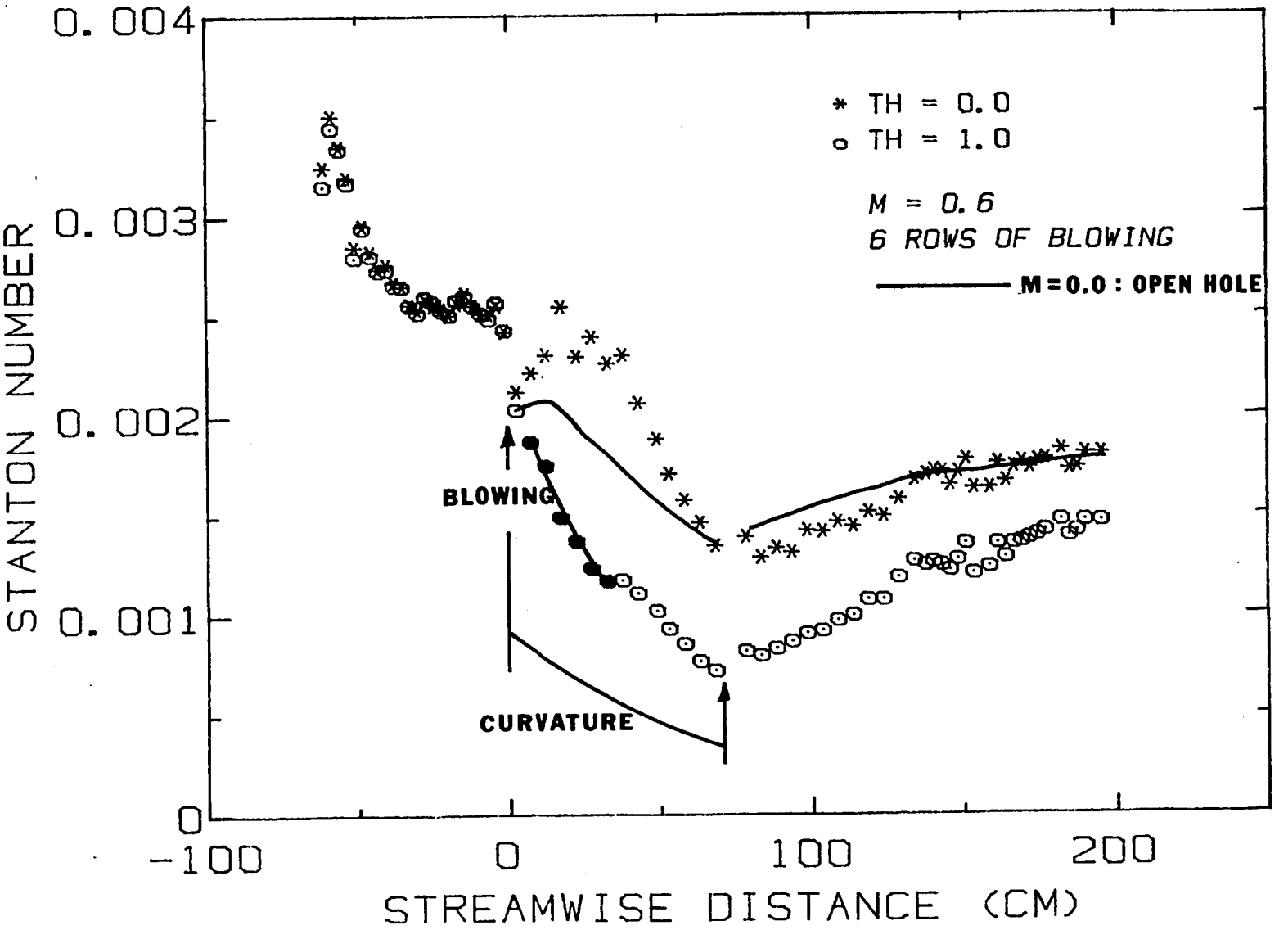

Fig. 5.15. Stanton number for partial-coverage cooling (six rows of injection) with m = 0.6

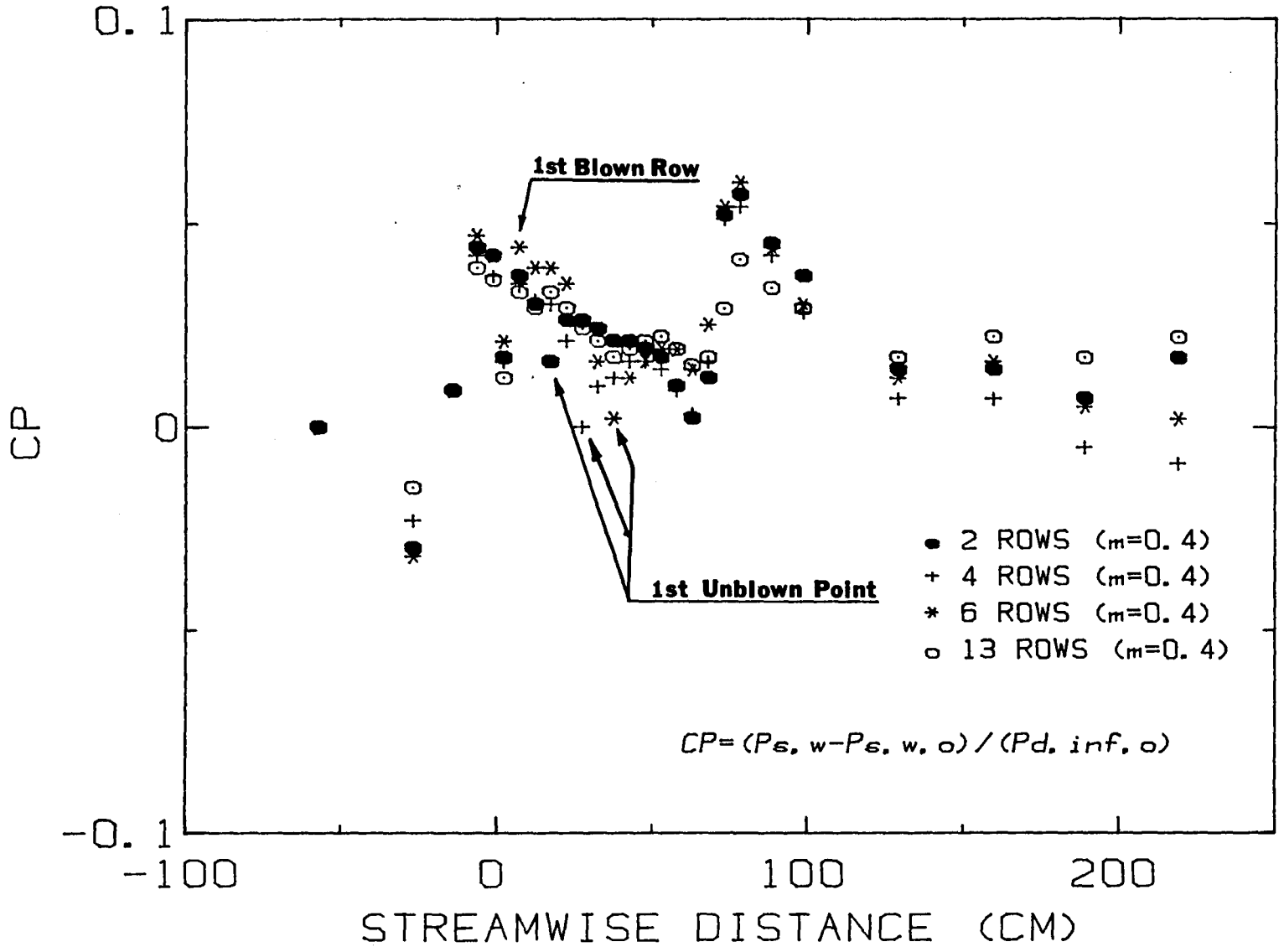

Fig. 5.16a. Wall static-pressure distribution for full- and partial-coverage cooling (two, four, and six rows) with m = 0.4

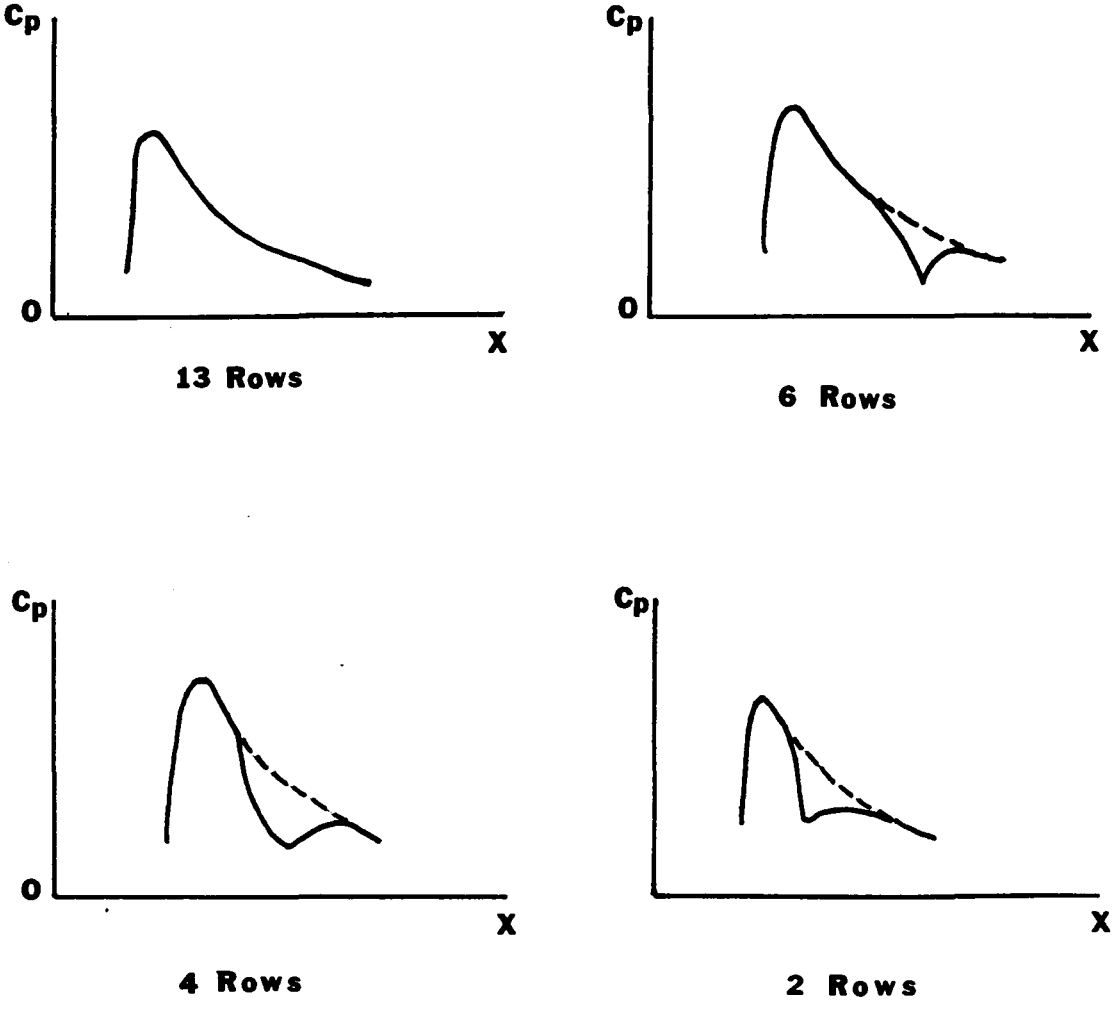

Fig. 5.16b. Illustration of the wall static-pressure distribution inside the injection region for full- and partial-coverage cooling

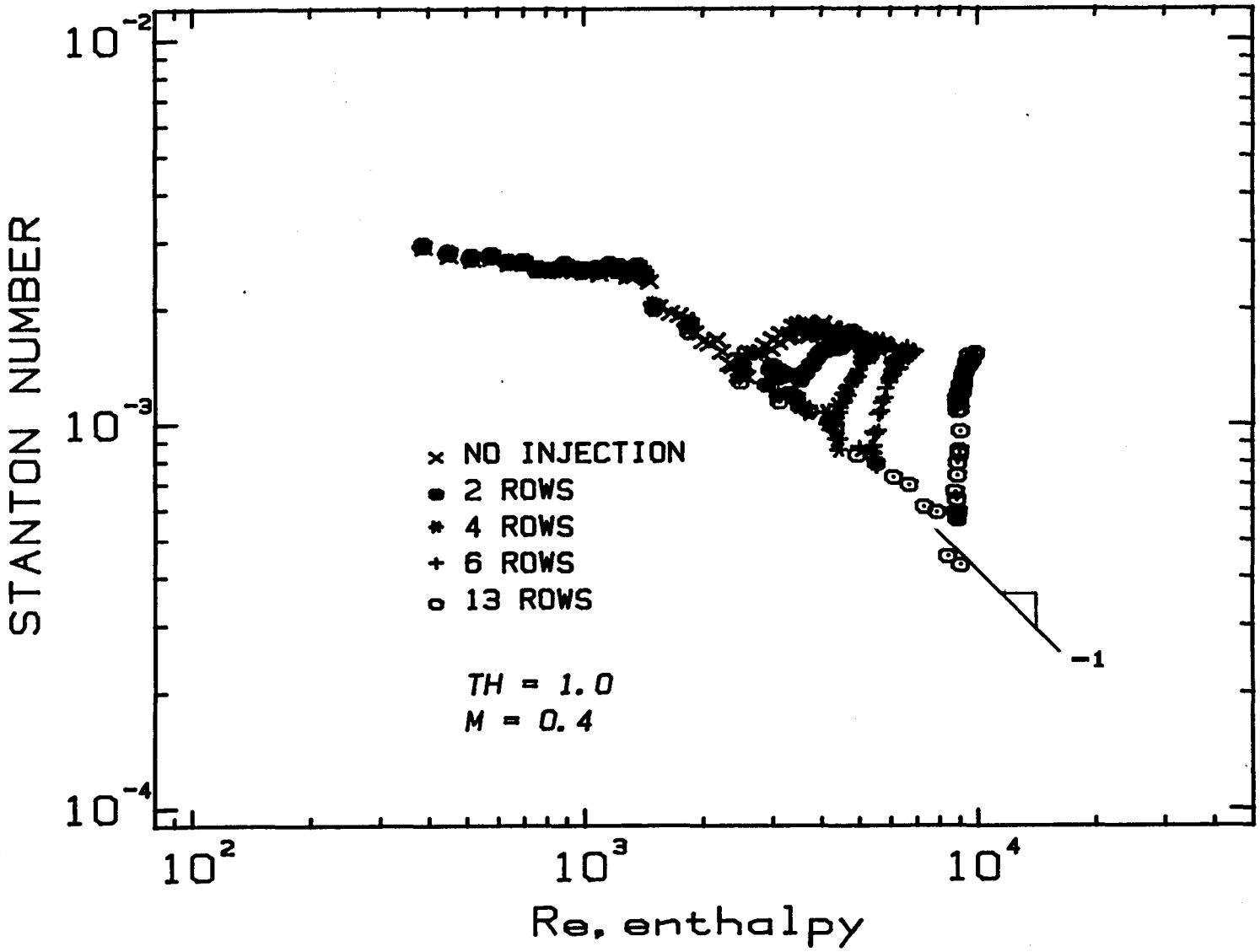

Fig. 5.17. Stanton numbr with $T_2 = T_w$ ($\theta = 1.0$) for full- and partial-coverage cooling: m = 0.4, on St-Re_{Δ_2} coordinates

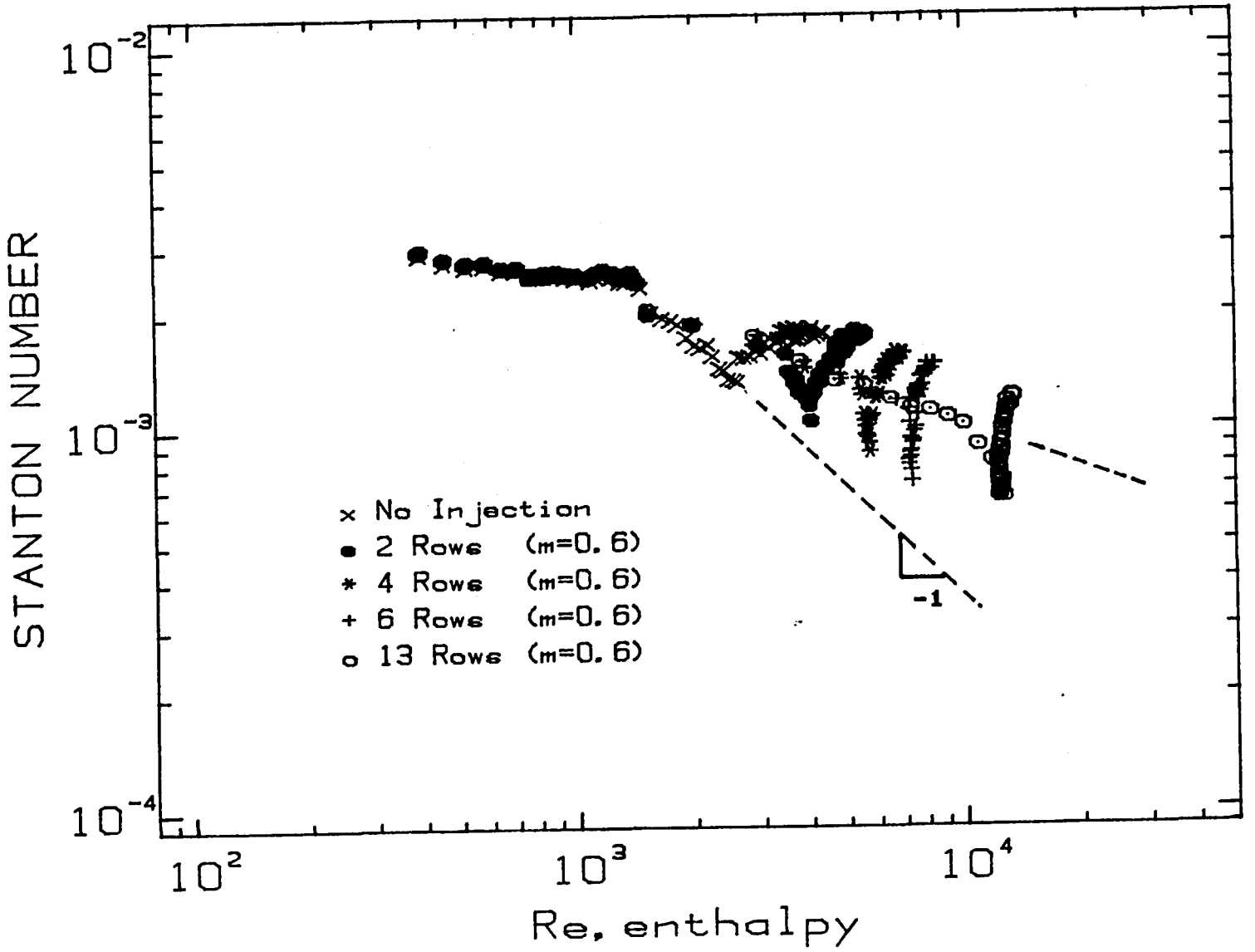

Fig. 5.18. Stanton number with $T_2 = T_w$ ($\theta = 1.0$) for full- and partial-coverage cooling: m = 0.6, on St-Re_{Δ_2}

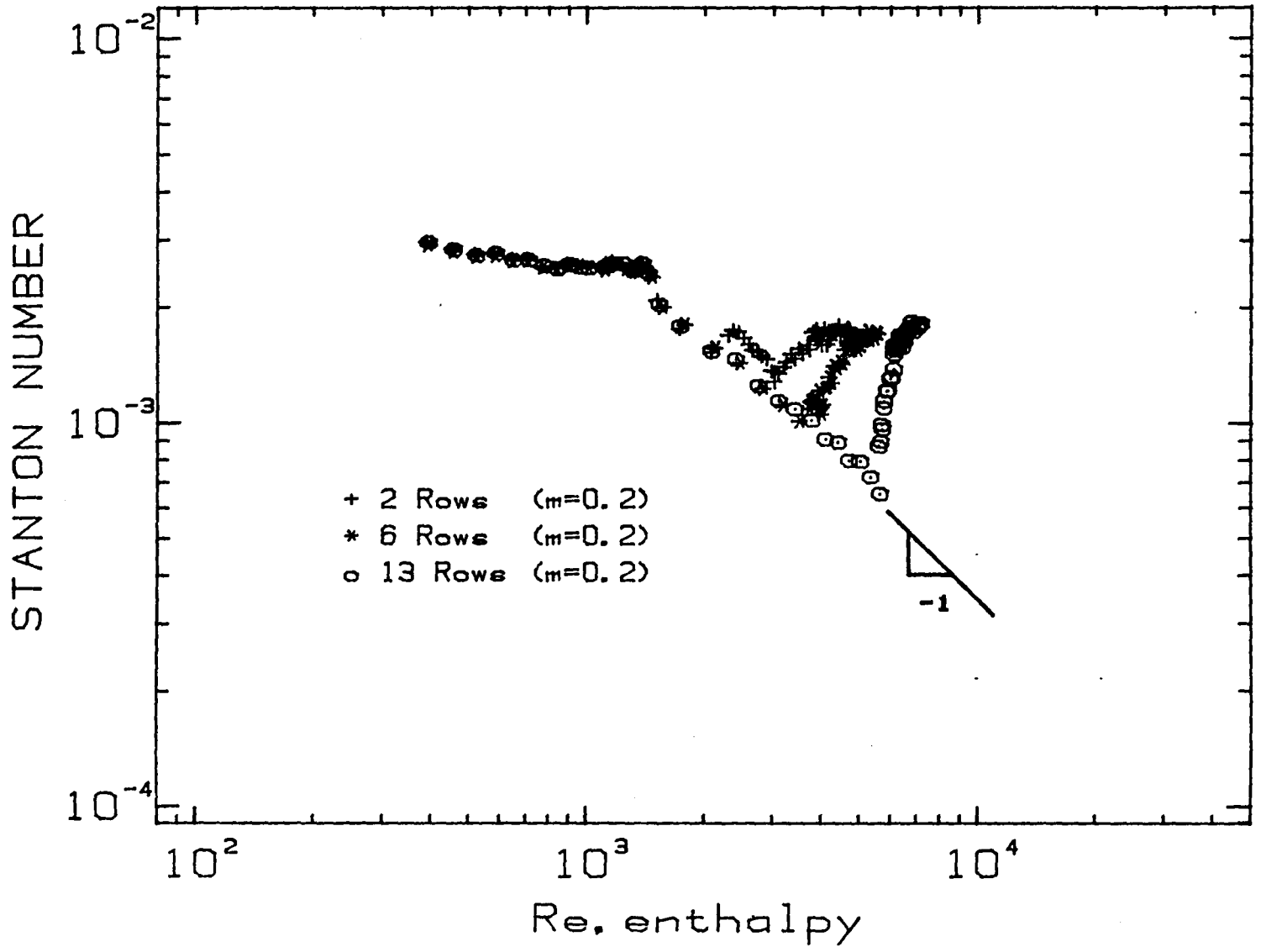

Fig. 5.19. Stanton number with $T_2 = T_w$ ($\theta = 1.0$) for full- and partial coverage cooling: m = 0.2, on St-Re_{Δ_2} coordinates

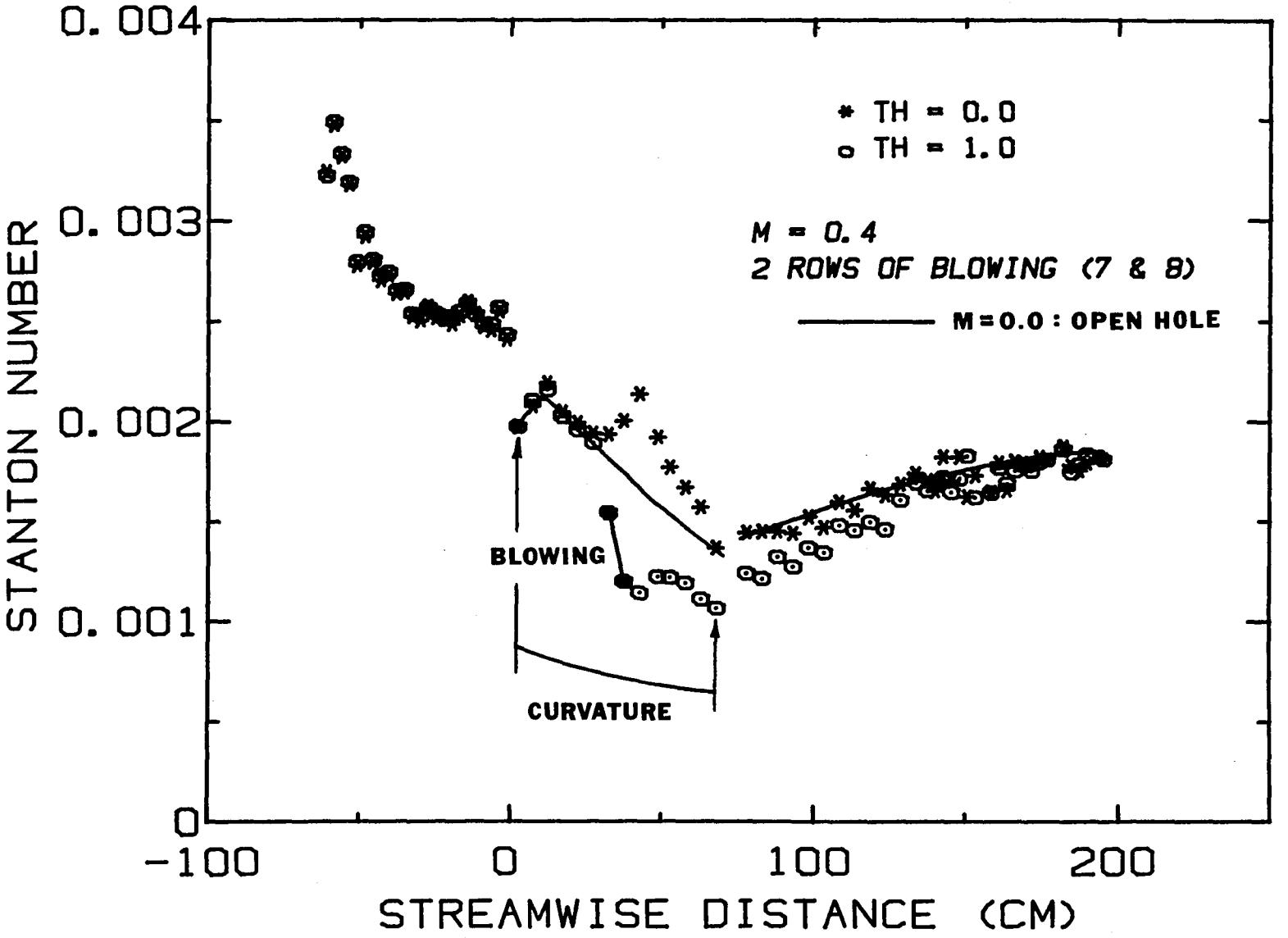

Fig. 5.20. Stanton number for two rows of injection with m = 0.4: injection rows located in the middle of the curved plate

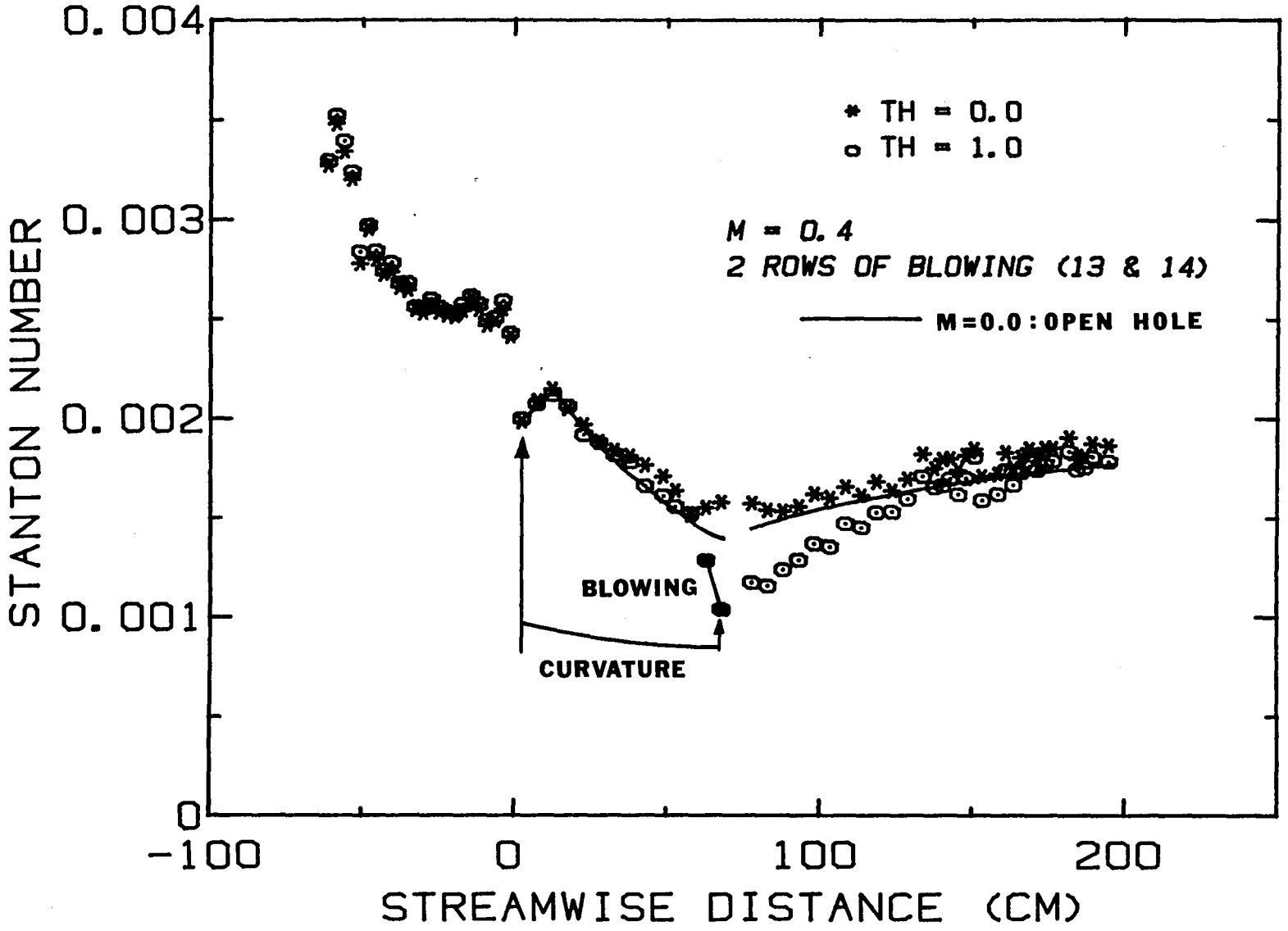

Fig. 5.21. Stanton number for two rows of injection with m = 0.4: injection rows located at the end of the curved plate

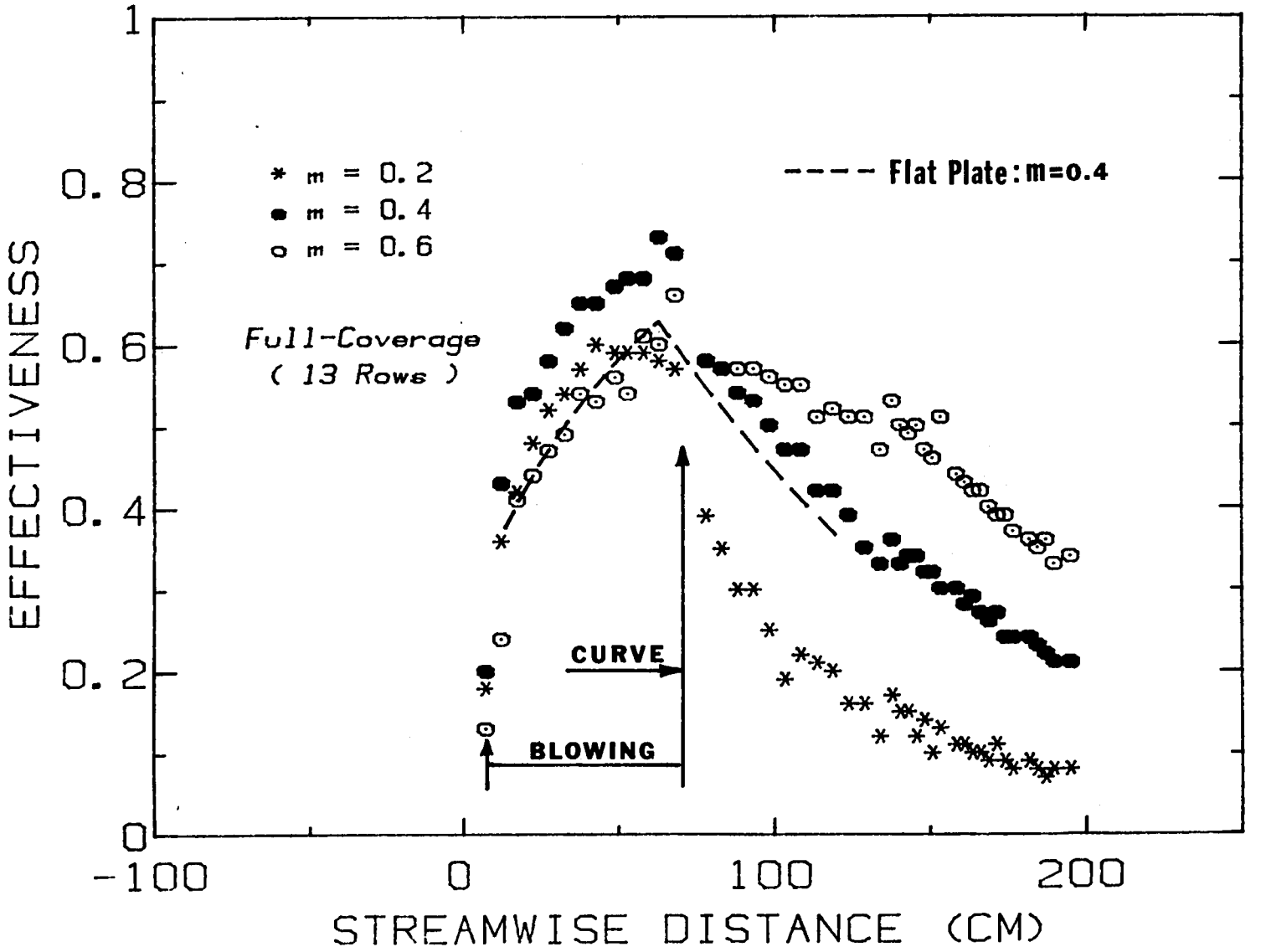

Fig. 5.22. Film-cooling effectiveness for full-coverage cooling: m = 0.2, 0.4, and 0.6

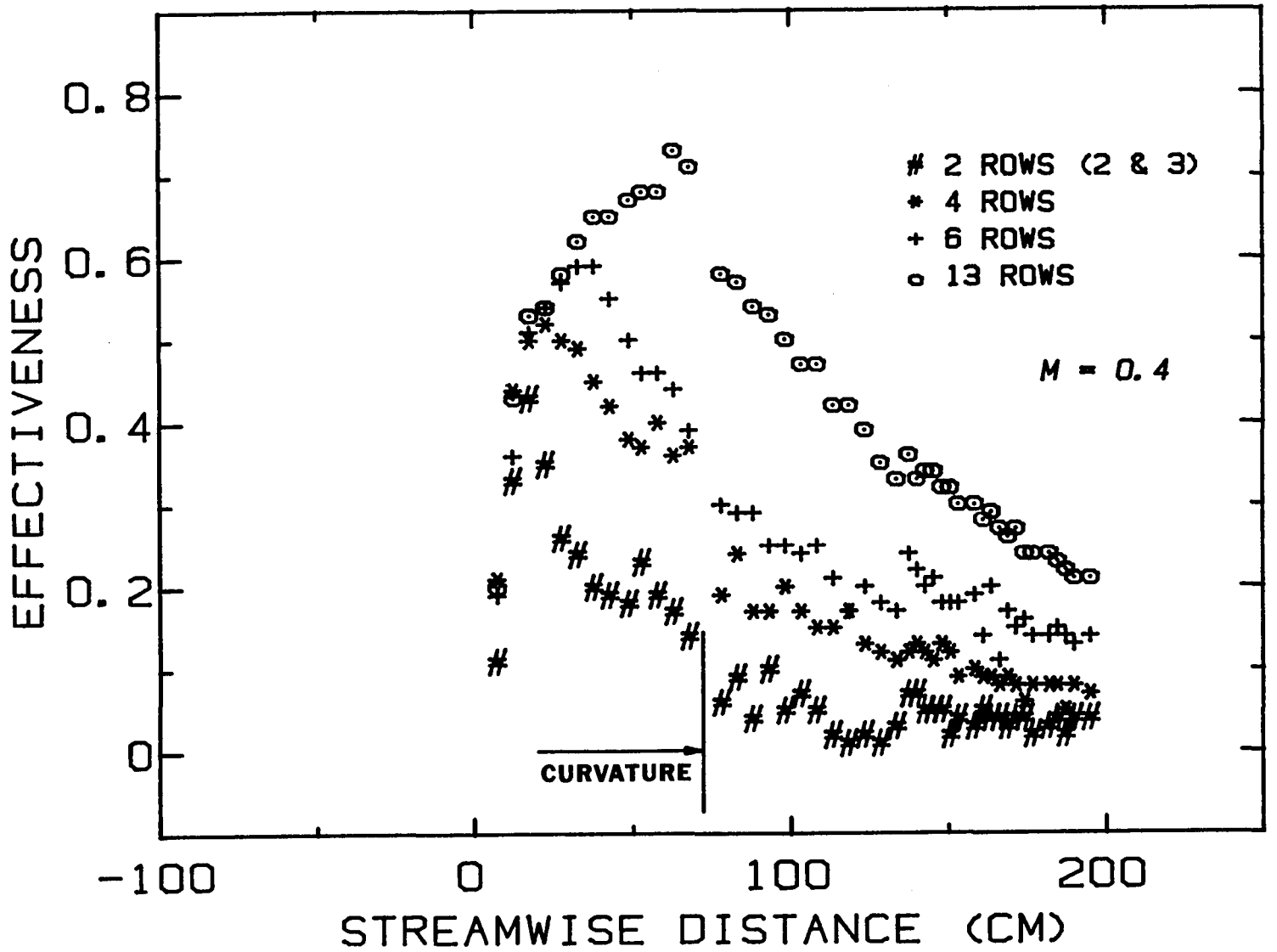

Fig. 5.23. Film-cooling effectiveness for full- and partial-coverge cooling with m = 0.4

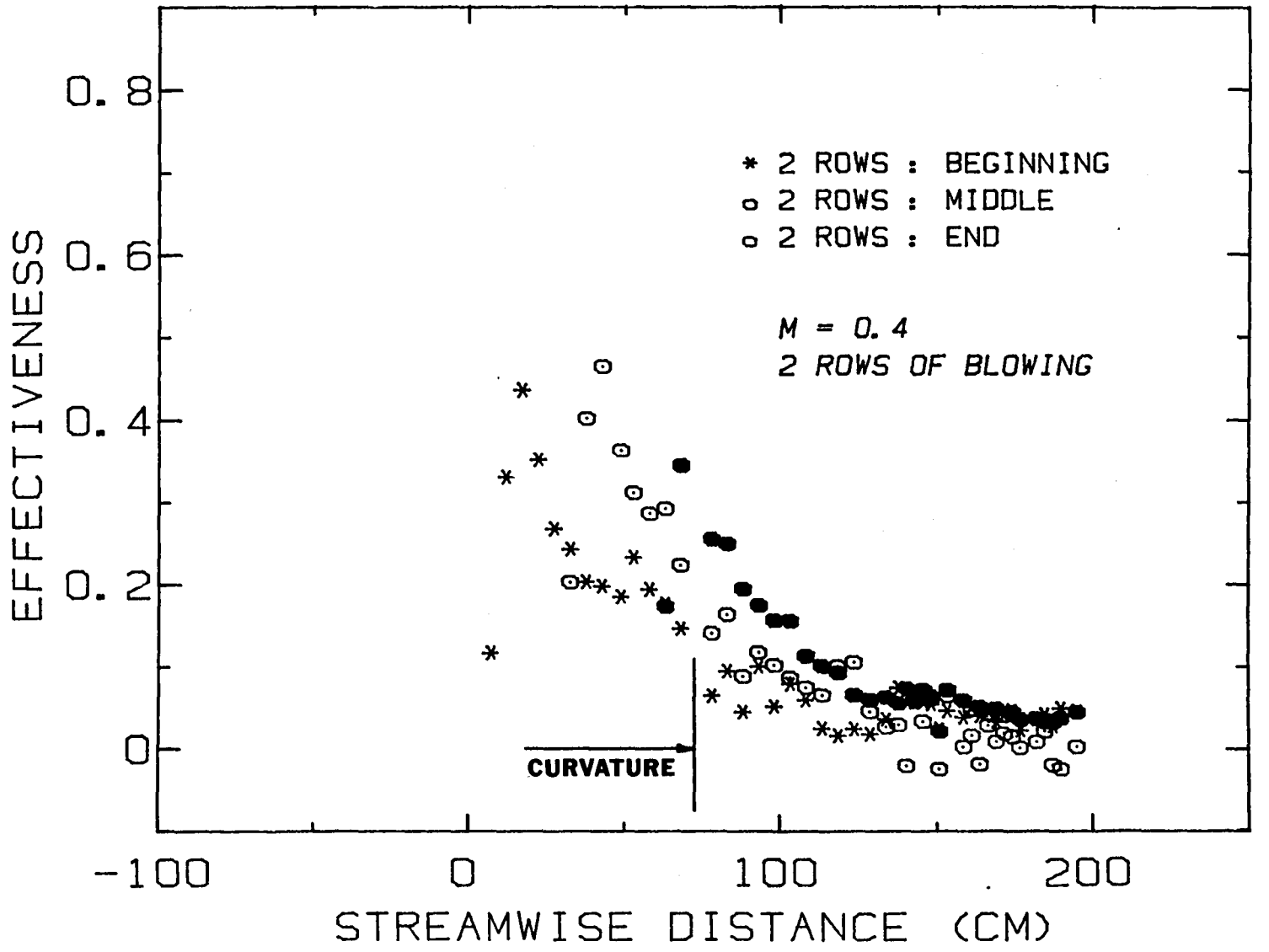

Fig. 5.24. Film-cooling effectiveness for two rows of injection: beginning, middle, and end of curved plate

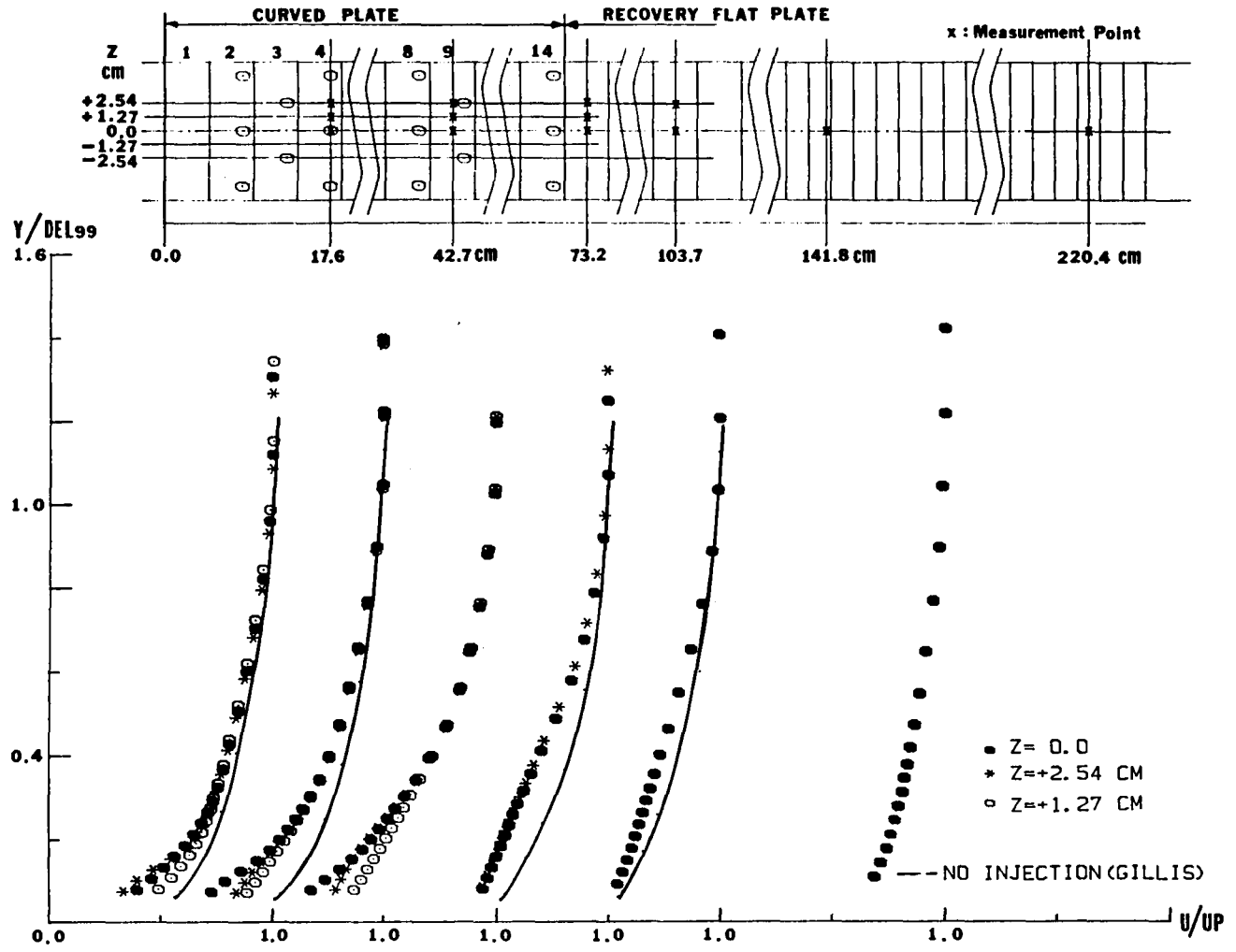

Fig. 5.25. Mean velocity profiles (U) for full-coverage cooling with m = 0.2

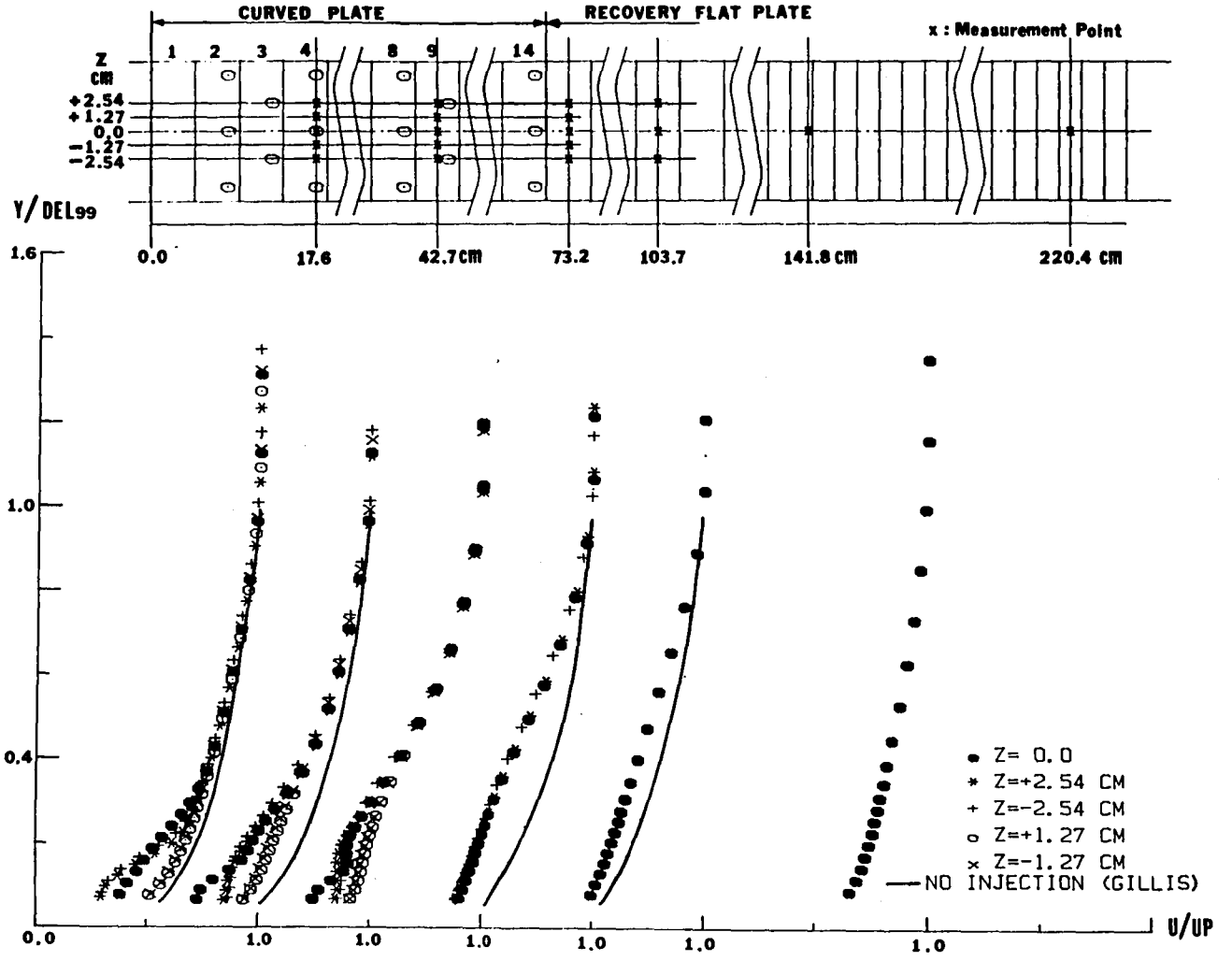

Fig. 5.26. Mean velocity profiles (U) for full-coverage cooling with m = 0.4

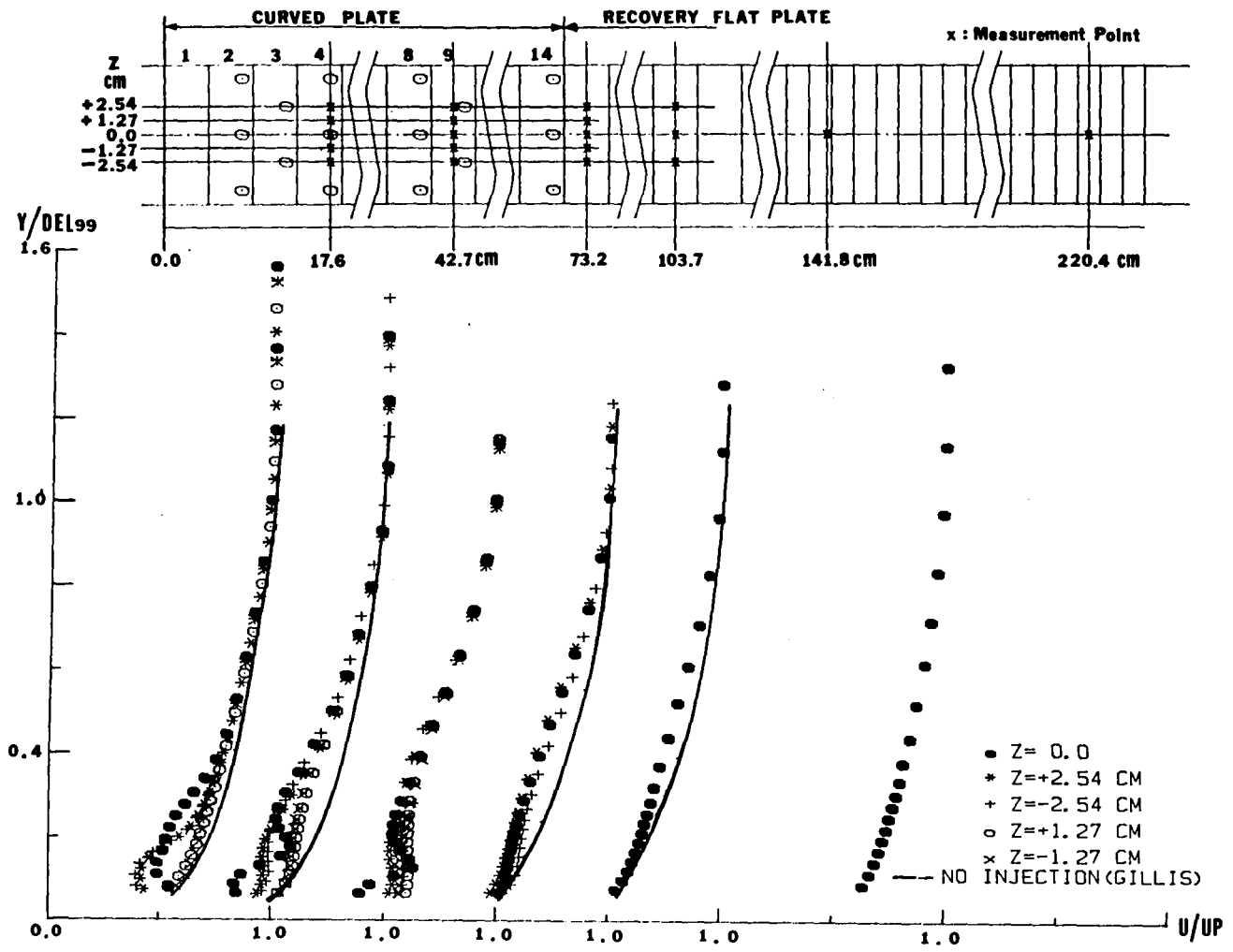

Fig. 5.27. Mean velocity profiles (U) for full-coverage cooling with m = 0.6

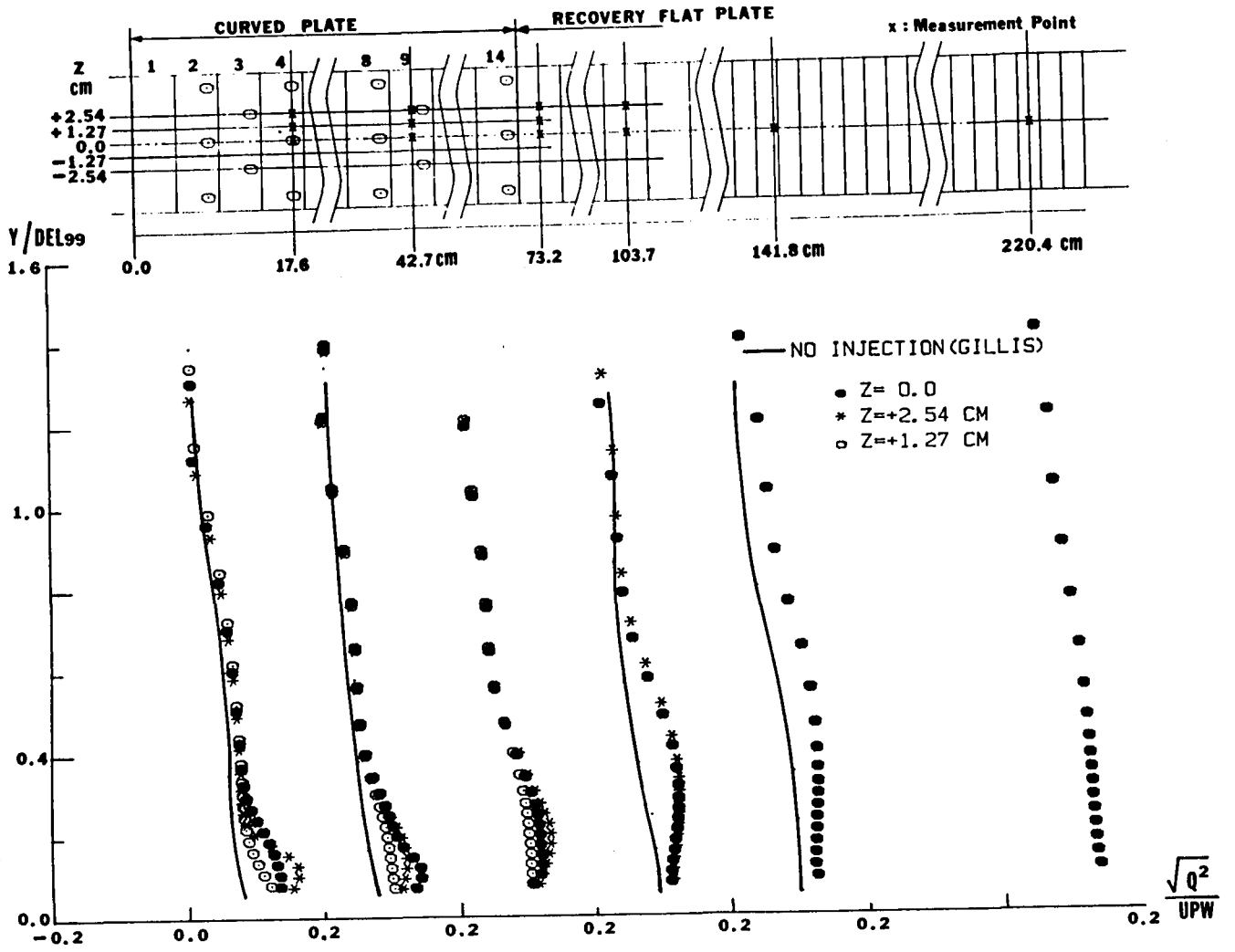

Fig. 5.28. Turbulence kinetic energy profiles (Q^2) for full-coverage cooling with m = 0.2

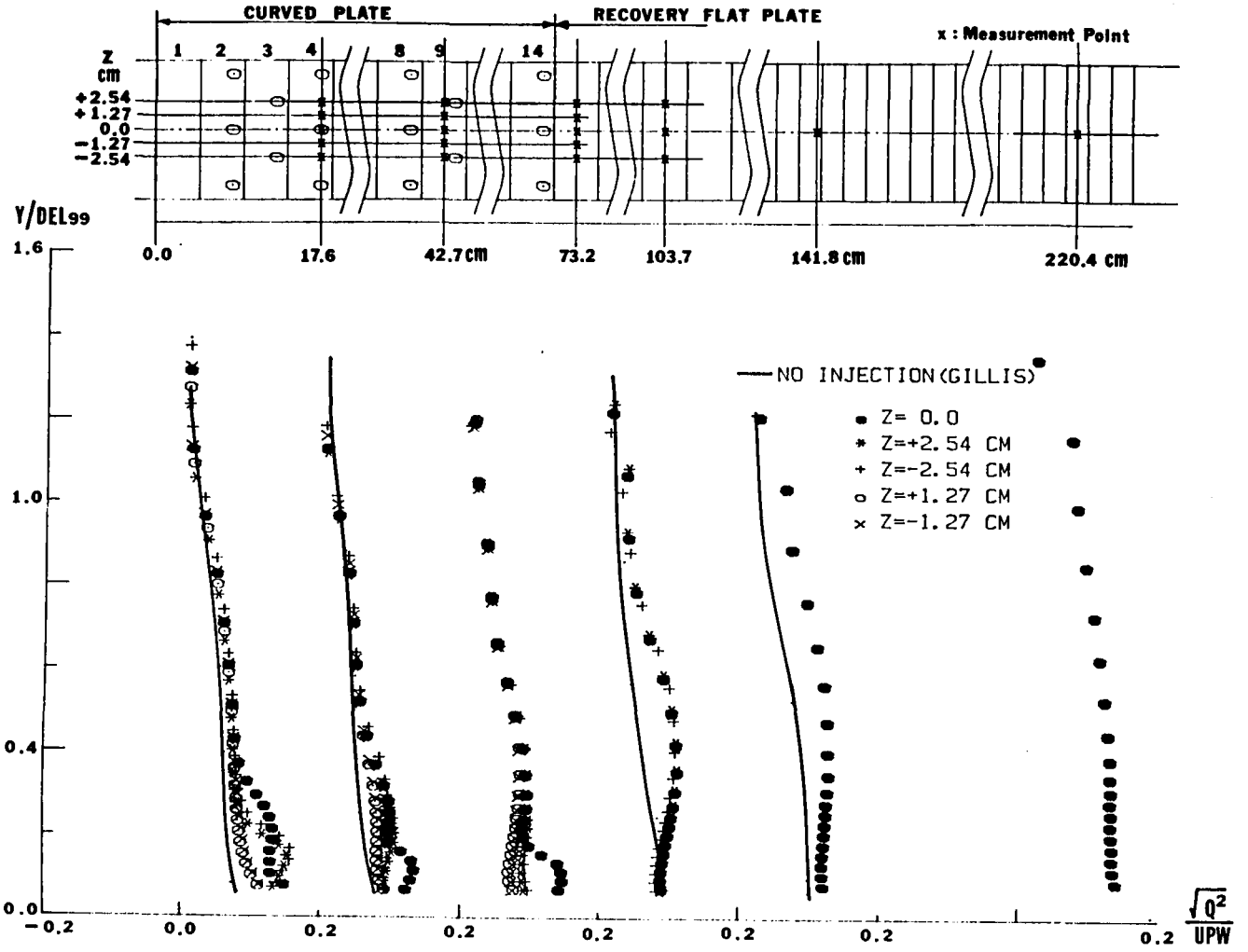

Fig. 5.29. Turbulence kinetic energy profiles (Q^2) for full-coverage cooling

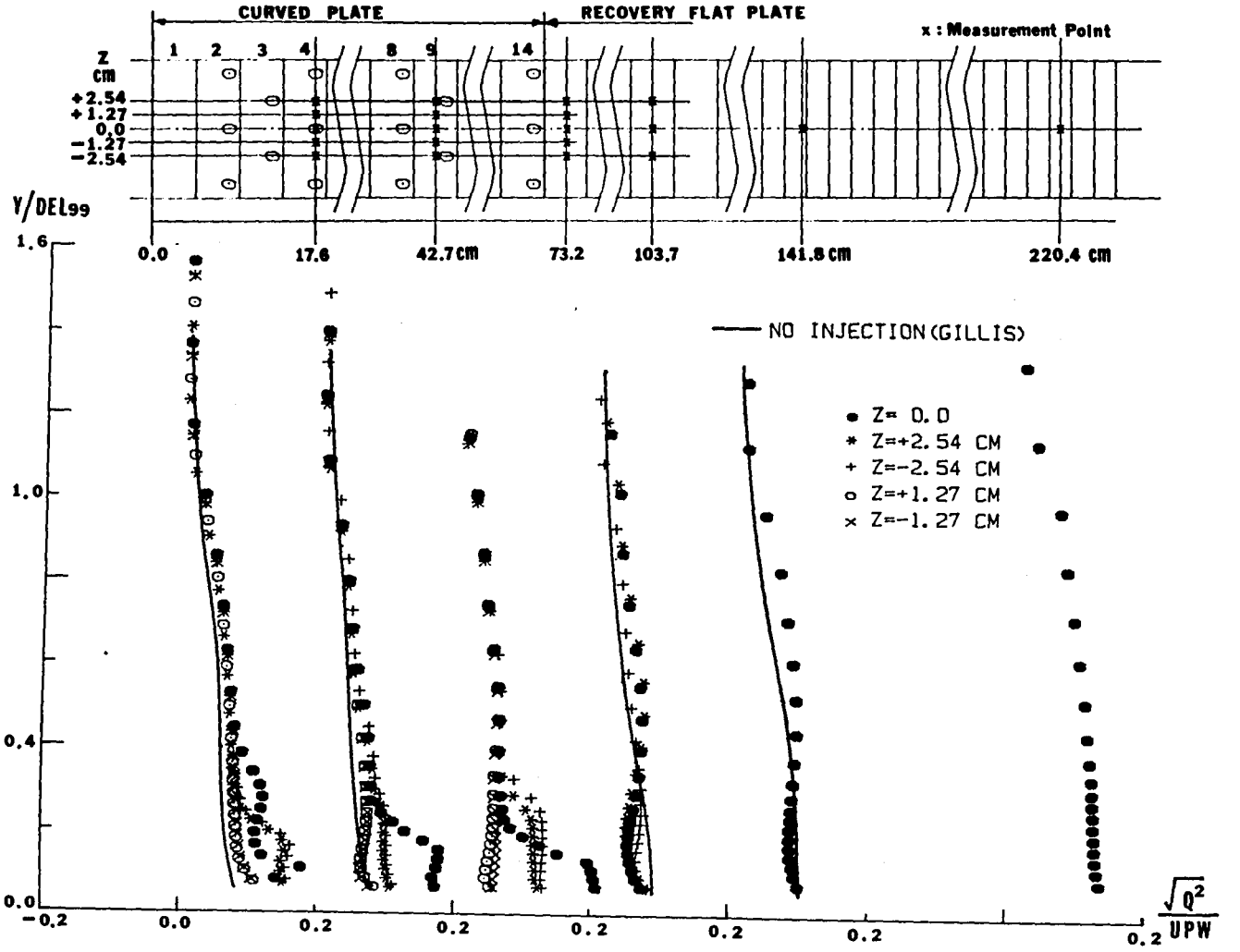

Fig. 5.30. Turbulence kinetic energy profiles (Q^2) for full-coverage cooling with m = 0.6

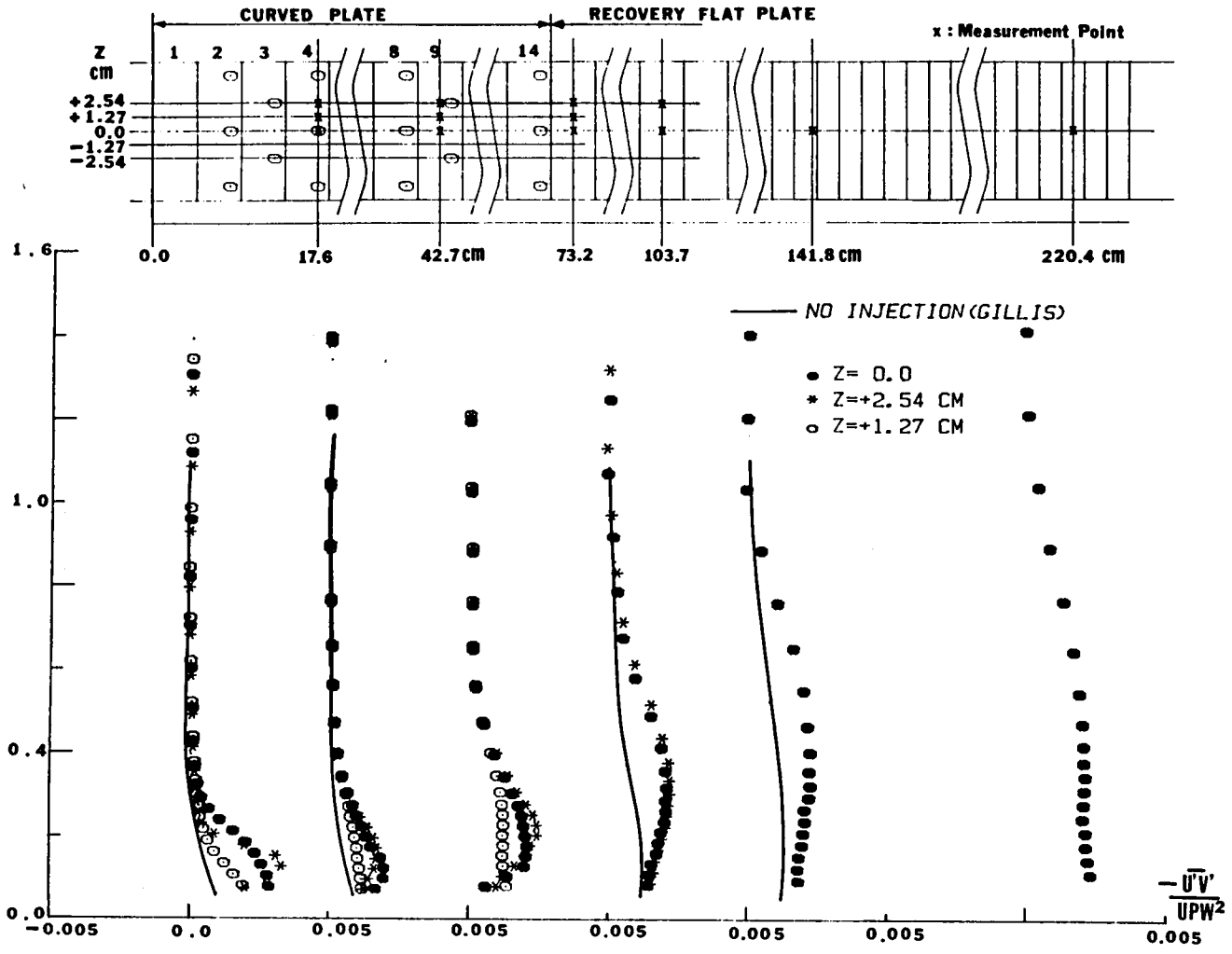

Fig. 5.31. Shear stress profiles ($-\overline{U'V'}$) for full-coverage cooling with m = 0.2

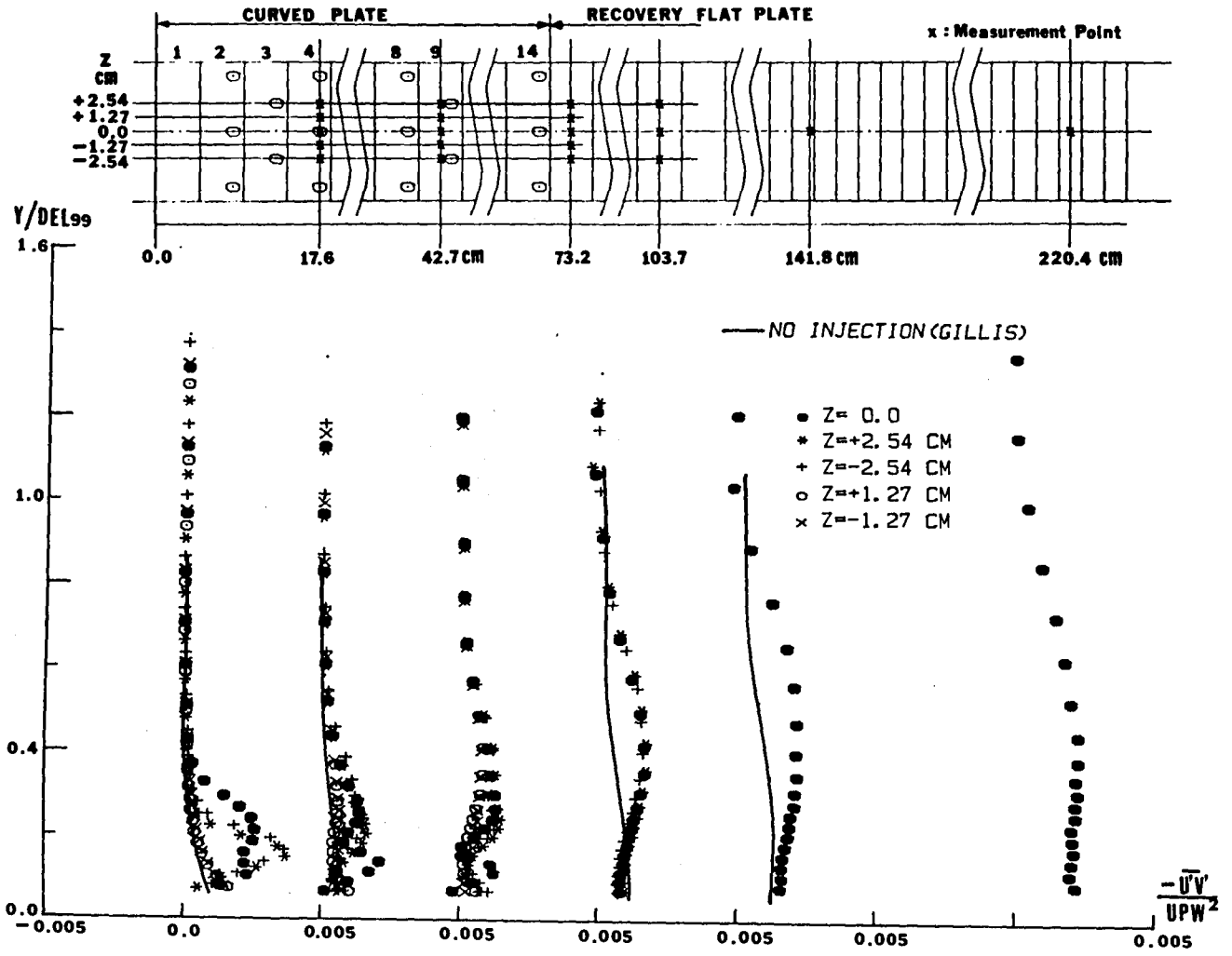

Fig. 5.32. Shear stress profiles $(-\overline{U'V'})$ for full-coverage cooling with m = 0.4

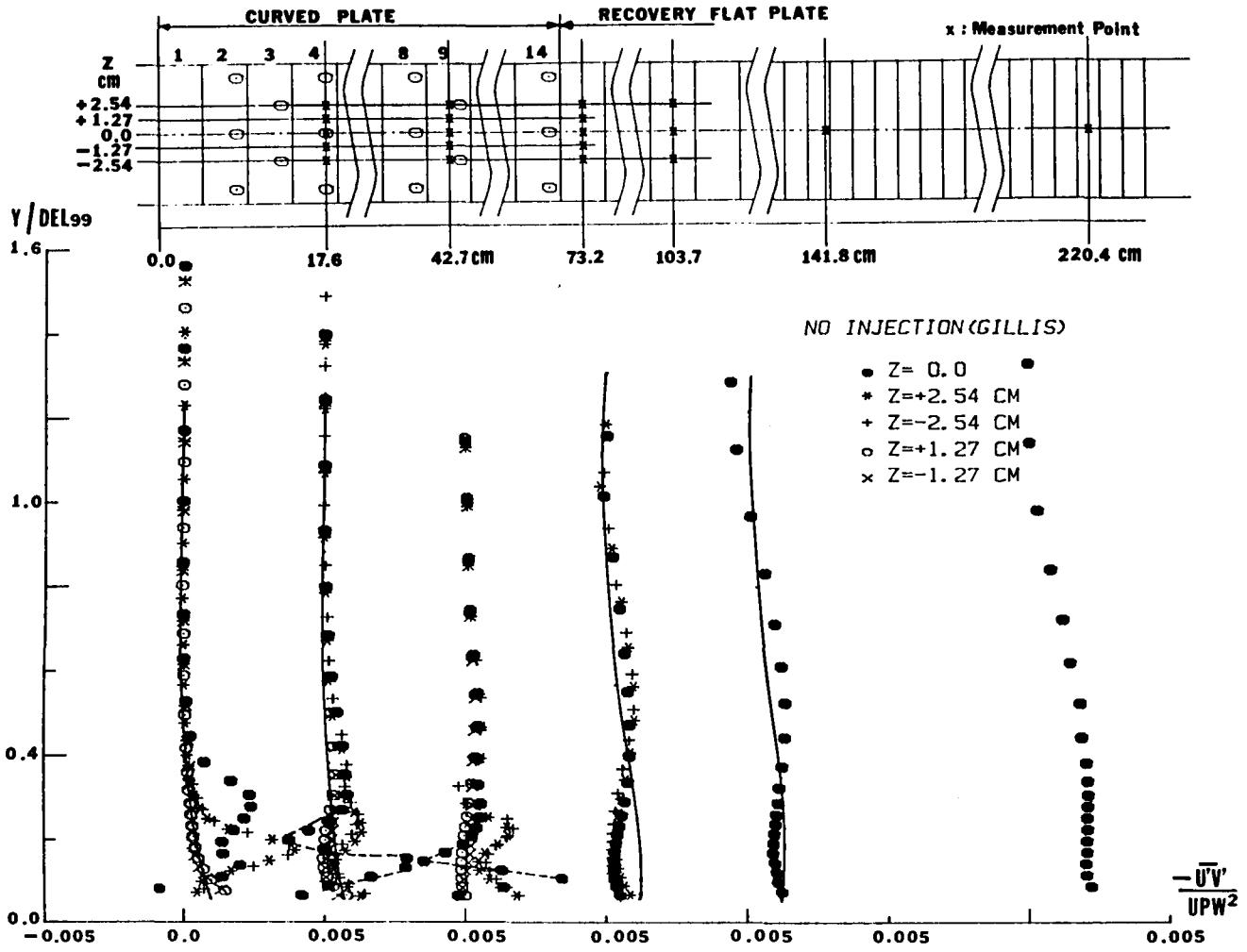

Fig. 5.33. Shear stress profiles $(\overline{U'V'})$ for full-coverage cooling with m = 0.6

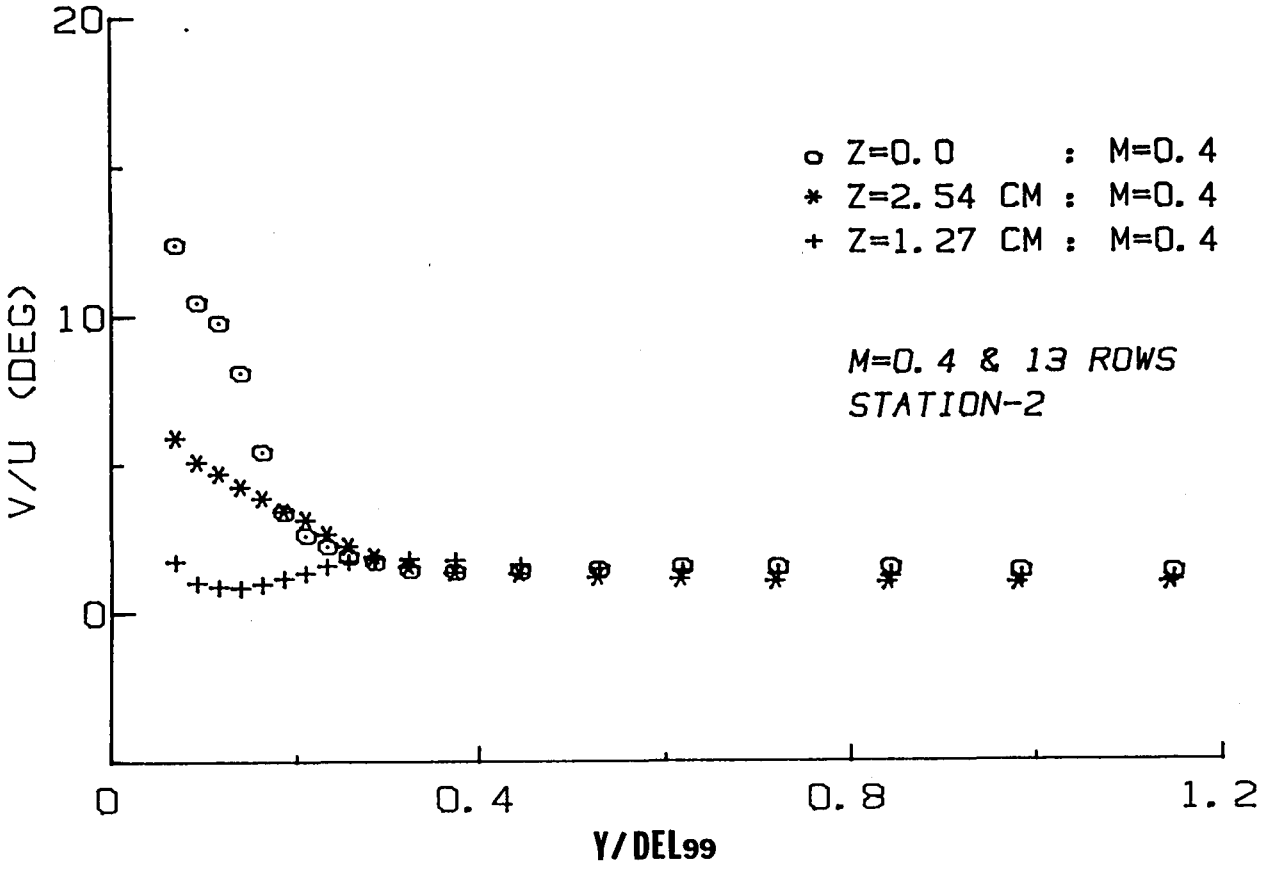

Fig. 5.34. Flow angle profiles (V/U) for full-coverage cooling with m = 0.4 at Station 2

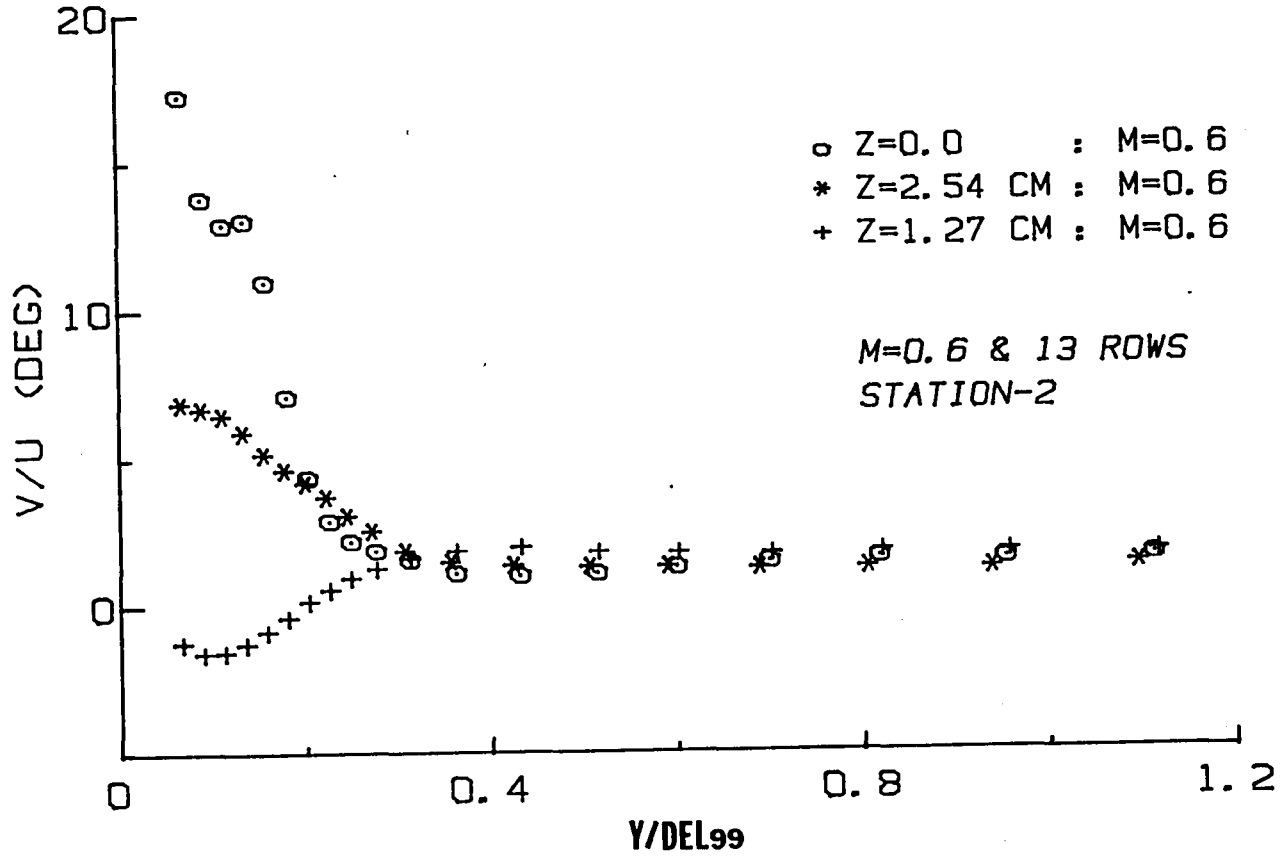

Fig. 5.35. Flow angle profiles (V/U) for full-coverge cooling with m = 0.6 at Station 2

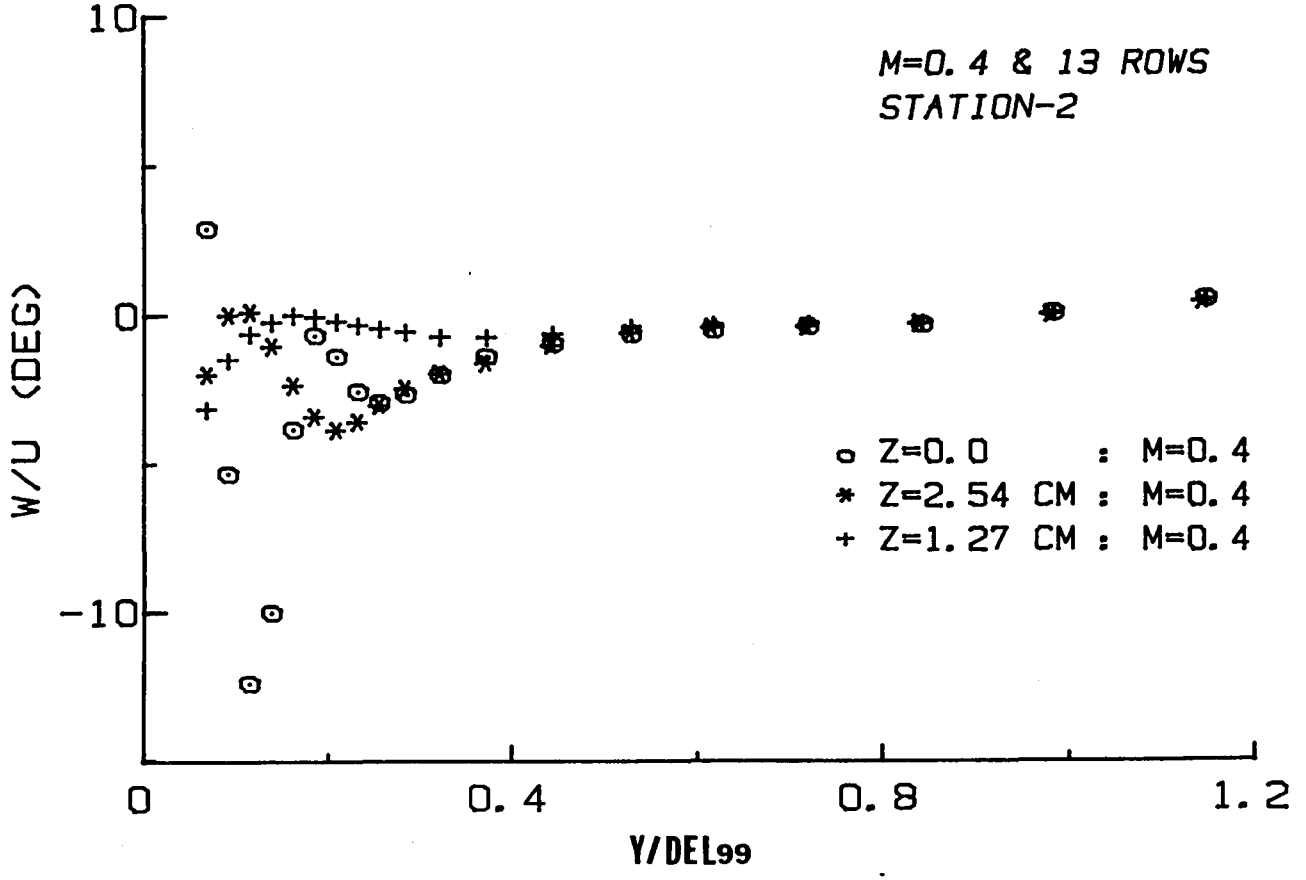

Fig. 5.36. Flow angle profiles (W/U) for full-coverage cooling with m = 0.4 at Station 2

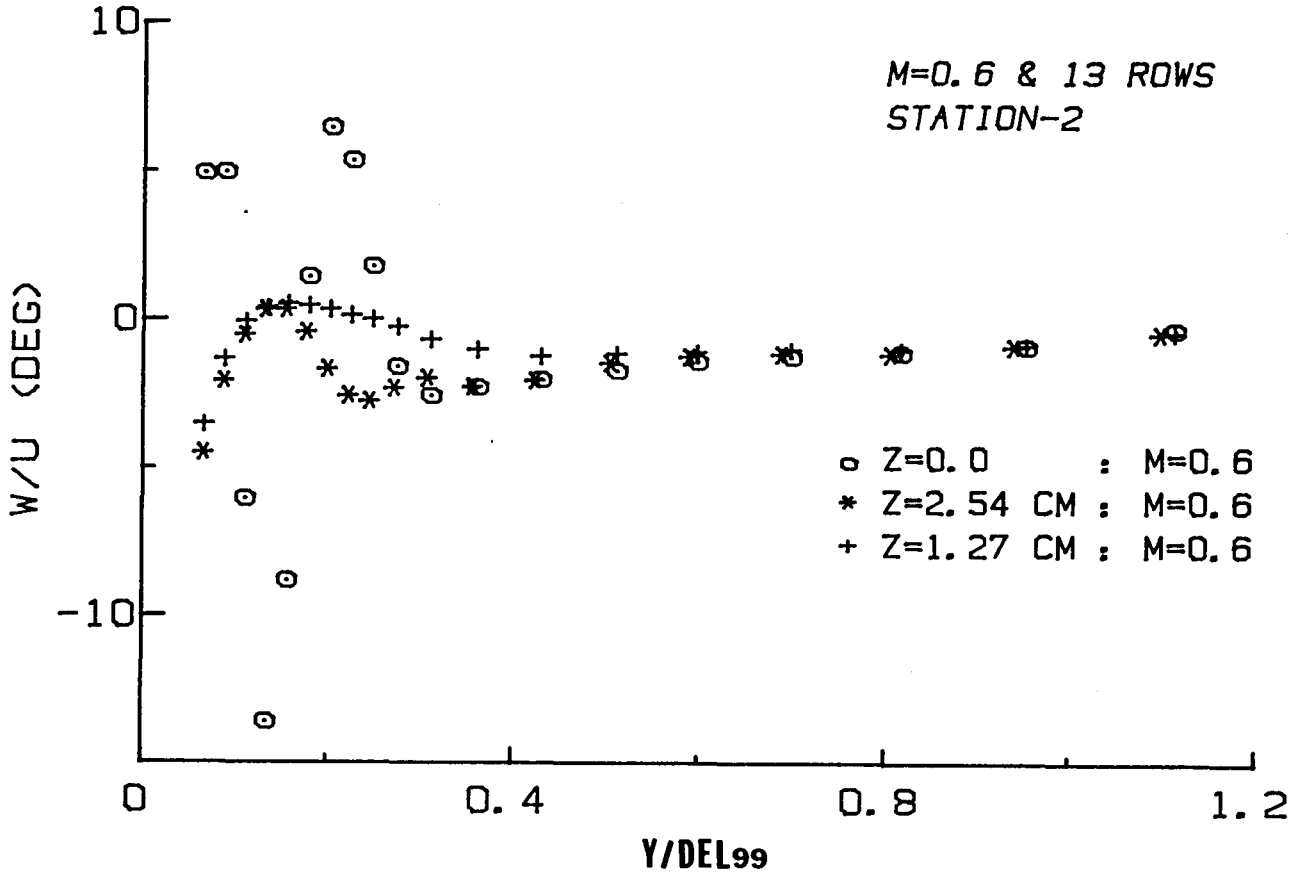

Fig. 5.37. Flow angle profiles (W/U) for full-coverage cooling with m = 0.6 at Station 2

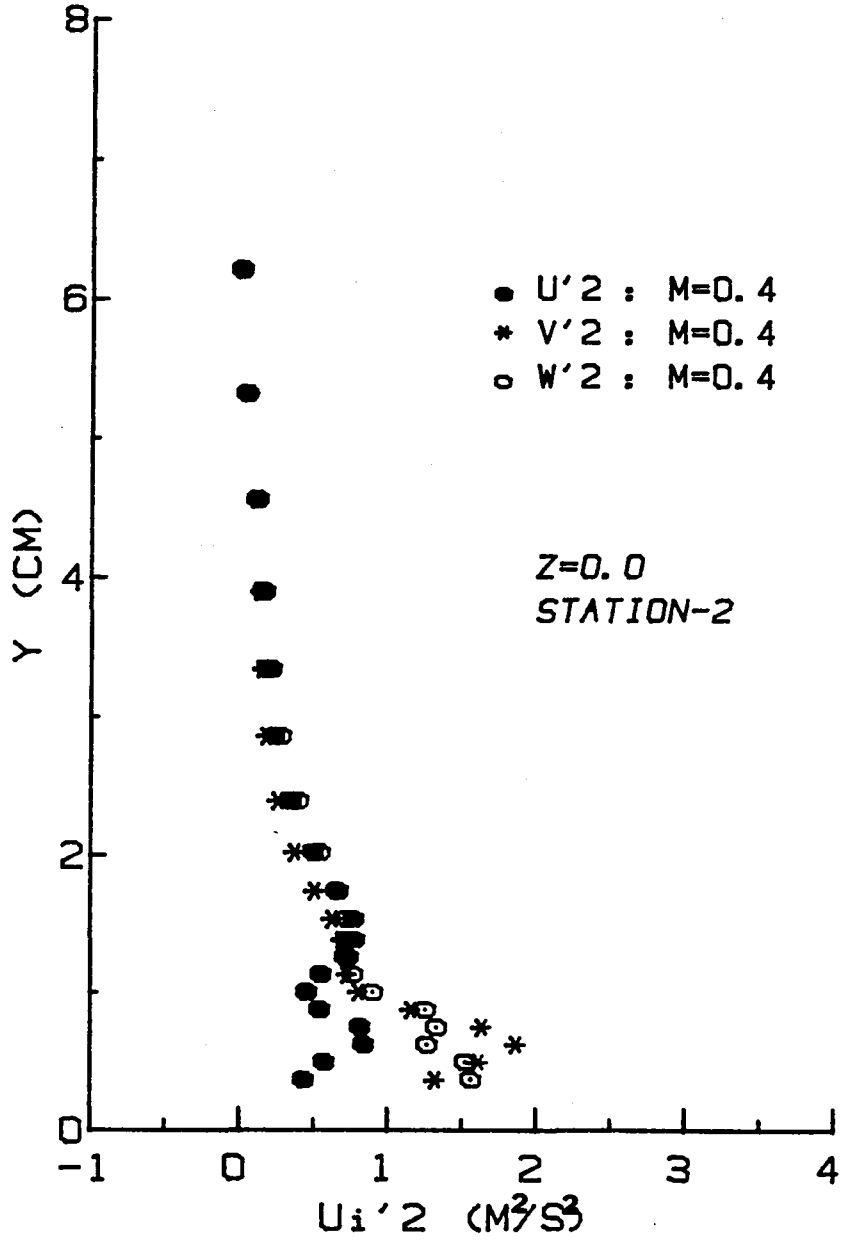

Fig. 5.38. Normal Reynolds stress profiles $(\overline{u_i'^2})$ for full-coverage cooling with m = 0.4 at Station 2

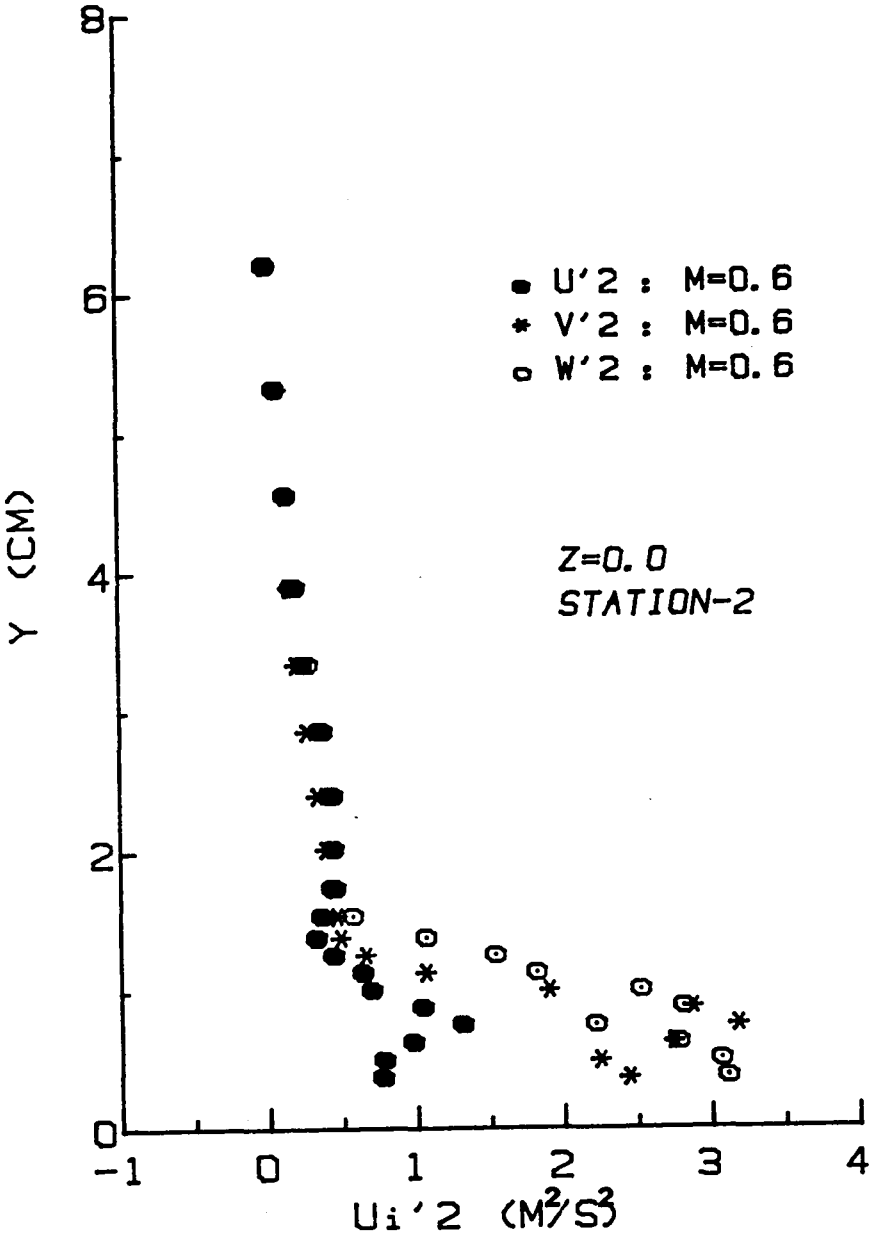

Fig. 5.39. Normal Reynolds stress profiles $(\overline{u_i'^2})$ for full-coverage cooling with m = 0.6 at Station 2

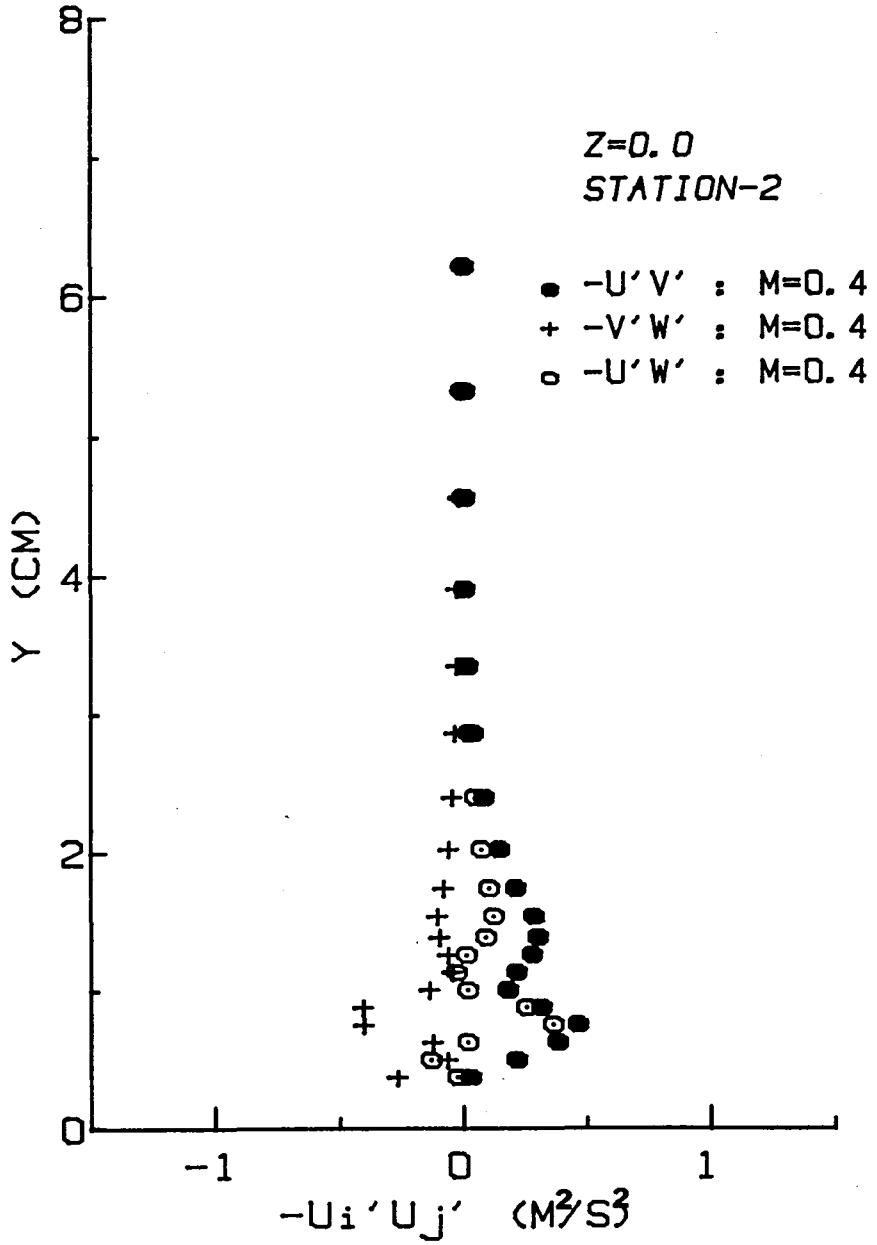

Fig. 5.40. Reynolds stress stress profiles for full-coverage cooling with m = 0.4 at Station 2

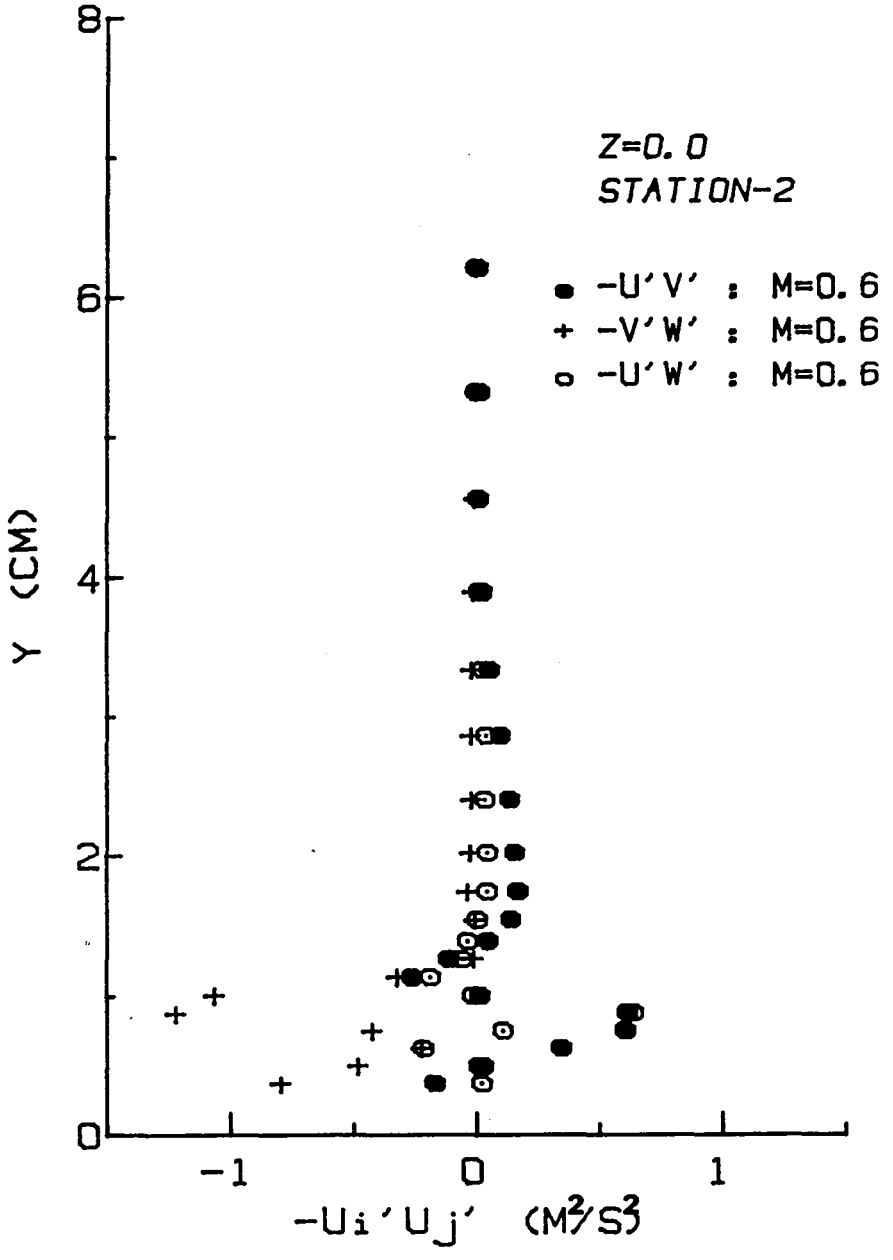

Fig. 5.41. Reynolds shear stress profiles for full-coverage cooling with m = 0.6 at Station 2

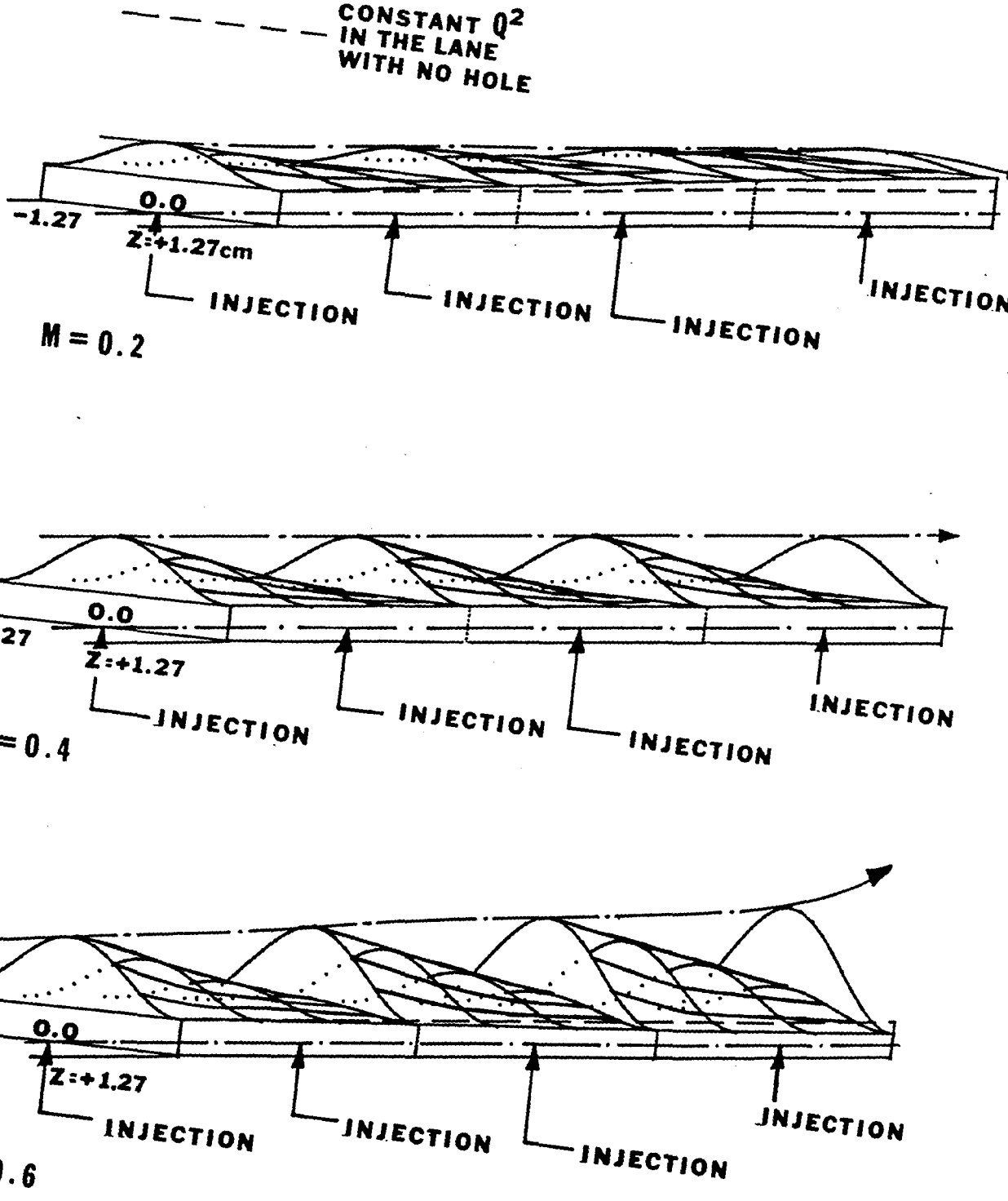

Fig. 5.42. Illustration of small and large evolutions of turbulence kinetic energy profiles: full-coverage cooling

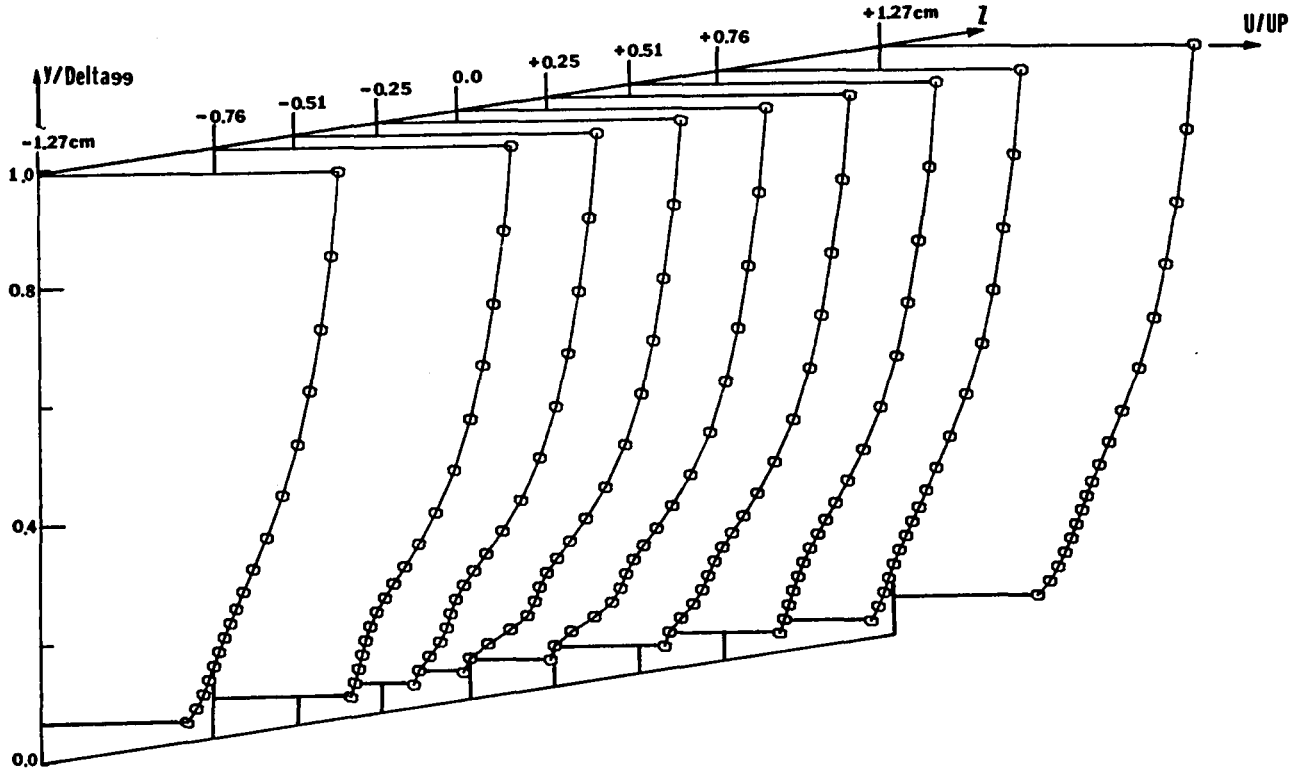

Fig. 5.43. Detailed mean-velocity profiles (U) at Station 2 for full-coverage cooling with m = 0.4 between a lane with holes and a lane without

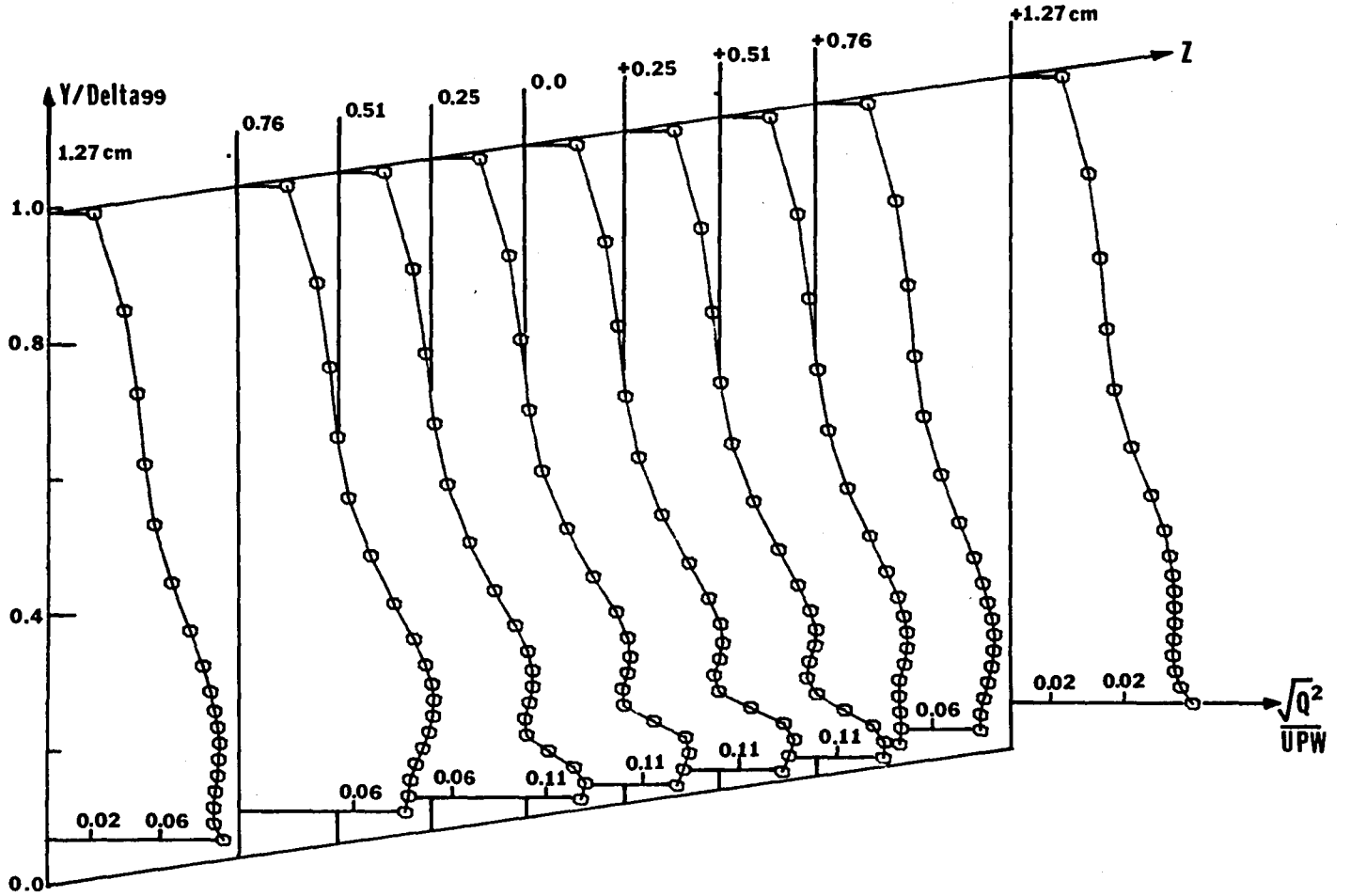

Fig. 5.44. Detailed turbulence energy profiles (Q^2) at Station 2 for full-coverage cooling with m = 0.4 between a lane with holes and one without

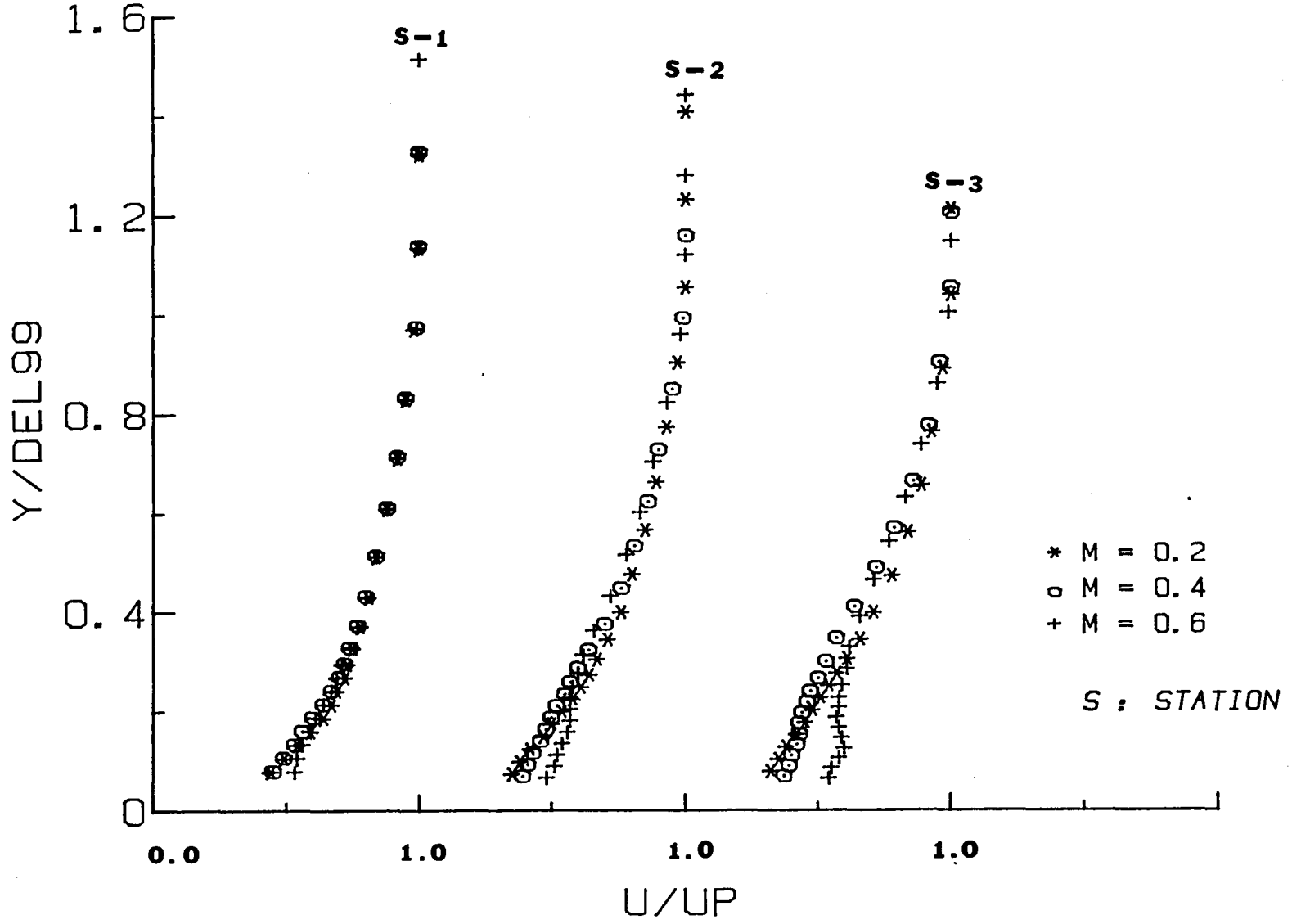

Fig. 5.45. Spanwise-averaged mean-velocity profiles (U) in the blown curved region

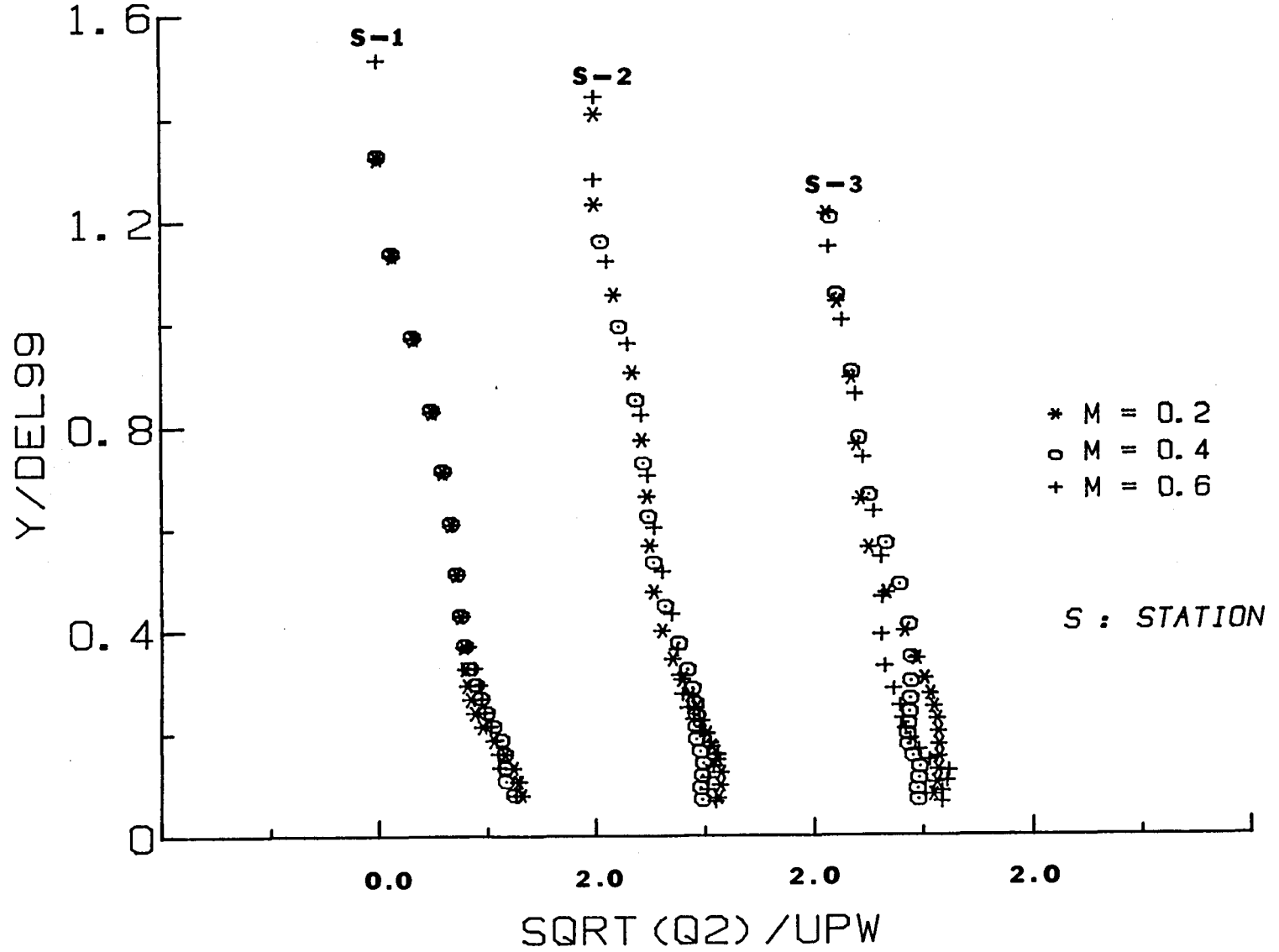

Fig. 5.46. Spanwise-averaged turbulence kinetic energy profiles (Q^2) in the blown curved reigon

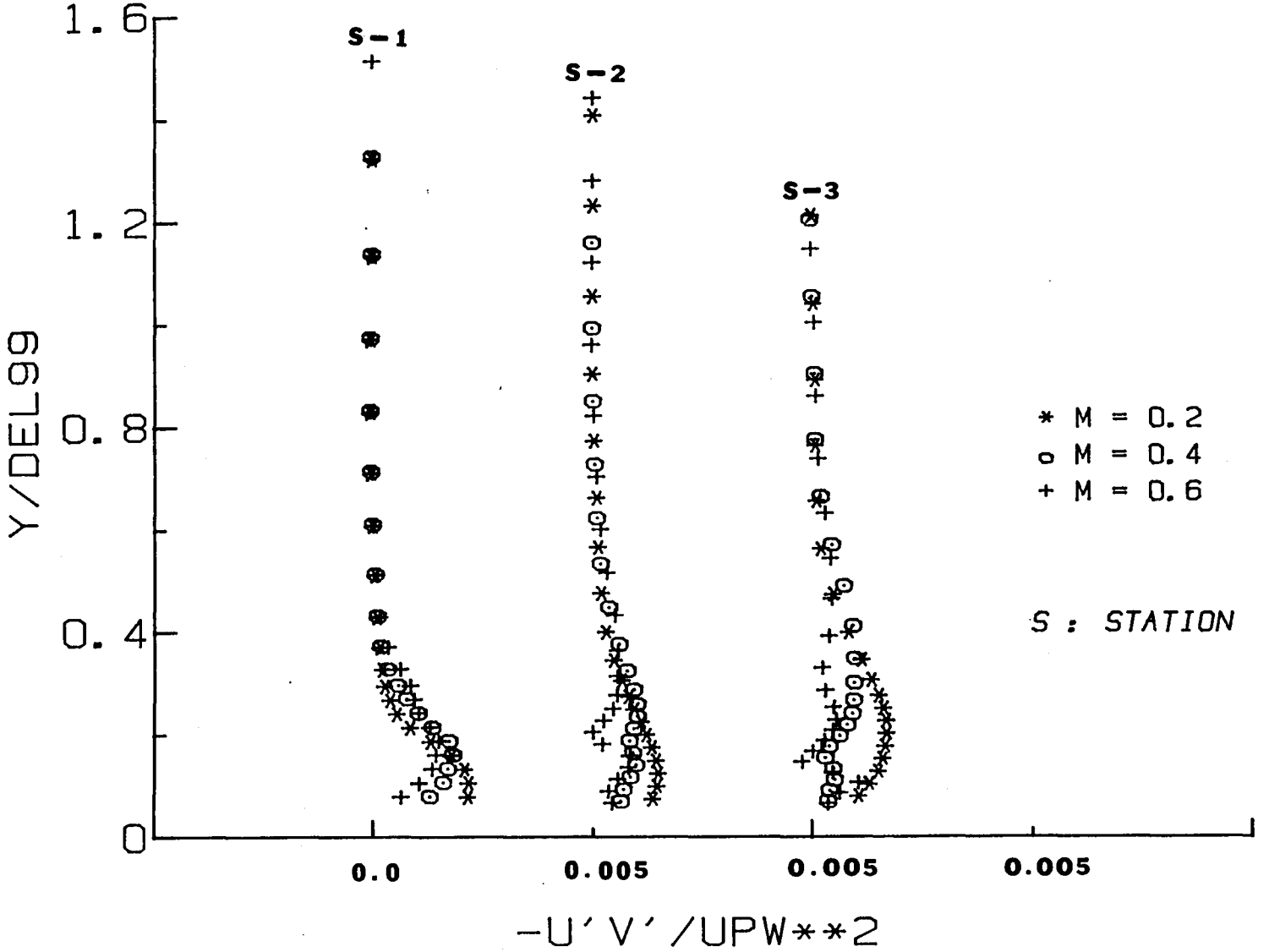

Fig. 5.47. Spanwise-averaged shear-stress profiles $(-\overline{U'V'})$ in the blown curved region

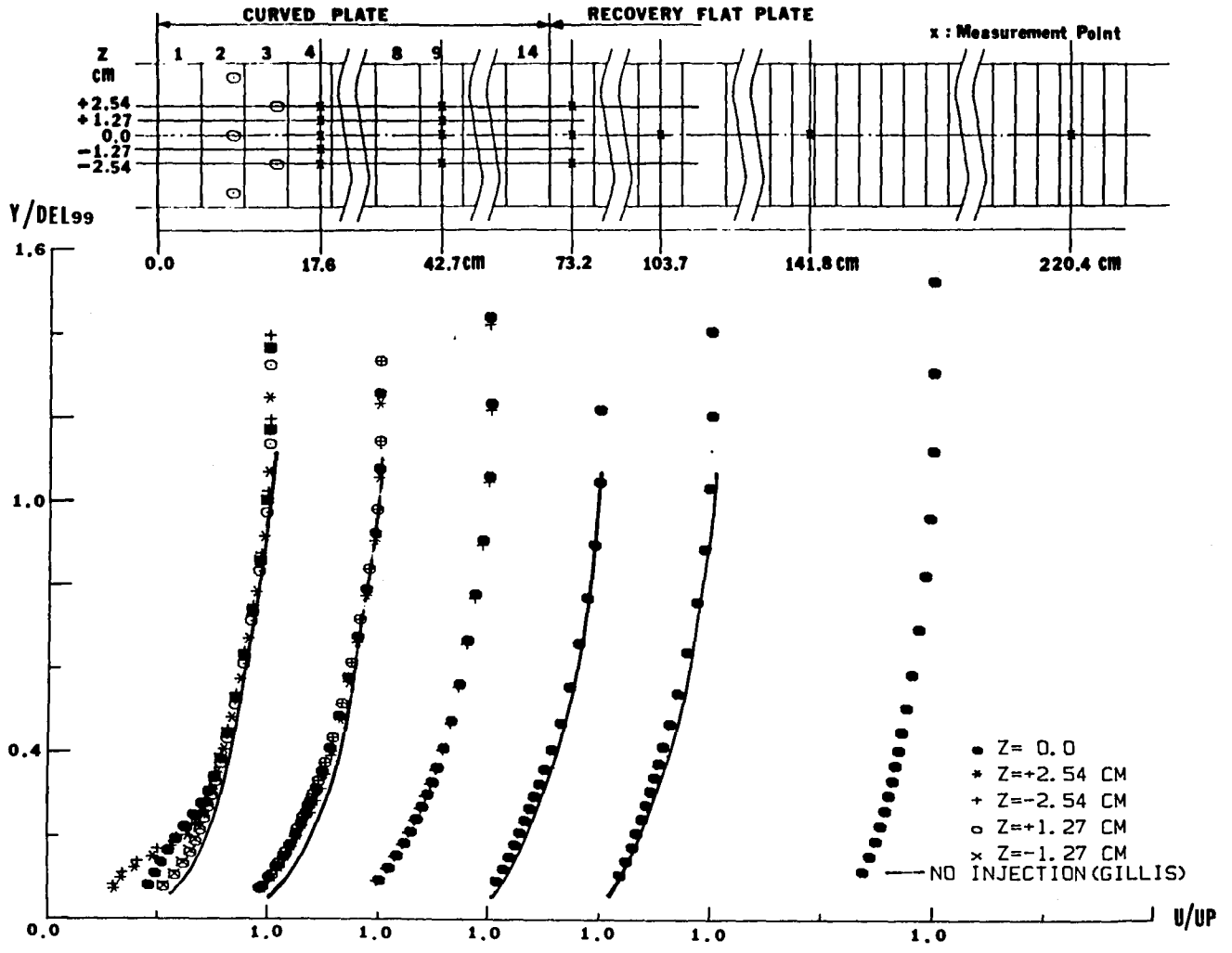

Fig. 5.48. Mean-velocity profiles (U) for two rows of injection with m = 0.4

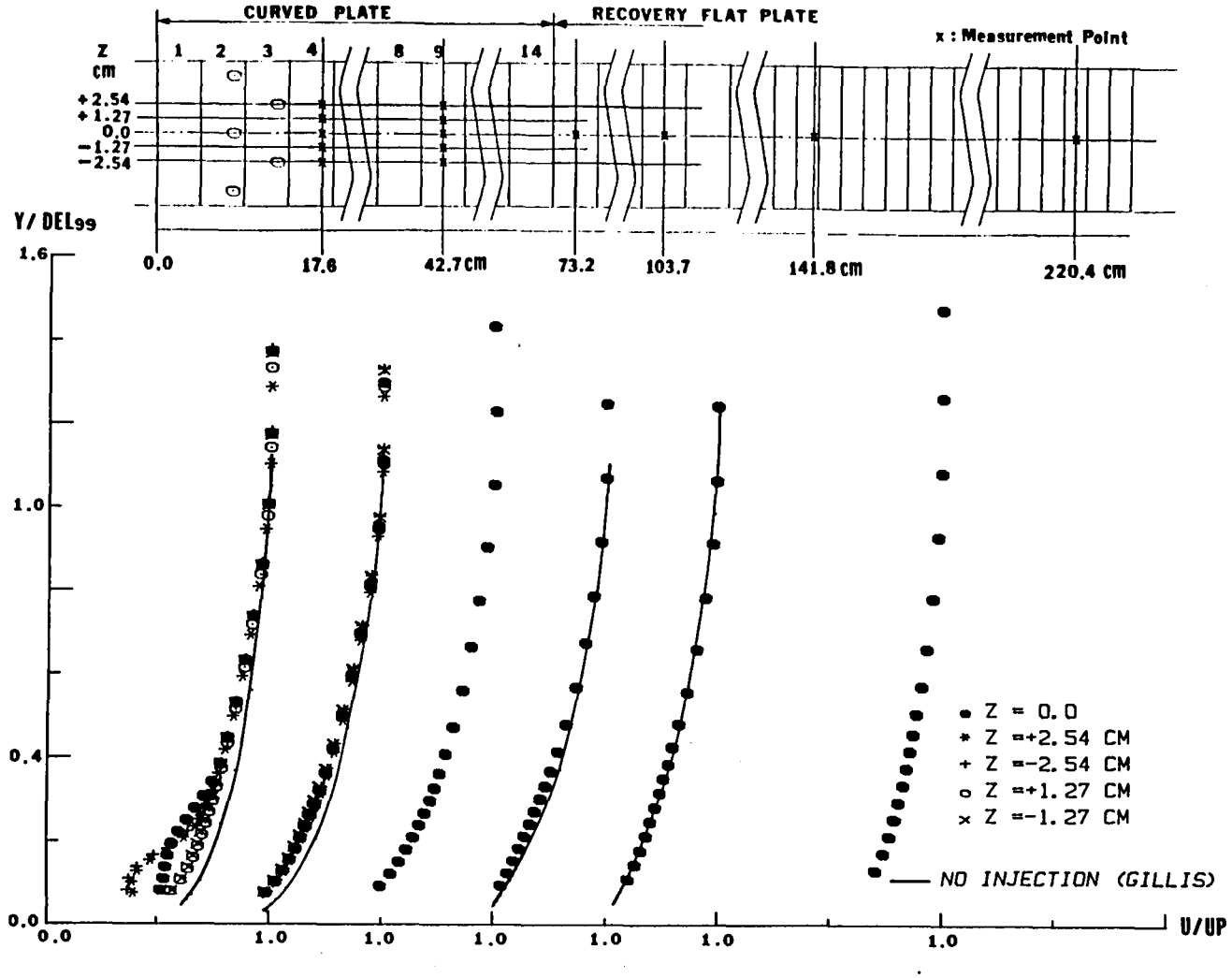

Fig. 5.49. Mean-velocity profiles (U) for two rows of injection with m = 0.6

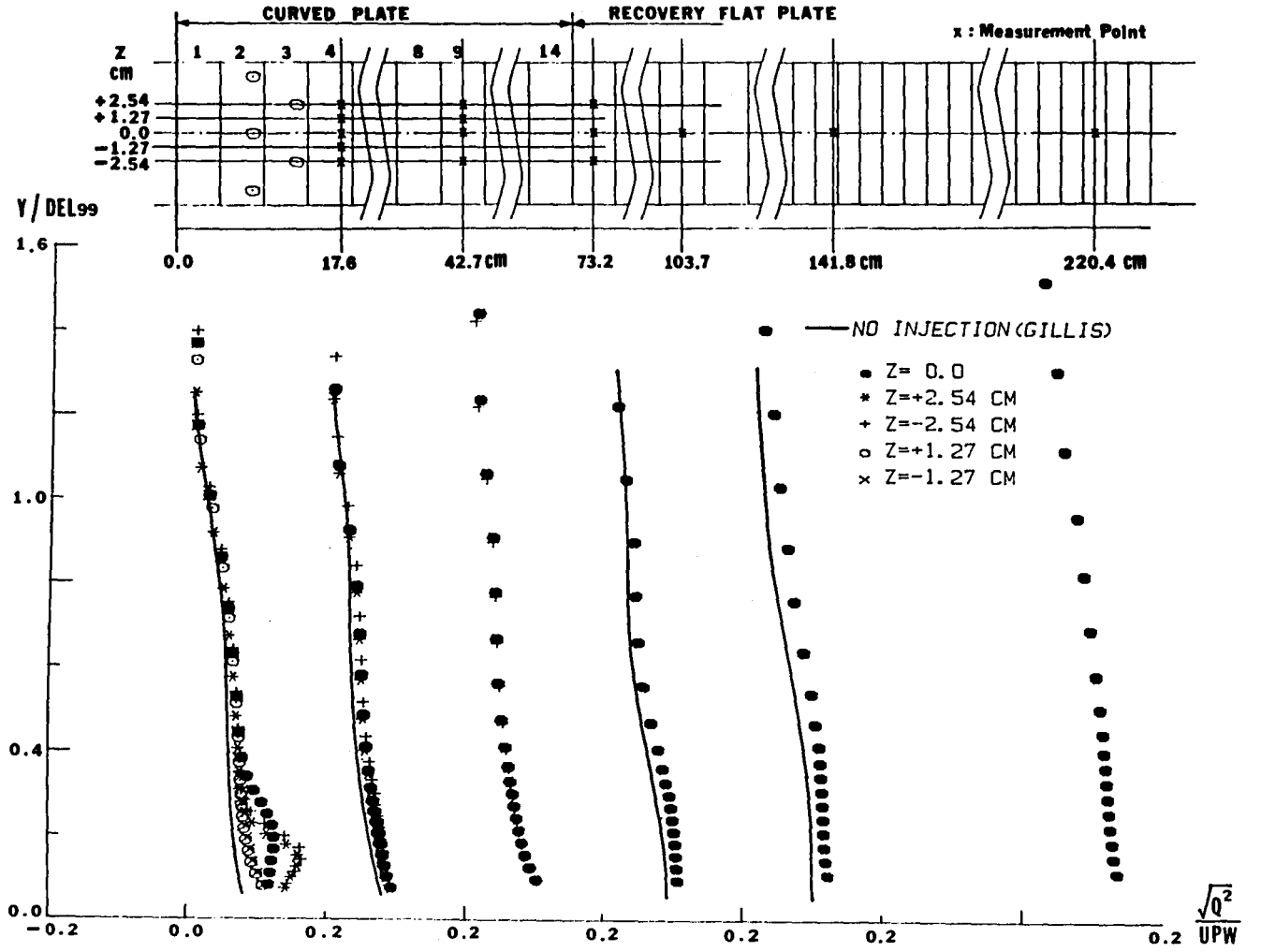
CURVED PLATE
RECOVERY FLAT PLATE
x : Measurement Point
Z
cm
+2.54
+1.27
0.0
−1.27
−2.54
1
2
3
4
8
9
14
0.0
17.6
42.7cm
73.2
103.7
141.8cm
220.4 cm
Y / DEL99
1.6
1.0
0.4
0.0
−0.2
0.0
0.2
0.2
0.2
0.2
0.2
0.2
NO INJECTION(GILLIS)
Z= 0.0
Z=+2.54 CM
Z=−2.54 CM
Z=+1.27 CM
Z=−1.27 CM
√Q²
UPW

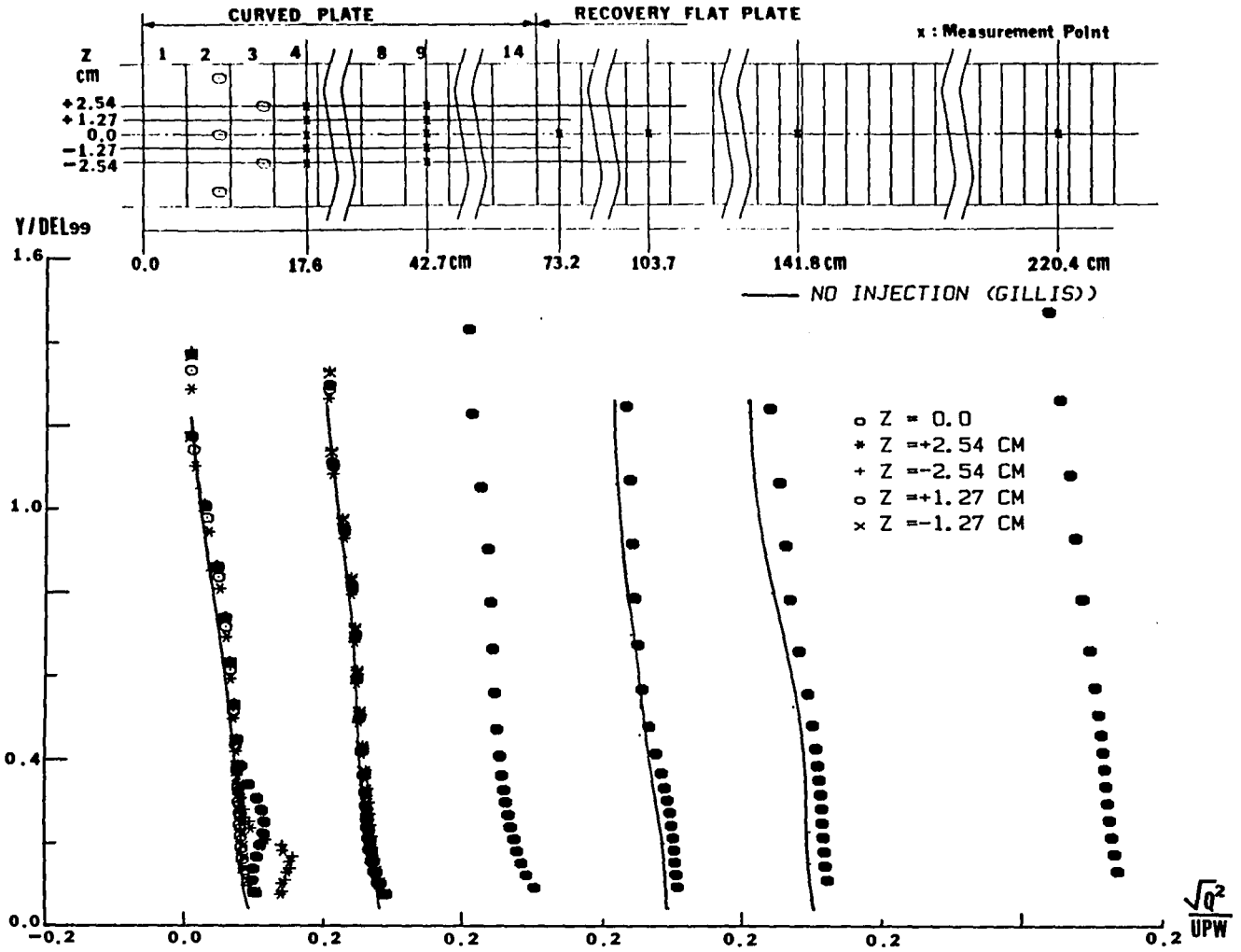

Fig. 5.51. Turbulence kinetic energy profiles (Q^2) for two rows of injection with m = 0.6

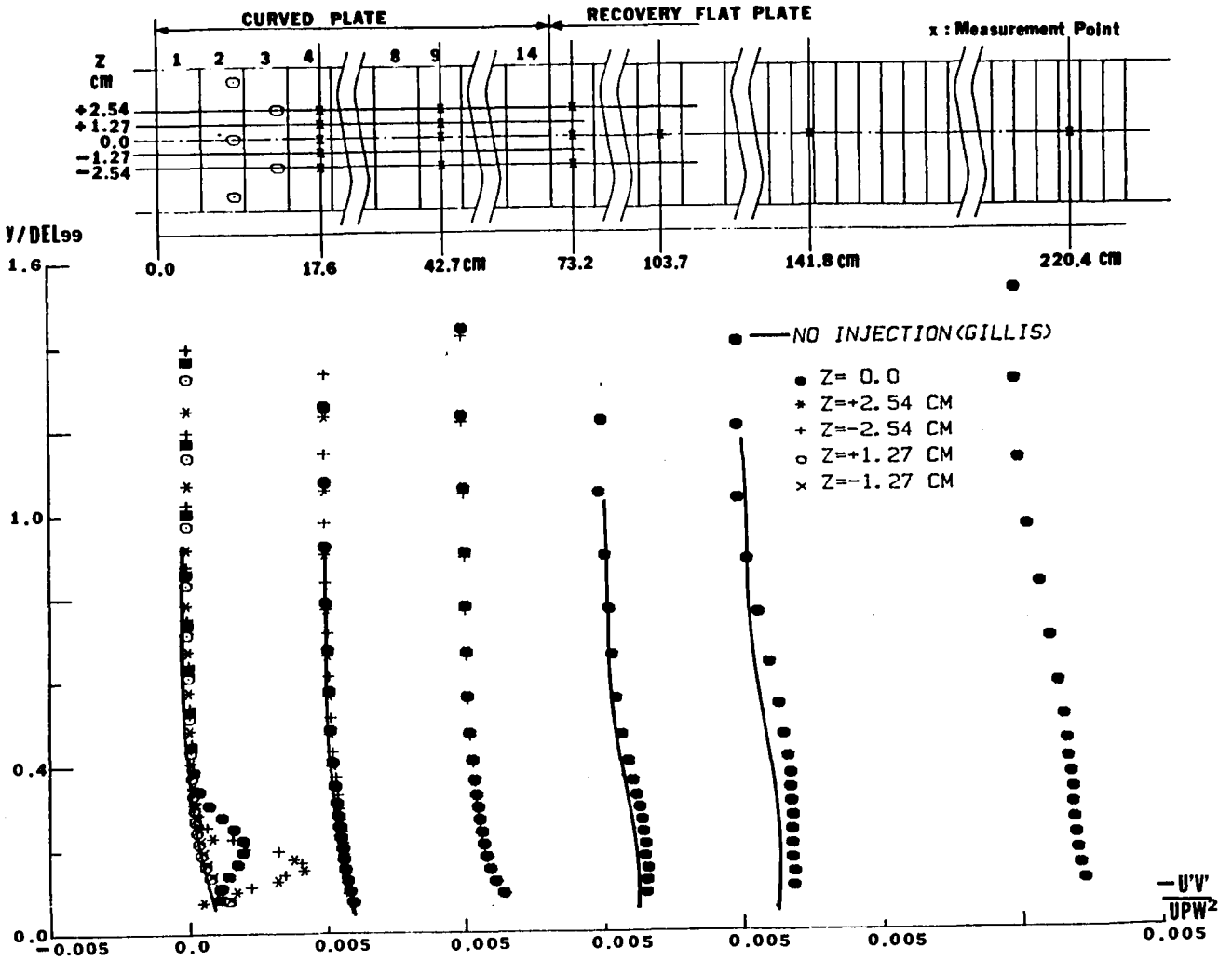

Fig. 5.52. Shear-stress profiles $(-\overline{U'V'})$ for two rows of injection with m = 0.4

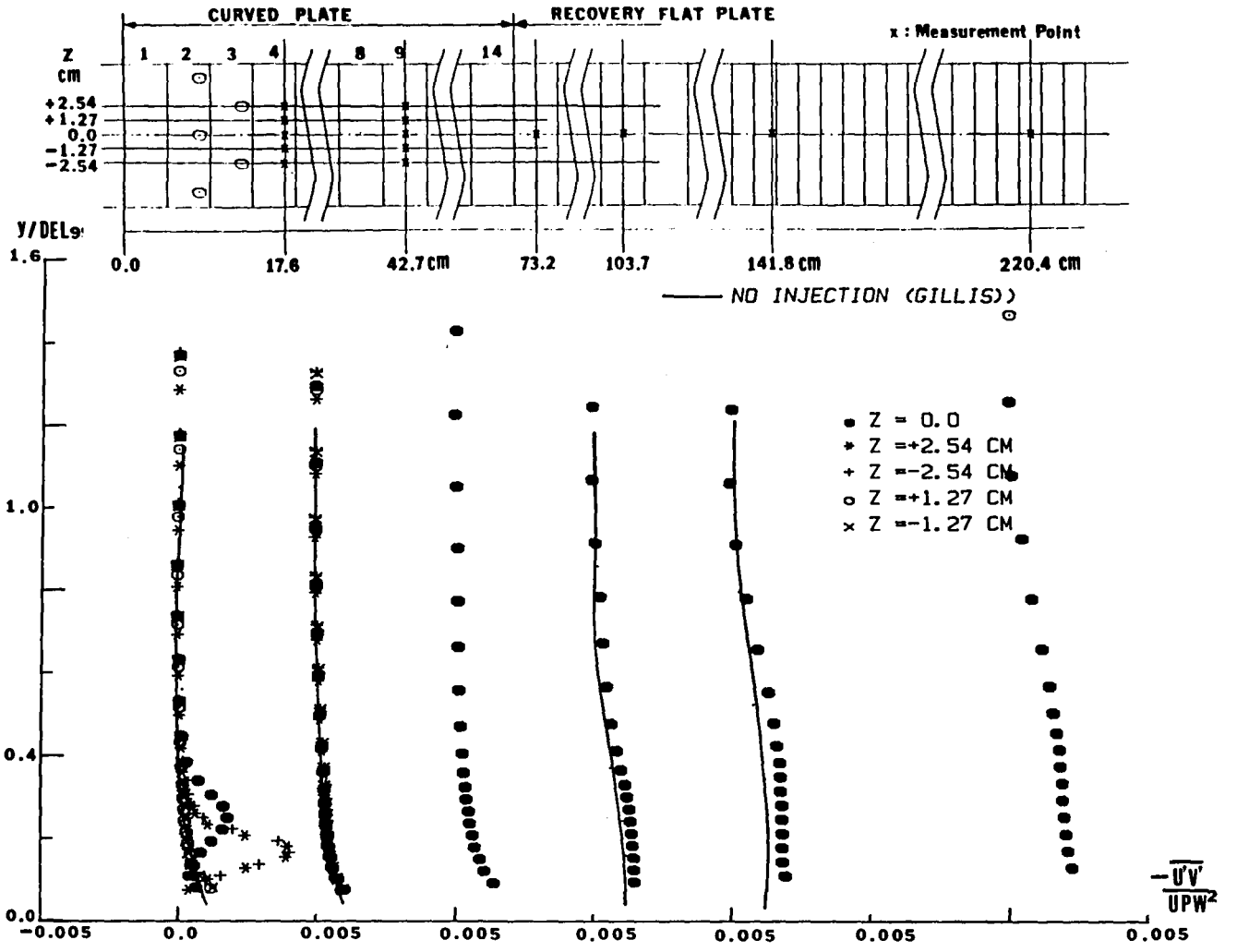

Fig. 5.53. Shear-stress profiles ($-\overline{U'V'}$) for two rows of injection with m = 0.6

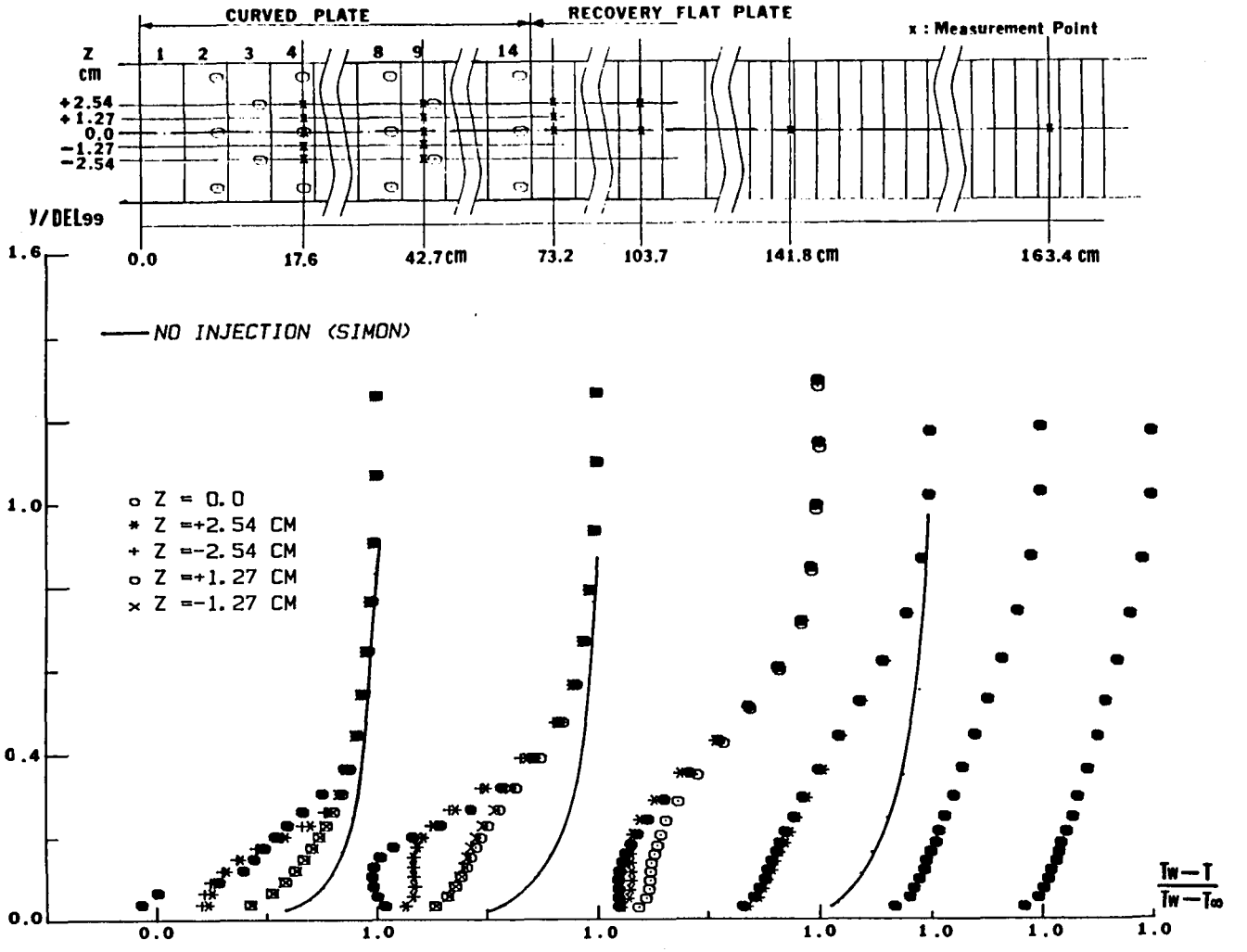

Fig. 5.54. Temperature profiles for full-coverage cooling with m = 0.4.: hot run ($\theta \sim 1.0$)

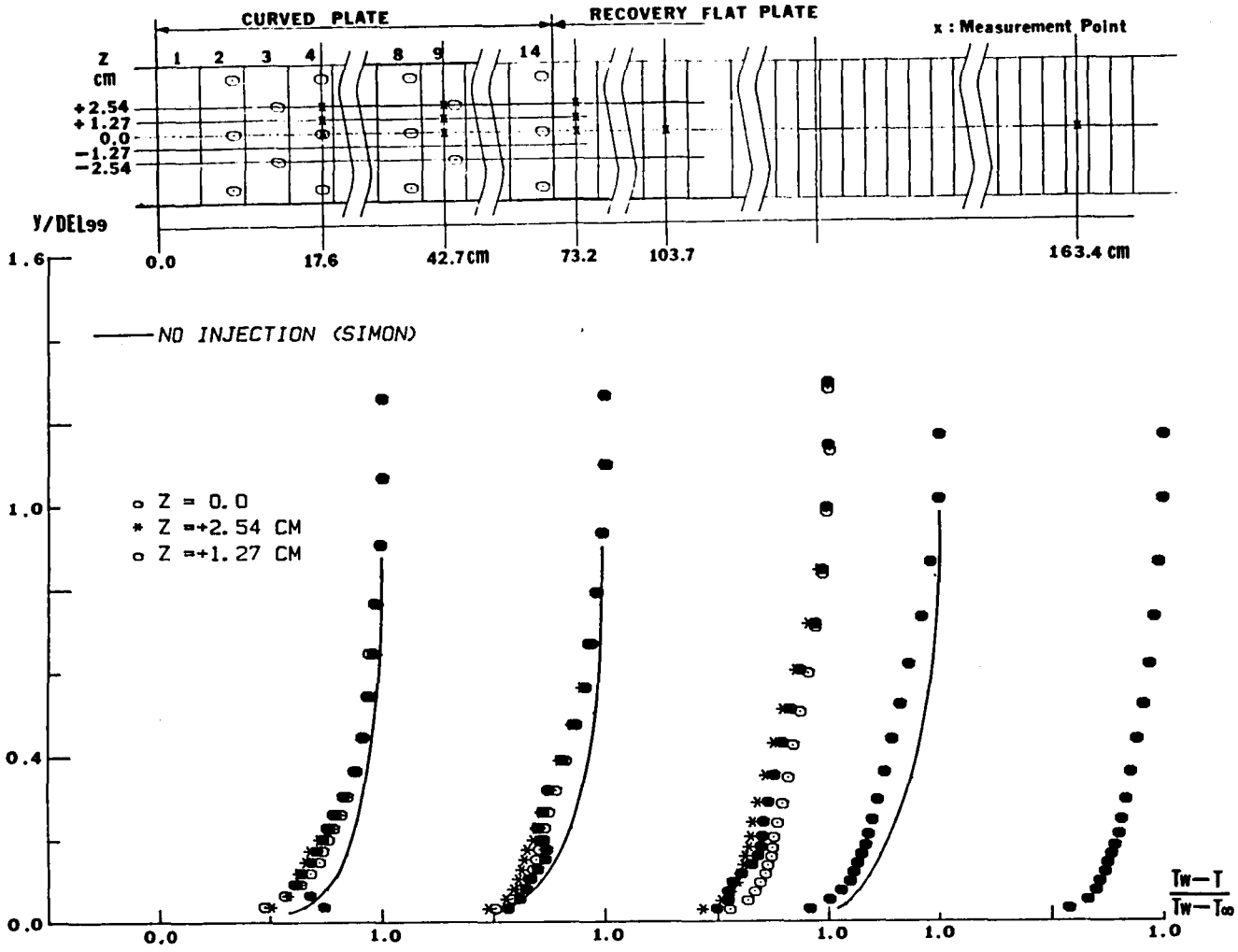

Fig. 5.55. Temperature profiles for full-coverage cooling with m = 0.4: cold run ($\theta \sim 0.2$)

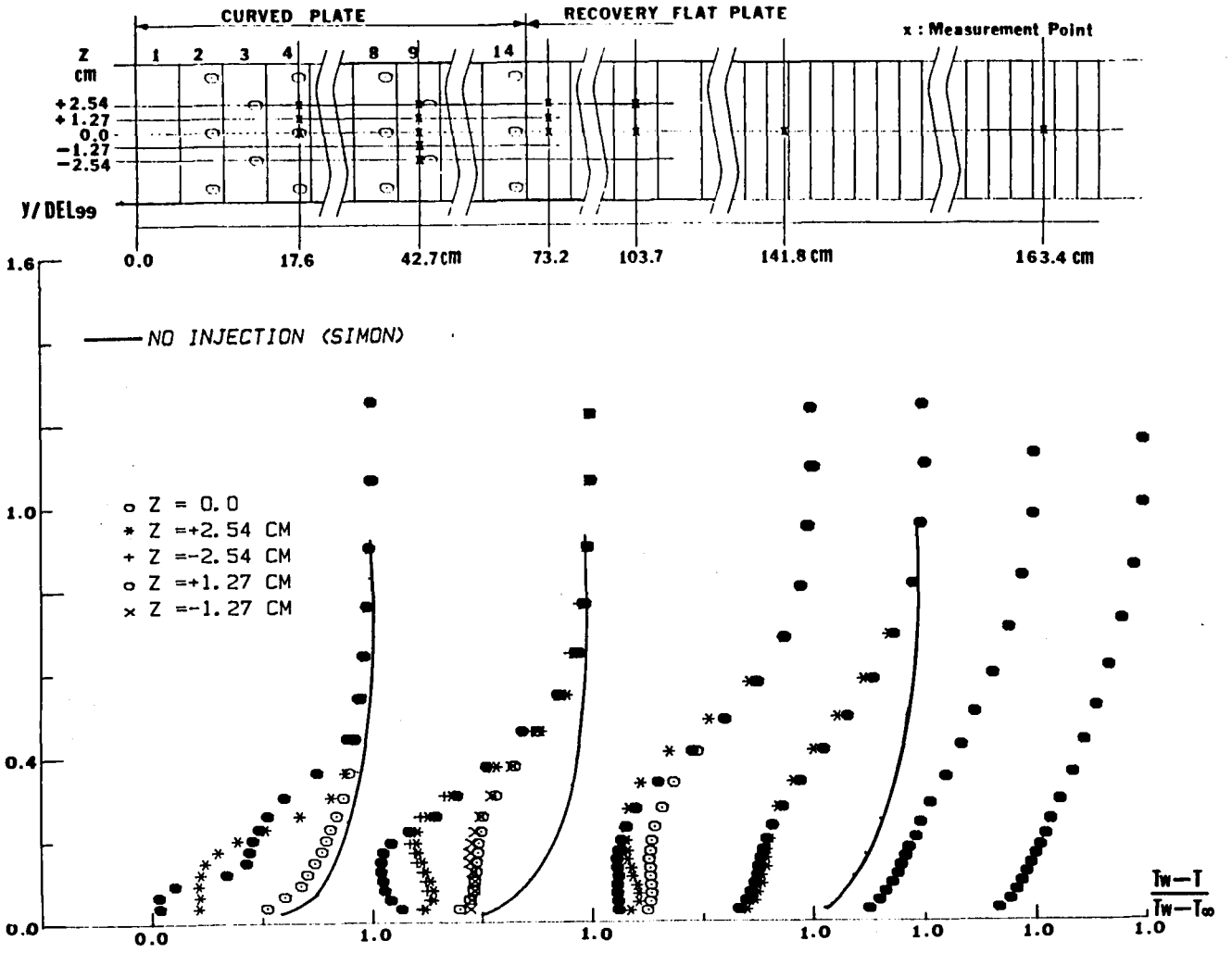

Fig. 5.56. Temperature profiles for full-coverage cooling with m = 0.6: hot run ($\theta \sim 1.0$)

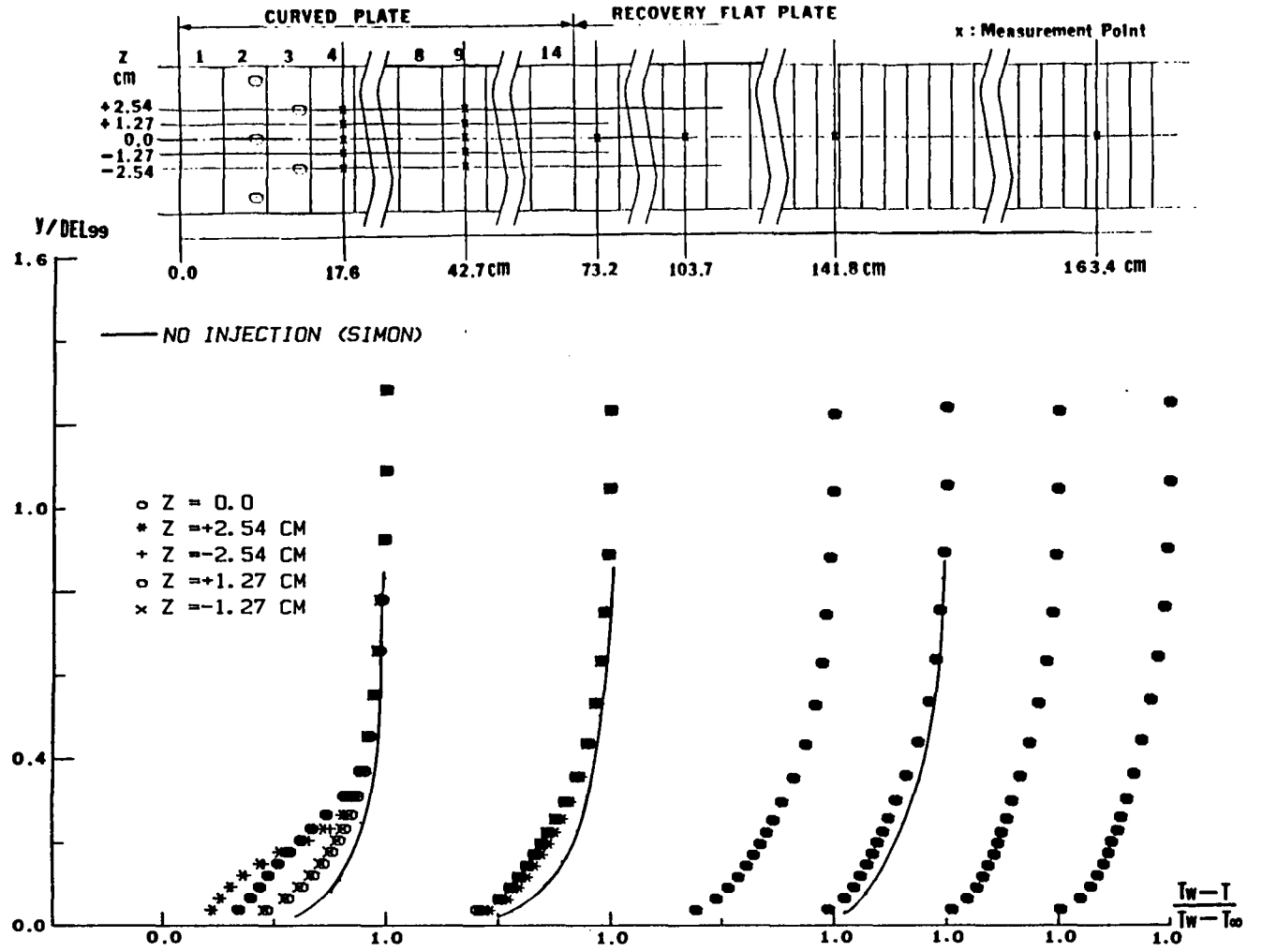

Fig. 5.57. Tempereature profiles for two rows of injection with m = 0.4: hot run ($\theta \sim 1.0$)

Chapter 6

PREDICTION OF THE DATA

6.1 Previous Work

Efforts to produce a prediction model have been made by several investigators, both for film-cooled flow and for flow over a curved surface. In this section, some representative approaches will be introduced.

Crawford et al. [12] created a subroutine for full-coverage film-cooled flow for insertion into the STAN5 [40] numerical program for boundary-layer flows. Their scheme was to solve differential conservation equations of mass, momentum, and energy, subject to a closure scheme which acknowledged the effect of injection. The effect of the injected air is accounted for as soon as the injection hole is encountered, i.e., at the x-location of the centerline of the injection hole. A mixing-length approach was used for the turbulence model, with augmentation of the turbulence in the near-wall region ($y/\delta < 0.4$). The program treats the film-cooled flow as two-dimensional, using spanwise-averaged values. This subroutine, together with the main program, has been widely used in the gas-turbine industry.

More recent studies on the prediction of film-cooled flows are as follows. Wang et al. [51] used integral conservation equations and predicted the film-cooling effectiveness downstram of a single hole. Stepka and Gaugler [52] predicted the heat-transfer behavior of a film-cooled cylinder. The prediction of aerodynamical losses is of practical importance. Goldman and Gaugler [53] used integral parameters for predicting the aerodynamic losses of film-cooled vanes.

Several prediction models for flow over a convex wall have been widely developed. The two-dimensional approach using a mixing-length turbulence model seems appropriate from a practical point of view. Bradshaw [54] proposed the analogy between streamwise curvature and buoyancy and suggested that the mixing length for curved flows be expressed as $\ell = \ell_0(1 - \beta Ri)$, where ℓ_0 is a flat-plate value, Ri is the Richardson numbr of curvature effects, and β is an empirical constant. This correction to the mixing length was used by Cebeci and

Hirsh [55], Adams and Johnston [56], and others. Gillis and Johnston [38] proposed a different scheme. The mixing length in the curved region was expressed as $\ell = 0.10\ (\delta_{SL} - \delta^*_{SL})$, where δ_{SL} is the width of the active shear layer and δ^*_{SL} is the displacement thickness integrated out to δ_{SL}. In the curved region, $\delta_{SL} = y_{crit}$, where y_{crit} is the value of y for which $S \equiv (U/R)/(dU/dy) = 0.11$, and in the recovery region, $\delta_{SL} = y_{SL}$, where y_{SL} is the location where the shear stress becomes zero. This model agrees with their experimental results quite well. Simon et al. [43] slightly modified this model for heat-transfer predictions, with reasonably good success. Adams and Johnston [56] made further modifications, especially for the recovery process, and tested it against other experimental data, with good agreement. A high-order turbulence model has been used by Gibson et al. [57], and an integral method by Cousteix and Houdeville [58].

Gaugler [59] integrated the discrete-hole injection model by Crawford et al. [12] with the curvature model by Adams and Johnston [56] and put both into the original STAN5 [40]. In principle, this should allow prediction of film-cooled boundary-layer flows over curved walls. In the following section, comparisons will be made between the calculation by this program and the experimental data in the present program.

6.2 Comparison of Prediction and Experimental Data

A special version of the STAN5 program [40] has been written by R.E. Gaugler [59] which includes both the subprogram STANCOOL [60] and the mixing-length model for the streamwise curvature STANCURVE [56]. The program will be called STAN-FC-CRV in this chapter.

The program was executed for four cases: full-coverage cooling with $m = 0.2$, 0.4, and 0.6, and partial-coverage cooling (first two rows) with $m = 0.4$. The results of three full-coverage cases are shown in Figs. 6-1, 6-2, and 6-3. The general conclusion on the comparison of prediction and experimental data follows the main trends in the curved blown region, but needs work in the recovery region and near the beginning of curvature with blowing. In the curved blown region, the prediction model does not work as well for small blowing ratios as it does for large, especially in the initial part of the blown region. In

the recovery flat-plate region, the predicted values are far lower than the experimental data for all cases.

Figure 6-1 shows the results for the full-coverage case with $m = 0.4$ compared with the experimental results of the present study. The line of the prediction is based on the averaged values over the same streamwise distance as for the experimental data: from 3.8 cm upstream to 1.35 cm downstream of the location of injection holes. In the curved region, the predicted values show reasonably good agreement with the experimental data. However, the predicted St(1) values do not follow the sharp decrease of Stanton number shown in the experimental data in the initial part of the blowing region.

The program takes account of both the thermal effect of injection and the altered turbulence structure caused by injection and curvature. The injection model used in the program is based on flat-plate blowing. For injection on a convex surface, as Ito et al. [47] suggested, the injected air is forced towards the wall and the thermal protection of the injection jet increases, due to the convex-curvature effect. Therefore, the injection model itself should be modified to acknowledge the curvature effect. According to Ito and Goldstein [47], convex curvature affects the injection jet favorably until a certain amount of the blowing ratio has been reached. Therefore, the curvature effect on the jet varies with m. A new injection model is needed for the curvature case, and the penetration parameter might have to be a function of the blowing ratios.

For the turbulence model, blowing increases turbulence mixing, but convex curvature suppresses it. The question is how these two opposite effects interact with each other. For $m = 0.4$, direct superposition of these two effects does not seem too bad, because the prediction of St(0) shows reasonable agreement with the experimental data, although a slight over-prediction is seen in the entire blown region.

In the recovery region, for both St(0) and St(1), the prediction shows much lower values than do the experimental data. This could be caused by the fact that the predicted recovery from the turbulence augmentation in the blowing region is too fast, while recovery from the

thermal effect is too slow. In the recovery region, further modification is necessary, based on the experimental data and their interpretation.

Figure 6-2 shows the prediction for $m = 0.6$. Both the $St(0)$ and $St(1)$ prediction in the blown region seems to agree with the data fairly well. The prediction of Stanton number in the blown region for $m = 0.6$ shows the best agreement among the three blowing ratios. Therefore, it might be that, for this large blowing ratio, the curvature effect on injected air is so small that the model based on the flat-plate behavior also represents the injection model on a curved wall for $m = 0.6$. In the recovery region, as was the case for $m = 0.4$, the predicted values of both $St(0)$ and $St(1)$ are lower than the experimental data.

For $m = 0.2$, the prediction does not work well; this is the worst of the three full-coverage cases. The very high values of $St(0)$ and $St(1)$ in the first part of the blowing region are unrealistic. For this small blowing ratio, the curvature effect must remain the dominant effect on the turbulence structure. It also seems true for $St(1)$ that the thermal protection by injection is not properly modeled, as discussed in the case of $m = 0.4$. In the recovery region, the prediction shows the same results: under-prediction for both $St(0)$ and $St(1)$, as seen in the other full-coverage cases.

The situation in Fig. 6-4 deals with two rows of blowing with $m = 0.4$. It agrees well with the experimental data except in the first one-third of the curved region. In the last part of the curved plate and in the recovery region, there is essentially only one effect, the curvature effect. Since the program has been proven to work well for the curvature effect by Adams and Johnston [6], the predicted values in the last half of the curved region and in the entire recovery region agree very well with the experimental data taken in the present study. On the other hand, the first one-half of the curved region is strongly affected by injection, and the relatively bad agreement in this region is seen because of the reasons discussed in the full-coverage cases.

From the four results discussed here, it is clear that modifications are necessary for the part predicting injection behavior. The

curvature effect should be included in the injection model, which predicts the thermal protection by the injected jet. The interaction between the turbulence augmentation caused by injection and the suppression by convex curvature seems to need modification: a more complicated coupling than simple superposition might be necessary, probably involving some function of a blowing ratio.

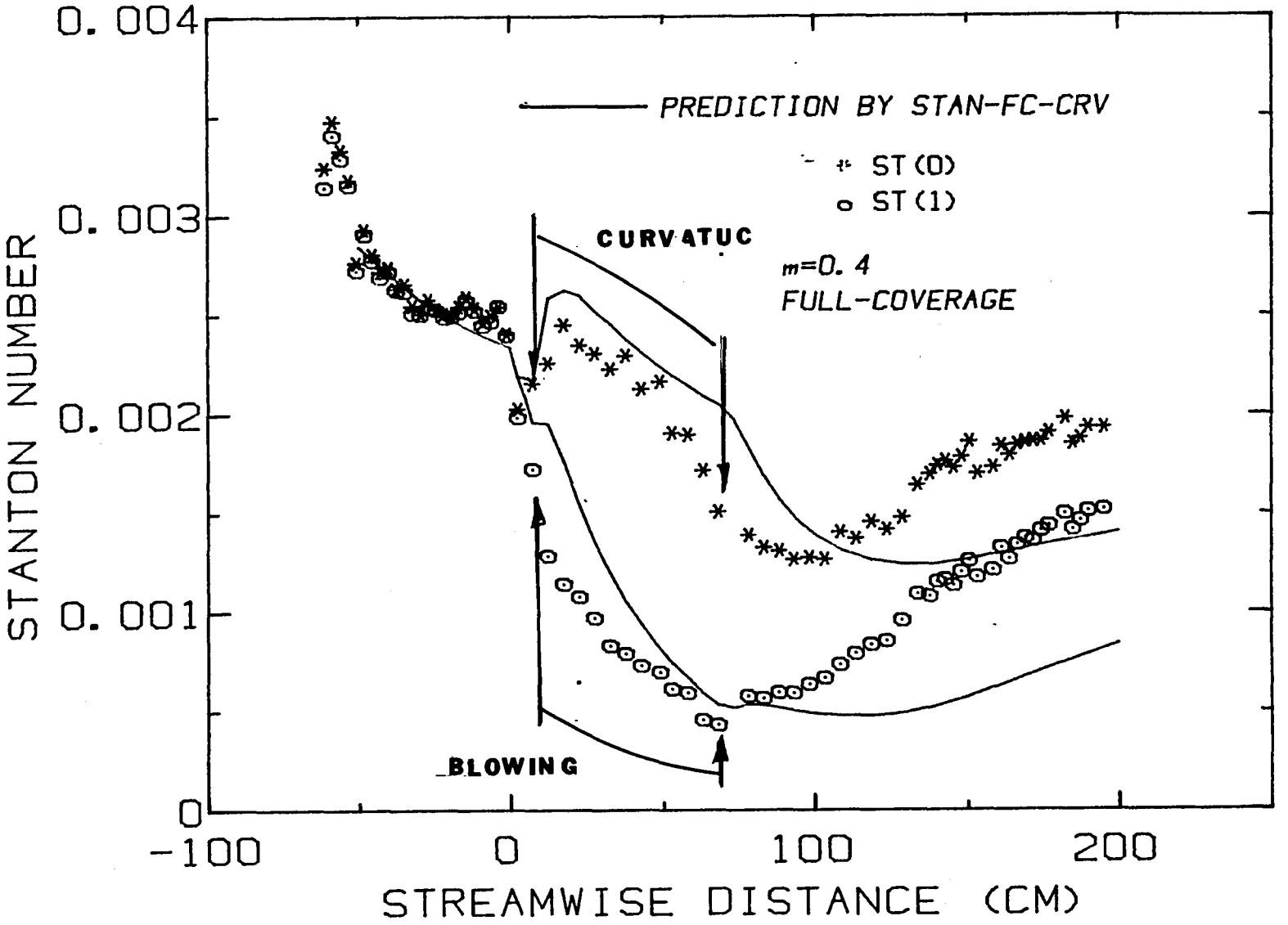

Fig. 6.1. Prediction of Stanton number for full-coverage cooling with m = 0.4: comparison with experimental data . .

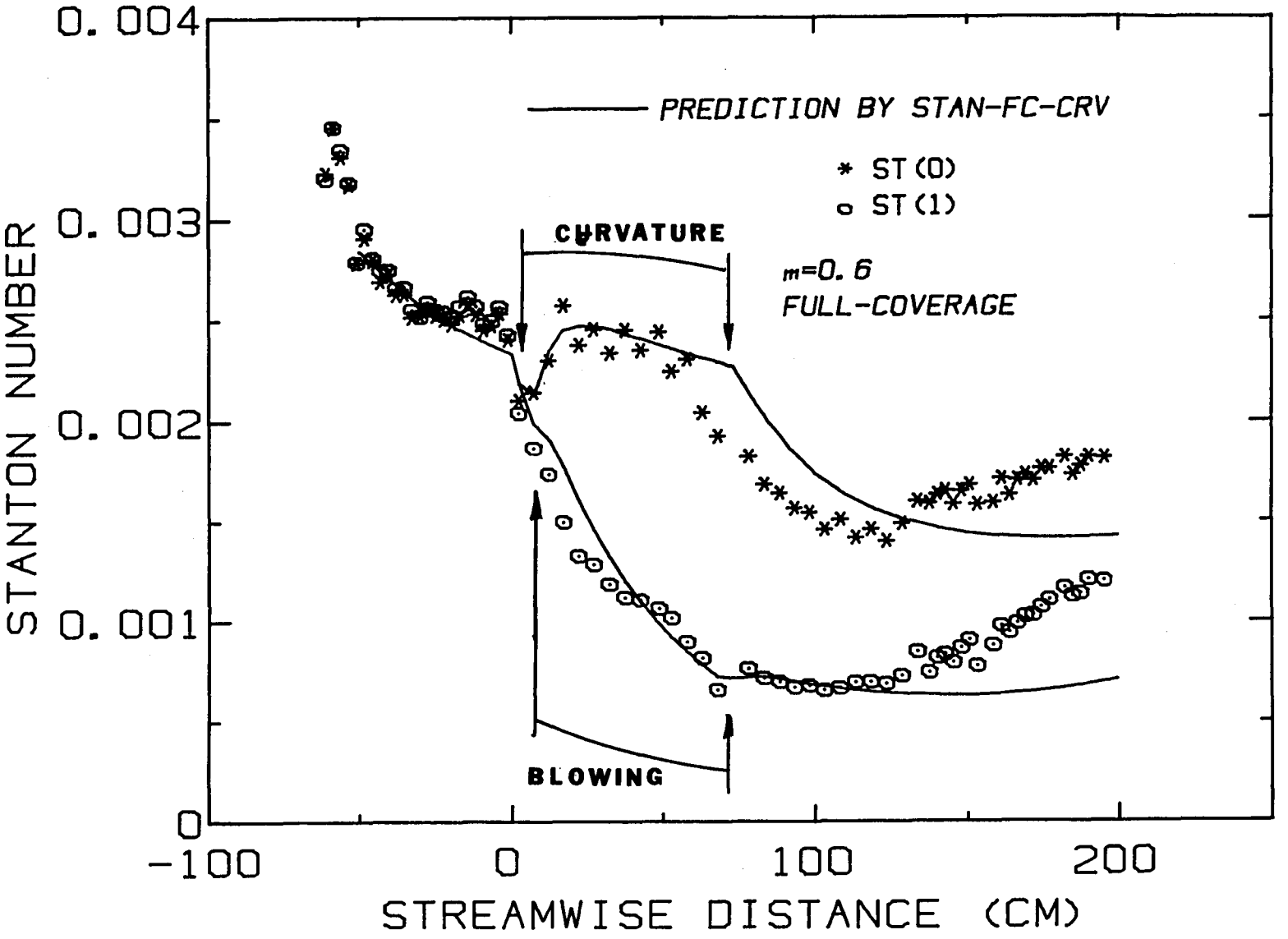

Fig. 6.2. Prediction of Stanton number for full-coverage cooling with m = 0.6: comparison with expeirmental data

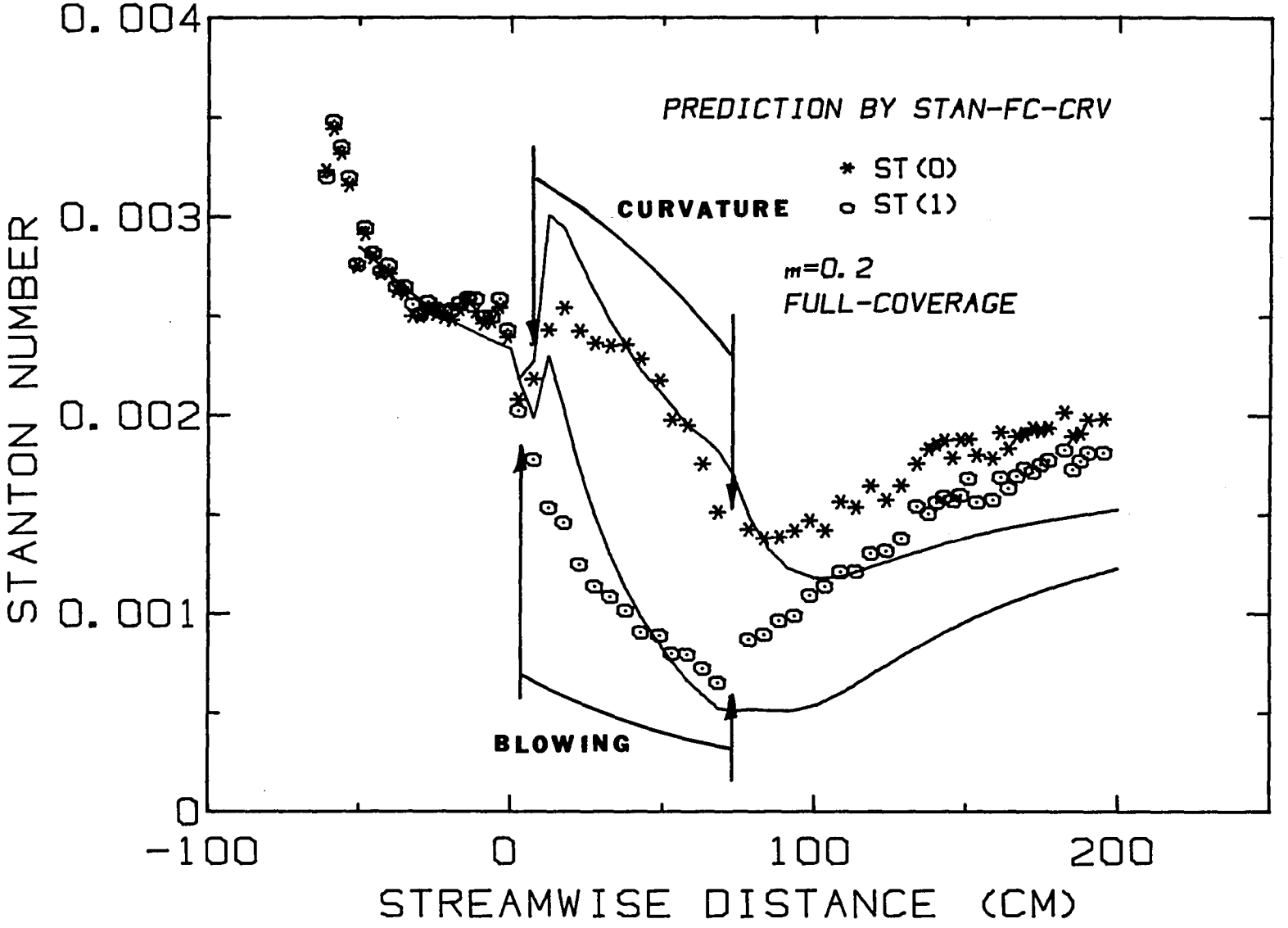

Fig. 6.3. Prediction of Stanton number for full-coverage cooling with m = 0.2: comparison with experimental data

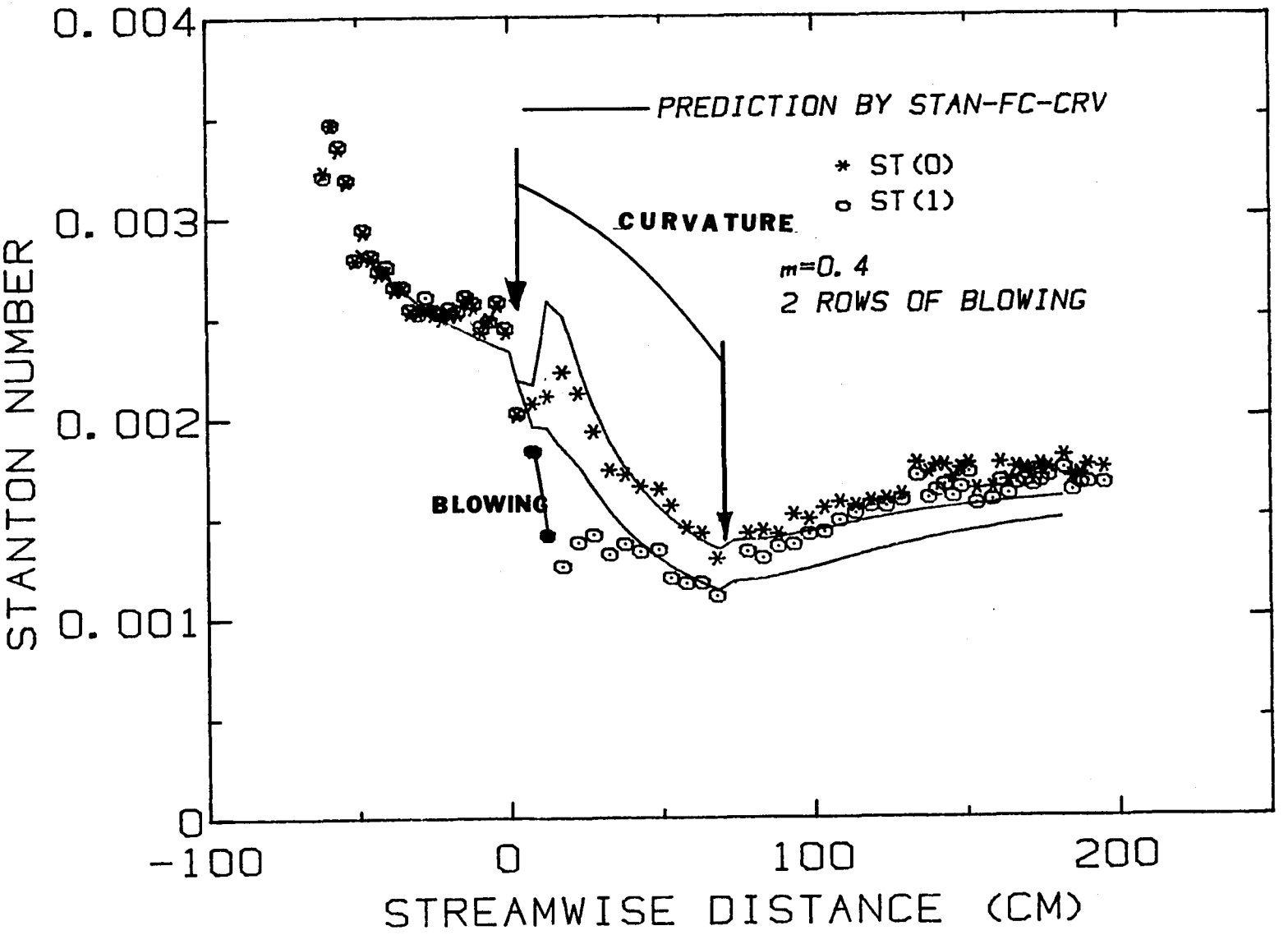

Fig. 6.4. Prediction of Stanton number for partial-coverage cooling with m = 0.4: comparison with experimental data

Chapter 7

CONCLUSIONS AND RECOMMENDATIONS

Measurements of spanwise-averaged heat-transfer coefficients were made on a convex wall with discrete-hole injection and on the following flat recovery plate for several values of the injection parameter and for both full and partial coverage. The injection holes were inclined downstream at 30° to the surface. The baseline data set is for full-coverage blowing with $m = 0.4$, and three parameters were altered--blowing ratio: $m = 0.2$, 0.4, and 0.6; number of rows of injection: thirteen rows (full coverage), six, four, and two rows (partial coverage); and location of the beginning of injection: beginning, middle, and end of the curved plate.

The experimental data are presented in terms of two fundamental Stanton number sets: $St(0)$, $T_2 = T_\infty$), and $St(1)$, ($T_2 = T_w$), where T_2 is the injection air temperature. These two sets allow one to calculate Stanton numbr values at any injection air temperature.

The case of $\theta = 1$ is representative of current gas-turbine practice, and the variation of $St(1)$ can be used to judge the heat-transfer effects in service reasonably well, without considering superposition effects. Injection on a convex wall depresses the Stanton number somewhat more than it does on a flat wall, i.e., the convex wall is easier to cool. This effect can be seen in both the $St(1)$ data and also in cooling effectiveness values deduced from the present data. There is an immediate drop in $St(1)$ with the onset of injection, and $St(1)$ remains low throughout the curved, blown region. When the curved surface is followed by a flat plate, the Stanton number recovers toward the expected flat-plate values, but very slowly.

$St(1)$ and $St(0)$ show complex responses to changes in blowing and/or curvature, but all aspects of this behavior can be explained in terms of three major effects: the thermal effect of the injected air, the turbulence augmentation by the jet/boundary layer interaction, and the convex curvature effect. Experiments with three blowing ratios for full-coverage cases (i.e., blowing throughout the curved region) reveal that, in the blown region itself, $m = 0.4$ is near optimum, but the

higher the blowing in the curved region, the lower the Stanton number in the recovery region.

When conditions change in the x-direction, it is difficult to separate a boundary layer's response to local conditions from the effects of the upstream history. The local response of the boundary layer heat-transfer behavior can be isolated from the historical effects (initial boundary-layer thickness, etc.) by plotting the data on $St\text{-}Re_{\Delta_2}$ coordinates. When this approach is applied to the present data, it is seen that the St(1) data for full-coverage blowing with $m = 0.2$ and 0.4 in the blown region lie on a line of (-1) slope, the same line which applies with no injection, on a convex wall. This result demonstrates that, for low values of m (i.e., $m \leq 0.4$), the local response of the boundary layer is governed by curvature effect, not the blowing effect. On the other hand, for $m = 0.6$, the St(1) data in the blown region lie on the line of a different slope, above the line of (-1) slope. The large amount of injection air at $m = 0.6$ tends to counteract the curvature effect on the local nature of heat transfer.

In the recovery region, for full-coverage blowing, both St(0) and St(1) gradually approach the no-injection values. The behavior of St(0) is complicated, showing both a minimum and a maximum point within the recovery region, while St(1) data monotonically increase in the recovery region. The recovery of St(0) from the injection effect can be divided into three regions, and the behavior in each region can be explained in terms of three effects: recovery from the thermal effect, recovery from the augmented turbulence, and the release of curvature. The recovery of St(1) is simpler, and is dominated by the recovery from the thermal effect.

The explanations of the recovery process of Stanton number after full-coverage blowing are supported by the boundary-layer velocity measurements, turbulence kinetic-energy profiles, and temperature profiles.

Boundary-layer profile measurements were made for several representative cases using a triple hot-wire probe for mean velocities and turbulence quantities and a thermocouple probe for temperature. From the measured boundary-layer profiles, it appears to be appropriate to divide the flow in the blown region into two types of lanes in the

spanwise direction: lanes with injection holes and lanes with no holes. In a lane with holes, both the hydrodynamic and the temperature profiles show a strong effect of injection, while in the lane without holes, only small effects are seen. For the full-coverage cases, the turbulence structure in the lane with injection holes can be described by a superposition of two streamwise evolutions: small scale and large scale. The small-scale evolution within a lane occurs between two consecutive holes, while the large-scale evolution can be seen by comparing different streamwise locations at the same relative position between holes. Both the small- and large-scale evolutions depend on the blowing ratio, m.

A prediction model, STAN-FC-CRV, which is a direct combination of a flat-plate injection model (STANCOOL) and a model for streamwise curvature (STANCURVE), was tested for four cases: full-coverage with $m = 0.2$, 0.4, and 0.6 and two rows of blowing with $m = 0.4$. Comparison of predicted values with the experimental data shows that this program does not predict the heat-transfer data very well in the recovery region and the prediction in the blown region for small m, 0.2 and 0.4 needs further modification. The injection model dealing with the thermal effect of injection must be modified to account for the curvature effect. The rate at which the boundary layer recovers from the effect of injection should also be modified, because the predicted recovery process is too slow.

Recommendations for Future Work

1. Heat-transfer experiments should be done with streamwise pressure gradient and with different initial boundary-layer conditions.
2. The effect of injection in the first part of the recovery flat plate should be determined.
3. Detailed measurements of the streamwise evolutions in the blown region should be undertaken to support the modeling efforts.
4. For a modeling effort, more work is necessary. The present study suggests that two parts of STAN-FC-CRV be modified.

5. The lanes with holes and without holes should be modeled separately, based on spanwise averages within those lanes. This approach will open the door to treatment of different P/D geometries using the same data base.

References

1. Kays, W. M., and Moffat, R. J., "The Behavior of Transpired Turbulent Boundary Layers," Rept. HMT-20, Thermosciences Div., Dept. of Mech. Engrg., Stanford University.

2. Goldstein, R. J., "Film Cooling," in Advances in Heat Transfer, Vol. 7, pp. 321-379.

3. Jabbari, M. Y., and Goldstein, R. J., "Adiabatic Wall Temperature and Heat Transfer Downstream of Injection through Two Rows of Holes," J. Engrg. for Power, Vol. 100, pp. 303-307, 1978.

4. Bergeles, G., Gosman, A. D., and Launder, B. E., "Double-Row Discrete Hole Cooling: An Experimental and Numerical Study," J. Engrg. for Power, Vol. 102, p. 498-503, 1980.

5. Afejuku, W. O., Hay, N., and Lampard, D., "Film-Cooling Effectiveness of Double Row Holes," J. Engrg. for Power, Vol. 102, pp. 601-606, 1980.

6. Metzger, D. E., Takeuchi, D. I., and Kuestler, P. A. "Effectivness and Heat Transfer with Full-Coverage Film Cooling," J. Engrg. for Power, Vol. 95, pp. 180-184, 1973.

7. Sasaki, M., Takehara, K., Kumagai, T., and Hamano, M., "Film Cooling Effectiveness for Injection from Multirow Holes," J. Engrg. for Power, Vol. 101, pp. 101-108.

8. Kasagi, N., Hirata, M., and Kumada, M., "Studies of Full-Coverage Film Cooling, Part 1: Cooling Effectivness of Thermally Conductive Wall," ASME Paper 81-GT-37, for March 9-12, 1981, meeting.

9. Kumada, M., Hirata, M., and Kasagi, N., "Studies of Full-Coverage Film Cooling, Part 2: Measurement of Local Heat Treatment Coefficient," ASME Paper 81-GT-38, for March 9-12, 1981, meeting.

10. Metzger, D. E., Carper, H. J., and Swank, L. R., "Heat Transfer with Film Cooling near Non-Tangential Injection Slots," J. Engrg. for Power, Vol. 90, pp. 128-133, 1968.

11. Choe, H., Kays, W. M., and Moffat, R. J., "Turbulent Boundary Layer on a Full-Coverage Film-Cooled Surface--An Experimental Heat Transfer Study with Normal Injection," Rept. HMT-22, Thermosciences Div., Dept. of Mech. Engrg., Stanford University, 1973.

12. Crawford, M. E., Kays, W. M., and Moffat, R. J., "Heat Transfer to a Full-Coverage, Film-Cooled Surface with 30° Slant-Hole Injection," Rept. HMT-25, Thermosciences Div., Dept. of Mech. Engrg., Stanford University, 1976.

13. Kim, H. K., Moffat, R. J., and Kays, W. M., "Heat Transfer to a Full-Coverage, Film-Cooled Surface with Compound Angle (30° and 45°) Hole Injection," Rept. HMT-28, Thermosciences Div., Dept. of Mech. Engrg., Stanford University, 1978.

14. Metzger, D. E., Kuenstler, P. A., and Takeuchi, D. I., "Heat Transfer with Film Cooling Within and Downstream of One to Four Rows of Normal Injection Holes," ASME Paper 76-GT-83, for March 21-25, 1976, meeting.

15. Kadotani, K., and Goldstein, R. J., "Effect of Mainstream Variables on Jets Issuing from a Row of Inclined Round Holes," ASME Paper 78-GT-138 for April 9-13, 1978, meeting.

16. Brown, A., and Saluja, C. L., "Film Cooling from Three Rows of Holes on Adiabatic, Constant Heat Flux and Isothermal Surfaces in the Presence of Variable Velocity Gradients and Turbulence Intensity," ASME Paper 79-GT-24 for March 12-15, 1979, meeting.

17. Jabbari, M. Y., and Goldstein, R. J., "Effect of Mainstream Acceleration on Adiabatic Wall Temperature and Heat Transfer Downstream of Gas Injection," 6th Int. Heat Transfer Conf., Toronto, 1978.

18. Talor, A.M.K.P., and Whitelaw, J. H. "Effectiveness of Leading-Edge Cooling Arrangements," 6th Int. Heat Transfer Conf., Toronto, 1978.

19. Luckey, D. W., Winstanley, D. K., Hanus, G. J., and Ecuyer, M. R., "Stagnation Region Gas Film Cooling for Turbine Blade Leading-Edge Applications," J. Aircraft, Vol. 14, pp. 494-501, 1977.

20. Sakata, K., Usui, H., and Takahara, K., "Cooling Characteristics of Film-Cooled Turbine Vane Having Multi-Rows of Ejection Holes," ASME paper 78-GT-21, for April 9-13, 1978m, meeting.

21. Dring, R. P., Blair, M. F., and Joslyn, H. D., "Experimental Investigation of Film Cooling on a Turbine Rotor Blade," J. Engrg. for Power, Vol. 102, pp. 81-87, 1980.

22. Bergeles, G., Gosman, A. D., and Launder, B. E., "Near-Field Character of a Jet Discharged through a Wall at 30° to a Mainstream," AIAA J., Vol. 15, pp. 499-504, 1977.

23. Kadotani, K., and Goldstein, R. J., "On the Nature of Jets Entering a Turbulent Flow, Part A: Jet-Mainstream Interaction," J. Engrg. for Power, Vol. 101, pp. 459-465, 1979.

24. Yavuzkurt, S., Moffat, R. J., and Kays, W. M., "Full-Coverage Film Cooling: Three-Dimensional Measurements of Turbulence Structure and Prediction of Recovery Region Hydrodynamics," Rept. HMT-27, Thermosciences Div., Dept. of Mech. Engrg., Stanford University, 1977.

25. Colladay, R. S., and Russell, L. M., "Streaklike Flow Visualization of Discrete-Hole Film Cooling for Gas Turbine Applications," J. Heat Transfer, Vol. 98, pp. 2455-250, 1976.

26. Russell, L. M., "Flow Visualization of Discrete-Hole Film Cooling with Spanwise Injection over a Cylinder," NASA Tech. Paper 1491, 1979.

27. Bradshaw, P., "Effect of Streamline Curvature on Turbulent Flow," AGARDograph No. 169, 1972.

28. Wattendorf, F. L, "A Study of the Effect of Curvature on Fully Developed Turbulent Flow," Proc. Royal Soc., Vol. 148, 1935.

29. Eskinazi, S., and Yeh, Y., "An Investigation of Fully Developed Turbulent Flows in a Curved Channel," J. Aero Sci., Vol. 23, 1956.

30. Schneider, W. G., and Wade, J.H.T., "Flow Phenomena and Heat Transfer Effects in a 90° Bend," Canadian Aeronautics and Space Journal, 1967.

31. Ramaprian, B. R., and Shivaprasad, B. G., "Mean Flow Measurements in Turbulent Boundary Layers along Mildly Curved Surfaces," AIAA J., Vol. 15, pp. 189-196, 1977.

32. Shivaprasad, B. G., and Ramaprian, B. R., "Turbulence Measurements in Boundary Layers along Mildly Curved Surfaces," J. Fluids Engrg., Vol. 100, pp. 37-46, 1978.

33. Rammaprian, B. R., and Shivaprasad, B. G., "The Structure of Turbulent Boundary Layers along Mildly Curved Surfaces," J. Fluid Mech., Vol. 85, pp. 273-303, 1978.

34. Meroney, R. N., and Bradshaw, P., "Turbulent Boundary Layer Growth over a Longitudinally Curved Surface," AIAA J., Vol. 13, 1975.

35. Hoffman, P. H., and Bradshaw, P., "Turbulent Boundary Layers on Surfaces of Mild Longitudinal Curvature," Imperial Coll. Sci. & Technol., 1978.

36. So, R. M. C., and Mellor, G. L., "Experiment on Convex Curvature Effects in Turbulent Boundary Layers," J. Fluid Mech., Vol. 60, pp. 43-62, 1973.

37. So, R. M. C., and Mellor, G. L., "Experiment on Turbulent Boundary Layers on a Convex Wall," Aero Quarterly, Vol. 16, 1975.

38. Gillis, J. C., Johnston, J. P., Kays, W. M., and Moffat, R. J., "Turbulent Boundary Layer on a Convex, Curved Surface," Rept. HMT-31, Thermosciences Div., Dept. of Mech. Engrg., Stanford University, 1980.

39. So, R. M. C., and Mellor, G. L., "Turbulent Boundary Layers with Large Streamline Curvature Effects," Z. Angew. Math. & Phys., Vol. 29, pp. 54-74, 1978.

40. Crawford, M. E., and Kays, W. M., "STAN5 — A Program for Numerical Computation of Two-Dimensional Internal and External Boundary-Layer Flows," NASA CR-2742, 1976.

41. Brinich, P. E., and Graham, R. W., "Flow and Heat Transfer in a Curved Channel," NASA TND-8464, 1977.

42. Mayle, R. E., Blair, M. F., and F. C. Kopper," Turbulent Boundary Layer Heat Transfer on Curved Surfaces," J. Heat Transfer, Vol. 101, 1979.

43. Simon, T. W., Moffat, R. J., Johnston, J. P., and Kays, W. M., "Turbulent Boundary Layer Heat-Transfer Experiments: Convex Curvature Effects, Including Introduction and Recovery," Rept. HMT-32, Thermosciences Div., Dept. of Mech. Engrg., Stanford University, 1980.

44. Nicolas, J., and LeMeur, A., "Curvature Effects on a Turbine-Blade Cooling Film," ASME Paper 74-GT-156, for March 30-April 4, 1974, meeting.

45. Folayan, C. O., and Whitelaw, J. H., "Effectiveness of Two-Dimensional Film Cooling over Curved Surfaces," ASME Paper 76-HT-31, for Aug. 9-11, 1976, meeting.

46. Mayle, R. E., Kopper. F. C., Blair, M. F., and Bailey, D. Z., "Effect of Streamwise Curvature on Film Cooling," J. Engrg. for Power, Vol. 99, pp. 77-82, 1977.

47. Ito, S., Goldstein, R. J., and Eckert, E.G.R., "Film Cooling of a Gas-Turbine Blade," J. Engrg. for Power, Vol. 100, pp. 476-482 1978.

48. Youssefmir, P., and Johnston, J. P., "Flow Studies of Full-Coverage Film Cooling on a Convexly Curved Surface," Engineering thesis, Thermosciences Div., Dept. of Mech. Engrg., Stanford University, 1982, HMT Report to be published.

49. Frota, M. N., and Moffat, R. J., "Analysis of the Uncertainties in Velocity Measurements Technique for Turbulence Measurements in Complex Heated Flow with Multiple Hot Wires," Rept. HMT-34, Thermosciences Div., Dept. of Mech. Engrg., Stanford University (to be published).

50. Honami, S., and Johnston, J. P., "A New Definition of Integral Thicknesses for Boundary-Layer Flow over Longitudinally Curved Surfaces," Rept. IL-26, Thermosciences Div., Dept. of Mech. Engrg., Stanford University, 1980.

51. Wang, C. R., Papell, S. S., and Graham, R. M., "Analysis for Predicting Adiabatic Wall Temperatures with Single-Hole Coolant Injection into a Low-Speed Crossflow," ASME Paper 81-GT-91, for March 9-12, 1981, meeting.

52. Stepka, F. X., and Gaugler, R. E., "Comparison of Predicted and Experimental External Heat Transfer around a Film-Cooled Cylinder in Crossflow," NASA Tech. Memo 83017, 1983.

53. Goldman, L. J., and Gaugler, R. E., "Prediction Method for Two-Dimensional Aerodynamic Losses of Cooled Vanes Using Integral Boundary-Layer Parameters," NASA Tech. Paper 1623, 1980.

54. Bradshaw, P., "The Analogy between Streamwise Curvature and Buoyancy in Turbulent Shear Flow," J. Fluid Mech., Vol. 36, pp. 177-191, 1969.

55. Cebeci, T., and Hirsh, R. S., "On the Calculation of Laminar and Turbulent Boundary Layers on Longitudinally Curved Surfaces," AIAA J., Vol. 17, pp. 434-436, 1979.

56. Adams, E., and Johnston, J. P., "A Mixing-Length Model for the Prediction of Convex Curvature Effects on Turbulent Boundary Layers," Rept. IL-42, Thermosciences Div., Dept. of Mech. Engrg., Stanford University, 1981.

57. Gibson, M. M., Jones, W. P., and Younis, B. A., "Calculation of Turbulent Boundary Layers on Curved Surfaces," Phys. Fluids, Vol. 24, pp. 386-395, 1981.

58. Cousteix, J., and Houdeville, R., "An Integral Method for the Calculation of a Turbulent Boundary Layer along a Longitudinally Curved Wall," Rech. Aerosp., No. 1, 1977.

59. Gaugler, R. E., "NASA-Lewis Version of STAN5 Computer Program," NASA-Lewis Research Center, 1982.

60. Crawford, M. E., Kays, W. M., and Moffat, R. J., "Full-Coverage Film Cooling on Flat, Isothermal Surfaces: A Summary Report on Data and Predictions," Rept. HMT-30, Thermosciences Div., Dept. of Mech. Engrg., Stanford University, 1978.

61. Adams, E. W., and Johnston, J. P., "A Mixing-Length Model for the Prediction of Convex Curvature Effects on Turbulent Boundary Layers," ASME Paper 83-GT-80 for the 28th International Gas-Turbine Conference and Exhibit, March 1983.

Appendix A

UNCERTAINTY ANALYSIS OF STANTON NUMBER MEASUREMENTS

The following pages show the listing of the program which calculates the uncertainty of the reduced Stanton number data. The listing program was applicable only to the curved region with full-coverage blowing with $T_2 = T_w$. The program of uncertainty analysis is a modified Stanton-number data-reduction program (see Appendix B). The programs for the other cases can be derived from the original data-reduction program. The results of the uncertainty analysis are also shown in this appendix; the developing region, the curved region (hot run and cold run), the first recovery region, and the second recovery region.

Appendix B

DATA-REDUCTION PROGRAMS FOR STANTON-NUMBER DATA

The following listings are those of the Fortran programs used to reduce the wall heat-flux data. There are four programs, each of which is used in each part of the test section: the developing region, the curved blown region, the first recovery region (capable of dealing with the injection in this region), and the second recovery region. For each program, one set of sample input data is also listed.

Appendix C

LIST OF STANTON NUMBER DATA

In the following pages, all reduced Stanton number data are listed. In each setup, there are two sets of experimental data, cold run and hot run. Also listed are the data of St(0) and St(1) calculated from experimental data by superposition.

Appendix D

DATA-ACQUISITION PROGRAM FOR HYDRODYNAMIC DATA

The following listing is that of the Fortran program used for hydrodynamic boundary-layer measurements with a triple hot-wire probe. The program can move the automatic traversing mechanism and position the probe; it can also read the output signal and store the data in a diskette.

Appendix E

LIST OF HYDRODYNAMIC DATA

In the following pages, the data for hydrodynamic boundary-layer measurements are listed. The data include the three mean-velocity components and six turbulence quantities. The data presented were all normalized by δ, U_p, or U_{pw}.

Appendix F

LIST OF TEMPERATURE-PROFILE DATA

List of temperature data are shown in the following pages. The measured temperature is normalized by T_w and T_∞ and expressed in terms of $(T_w - T)/(T_w - T_\infty)$.

1. Report No.	2. Government Accession No.	3. Recipient's Catalog No.
NASA CR-174964		

4. Title and Subtitle	5. Report Date
Film Cooling on a Convex Wall: Heat Transfer and Hydrodynamic Measurements for Full and Partial Coverage	August 1985
	6. Performing Organization Code
7. Author(s)	8. Performing Organization Report No.
K. Furuhama, R.J. Moffat, J.P. Johnston, and W.M. Kays	None
	10. Work Unit No.
9. Performing Organization Name and Address	11. Contract or Grant No.
Stanford University Thermosciences Division Department of Mechanical Engineering Stanford, California 94305	NAG 3-3
	13. Type of Report and Period Covered
12. Sponsoring Agency Name and Address	Contractor Report
National Aeronautics and Space Administration Washington, D.C. 20546	14. Sponsoring Agency Code
	505-31-04

15. Supplementary Notes

Final report. Project Manager, Raymond E. Gaugler, Internal Fluid Mechanics Division, NASA Lewis Research Center, Cleveland, Ohio 44135. The microfiche supplement at the back of this report contains the data in appendixes A to F.

16. Abstract

Turbine-blade cooling is an important issue for high-efficiency turbine engines, and discrete-hole injection is widely used as a cooling method. In the present study, detailed measurements were made of the heat transfer and hydrodynamics of a film-cooled flow on a convex wall, both for full and partial coverage. Two important parameters were altered: the blowing ratio, m, and the number of rows of injection holes. Three values of m were tested: m = 0.2, 0.4, and 0.6. In the blown region, m = 0.4 results in the lowest Stanton numbers of the three blowing ratios tested. This indicates that the value of m = 0.4 is near optimum on the convex wall from the point of view of cooling effect by injection. In the recovery region, Stanton numbers gradually approach the no injection values. Although the heat-transfer behavior during recovery from injection looks relatively complicated, the behavior of Stanton number can be explained in terms of two mechanisms: recovery from the thermal effect of injection and recovery from the turbulence augmentation. This interpretation of the data is supported by the hydrodynamic and temperature-profile measurements. For partial blowing cases, the data follow the full-coverage values inside the blown region. In the unblown region, both in the curved and in the flat plate, the effect of the number of blown rows is clearly seen. Hydrodynamic boundary-layer profiles were measured with the aid of a triple hot-wire probe. Three mean-velocity components and six turbulence quantities were simultaneously measured, and inside the blown region strong three-dimensionality was observed. It seems appropriate to divide the flow field in two alternate lanes in the spanwise direction—lanes with injection holes and lanes without. The profiles in the lane with holes were strongly affected by the injection, but in the lane without holes only small effects were observed. The turbulence structure in the blown region can be described by the superposition of two streamwise evolutions: a small-scale evolution (between consecutive holes) and a large-scale evolution. The patterns shown in both evolutions depend upon the blowing ratios. A prediction program was tested for four representative cases. The comparison between the prediction and the experimental data reveals that further modification is necessary for the injection model.

17. Key Words (Suggested by Author(s))	18. Distribution Statement
Film cooling; Curvature; Boundary layer	Unclassified - unlimited STAR Category 34

19. Security Classif. (of this report)	20. Security Classif. (of this page)	21. No. of pages	22. Price*
Unclassified	Unclassified		

*For sale by the National Technical Information Service, Springfield, Virginia 22161

End of Document